DEPARTMENT OF MECHANICAL & AEROSPACE ENGINEERING

University of Strathclyde Engineering

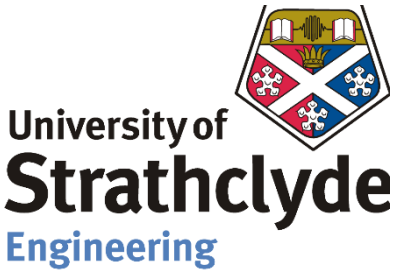


Department of Mechanical and Aerospace Engineering

# Modelling and Assessing CSP and PV systems technical and economic performances to supply power to a mining context in Zimbabwe.

Author: Anesu Maronga

Supervisor: Dr Paul Tuohy

A thesis submitted in partial fulfilment for the requirement of degree in

Master of Science in Sustainable Engineering: Renewable Energy Systems and the Environment

2020

# Copyright Declaration



Signed: Anesu Maronga Date: 19/08/2020

# Abstract

The current electricity supply in Zimbabwe is not stable due to mainly drought that affected the utility's main hydro power station. This challenge resulted in load shedding something that is not desirable to mining companies that require constant and reliable power for their operations. Like any other power consumers in the country, mining companies are now compelled to look for alternative ways to power their operations in an efficient, clean, and cost-effective way. In this context, this report is aimed at evaluating the potential of integrating Concentrated Solar Power (+ thermal storage) and Photovoltaics (+ battery storage) to supply power at a typical mine in Zimbabwe.

The techno-economic analysis of the systems was carried out using System Advisory Model (SAM) and PVSyst software packages. The climate data of the area was gathered together with the typical annual demand profile which were then used as inputs to the designed models. The PV system was designed and optimised based on the tilt angle, interrow distance, and battery storage capacity. CSP system was designed and optimised based on the solar multiple, design point direct normal irradiation value, and thermal energy storage capacity. Two scenarios were simulated – base case with no exports to the grid and another case where exports are allowed. The models were evaluated based on the generated renewable energy offsetting the mine demand, energy exported, grid contribution, Localised Cost of Energy and Net Present Value.

The addition of battery storage system to PV improved the percentage of load offset by renewable system and the generated energy by the renewable system by almost double. However, the installation cost, required land, LCOE, and simple payback also increased by approximately a factor of 2 while the NPV reduced by nearly half. The addition of thermal storage system to CSP increased the generated energy, capacity factor, and renewable energy contribution by approximately a factor of 2. Also, the LCOE improved due to increase in generated energy. However, the land required for development and installation costs also nearly doubled.

The PV + Battery model performed better (hence recommended for implementation) on both simulated scenarios offsetting about 63% of the annual mine load at a localised cost of US cents 10.67/kWh (for no exports case) and US cents 9.4/kWh (for export case). The analysis showed that the CSP system perform better when exports are allowed than with base case scenario. The localised cost of energy of CSP + TES with no exports was predicted at US cents 15.44/kWh while the one with exports case had a localised cost of energy at US cents 10.45/kWh and the annual mine load offset by the system was around 41%.

# Acknowledgements

Firstly, I wish to give my special appreciation to my dissertation supervisor, Dr Paul Tuohy, for his continuous guidance and encouragement in making this dissertation complete. Without his efforts, this dissertation would have not been the same as presented here.

I want to thank the Beit Trust Scholarship for the opportunity they gave me to study this Master's program. Without this scholarship, it would have been impossible for me to study this course.

I am also indebted to my family who have been supportive to me during this time of Covid - 19 pandemic while I complete this dissertation. Thanks for their encouragement, love, and emotional support that they have given me.

Finally, my appreciation goes to all my colleagues and others who contributed either directly or indirectly in process to finish this dissertation.

# Table of Contents

# List of Figures

# List of Tables

# Nomenclature

| Symbol | Description |
|---|---|
| AC | Alternating Current |
| CSP | Concentrated Solar Power |
| DC | Direct Current |
| DNI | Direct Normal Irradiation |
| GHI | Global Horizontal Irradiation |
| GWH | Giga Watt Hour |
| kWh | Kilo Watt Hour |
| kV | Kilo Volt |
| Kg | Kilo gram |
| LCOE | Localised Cost Of Energy |
| MVA | Mega Volt Amperes |
| M | metres |
| MW | Mega Watt |
| NPV | Net Present Value |
| PV | Photovoltaic |
| TES | Thermal Energy Storage |
| USD | United States Dollars |
| W | Watts |
| $^{o}C$ | Degrees Celsius |

# 1.0 Introduction

## 1.1 Background

About 11% of the final worldwide energy consumption is attributed to the mining sector according to the International Energy Agency (IEA) (IEA database, 2019). The energy demand in mines is expected to increase by 36% by the year 2035 (Columbia Center on Sustainable Investment, 2018). The industry, however, is currently powered predominantly by convectional energy sources which contribute to greenhouse gas emissions (Australian Renewable Energy Agency, 2017). Mining organisations including the International Council on Mining and Metals (ICCM), South African Chamber of Mines, Minerals Council of Australia among others have acknowledged the need to incorporate renewable energy systems and improving efficiency in their operations to reduce greenhouse gas emissions (Australian Renewable Energy Agency, 2017).

The current power situation in Zimbabwe is not favourable for mining companies who require reliable power for their operations. According to the power utility 1$^{st}$ quarter figures of 2020, the generated electricity was approximately 20% short from the target (Zimbabwe Power Company, 2020). This was mainly caused by the low levels of water in Kariba dam which is the main hydro power station and technical challenges at one of the thermal power stations (Zimbabwe Power Company, 2020). Mining companies are now compelled to look for alternative ways to supply power in case of load shedding from the utility. Renewable energy systems, particularly solar, has the potential to provide an alternative solution to this conundrum due to generally good solar resource in the country (Ziuku et al, 2014).

Renewable energy systems like Solar – Photovoltaic (PV) and Concentrated Solar Power (CSP) - and wind have matured enough to be economically competitive to power mining operations. The possibility of combining the systems with storage presents an opportunity to solve the challenge of intermittence of renewable energy sources there by providing predictable power. Thermal storage (in the case of CSP) and battery storage could be used as technological enablers to help renewable energy systems to provide reliable and dispatchable power. In addition, the hybrid renewable energy systems can have their dispatch automated to provide high return on investment by supplying the lowest cost renewable electricity at any given time.

Currently there is not much research available to access the possibility of powering mining operations using hybrid renewable energy systems. However, a significant number of scholars have evaluated quite diverse combinations of renewable systems to supply certain needs. Zurita et al (2018) evaluated the hybrid CSP + PV + battery energy system to supply a base load. One of the key results of the study was that integrating the battery storage would make the system not economically competitive. Parrado et al (2016) projected the Localised Cost of Energy (LCOE) of a hybrid PV-CSP located in Chile in the year 2050. The results show that it is feasible to supply sustainable continuous electricity that could benefit industries like mining. Green et al (2015) analysed factors that are important to have a high capacity factor from a CSP-PV hybrid system. The analyses concluded that there is need of an effective configuration, dispatch strategy and good sunlight to have high capacity factor from the system.

Despite the high promise in the potential of hybrid renewable systems, there is still uncertainty on whether the systems can reliably provide power to the mining sector while providing economic benefit. Hybrid renewable energy systems in mining systems are relatively still new and offtakers have no first-hand experience on their ability to reliably provide power (Australian Renewable Energy Agency, 2017). Another limitation facing the hybrid systems has to do with amortisation. There is usually a mismatch between the life of the mine and the hybrid system asset life (Australian Renewable Energy Agency, 2017).

In this context, this project intends to analyse and propose renewable energy hybrid system that can be technically and economically integrated into mining operations. The system should be configured carefully to meet the electrical demand of the mine at most risk period of load shedding at a lowest cost possible.

## 1.2 Aim

The aim of the project is to evaluate the potential of integrating CSP + Thermal storage and PV + Battery storage systems to supply power at a mine in Zimbabwe. The systems will be optimised based on the following design parameters:

- Thermal energy storage capacity (CSP)
- Tilt angle (PV)
- Inter-row distance (PV)
- Solar multiple (CSP)
- Battery storage hours (PV)

The evaluation will be assessed based on energy generated and economic performance.

## 1.3 Project Scope and Assumptions

The project scope will be limited to PV and CSP renewable technologies. Other potential renewable energy sources such as wind and hydro will not be analysed. The project will assume other development stages like Environmental Impact Studies and Grid impact studies have been carried out and the results thereof will not affect the analysis. Also, the model assumes that a Power Purchase Agreement (PPA) with the utility is in place in case of energy exports. The land required to develop the hybrid system is assumed to be available near the mine without restrictions.

## 1.4 Objectives

The objective for this project is to simulate and evaluate/optimise the effect of:

- Tilt angle and interrow distance on PV system
- Thermal energy storage capacity on CSP system
- Battery capacity on PV system
- Solar multiple on CSP system
- Offsetting mine load with PV and PV + Battery systems
- Offsetting mine load with CSP and CSP + Thermal storage systems

## 1.5 Project Method

The table 1.1 below shows the methodology to be used to deliver the outcomes of the project:

Table 1. 1: Project methodology

| Item | Description |
|---|---|
| Project definition | Define the project title, aim, and expected outcomes |
| Literature review | • Investigate the characteristics of general mine power systems<br>• Review the PV and CSP technologies<br>• Research about modelling software packages for CSP and PV systems |
| Methodology | • Gather the demand profile and weather data for the mine<br>• Identify economic metrices used to evaluate candidate technologies<br>• Model and evaluate the impact of tilt angle, interrow distance, and battery capacity on PV systems using SAM<br>• Model and evaluate the impact of thermal energy storage, and solar multiple using SAM<br>• Design, model and evaluate the technical and economic performance of PV, PV + Battery, CSP, CSP + Thermal storage using SAM and PVSyst software packages |
| Result analysis | • Analyse the results |

## 1.6 Tools and Resources

The list below shows the major tools and resources that will be used in the project:

- PVSyst – Used to evaluate PV systems
- SAM – Used to evaluate CSP and PV systems
- Weather data – the data for the case study to be purchased from Solcast and used by SAM and PVSyst
- Demand profile – data from Mimosa mine in Zimbabwe as a case study to be used as an input to the model

## 1.7 Milestones

The schedule of key deliverables of the project is presented in the table 1.2 below:

Table 1. 2: Project Milestones

| Deliverable | Deliverable date |
|---|---|
| Project proposal | 01/06/2020 |
| Literature review | 15/06/2020 |
| PV and CSP Economic metrics | 22/06/2020 |
| Evaluation of key design parameters | 06/07/2020 |
| PV, PV + Battery models | 13/07/2020 |
| CSP, CSP + Thermal storage models | 22/07/2020 |
| First draft report | 03/08/2020 |
| Final report | 17/08/2020 |

## 1.8 Risk management

Potential obstacles to the completion of the project and their respective control strategies are presented in the table 1.3 below:

Table 1. 3: Project Risk Management

| **Risk** | **Control measure(s)** |
|---|---|
| Change in scope or unsustainable scope risking project overrun/failure | • Define the scope boundaries and agree with the supervisor early on |
| Inability to model the hybrid technologies | • Perform comprehensive literature review of the technologies<br>• Make reasonable engineering assumptions where necessary |
| Lack of key data /inaccurate data like weather and demand profile | • Use industrial links to source the demand profile data<br>• Communicate with supervisor to identify substitute data<br>• Find economical yet accurate weather data accepted in the industry<br>• Make reasonable engineering assumptions where there is no data |
| Lack of funding for software licence and weather data | • Try to use as much as possible free software packages<br>• Communicate with the supervisor to explore avenues available |
| Challenges with SAM and PVSyst software | • Learn in advance the functionality of these software packages using YouTube and help forums |
| Loss or corruption of project files | • Always keep up to date back up files on google drive and removable flash drive |
| Project time overrun | • Adhere to the project timeline developed and agreed by the supervisor<br>• Review progress weekly and adjust where necessary with the consent of the supervisor<br>• Communicate with the supervisor every week |
| COVID-19 pandemic | • Adhere to the given guidelines to stay safe<br>• Communicate with the supervisor/department if anything happens |

# 2.0 Literature Review

## 2.1 Mining Power Systems and Renewable Energy

### 2.1.1 Role of power in mines

In general, mines are high electrical power intensive sector requiring constant and reliable electrical energy for its operations. Electrical cost constitutes about 15-40% of the total annual operating expenditure (OPEX) of a typical mine with approximately 15% of a typical capital expenditure (CAPEX) budget set aside for electrical infrastructure and equipment (Australian Renewable Energy Agency, 2018). In most instances, the mining sector values more the reliability and stability of the power than the marginal cost saving of its supply (Australian Renewable Energy Agency, 2018).

The electricity consumed at the mine depends on the extend of processing required to liberate the mineral from its ore (Australian Renewable Energy Agency, 2018). The table 2.1 below shows some of the process that consumes a lot of electricity at a mine:

Table 2. 1: High electric intensive activities typical at a mine (Australian Renewable Energy Agency, 2018)

| Mine department | High Electricity consumption activity |
|---|---|
| Mining | Underground mining<br>• Mine ventilation<br>• Drilling<br>Open Cast mine<br>• Pumping |
| Processing | Crushing plant<br>• can include primary, secondary, and tertiary crushers<br>• installed power capacity ranges from 0.2 – 1.2 MW per crusher<br>Milling plant<br>• can consume up to 75% of the plant processing electrical demand<br>• start-up power can be 1.5 times the rated power<br>• installed power capacity can range from 0.2 – 25 MW per mill<br>• requires 24/7 operation<br>Benefaction<br>• smelting |
| Tailings | • conveying or pumping |
| Product delivery | • rail transport (electric) |

### 2.1.2 Demand profile

The demand profile of mines both in the short term and long term has relatively the same pattern. Mines usually operate 24/7 with very limited fluctuations in their daily profile hence its relatively flat (Australian Renewable Energy Agency, 2018). The intra-day variability on the demand profile is caused by maintenance activities. These include planned (scheduled or condition based) or unplanned (faults) (Shahin et al, 2012). The figure 2.1 below shows a typical demand profile (daily and annual) of Spencer copper mine in Northern Chile:

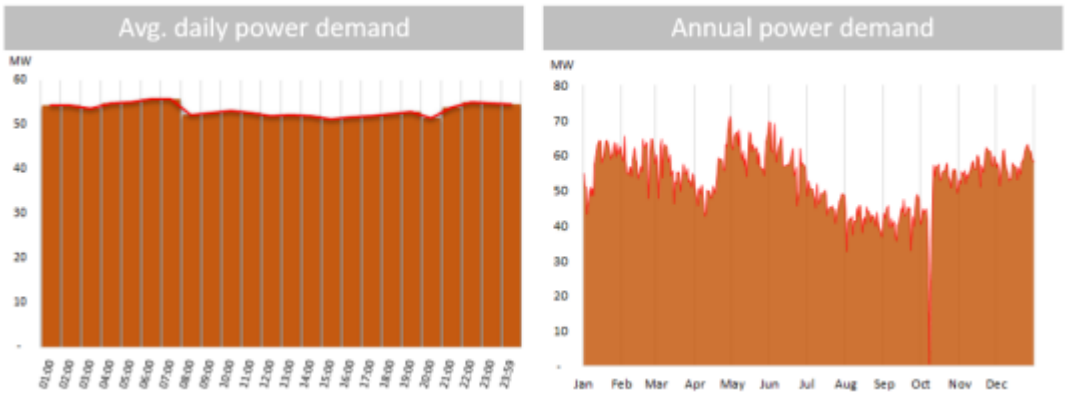


Figure 2. 1: Typical power demand of Spencer copper mine, Chile (Bravo and Friedrich, 2018)

The yearly demand profile, from above figure 2.1, shows that there is limited seasonal variability with the major contributor being the maintenance strategy employed at the mine.

### 2.1.3 Renewable energy integration in mines

#### 2.1.3.1 Technology

There has been a surge in interest in renewable power in the mining sector in recent years. By November 2019, the total capacity of renewable energy either in construction or commissioned was 5.032GW – total installed was 1.760GW and total announced was 3.272 – spanning over 26 countries and 65 mining companies (Rocky Mountains Institute, 2019). The graphs in figure 2.2 and 2.3 below show the renewable energy commissioned capacity in mining by year and the cumulative commissioned plus announced renewable energy project in mining.

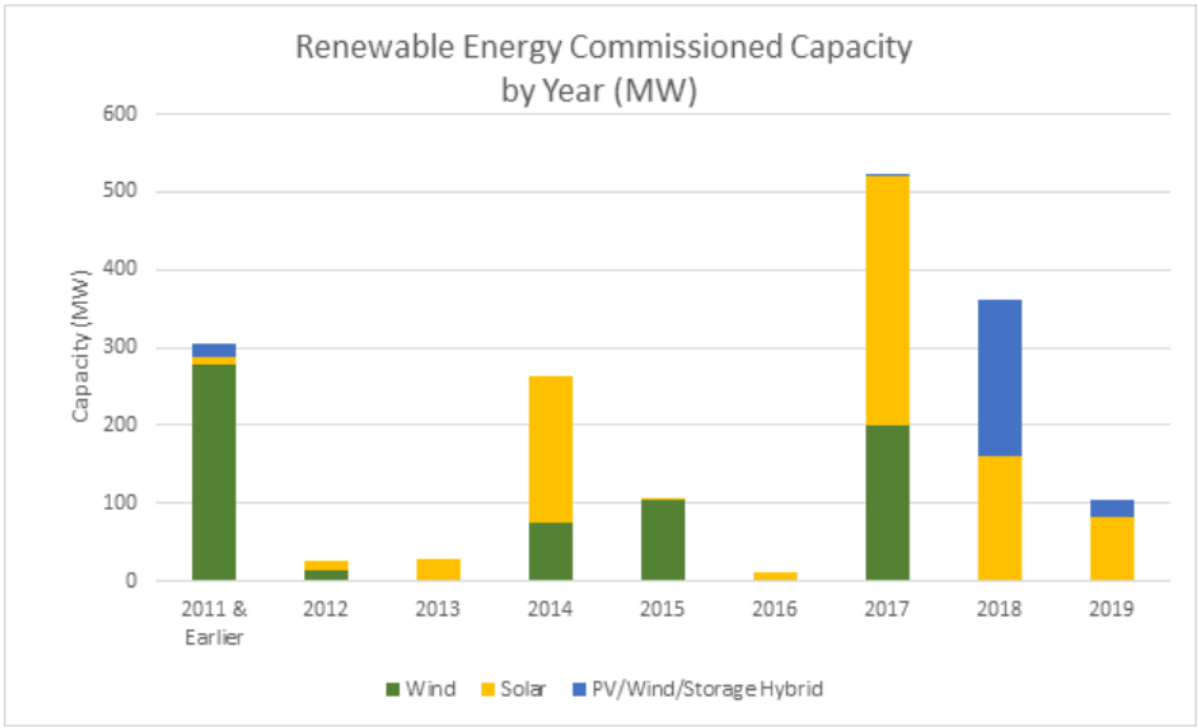


Figure 2. 2: Installed renewable energy in mining sector (Rocky Mountains Institute, 2019)

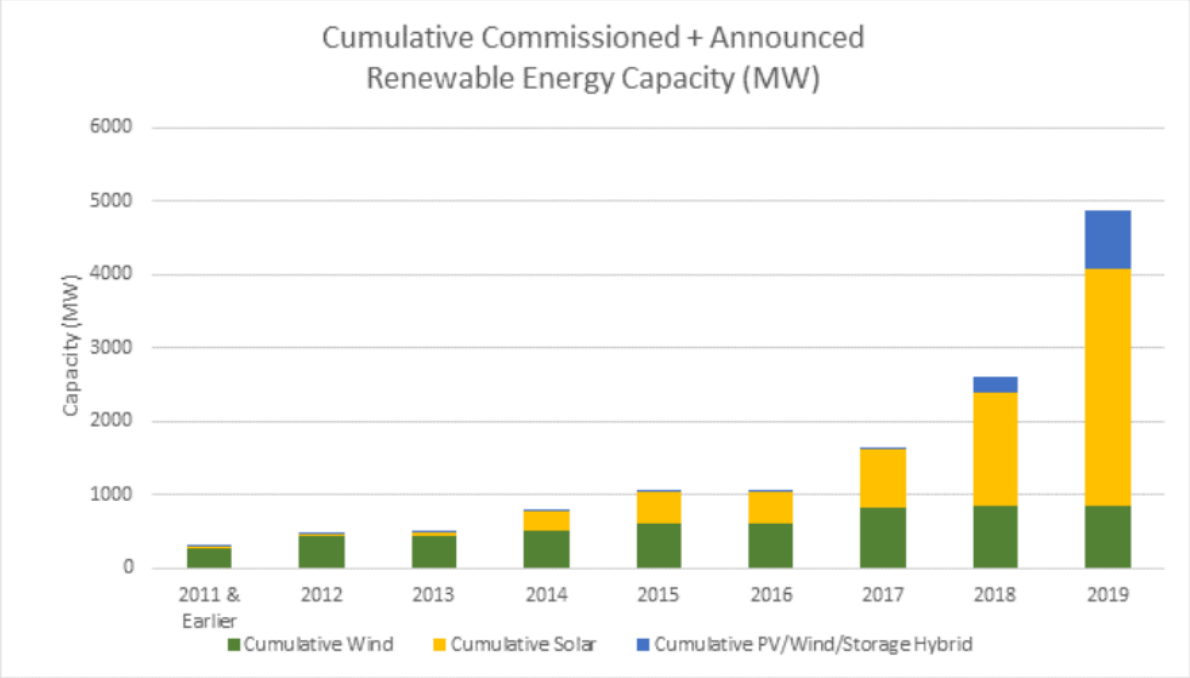


Figure 2. 3: Cumulative commissioned plus announced renewable energy in mining sector (Rocky Mountains Institute, 2019)

The trend is expected to continue to increase as the demand of minerals coupled with reduction in ore grades will increase the required energy per output (Columbia Centre on Sustainable Investment, 2018). In addition, mines are becoming automated and electrified further increasing the potential of renewable integration. This also coincides with the falling cost of renewables, renewable energy aligned polices from governments and increased expertise of renewable energy that will further encourage the uptake of renewables into mining (Columbia Centre on Sustainable Investment, 2018).

Before integrating renewables into mining industry there are several factors that need to be considered to determine the scope of the power system and the design required. The table 2.2 below shows some of the factors needed to be considered when determining the renewable power source to develop for use at a mine:

Table 2. 2: Key factors to consider when integrating renewable energy into a mine (Columbia Centre on Sustainable Investment, 2018)

| Factor | Key questions |
|---|---|
| Potential for renewables | • location of the mine<br>• demand profile<br>• power source options |
| Access and stability of grid | • off or on grid<br>• grid stability |
| Stage of mine project | • Exploration<br>• Operation<br>• Post closure |
| Regulation framework | • Taxes and subsidies<br>• National utility |

| | |
|---|---|
| | • Independent Power Producer (IPP) opportunities |
| Beneficiaries | • Mine<br>• Grid<br>• Community |

**Potential for renewables**

Geographical characteristics around the mine will play a huge role in deciding the best renewable energy mix to develop. This include weather conditions (things like wind profile, radiation, and temperature) and the land terrain. The life of the mine and the load profile will also help in designing the required renewable power source. The cost and reliability of the available renewable source will be important factors to consider as well. (Columbia Centre on Sustainable Investment, 2018)

**Access and grid stability**

Renewable power sources in the mining sector can be categorised as grid connected or off-grid with the former further divided into central and distributed (Australian Renewable Energy Agency, 2018). Central connected implies that renewable energy sources feeds into the central grid (usually at transmission voltage levels) while distributed connected implies that the renewable power source supply the on-site demand. Grid connected projects will depend on technical capability of integrating them to the grid (Columbia Centre on Sustainable Investment, 2018). This is usually assessed by carrying out the grid impact study. On the other hand, off-grid systems are isolated from the central grid operating autonomously.

**Stage of project**

Most renewables in mining sector have been integrated at the production stage of the mine. There are however significant number of renewable projects integrated during exploration and post closure (Columbia Centre on Sustainable Investment, 2018). Mine exploration is usually done in remote areas which have limited grid access. Electrical power at this stage is needed for drilling and domestic use in camps. PV modules provide an alternative clean option to the diesel generators that are normally used at this stage (Columbia Centre on Sustainable Investment, 2018).

At the end of life of the mine, companies are required to decommission and carryout activities like reclamation, maintenance and monitoring the site (Columbia Centre on Sustainable Investment, 2018). At this stage, these activities will be an expense to the company hence renewable energy presents an opportunity to generate revenue from the site (for example developing floating PV on tailings dams). The table 2.3 below shows the viability of different renewable technologies in relation to the life of the mine:

Table 2. 3: Viability of renewable technologies in relation to life of mine (Australian Renewable Energy Agency, 2018)

| Power source | Life of mine 3-7 years | Life of mine >10 years |
|---|---|---|
| Diesel generator | ✔ | ✔ |

| | | |
|---|---|---|
| PV | ✔ | ✔ |
| Wind | ✗ | ✔ |
| CSP | ✗ | ✔ |

**Regulation framework**

Policy and regulation will determine the economies of scale of the renewable energy source hence the viability thereof. These include the type of contracts (like power purchase agreements), net metering, existence of feed in tariffs, among others (Columbia Centre on Sustainable Investment, 2018).

**Beneficiaries**

The choice and design of the renewable power source will also depend on the target users. Taking for example the demand profiles for a mine is different to that of the community and in addition the infrastructure required to connect to the grid is different to that for off-grid systems (Columbia Centre on Sustainable Investment, 2018).

**2.1.3.2 System design**

The design of renewable energy source should be compatible with the operations of the mine. This means it is very important to know inherent characteristics of different renewable resources and how they interact with the mine system (Australian Renewable Energy Agency, 2018). Four key parameters that affect this system design are listed below (Australian Renewable Energy Agency, 2018):

- Mine demand profile
- Characteristics of the renewable technology
- Operating control philosophy
- Commercial arrangements

Mine demand profile has been explained in section 2.1.2 above while the second point will be explored in detail in the next sections

**Operating control philosophy**

The control philosophy basically has two nodes – load and generation – automated by software to achieve stable and reliable power (Australian Renewable Energy Agency, 2018). Load management involves controlling the demand to match power supply fluctuations. This primarily involves load shifting and load shedding. Load shedding is the automatic disconnection of load from supply feeders in response to a strain in the power supply network (this could be a fault or intermittence of renewable energy). This form of control is not encouraged at mine since it results in revenue loss if critical equipment is switched off. Load shifting on the other hand, involves scheduling loads to coincide with available generation. This could work in cases of non-critical, electrically intensive activities that can be scheduled to capitalise solar PV output for instance. (Australian Renewable Energy Agency, 2018)

The other control node involves generation management. Spinning reserve and curtailment are the typical methods used to control the generation side. Spinning reserve is extra online generation capacity on stand-by to cover an increase in power demand due to either of the following (Australian Renewable Energy Agency, 2018):

- Fault on one of the power sources
- Unexpected increase in demand
- Sudden increase in demand due to reduced generation from a variable renewable source

In mining context, spinning reserve can be used to support start-up of large motors (like those typically found at mills) and intermittent loads like conveyer belts. On the other hand, power curtailment involves reducing the energy generated from the power source to enhance system stability. In variable generation, power curtailment is used to provide voltage and frequency control to improve the power quality supplied. (Australian Renewable Energy Agency, 2018)

**Commercial arrangements**

The economic viability of renewable energy systems is affected by the characteristics of the mine including life of mine, legacy contracts, and source of project finance (Australian Renewable Energy Agency, 2018). The figure 2.4 below shows mostly used commercial arrangements for renewable energy in the mining sector. Power purchase agreements (PPA) and self-generation are the most popular on the list (Columbia Center on Sustainable Investment, 2018).

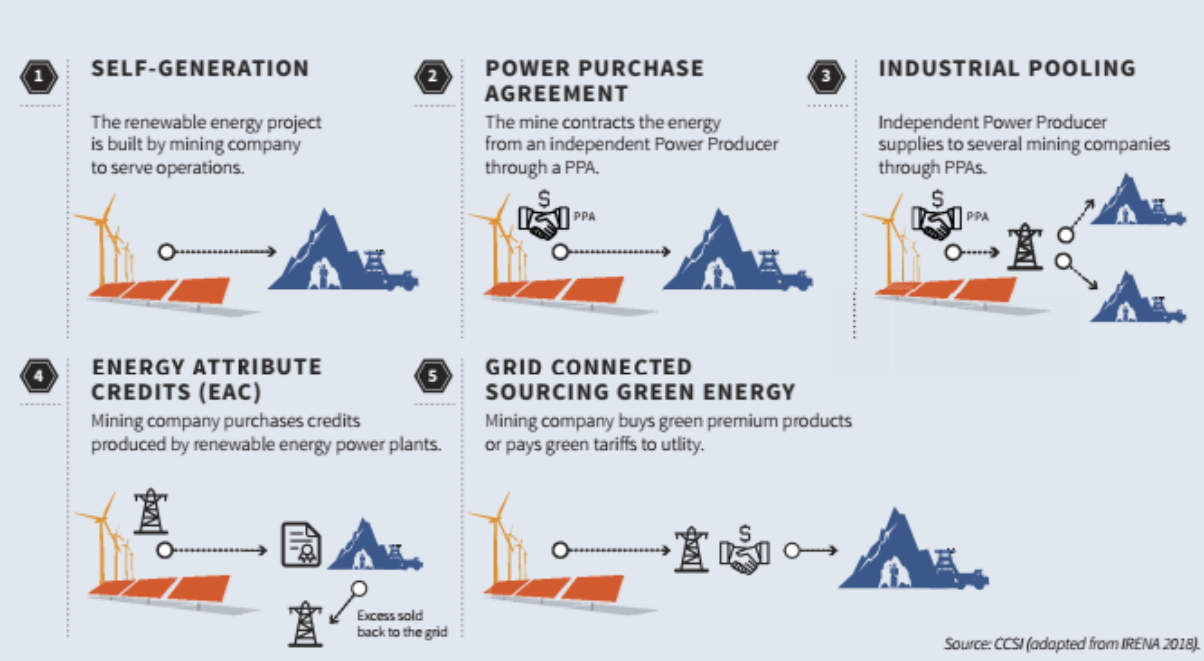


Figure 2. 4: Mostly used commercial arrangements in mining for renewables (Columbia Center on Sustainable Investment, 2018)

## 2.2 Concentrated Solar Power (CSP)

### 2.2.1 Technology Overview

The cumulative installed CSP plants around the globe in 2019 was 6.3GW (IRENA, 2020). Compared to other renewable energy systems, this number is in its infancy. The technology however is expected to grow to the point of supplying 25% of global electricity in 2050 (Islam et al, 2018). The ability to provide dispatchable power on demand and firm capacity coupled with decrease in generation costs, are some of the reasons expected to drive the uptake of CSP systems (Islam et al, 2018).

CSP systems function by concentrating the sun's rays using lenses or mirrors to produce heat energy (IRENA, 2012). The produced heat is then transferred to a Heat Transfer Fluid (HTF) which will be used to drive the steam cycle to produce electrical energy. Thermal energy storage can be integrated to the system enabling the CSP system to operate continuously even during the night or on a cloudy day. Generally, CSP plants consists of solar concentrators, solar receivers, steam turbines, and generators (Islam et al, 2018). Figure 2.5 below shows the main parts and components of CSP:

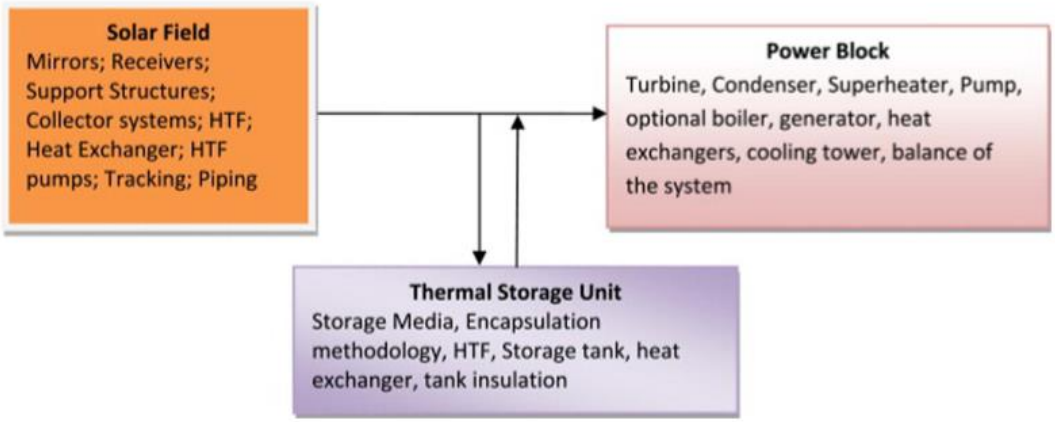


Figure 2. 5: Main parts and components of CSP plant (Islam et al, 2018)

### 2.2.2 Types of CSP plants

CSP plants can be categorised based on how they focus the sun rays (IRENA, 2020). The solar concentrators can focus the solar rays either through line focussing or point focussing as shown on the figure 2.6 below:

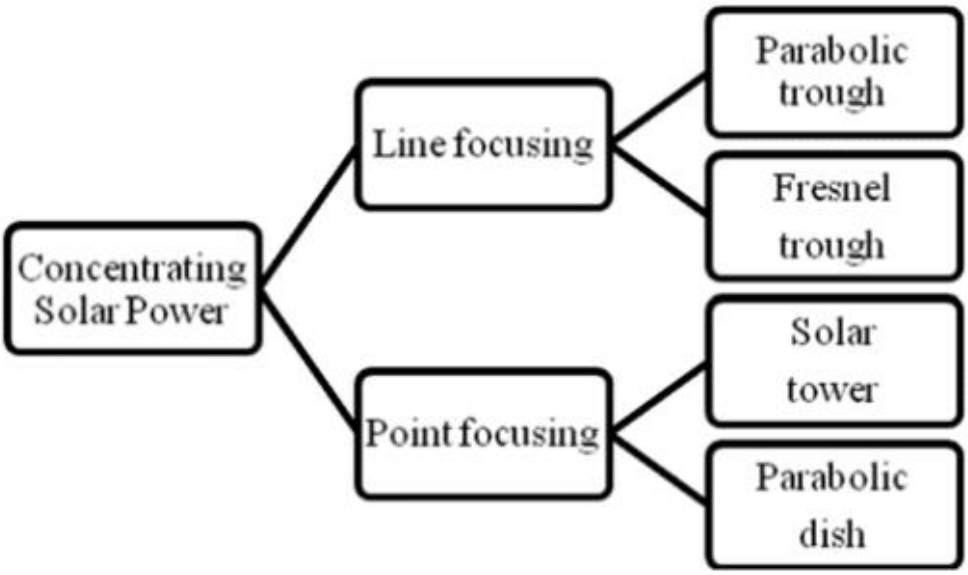


Figure 2. 6: Types of CSP technology (Gharbi et al, 2011)

The figure 2.7 below shows the installed ratios, by 2018, of the CSP technologies together with the pictorial view of each of the systems:

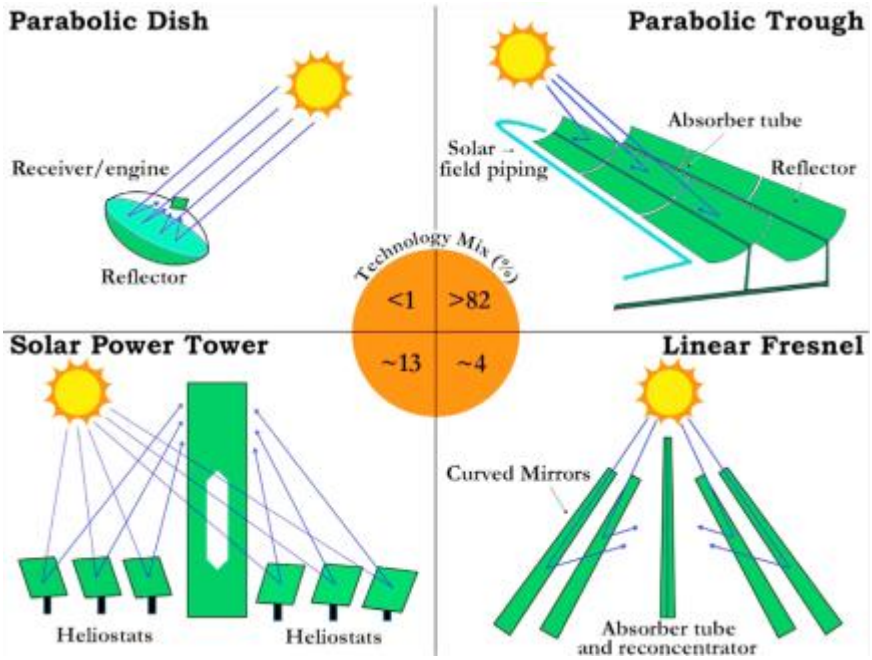


Figure 2. 7: CSP technologies with their respective installed ratios (Islam et al, 2018)

### 2.2.2.1 Parabolic Trough Collector (PTC)

The PTC CSP system is the most widely used technology with the first plant have been developed in Egypt in 1912 (Islam et al,2018). Currently most PTC plants are found in United States of America (USA) and Spain. In 2018, there were 77 PTC plants in commercial operation – 39 in Spain, 25 in USA, 3 in India, 2 in Morocco, 2 in Italy, 2 in South Africa, 1 in Canada, 1 in Egypt, 1 in United Arab Emirates and 1 in Thailand (Islam et al, 2018).

In a PTC system, U-shaped mirrors are used to reflect solar radiation onto a receiver. The mirrors will be in a collector field placed in parallel to each other aligned in a north-south axis (IRENA, 2012). The tracking mechanism will then be employed to track the sun from East to West to maximise energy collection. The receiver is made up of an absorber tube – usually a metal tube – inside an evacuated glass envelop. This stainless-steel tube is usually painted with a coating that absorbs short wave irradiation well but emits very little long wave irradiation to help reduce heat loss (IRENA, 2012).

The absorber tubes are filled by heat transfer fluid which is circulated to collect the solar energy from the receiver and transfer it to the steam generator and/or heat storage system. The fluid could be molten salts or synthetic oil or any other fluid that holds heat well (Islam et al, 2018). The position of the absorption tube in the focal point of the trough and the absorption coefficient of the tube are the two most important design parameters needed for efficient heating of the transfer fluid (Islam et al, 2012). The temperature of the working fluid will mainly depend on solar intensity, fluid flow rate and concentration ratio. Synthetic oils can reach an upper limit temperature of 400$^{o}$C (IRENA, 2012) while molten salts can reach 550$^{o}$C (Islam et al, 2018).

When the trough system is coupled directly to the steam turbine, without thermal storage, the system is called direct steam generation (Islam et al, 2018). The hot working fluid heats the water through the heat exchanger turning it into steam used to drive a convectional Rankine cycle. After the heat transfer, the working fluid is recycled again by pumping it to the receiver to collect heat energy. The typical solar to electrical energy efficiency of this system is 15% (Islam et al, 2018). The working fluid can also be stored and used at a latter stage when there is no sunlight. The most used design is the two-tank molten salt storage system shown in the figure 2.8 below:

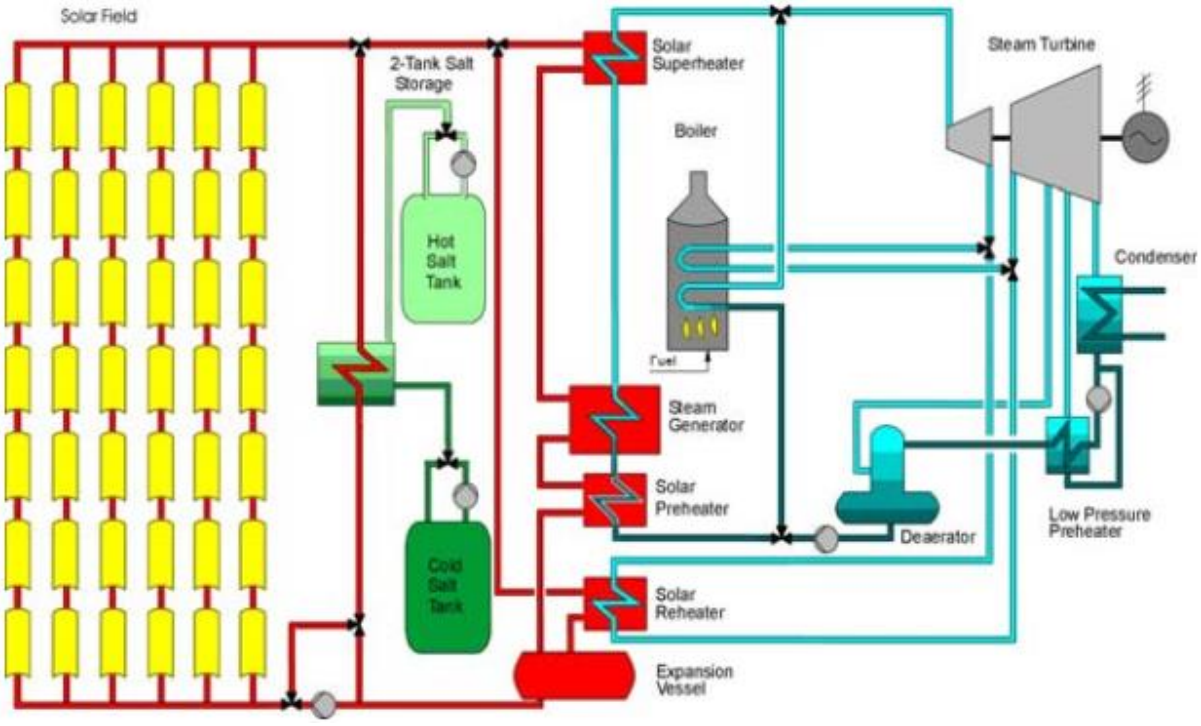


Figure 2. 8: Typical design of a two-tank molten salt storage system for PTC (Kuravi et al, 2013)

### 2.2.2.2 Linear Fresnel Reflector (LFR)

Linear Fresnel reflector is a linear focusing CSP technology, like PTC, but much less developed in comparison to PTC (IRENA, 2020). In 2018, there were only 7 operational LFR-CSP plants (Islam et al, 2018). The highest installed capacity of this technology is in India with a capacity of 125MW with designed generation capacity of 280GWh/year (Islam et al, 2018).

LFR-CSP plants consists of an array of linear mirror strips that concentrate sun's rays to a receiver placed at height above them (IRENA, 2012). Figure 2.9 below show the schematic of LFR-CSP plant and a typical plant in Spain with a capacity of 1.4MW.

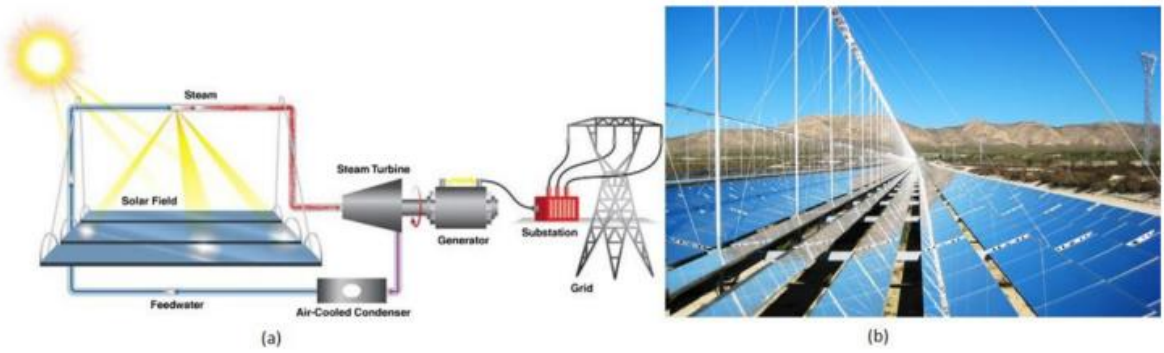


Figure 2. 9: (a) Schematic diagram of LFR-CSP plant and (b)1.4 MW Power Plant at Calasparra, Spain (Islam et al, 2018)

The system consists of reflectors, receivers, steam turbine, generator, and tracking system. During the day, the reflectors are directed towards the sun and the solar irradiation is reflected towards the receiver. The receiver is shaped like long cylinders containing tubes filled with water (Islam et al, 2018). The solar energy will cause the water to evaporate under pressure and this steam will be used in Rankine cycle to produce electricity. The solar to electric efficiency is estimated to be 8-10% (Islam et al, 2018).

The advantages of LFR over parabolic trough systems are (IRENA, 2012):

- The glass mirrors used are cheaper
- The support structure is lighter – less steel and concrete required
- There is better structure stability due to smaller wind loads on LFR. This also reduce mirror/glass breakages
- LFR have higher mirror surface per receiver. This is important since the receiver is the most expensive component in both technologies

However, due to the geometric orientation of the LFR, the optical efficiency of LFR is lower than that of PTC solar field (IRENA, 2012). There are higher cosine losses in the morning leading to lower direct solar irradiation on the cumulated mirror aperture when compared to PTC (IRENA, 2012).

### 2.2.2.3 Solar Power Tower (SPT)

The most widely developed focal point CSP technology is the solar power tower (IRENA, 2020). As of 2018, there were 13 operational SPT-CSP plants with a total capacity of around 618MW (Islam et al, 2018). The largest SPT-CSP plant currently is Ivanpah Solar Electric

generation located in USA with a design capacity of 392MW. It covers a land area of 3500 acres with energy generation capacity of about 1079GWh/year (Islam et al, 2018).

In a solar power tower, ground-based field of mirrors are used to focus direct solar irradiation onto a receiver located at the top of a central tower (IRENA, 2012). At the receiver, the directed light is captured and converted into heat energy. The receiver is usually made up of metal or ceramics which are stable at high temperatures (Islam et al, 2018). The energy will be transferred to the working fluid which will in-turn drive the Rankine cycle. Molten salt, water/steam or air can be used as working fluid. The upper working temperature of the working fluid ranges from 250-1000$^{o}$C depending on the receiver design and heat transfer fluid (molten salts can reach up to 600$^{o}$C) (Islam et al, 2018).

The solar field consists of mirrors called heliostats arranged in a circle or semi-circle around the central tower (IRENA, 2012). Each heliostat is programmed to track the sun, using two axis tracker, to direct as much solar irradiation to the receiver at the top of the tower (IRENA, 2012). The figure 2.10 below shows the typical schematic of SPT-CSP plant:

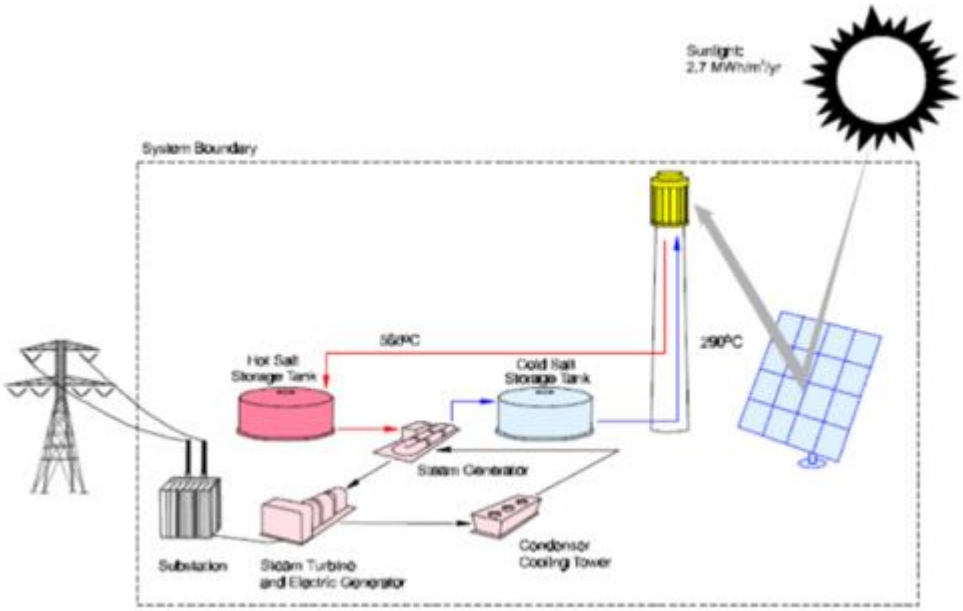


Figure 2. 10: Typical molten salt driven SPT-CSP plant

As seen on figure 2.10 above, the system consists of thermal storage just like the parabolic-trough system. However, SPT have a higher solar to electric efficiency ranging from 20 to 30% (Islam et al, 2018). Solar towers achieve higher concentration factors (ratio between sunlight collected area and solar receiver where it is directed) which means higher potential of achieving high operating temperatures (IRENA, 2012). This helps increase the steam cycle efficiency, reducing the cost of thermal energy storage, reducing the cost of generation and result in higher capacity factor. Unlike other CSP plants, SPT require large amounts of water and the largest development land (IRENA, 2012).

### 2.2.2.4 Solar Parabolic Dish

Currently there is only one commercial operational SPD plant located at Tooele Army Deport in Utah, USA. The design capacity is 1.5MW consisting of 429 solar dishes with a Stirling engine. The plant supply 30% of the electrical load requirements at Tooele US army facility (Islam et al, 2018).

A parabolic dish shaped point focus concentrator is used to reflect solar irradiation onto a receiver at the focal point. The system requires two axis tracking and this help generate high concentration ratio (IRENA, 2012). The working fluid upper limit temperature ranges from 700 to 750$^{o}$C at 200 bars (Islam et al, 2018). A Stirling engine or micro turbine is placed at the focal point to drive an electrical generator (Islam et al, 2018). A typical arrangement of SPD-CSP system is shown in figure 2.11 below:

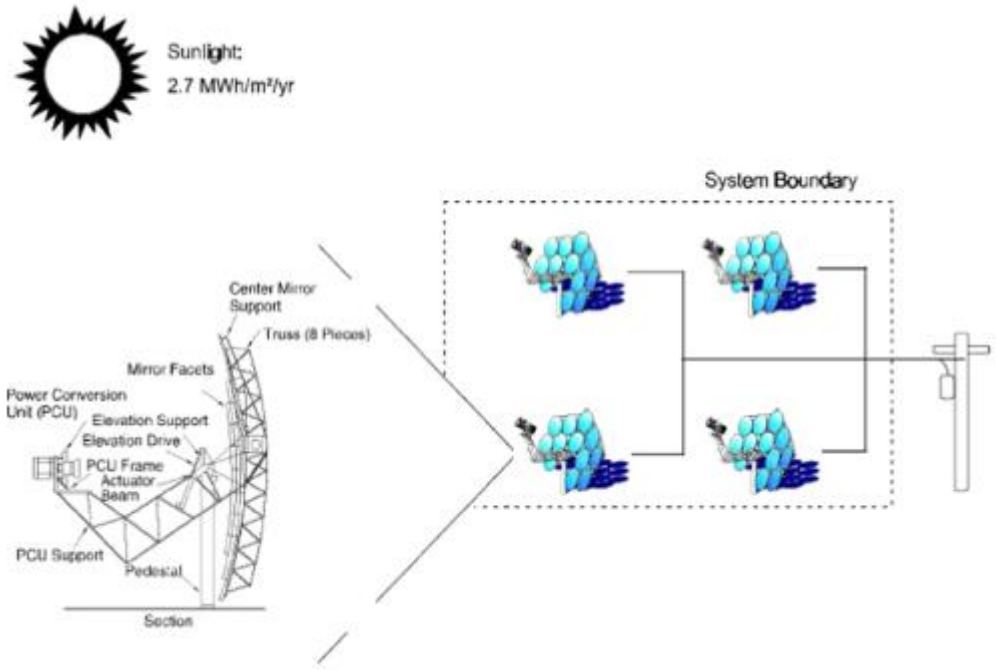


Figure 2. 11: Typical arrangement of SPD-CSP plant (Islam et al, 2018)

The diameters of the parabolic dishes range from 5m to 10m with surface area ranging from 40m$^2$ to 120m$^2$ (Islam et al, 2018). The dish should be constructed in a way to achieve high solar reflectance (typical values of 90 – 94%). There are usually constructed with silver or aluminium, with a thickness of 1µm, coated with plastic or glass. Typical generation capacity of a single dish ranges from 0.01 - 0.5MW (Islam et al, 2018).

SPD systems with Stirling engine have efficiency that ranges between 25 – 30% (Islam et al, 2018). The curved mirrors always point to the sun unlike other CSP technologies which are affected by cosine losses – reduced projected area. Another advantage of SPD system over other CSP systems is that it does not need a level ground for development (IRENA, 2012). The major characteristics and comparison of the 4 CSP technologies is given in the table in Appendix A.

### 2.2.3 CSP System design

#### 2.2.3.1 Efficiency

The generalised system efficiency of a CSP plant can be written as (Cirocco et al, 2014):

$$\eta_{system} = \eta_{optical}\, x\, \eta_{receiver}\, x\, \eta_{transport}\, x\, \eta_{storage}\, x\, \eta_{conversion} x\, \eta_{electrical}$$

**Optical efficiency**

This comprises of all the losses of the concentrator up to but not including the receiver. In the case of solar power tower, these losses include cosine losses, atmosphere attenuation, spillage losses, shading and blockage losses and mirror reflectivity

**Cosine efficiency**

For maximum energy interception by a heliostat, the frame thereof should be normal to the sun's rays (Arrif et al, 2018). Any deviation to this position will cause a decrease in the intercepted energy which is proportional to the cosine angle (Arrif et al, 2018).

**Atmospheric attenuation**

This is the scatter of reflected radiation as it moves from the heliostat to the receiver. This loss is dependent on distance between the receiver and the heliostat (Arrif et al, 2018).

**Spillage loss**

A fraction of reflected radiation loses its path and do not hit the receiver. This is mainly caused by tracking accuracy and mirror quality (Eddhibi et al, 2015)

**Blocking and shading loss**

Blocking refers to when the heliostat behind its neighbour cannot reflect its whole surface to the receiver. Shading is similar to blocking principle expect it refers to incident ray (Arrif et al, 2018).

**Mirror reflectivity**

This the quality of the reflective surface. It depends on cleanliness and degradation of the mirror (Eddhibi et al, 2015).

**Receiver efficiency**

This includes any losses associated with the receiver which include thermal losses (radiation and convection from the receiver) and absorptivity (reflection of solar radiation from the receiver surface) (Cirocco et al, 2014).

**Transport efficiency**

This refers to the efficiency of the heat transfer fluid and it also includes losses from heat exchangers (Cirocco et al, 2014).

**Thermal storage efficiency**

This captures the charging and discharging efficiency of thermal energy storage (Cirocco et al, 2014).

**Conversion efficiency**

This the heat to electrical efficiency which is theoretically limited to the Carnot efficiency of the Rankine cycle (Cirocco et al, 2014).

**Electrical efficiency**

Any other losses like transformer losses, copper losses ($I^2R$) in the conductors (Cirocco et al, 2014).

### 2.2.3.2 Parameter sizing

Solar field size, solar multiple and thermal storage are important parameters to consider when designing CSP plant (IRENA, 2012). Thermal energy storage increases the costs but allows the system to attain dispatchable generation and higher capacity factors. The increase in cost is due to thermal system investment and increase in solar field size to cater for both plant operation and storage. There is a trade-off between the incremental costs of the increased solar field size and storage system against the anticipated revenue from increased production and ability to dispatch power (IRENA, 2012).

Solar multiple is also important in plant optimisation. This is defined as the actual size of the solar field relative to what is required to meet the rated electrical capacity at the design point (IRENA, 2012). To ascertain that the power block is effectively being utilised, the solar multiple value should be greater than 1 with typical value of 1.3 being used in industry (IRENA, 2012). The solar multiple increase as the amount required for storage increases. The figure below 2.12 shows the relationship between capacity factor and thermal storage for different solar multiple at a good solar resource:

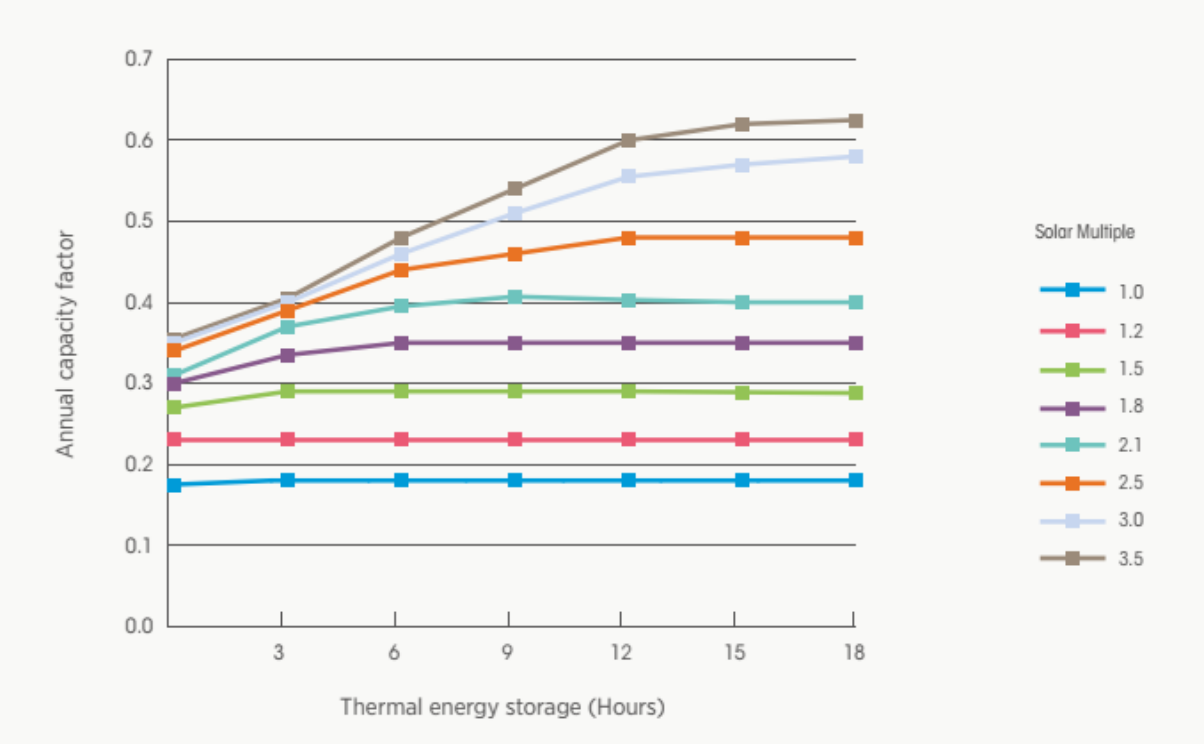


Figure 2. 12: Relationship between capacity factor, thermal storage hours and solar multiple of a typical 100MW PTC-CSP plant (IRENA, 2012)

Finding the optimal design parameters is a challenge given that the goal is to minimise the levelized cost of energy. There is need to strike the right balance as a smaller than optimal solar size will under-utilize the thermal storage and designed power block. On the other hand,

a bigger than optimal solar field would increase the costs but with no guarantee of financial gain (IRENA, 2020).

The overall cost of thermal storage has decreased due to decrease in cost of thermal energy storage investment coupled with increased operating temperatures (IRENA, 2020). This increased the optimal level at which storage can minimise localised cost of energy at a given location. For a given DNI level and fixed plant configuration, a higher heat transfer fluid temperature allows a bigger difference in temperatures between the hot and cold storage tanks. This means greater energy can be extracted for a given physical storage size. In essence, a smaller (hence cheaper) storage medium volume is now required to achieve a given number of storage hours (IRENA, 2012).

### 2.2.3.3 CSP capacity factor

For a given location and technology, the capacity factor is largely depended on the quality of the solar resource along with the configuration of the technology (IRENA, 2020). The addition of thermal storage increases the capacity factor up to a certain point, given there are diminishing marginal returns. The figure 2.13 below shows the trend of capacity factor for different technologies and storage capabilities.


Figure 2. 13: Capacity factor trends for different configurations of CSP plants (IRENA, 2020)

### 2.2.3.4 Localised Cost of Energy (LCOE)

The International Renewable Energy Agency (IRENA) cost database shows that the weighted average for LCOE is on a downward trend from USD 0.346 kWh in 2010 to USD 0.182 kWh in 2019 as shown in figure 2.14 below:

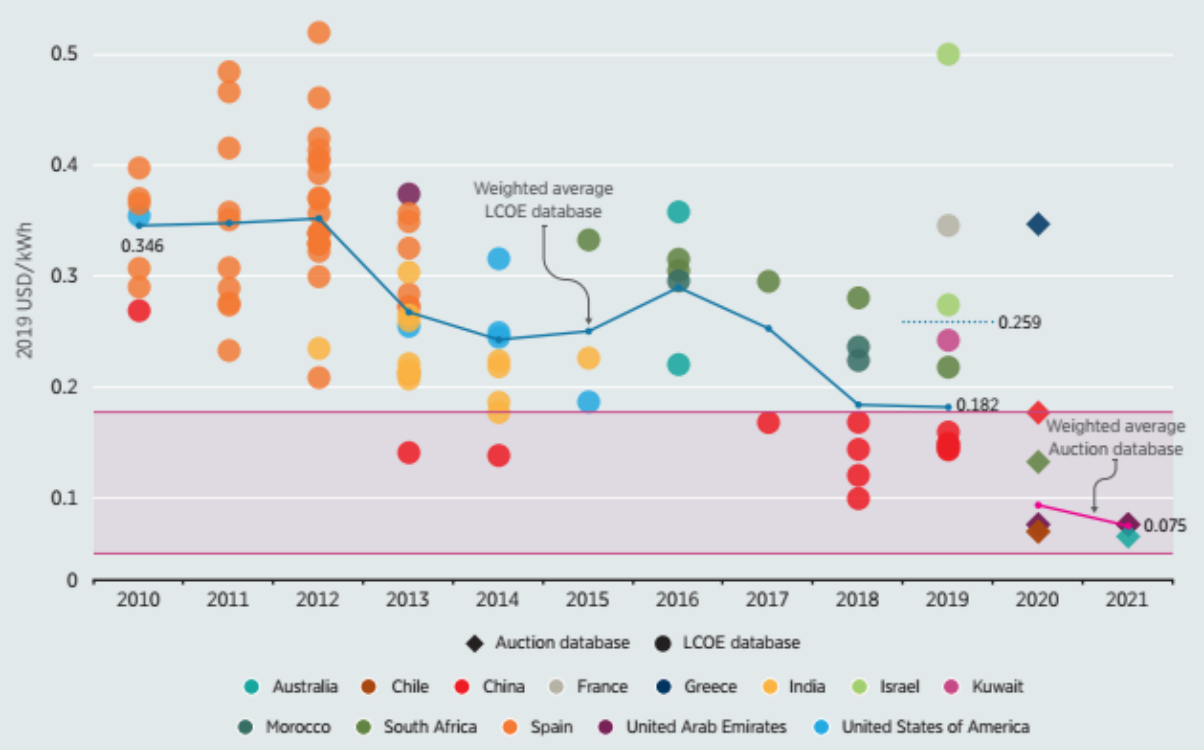


Figure 2. 14: CSP LCOE trend (IRENA, 2020)

The downward trend can be attributed to several reasons including but not limited to projects moving to areas with higher DNI, projects having higher storage capacity (both increase the capacity factor) and reduced cost of thermal storage system (IRENA, 2020). The important parameters when determining the LCOE of CSP plants are (IRENA, 2012):

- Initial investment cost – site development, components and system cost, assembly, grid connection
- Plant capacity factor and efficiency
- Operations and maintenance cost
- Cost of capital and economy life

The amount of thermal energy storage and size of solar multiple, together with the location DNI are important parameters to consider when reducing the LCOE (IRENA, 2012). The figure 2.15 below shows the variation of LCOE in response to changes in solar multiple and thermal energy storage:

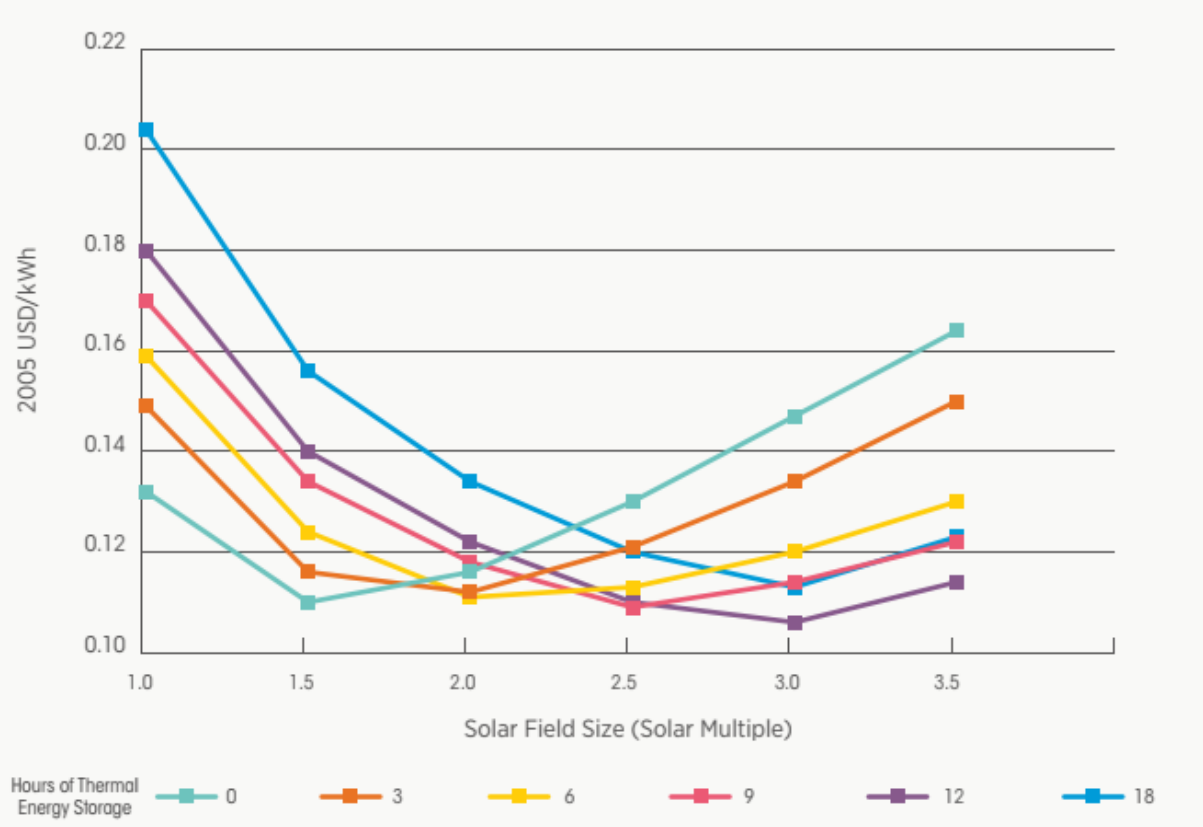


Figure 2. 15: Effect of varying solar multiple and hours of thermal storage on LCOE (IRENA, 2012)

## 2.3 Photovoltaic (PV) Plant

### 2.3.1 PV Plant Overview

By the year 2019, the cumulative installed solar PV System was over 580GW worldwide and this is a 14-fold increase in capacity since 2010 (IRENA, 2020). One of the reasons for this growth is due to decrease in the solar PV module costs. This has been attributed to more efficient manufacturing processes and high efficiency gain in the modules. Higher efficiency means a smaller area is required per unit watt hence reducing cost per watt of the module together with that of balance of system (racking and mounting structures, cable, etc) (IRENA, 2020).

The basic building block of a photovoltaic plant system consist of solar arrays, mounting structures, inverters, and transformers (in case of grid connected systems) as shown in the figure 2.16 below:

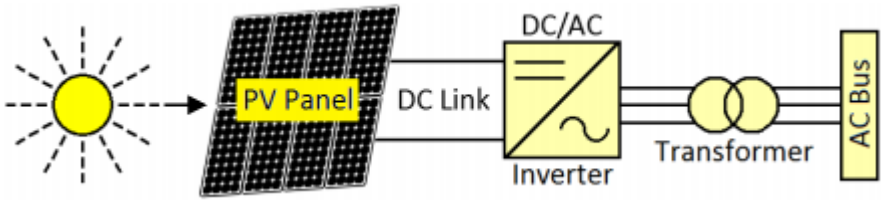


Figure 2. 16: A basic PV system arrangement (Vidyanandan, 2017)

### 2.3.1.1 Solar PV modules

A PV module consist of individual solar cells connected in series. A solar cell is a semiconductor responsible for converting solar irradiation into electrical energy (Vidyanandan, 2017). Commonly used PV cells can be classified as silicon wafers or thin-films technologies. These are further divided according to the long-range structure of the semiconductor material – monocrystalline, polycrystalline, and amorphous material (International Finance Corporation, 2015). In 2017, crystalline modules represent about 85% of the market share due to reduced manufacturing cost and maturity of the technology (Vidyanandan, 2017). Appendix B shows the most used technologies with their characteristics.

### 2.3.1.2 Mounting structure

Mounting structures provides structural support and protection, and make sure modules are oriented in the right direction. The structures can be classified as fixed or tracking:

- Fixed mounting – this maintains the modules at a fixed tilt angle and fixed angle of orientation (azimuth). Optimum tilt angle is estimated to be equal to the latitude while modules in a northern hemisphere should be geographical south facing and those in south hemisphere should be geographical north facing (Fouad et al, 2017).
- Single axis tracker – the trackers either alters the tilt angle or the azimuth angle. Tilt angle trackers follow the sun from east to west about the north-south axis. It might also have backtracking to avoid interrow shading. Azimuth tracking rotates in a horizontal plane altering the orientation angle (Fouad et al, 2017).
- Dual axis tracking – altering both the tilt angle (from east to west) and the orientation angle (catering for seasonal variations). The figure 2.17 below shows the orientation of the three systems. (Fouad et al, 2017)

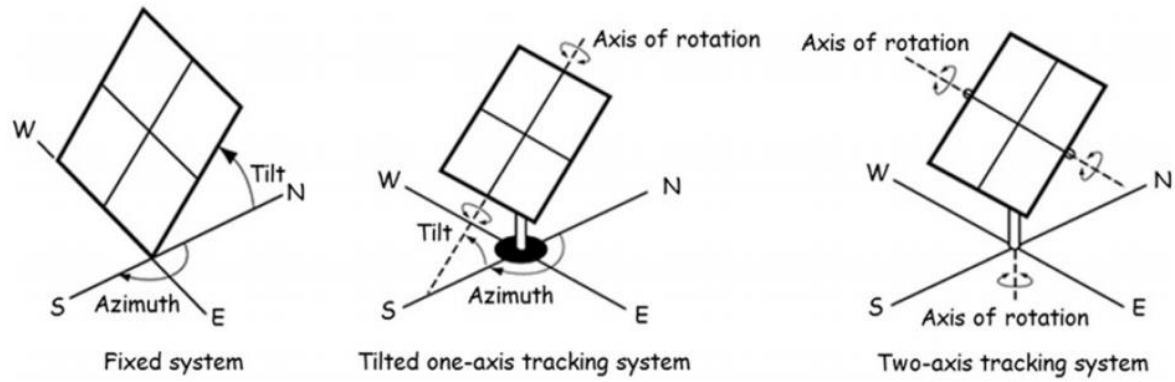


Figure 2. 17: Fixed, single, and double axis tracking systems (Fouad et al, 2017)

Single axis trackers can improve the yield by a range of 15 – 30% while dual axis trackers can increase the yield up to 45% (Fouad et al, 2017). However, trackers increase the capital cost of installation and maintenance cost due to existence of moving parts.

### 2.3.1.3 Inverters

These are solid state electronic devises responsible to convert DC electricity from the PV modules into AC electricity. They also perform the following functions in a solar power plant (International Finance Corporation, 2015):

- Grid code compliance in a grid connected system (like adhering to voltage limits)
- Performance monitoring and data logging
- Protection from electrical faults and plant isolation and sectionalisation
- Optimising output through maximum power point tracking

There are basically two orientation in which inverters can be configured in a solar power plant as shown in the figure 2.18 below:

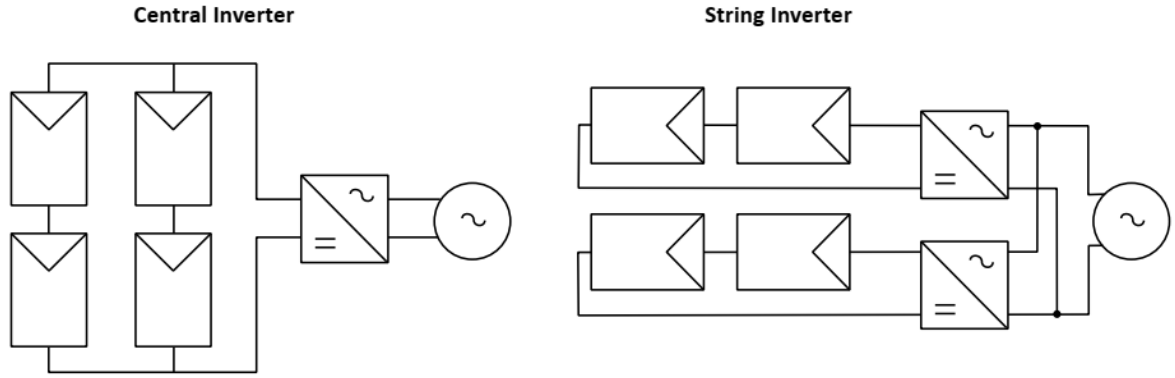


Figure 2. 18: Inverter configurations (International Finance Corporation, 2015)

- Central inverters – the main advantage of central inverters is simplicity in installations and lower cost per watt. However, they reduce the overall plant availability and lower efficiency due to lack of performance optimisation - Maximum Power Point Tracker (MPPT) (International Finance Corporation, 2015)
- String inverters – In contrast, string inverters provide MPPT function hence improved efficiency. They also improve the overall plant availability as it makes it easier to isolate and sectionalise a faulty part. However, string inverters have a higher cost per watt.

Another inverter type configuration that is not popular in utility PV system due to high cost is microinverters (Vidyanandan, 2017). These are connected to each module hence providing effective optimisation than string inverters. Figure 2.19 below shows a typical connection of such a system:

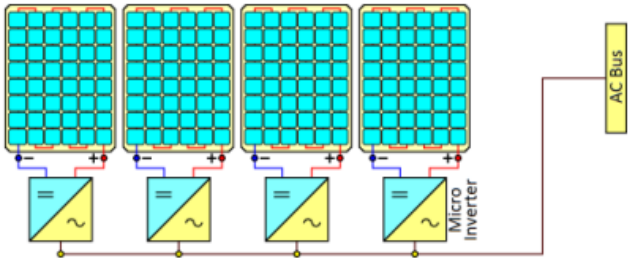


Figure 2. 19: Arrangement of micro-inverters (Vidyanandan, 2017)

### 2.3.2 System efficiency

There are a variety of factors that affect the performance of utility PV plants with some related to the components while others are related to the operating conditions at a given location:

#### (a) Module degradation

The performance of PV modules decreases with time due to mainly effects of module exposure to irradiation, ambient temperature, humidity, and voltage bias effects. Crystalline modules have a higher degradation rate during the first year of exposure to light and then stabilises thereafter. This process is called light induced degradation and varies between 0.5 – 2%. Typical long-term degradation rate of crystalline modules is 0.4% per year (International Finance Corporation, 2015).

Amorphous silicon cells on the other hand undergoes a process called Staebler-Wronski effect. This degradation can cause between 10 - 30% reduced output during the 6 months of exposure to light. The rate is expected to stabilise and continues at a rate between 0.7 – 1% per annum (International Finance Corporation, 2015). Manufactures usually guarantees module performance life of 25 years as shown in figure 2.20 below:

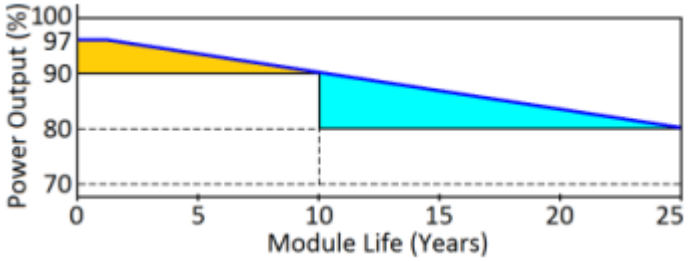


Figure 2. 20: Typical life span of PV modules (Vidyanandan, 2017)

#### (b) Irradiance Levels

The conversion efficiency of PV modules is affected by the level of irradiance falling on the module. Low irradiance relative to standard test conditions (STC) of 1000 W/m$^2$ will reduce the performance of the module (Vidyanandan, 2017).

#### (c) Module temperature

PV modules characteristics are determined at 25$^o$C (Vidyanandan, 2017). An increase in cell temperature increases the current slightly but reduce the voltage significantly leading to reduced power as shown in figure 2.21 below. The opposite occurs when temperature decrease below 25$^o$C – current falls slightly but voltage and power increases. Silicon cells have a typical 0.5% loss in efficiency per degree (Vidyanandan, 2017). The impact of temperature depends on the type of the module however, allowing conducive airflow behind the panels helps to cool them (International Finance Corporation, 2015).

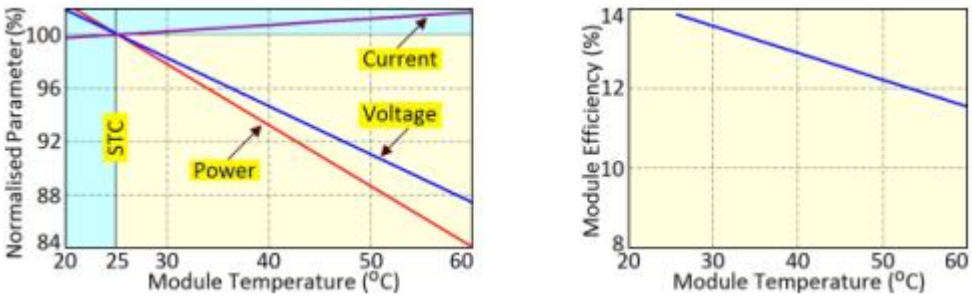


Figure 2. 21: Effect of temperature on solar cell (Vidyanandan, 2017)

**(d) Soiling**

Soiling can reduce the performance of a PV module by a range of 5 – 17% per year depending on location (Vidyanandan, 2017). Accumulation of dust, dirty and other contaminants affect the amount of incidence irradiance that reach the PV module. Contaminants settlement on PV module will depend on weather (rain, snow, humidity, wind), particle properties (size, shape, weight), location (coastal, desert, dusty), surface finish, tilt angle, and operation and maintenance strategy (Vidyanandan, 2017).

**(e) Air pollution**

Air pollution from industries and agriculture can reduce the incident irradiation on PV modules there by affecting the power output (International Finance Corporation, 2015).

**(f) Shading**

These are losses caused by obstruction on PV modules by objects in the vicinity. This can be categorised into far shading, near shading, and mutual shading (International Finance Corporation, 2015). Far shading involve shadow losses due to mountains or buildings on the far horizon. Near shading is usually caused by trees, buildings, and other infrastructure close by. Mutual shading refers to the shading between row modules. Common solutions include due diligence in site selection, optimum row spacing, modelling near shading, and designing modules and strings with bypass diodes (International Finance Corporation, 2015).

**(g) Incident angle**

This is reduced irradiation caused by reflection on PV modules of the incident radiation that is not normal to the surface of the module. This means that the optimal position for PV modules should always be facing the sun. This, however, is not possible due to daily and seasonal variations in the sun's position unless the system utilises tracking systems (Fouad et al, 2017).

**(h) Module mismatch**

This is when modules connected in strings do not present same voltage and current profiles. This usually caused by different properties of modules or different operating conditions (International Finance Corporation, 2015). Average annual loss from module mismatch is typically 2% (Fouad et al,2017).

**(i) Inverter performance**

The conversion efficiency from DC to AC will affect the output power of the PV system. Typical datasheet values of inverter efficiency ranges from 94 – 98% for string inverters (International Finance Corporation, 2015).

**(j) Ohmic losses**

These are power losses ($I^2R$) in power cables (both DC and AC) and transformer which affect the overall efficiency of the PV system (International Finance Corporation, 2015).

### 2.3.3 Parameter sizing

Designing a PV system usually involves finding the right balance between the yield and cost. Most projects value reducing the LCOE hence any optimisation should be analysed to ascertain the economic benefit is larger than the cost of implementing it (International Finance Corporation, 2015).

Typical layout design will involve choosing the configuration, tilt angle, interrow distance and orientation:

- Tilt angle – each location has an optimal tilt angle which lies +/-15$^o$ from the latitude of the given location (Vidyanandan, 2017). However, there is need to take account of the trade-off that exist between the tilt angle and interrow distance (hence capacity density). It is also important to consider seasonal irradiation distribution when choosing the tilt angle. Figure 2.22 below shows the typical relationship between tilt angle and yield:

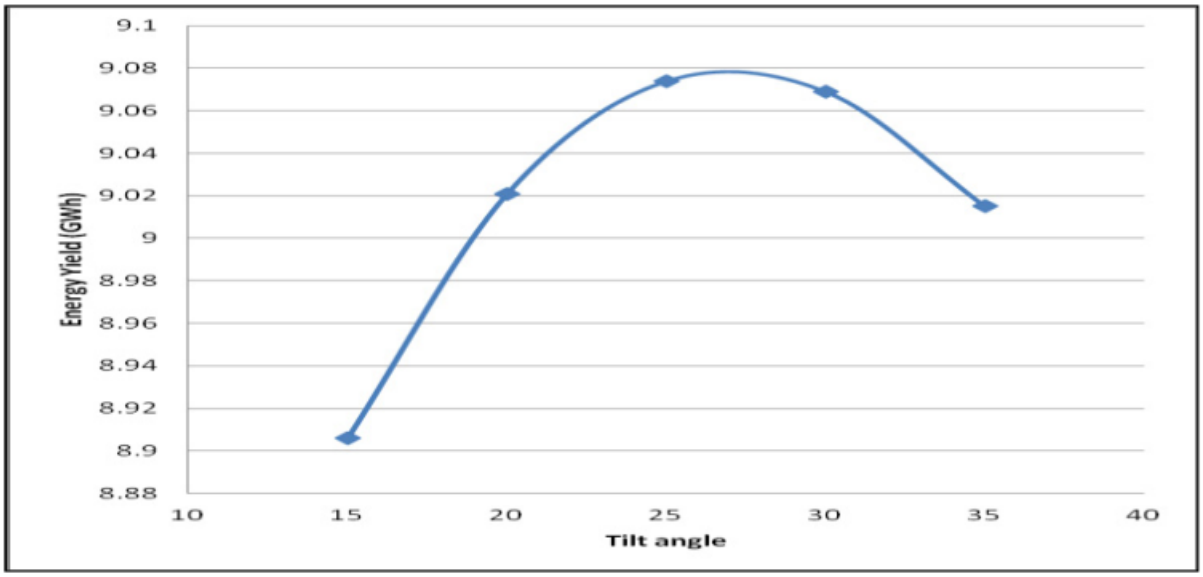


Figure 2. 22: Typical relationship of tilt angle and energy yield (Bhattacharya et al, 2014)

- Orientation – the rule of thumb in designing PV systems is that the modules should face the equator. However, azimuth can be varied to optimise PV output at a certain time – taking for example, a westly facing module has its peak late in the afternoon (International Finance Corporation, 2015).
- Configuration – PV modules can be configured in landscape or in portrait position. PV module configurations are affected differently by shading. Modules in landscape

typically have less electrical shading losses (hence produce more as seen in Figure 2.23 below) since most bypass diodes are connected along the module's length (International Finance Corporation, 2015).

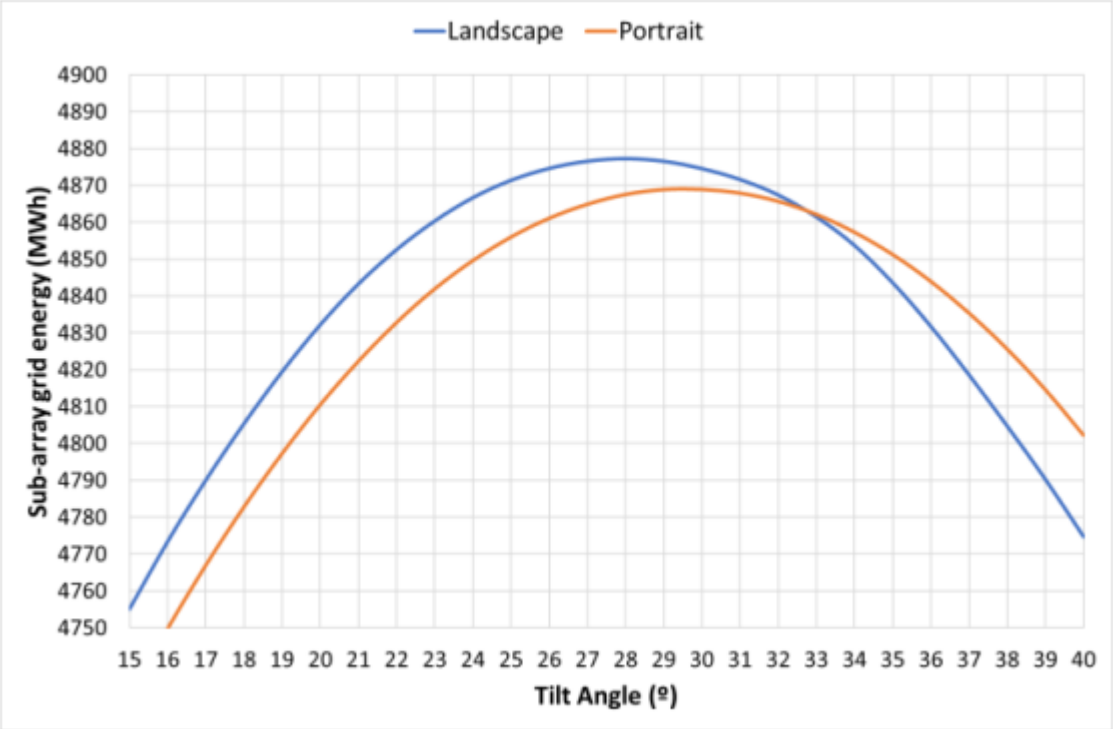


Figure 2. 23: Different module configurations varying with tilt angle (Silver et al, 2020)

- Interrow space – this involves sticking the balance between reducing the interrow shading and the area for development (hence cost). Interrow spacing can be calculated using shadow analysis or the ground cover ratio (International Finance Corporation, 2015). Figure 2.24 below shows the typical impact of varying the pitch (distance between rows) on output energy.

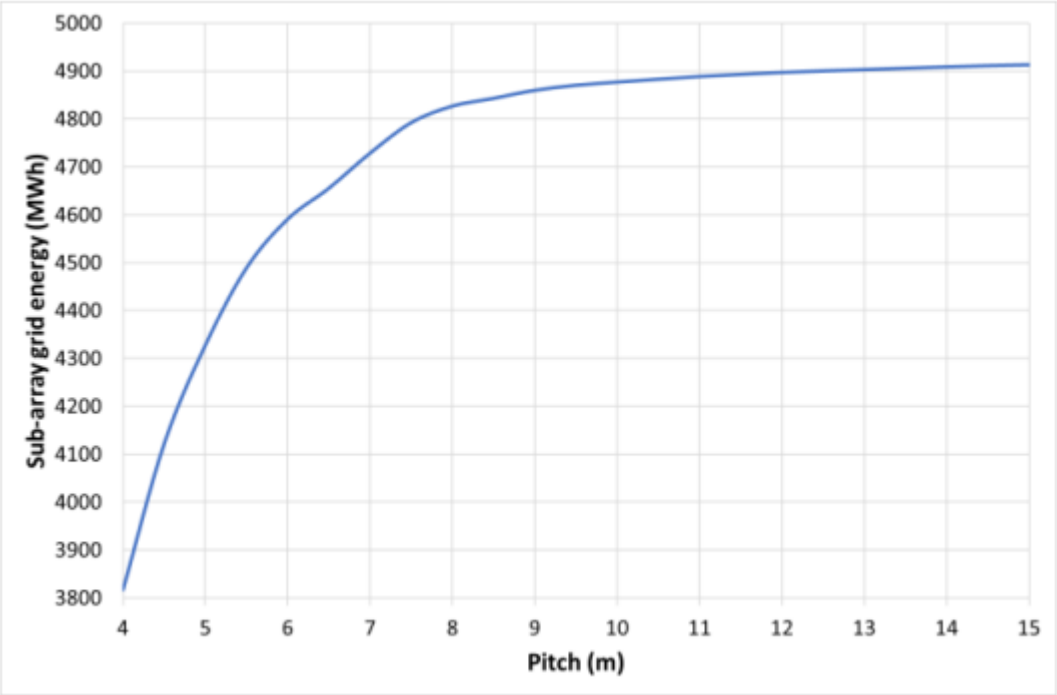


Figure 2. 24: Impact on output energy with varying interrow distance (Silver et al, 2020)

Typical electrical design of the plant will involve PV array design, inverter sizing and cable sizing.

- PV Array design – the system architecture and inverter specifications will determine the number of modules in a string. The maximum number of modules will depend on the maximum allowable string voltage into the inverter. This voltage is the open circuit voltage of the string on a coldest day (-10$^{o}$ used in Europe) (International Finance Corporation, 2015). The maximum number of modules (N) will be determined using the following relationship:

$$V_{oc}(module\ @\ coldest\ operating\ temperature)x\ N < V_{max}(Inverter\ DC)$$

  The minimum number of modules in a string depend on the operating MPPT range of the inverter. If the string voltage drops below the MPPT lower limit, the inverter will underperform with worst case scenario being switching off. The minimum operating voltage on a typical hot day (70$^{o}$C used in Europe) (International Finance Corporation, 2015) is used to calculate the minimum number of modules (n) using the following relationship:

$$V_{mpp}(module\ @\ highest\ module\ operating\ temperature)x\ n > V_{mpp}(\min inverter)$$

- Inverter sizing – the form factor is used to size an inverter. This is the ratio of DC power from solar array to AC power produced by the inverter. Typical industrial values used range between 1.1 – 1.2. A value greater than 1.2 will increase the chances of clipping losses while a value less than 1 means the inverter is undersized (which is not economical) (International Finance Corporation, 2015).
- Cable sizing – generally, cables should be sized according the cable voltage rating, current carrying capacity and maximum allowable voltage drop.

### 2.3.4 PV LCOE

The weighted average of LCOE of PV plants at utility level dropped from USD 0.378/kWh in 2010 to 0.068/kWh in 2019 (IRENA, 2020) as shown in the figure 2.25 below:

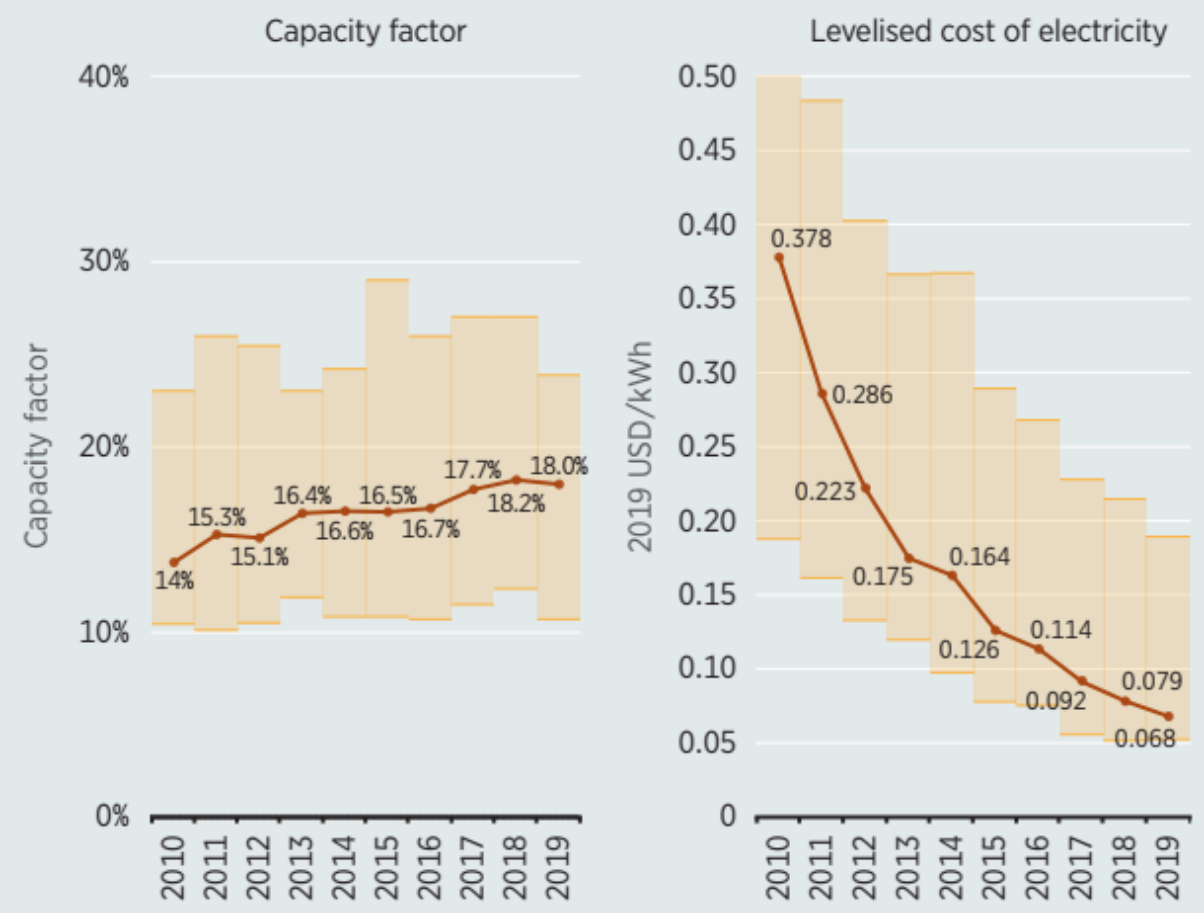


Figure 2. 25: Global weighted average trend for PV capacity factor and LCOE, 2010-2019 (IRENA, 2020)

This decline in trend is attributed to reduced investment cost of PV system, increased capacity factor – as shown in the graph above in figure 2.25 – and falling operation and maintenance cost. The following parameters are important when determining the LCOE of the PV plant (IRENA, 2020):

- Initial investment – land, modules, mounting systems, grid connection, balance of system cost
- Operation and maintenance cost
- Energy produced – efficiency and power factor
- Financial terms

## 2.4 PV + Battery Storage

### 2.4.1 Overview

There is a growing push to take the advantage of declining cost for both PV and Energy storage technologies to implement hybrid PV – Battery storage system (NREL, 2017). The hybrid system has the potential to create a more flexible renewable energy system that can be integrated in a flexible and reliable manner. The increase in flexibility is due to the unique

nature of batteries of being able to quickly absorb, hold, and reinject electricity (IRENA, 2019).

In 2017, the total worldwide stationery battery capacity was 11GWh and this value is expected to increase to 167GWh by the year 2030 (IRENA, 2019). This increase is anticipated due to the decline in the cost of battery storage technologies caused by the growing consumer market, development of Electric Vehicles (including plug-in hybrid Electric Vehicles), and increase in development of distributed renewable energy generation together with development of smart grids (IRENA, 2019).

### 2.4.2 Types and Uses of Batteries

Batteries can be categorised as in-Front of the Meter (FTM) or Behind the Meter (BTM). FTM batteries (sometimes called utility scale batteries) are connected to the distribution or transmission network or in connection with generation asset. BTM batteries are interconnected behind the utility meter of industrial, commercial, and residential customers, primarily aimed to reduce the electricity bill through demand side management (IRENA, 2019).

### FTM Batteries

Utility scale batteries can play a key role in energy transition to renewable energy. From operational point view, battery storage system will facilitate grid services like frequency response and ramp rate control (IRENA, 2019). It will also help in deferring investments in peak generation and grid reinforcements. FTM can be an enabler of renewable energy penetration into the grid by storing excess generation and firm the renewable energy output (IRENA, 2019). Figure 2.26 below shows the summary of services that can be provided by FTM batteries:

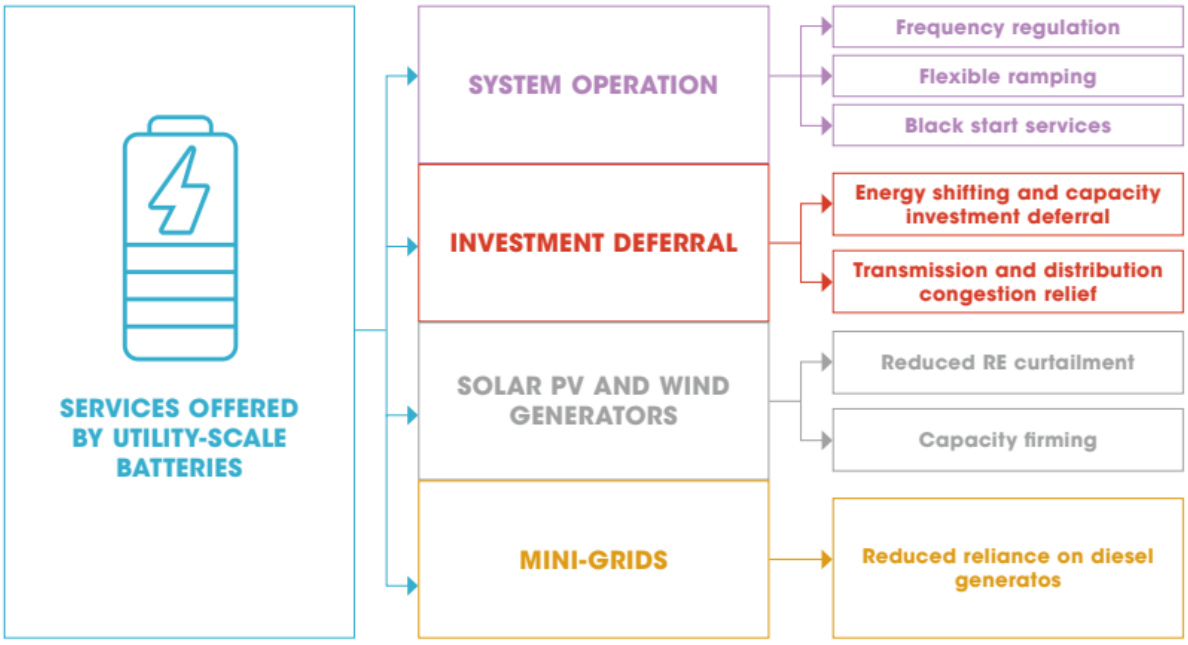


Figure 2. 26: Summary of services provided by FTM batteries (IRENA, 2019)

**BTM batteries**

A BTM battery is installed at the consumer premises to provide energy storage either from the renewable energy system or from the distribution grid when the tariff is low (IRENA, 2019). The stored energy can be used to meet the local load or exported to the grid when the price is high. The major enabler of deploying BTM batteries is to provide back-up power to consumers in case of black outs occurring on the grid hence improving the power system resilience and reliability (IRENA, 2019).

BTM batteries can play a key role in the development of renewable energy technologies. This is done by facilitating integration of local renewable energy by maximising self-consumption and its revenues (IRENA, 2019). In areas where time of use tariffs exist, consumers can reduce the electricity bill by using the energy stored in batteries when the tariff is high maximising the installed renewable energy. Just like the FTM batteries, BTM batteries can be used to provide voltage and frequency support (IRENA, 2019). Figure 2.27 below shows the summary of services offered by BTM batteries:

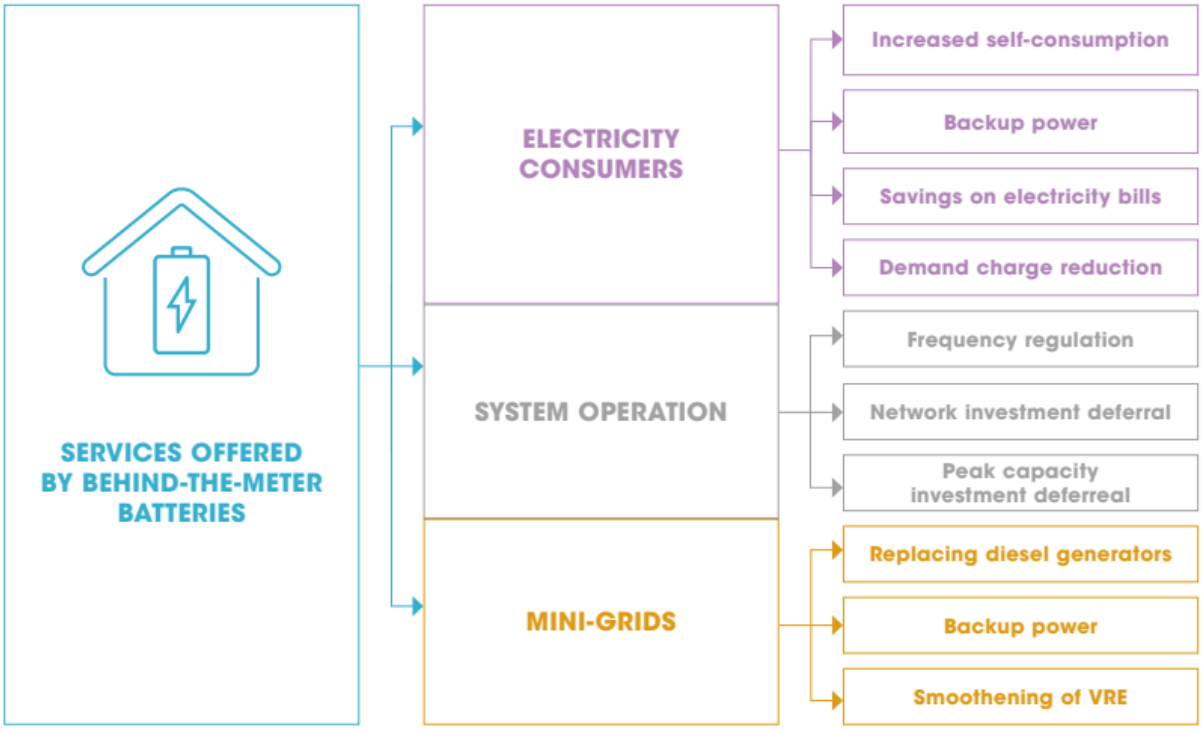


Figure 2. 27: Summary of services offered by BTM batteries (IRENA, 2019)

### 2.4.3 PV + Batteries Configurations

The table 2.4 below shows the typical configurations that currently exist to couple battery systems:

Table 2. 4: Typical coupling for PV + Batteries (NREL, 2017)

| Type of coupling | Point of common coupling | Energy stored |
|---|---|---|
| Independent | - | Grid |
| AC – coupled | Transmission line/feeder | Grid or PV |
| DC – coupled | DC side of inverter | Grid or PV |
| DC – tightly coupled | DC side of inverter | PV |

**Independent coupling**

The figure 2.28 below shows an orientation of an independent PV and battery storage system. With this set-up, there is no physical connection between the PV system and battery system. The battery system responds to the overall grid providing peak capacity, shifting energy from off-peak to on-peak period. The battery can charge with any grid resource that provides low cost energy (like off peak wind, coal or nuclear) and discharge it during periods of peak demand (NREL, 2017).

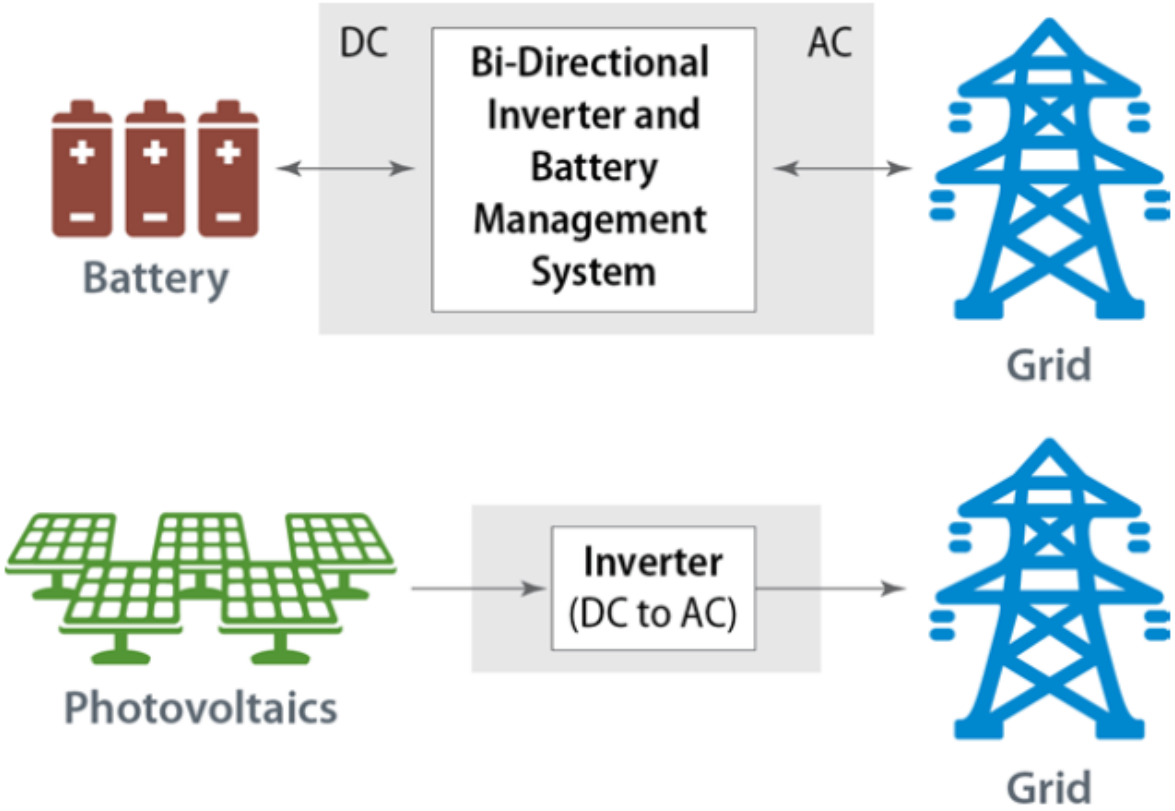


Figure 2. 28: Schematic of independent PV and storage systems (NREL, 2017)

**AC coupled**

The figure 2.29 below shows an AC coupled system in which storage and PV are co-located and sharing the same point of connection to the grid. However, the battery system does not share any components hence can operate independently of the PV system (NREL, 2019).

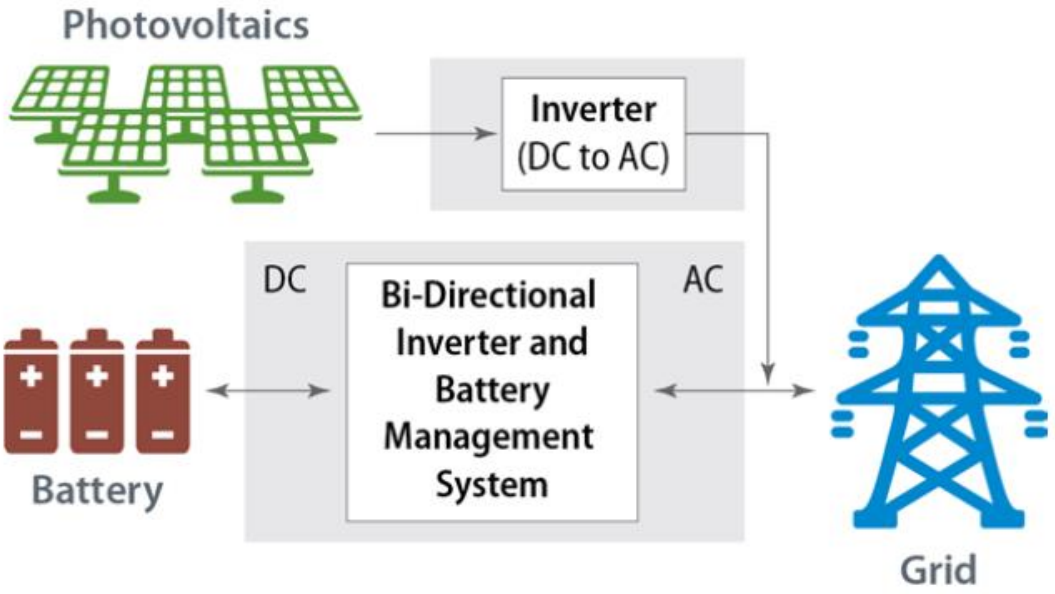


Figure 2. 29: Schematic of AC coupled PV + Battery system (NREL, 2017)

**DC Coupled systems**

The figure 2.30 below shows both dc-coupled and tightly coupled battery systems. The DC coupled systems include a bi-directional meter that enables battery system to be charged by both the grid and PV system (NREL, 2017). The DC tightly coupled system can only be charged by PV system and not from the grid. One advantage of DC coupled systems is that they can store otherwise clipped energy that occurs when the inverter loading ratio exceeds 1 (NREL, 2017).

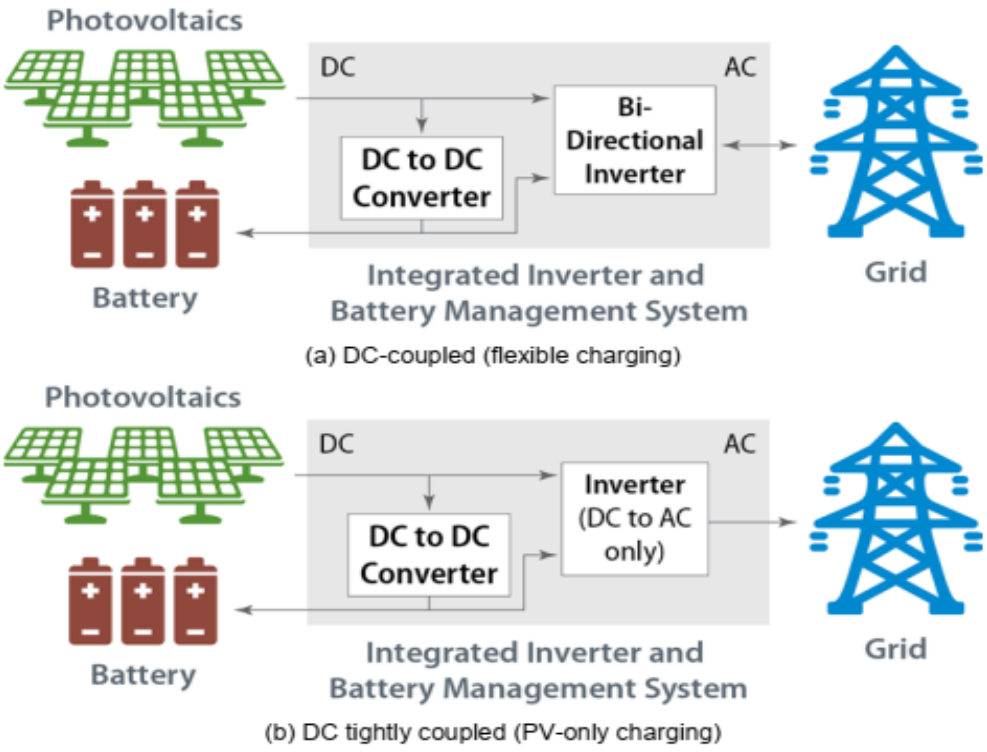


Figure 2. 30: Schematic of DC coupled PV + Battery systems (NREL, 2017)

### 2.4.4 Battery technologies

The mostly used battery technologies for FTM batteries include lithium ion, lead acid and sodium sulphur while lithium ion and lead acid are mostly used for BTM batteries (IRENA, 2019). However, market growth is more in lithium ion technology as it constituted about 90% of large-scale battery storage projects in 2017 (IRENA, 2019).

**Lithium ion batteries**

Lithium ion batteries consists of positive electrode materials made up of lithium compounds capable of reversible intercalation of lithium ions (May J.G. et al, 2018). Negative electrodes are made up of carbon or graphite that can accommodate lithium ions in solid state. Non-aqueous electrolyte is used in lithium ion batteries and is made up of ionisable organic solvents such as propylene carbonate with suitable lithium salts in solution (May J.G. et al, 2018). The cells also include separators which are microporous plastics films which may be coated with ceramic particles to enhance the safety of the cells as shown in the figure 2.31 below:

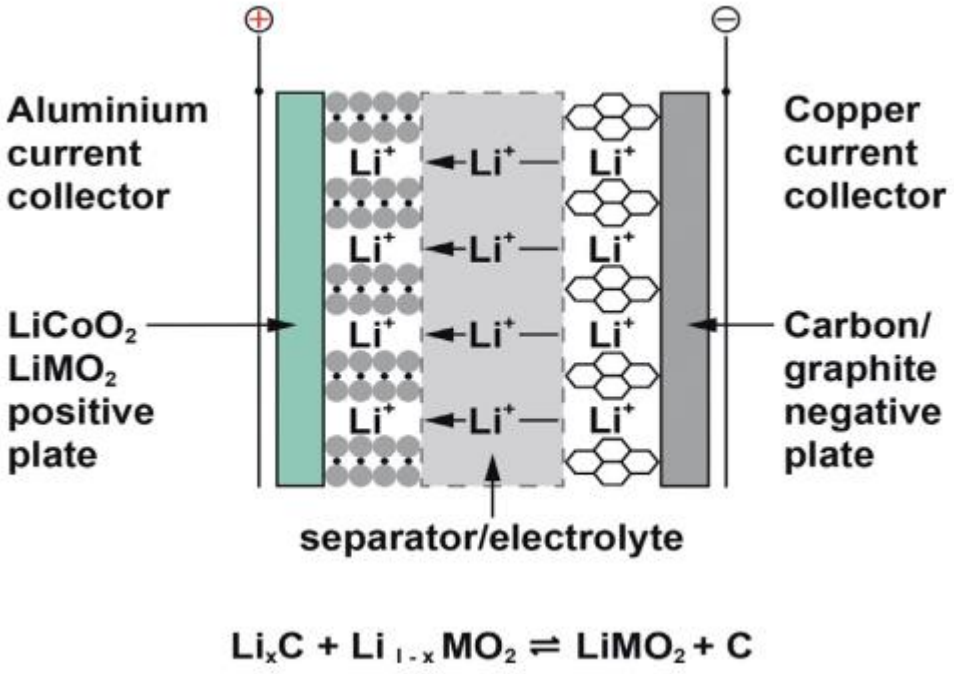


Figure 2. 31: Chemical and principal components of lithium ion battery (May J.G. et al, 2018)

For small scale batteries, lithium cobaltite (LCO) is the most used as the positive electrode material, however, this is too expensive for large scale storage systems. Low cost alternatives are used instead which include nickel, mixed oxides of nickel - cobalt and aluminium (NCA), and cobalt and manganese (NCM). For the anode, the most common material used is graphite or carbon (May J.G. et al, 2018).

Lithium ion cells have a high energy density and organic electrolyte which is flammable hence safety is a key issue (May J.G. et al, 2018). Thermal runaway is a huge challenge hence the materials – cells, batteries, and charging systems – need to be carefully chosen to

reduce the risk. Battery monitoring systems with thermal sensors, voltage and current measurements, and fuses are typically used for safe operation (May J.G et al, 2018).

**Lead acid battery**

Lead-acid cells are constructed from lead alloy grids which mechanically support the positive and negative active materials and act as current collectors (May J.G et al, 2018). The grids are stacked together as positive and negative plates and interleaved with a porous electrically insulating separator as shown in the figure 2.32 below:

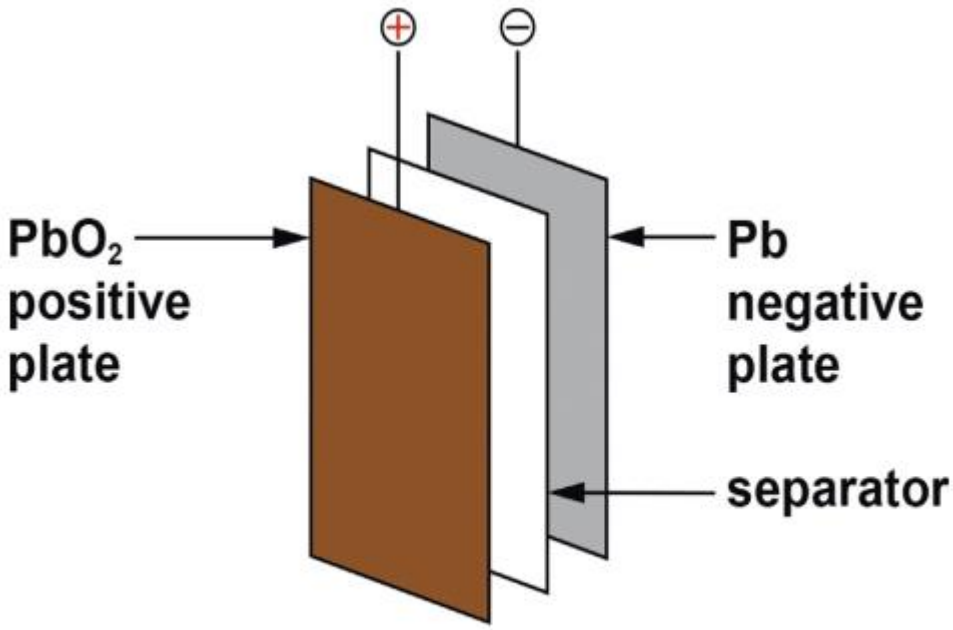


$$Pb + PbO_2 + 2H_2SO_4 \rightleftharpoons 2PbSO_4 + 2H_2O$$

Figure 2. 32: Chemistry and principal components of lead-acid battery (May J.G et al, 2018)

There are two main types of positive plates namely flat pasted plates and tubular plates while negative plates are always flat pasted type. The cells can also be categorised as flooded or valve regulated lead acid (VRLA) type (May J.G et al, 2018). The positive active material is highly porous lead dioxide and the negative material is finely divided lead. The electrolyte comprises of a dilute aqueous sulphuric acid. One operational challenge associated with lead acid batteries is the loss of water due to overcharging. This makes it imperative to control the charging voltage of the battery. For flooded batteries, water loss (hence the need for adding water during operation) can be reduced by correct selection of grid allows and charging parameters (May J.G et al, 2018).

**Sodium Sulphur batteries**

Sodium sulphur batteries consist of molten liquid sodium and sulphur as the electrode materials and operate between 300$^{o}$C and 350$^{o}$C (May J.G. et al, 2018). This is done to maintain electrodes in liquid form and achieve good ionic conductivity in the electrolyte which is a solid ceramic material. The advantages of these batteries over lead acid batteries is

that they have a higher energy density and a longer cycle life. However, safety is an issue in sodium-sulphur batteries with the need for insulation, heat and thermal management which make this type of batteries expensive (May J.G. et al, 2018). The figure 2.33 below shows the chemical and principal components of sulphur batteries.

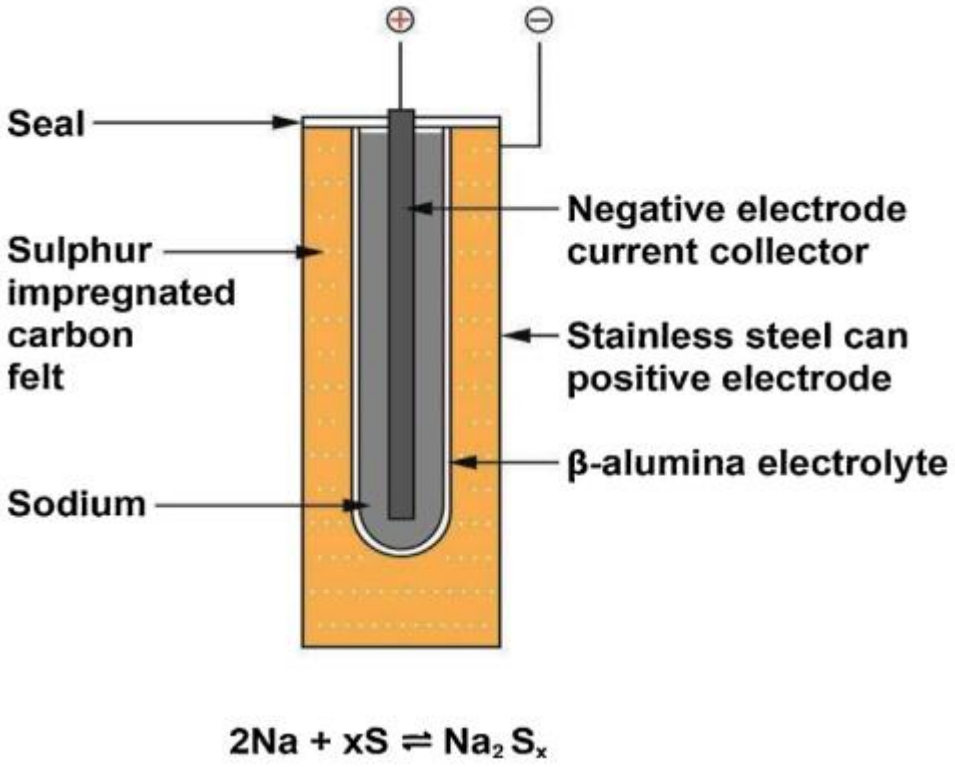


Figure 2. 33: Chemical and principal components of sulphur batteries. (May J.G. et al, 2018)

**Lead acid battery vs Lithium ion battery**

The table 2.5 below shows the summary of key parameters between the two technologies:

Table 2. 5: Summary of key parameters between Lead-acid and Lithium ion (May J.G. et al, 2018)

| Parameter | Lead acid | Lithium ion |
|---|---|---|
| Energy density | 35 – 40Wh/kg | 150 – 180Wh/kg |
| Power density | 250W/kg | 800W/kg |
| High temperature performance | To 40$^{o}$C | To 50$^{o}$C |
| Low temperature performance | To -30$^{o}$C | To -20$^{o}$C |
| Charge acceptance | Good | Better |
| Circle life | 1500 - 5000 | 1000 - 5000 |
| Overall service life | 15 years | 10 – 15 years |
| Reliability | Proven | Needs to be accessed for longer times |
| Sustainability | Excellent | Recovery methods uneconomical |
| Safety | Excellent | Issues to be resolved |

| | | |
|---|---|---|
| Cost (battery system only) | 250/kWh | 350/kWh |

### 2.4.5 PV + Battery system specifications

The energy content (storage hours) and power capability of battery system are the most important parameters in the design of battery storage (Hesse et al, 2017). For systems integrated with PV, the inverter loading ratio (or DC – to - AC ratio) determines the size of the PV plant. Parametric analysis is usually used to determine the right balance between the investment cost, operational cost and the anticipated revenue based on the given load profile and PV generation profile (Hesse et al, 2017).

The capacity factor of PV Battery plant can be increased by increasing the inverter loading ratio – PV plant size relative to the desired output power – as shown in the figure 2.34 below (NREL, 2016). Having very large inverter loading ratio (typical value of +2.4) means higher chances of curtailing excess energy produced. However, having low Inverter Loading Ratio (ILR) also translated to reduced capacity factor of the system as the plant rarely operates at rated output (NREL, 2016).

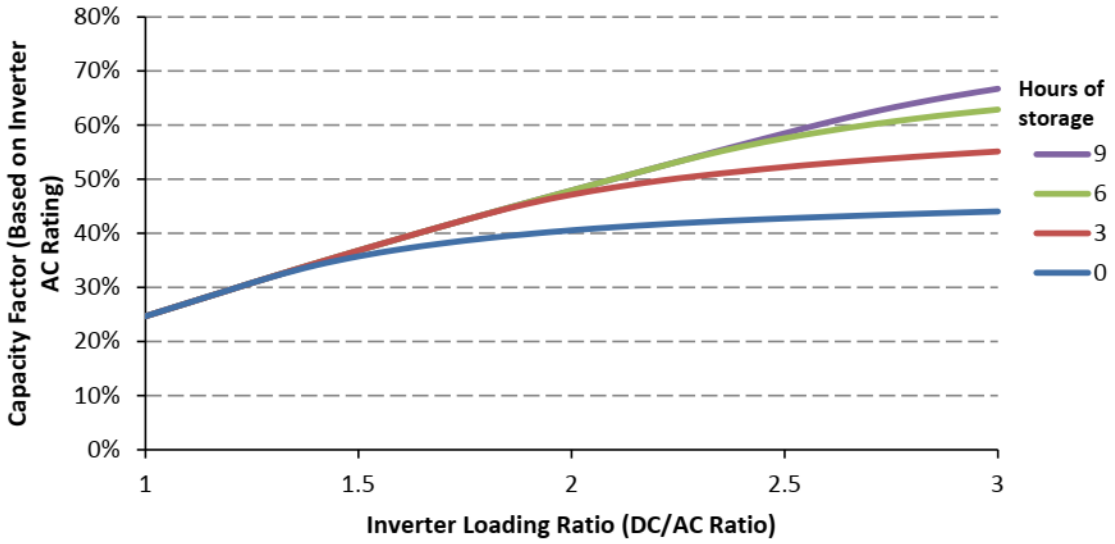


Figure 2. 34: Relationship between capacity factor and ILR with different amount of storage (NREL, 2016)

### 2.4.6 PV + Battery Economics

The table 2.7 below shows the anticipated cost from NREL Annual Technology Baseline for PV + Battery systems. AC coupled battery systems are interpreted to be 10% lower than DC coupled systems due to lesser equipment.

Table 2. 6: Estimated PV + Battery costs in 2020 (IRENA, 2019)

| Component | Cost |
|---|---|
| PV system | 912/kW DC |
| PV Operation and Maintenance (O&M | 11/kW-year |
| Batteries | 217/kWh |
| Battery BOS | 398/kW |
| Battery O&M | 9/kW-year |

## 2.5 Hybrid PV-CSP

### 2.5.1 Overview

The possibility of complementing CSP systems with PV systems promises to have high returns both technically and economically. PV systems have matured in the market, but their adoption is limited due to their instability caused by the intermittency nature of solar radiation (Bousselamti and Cherkaoui, 2019). This challenge makes it very difficult for PV systems alone to match demand. CSP systems on the other hand have the capability to match demand and overcome the intermittency challenge by using thermal energy storage. However, the current LCOE of CSP systems is more than double that of PV systems, according to IRENA 2019 weighted averages (IRENA, 2020), which makes it unattractive to developers (Singh and Singh, 2019).

There are a couple of PV-CSP commercial projects that are currently under development. Cerro Dominador in Chile, Atacama Desert, is coupling 100MW PV plant with 110MW CSP PTC with 17.5hours of thermal storage in molten salts (Bousselamti and Cherkaoui, 2019). According to Cerro Dominador website, the PV plant is now operational (grid connected), while the CSP is still in development (Cerro Dominador, 2020). There is also another plant in Chile, Atacama Desert in Copiapo, which is still in development with a plan to combine 130MW CSP with 14hours molten salt storage with 150MW PV plant (Bousselamti and Cherkaoui, 2019). The aim is to supply base load of 260MW 24/7 for local mining industries (Ju et al, 2017). In South Africa, two PV plants – 96MW Jasper plant and 75MW Lesedi plant – are planning to combine with a 100MW Redstone CSP plant that is currently under development (Bousselamti and Cherkaoui, 2019).

### 2.5.2 PV-CSP Hybrid Types

PV-CSP hybrid plants can be categorised based on the characteristics of optical system, system integration and operating temperature (Ju et al, 2017). Figure 2.35 below shows the two types of PV-CSP hybrid systems - compact and non-compact. The two types are at different stages of development with non-compact about to enter commercialisation while the compact is still in research and pilot projects (Ju et al, 2017). This report will therefore focus on non-compact PV-CSP.

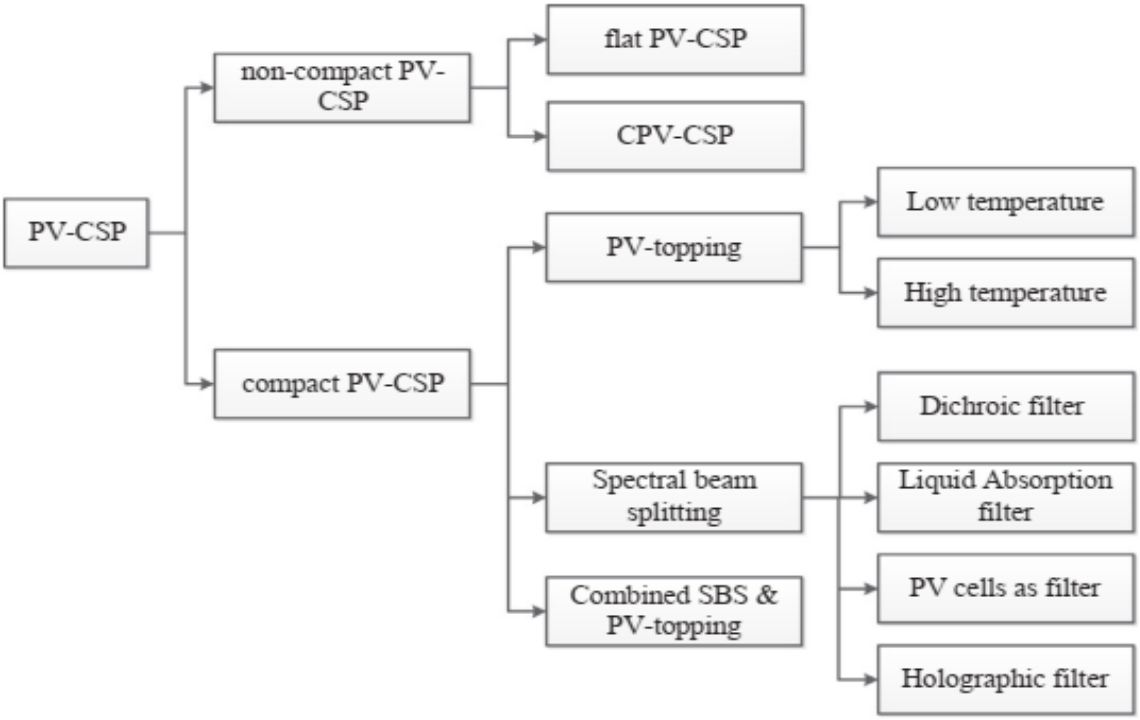


Figure 2. 35: Classification of PV-CSP hybrid system (Ju et al, 2017)

#### 2.5.2.1 Non-Compact PV-CSP hybrid

With a non-compact PV-CSP, PV system (both flat PV and concentrator PV) and CSP system can be operated independently of each other (Ju et al, 2017). Typical schematic diagram for a flat PV – CSP hybrid plant is shown in figure 2.36 below. The hybrid system is then operated by a dispatch control system to optimise the power output. SolarReserve, which is developing hybrid plants in Chile and South Africa, analysed the dispatch program they intent to implement for the plant in Chile. They discovered that if the CSP plant follows the output of PV plant, the capacity factor could reach a range of 80 – 90% (Ju et al, 2017). This value is comparable to convectional thermal power plants and is way above for individual CSP plants. The LCOE of the PV-CSP is expected to decline by a range of 8 – 13% when compared to CSP alone with thermal storage (Ju et al, 2017).

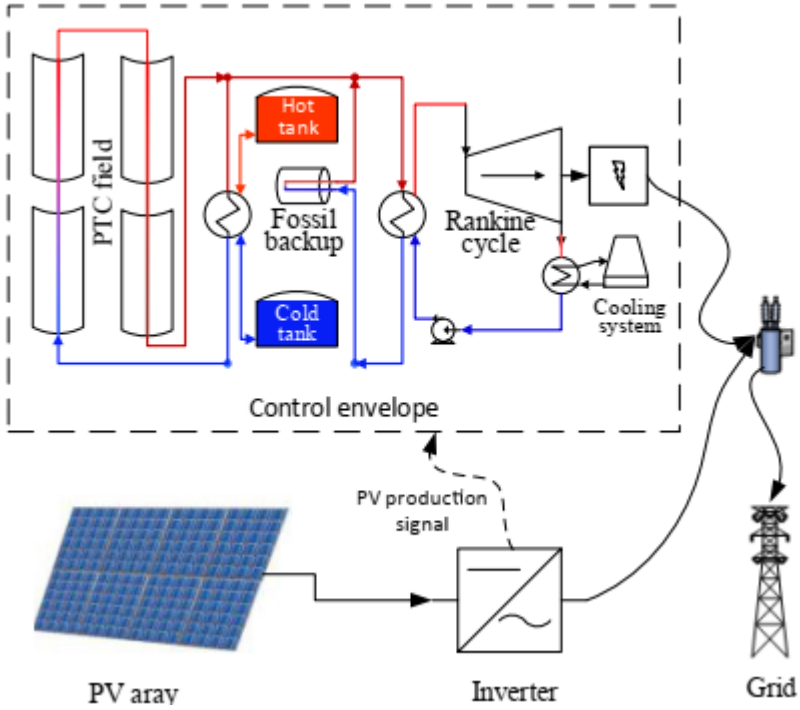


Figure 2. 36: Typical schematic flat PV-CSP hybrid plant (Starke et al, 2018)

### 2.5.2.2 Addition of Battery Storage

Battery energy system can be added to the non-compact PV-CSP hybrid system to minimise the variations of PV systems (Zurita et al, 2018). Currently, this type of system has only been analysed by scholars and a few pilot projects are currently under development with non at commercial level. A conceptual design to power Square Kilometre Array radio station telescope project was proposed by the Institute of Fraunhofer. The system constituted of a Concentrated PV (CPV) and linear Fresnel CSP combined with lithium and redox flow batteries (Ju et al, 2017). In Italy, a CPV plant with a bank of Sodium Nickel batteries is being coupled to linear Fresnel collector CSP system, with thermal oil as Thermal energy storage, coupled to an organic Rankine cycle is being built as a pilot project (Zurita et al, 2018). The schematic diagram and pictorial view of the pilot plant are shown in figure 2.37 below:

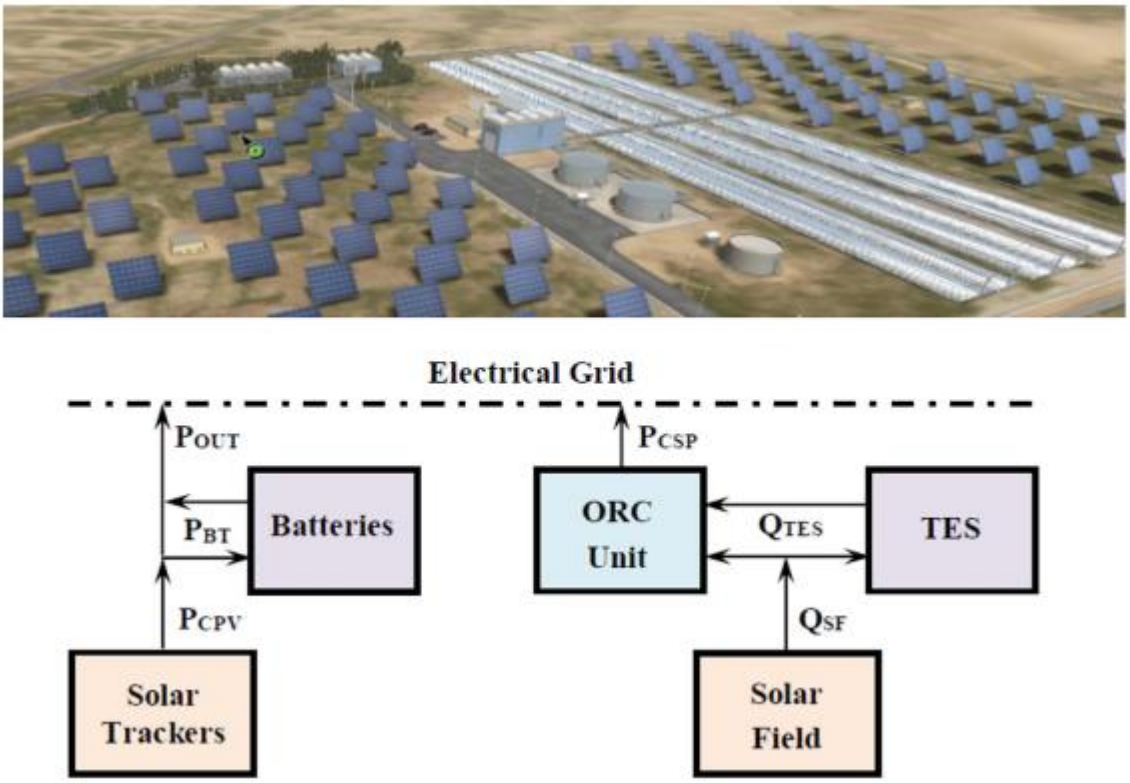


Figure 2. 37: Pilot CPV-CSP with battery storage under construction in Italy (Ju et al, 2017)

Zurita et al (2018) performed a parametric study to analyse the impact of solar multiple, PV size, Battery size and thermal storage size on PV-CSP hybrid with battery storage. The results showed that investment costs of the battery need to fall by a range of 60 – 90% to make the hybrid system competitive when compared to without battery system. The results were echoed by Zhai et al (2018) who found out that the battery storage size must be very small to make the hybrid system economically competitive.

### 2.5.3 PV-CSP dispatch strategies

#### 2.5.3.1 Overview

An area of active study in the PV – CSP hybrid systems is to find the dispatch strategy that will help optimise the two individual systems. The dispatch strategy has the potential to raise the capacity factor of the hybrid system when compared to uncoordinated power generation of the two systems (Pan and Dinter, 2017). There is also the potential to reduce the solar field size (solar multiple) which leads to reduced LCOE (Pan and Dinter, 2017).

Zhai et al (2017) analysed the technical and economic performance of thermal storage of PV – CSP when dispatched differently. The analyses showed that the LCOE reduced by 19% when PV is prioritised for dispatch during the day than when using uncoordinated strategy. The results also showed that the power output curve is more stable and fluid for coordinated dispatch. Liu et al (2019) also concluded that independent dispatch strategy for PV – CSP has a higher LCOE and less stead power output.

### 2.5.3.2 Typical dispatch strategies

There are typically two types of strategies from literature of dispatching PV – CSP hybrid system– PV advanced and Independent (Zhai et al, 2017).

### PV advanced strategy

With this dispatch strategy the PV system and CSP system are operating in synergy (Zhai et al, 2017). When the PV output is larger enough to cover the load, the PV system operate alone to satisfy the load while the thermal energy from CSP receiver is stored. If the PV output is not enough, CSP will cover the missing section. When there is no sunlight, the energy from the storage tank will be used to power the load as shown on the figure 2.38 below (Zhai et al, 2017):

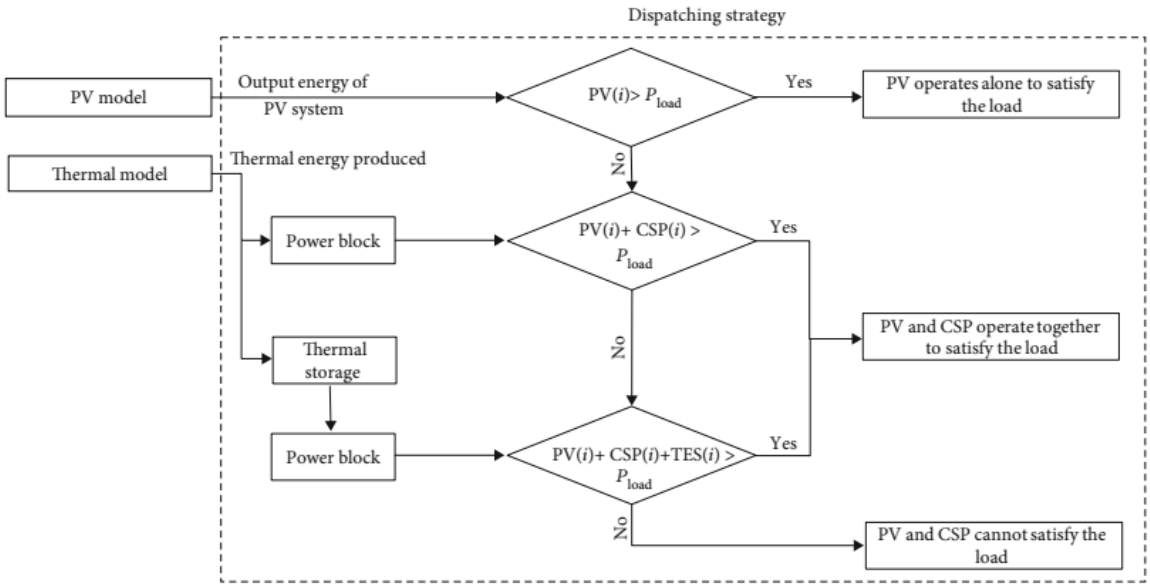


Figure 2. 38: A typical dispatch strategy prioritising PV output (Bousselamti and Cherkaoui, 2019)

### Independent strategy

With this strategy, the output from CSP system is summed up with that from the PV to supply the load as shown in the figure 2.39 below (Zhai et al, 2017):

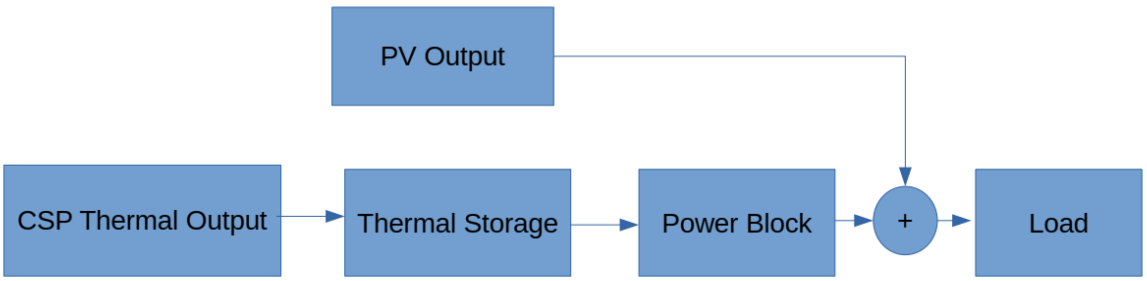


Figure 2. 39: A typical independent strategy for PV – CSP (Zhai et al, 2017)

## 2.6 Software review for PV – CSP hybrid

Performance and financial modelling are very critical when designing PV – CSP hybrid systems. Performance models are used to predict the expected output of the system at a given location under expected operating conditions (Alsadi and Khatib, 2018). Financial models are used to evaluate the economic performance of the system. Software packages differ in their operations, but they generally perform one or more of designing, simulation, and optimising. (Alsadi and Khatib, 2018). The table 2.7 below show different projects and approaches used by some scholars to model and analyse PV – CSP systems:

Table 2. 7: Typical software packages and methodologies involving PV – CSP systems

| Title | Project Aim | Methodology used | Reference |
|---|---|---|---|
| "Combination of PV and central receiver CSP plants for base load power generation in South Africa" | To simulate and access if PV – CSP can produce base load in South Africa | • SAM software to simulate PV and CSP independently<br>• Modified the thermal energy storage dispatch to emulate operational strategy<br>• Combined the systems in SAM | (Pan and Dinter, 2017) |
| "Techno-Economic Evaluation of Renewable Energy Projects using the Software GREENIUS" | Simulated the performance of 50MW CSP and 50MW PV plant in Jordan | • GREENIUS software used to simulate CSP and PV plant independently<br>• Added the two outputs and analysed | (Dieckmann and Dersch, 2015) |
| "Optimal Design Method of a Hybrid CSP-PV Plant Based on Genetic Algorithm Considering the Operation Strategy" | To optimise the design of PV – CSP plant considering operational strategy | • Modelled PV – CSP hybrid (performance and economic) in MATLAB | (Zhai et al, 2018) |
| "High capacity factor CSP-PV hybrid systems" | To investigate ways in which SolarReserve can increase the capacity factor of the hybrid PV – CSP plant they are constructing in Chile | • PV plant was modelled using PVSyst<br>• CSP was modelled using a proprietary software belonging to SolarReserve company<br>• Dispatch strategy was implemented using an inhouse | (Green et al, 2015) |

| | | | |
|---|---|---|---|
| | | software SmartDispatch | |
| "Multi-objective optimization of hybrid PTC + PV system using genetic algorithm" | To develop a methodology to design and size PV – CSP hybrid | • Used TRNSYS and GenOpt to simulate and optimise PV – CSP system respectively<br>• MATLAB used to develop genetic algorithm | (Starke et al, 2018) |
| "Techno-economic evaluation of a hybrid CSP + PV plant integrated with thermal energy storage and a large-scale battery energy storage system for base generation" | To investigate the impact of PV size, solar multiple, thermal storage size, and battery size on technical and economic performance | • Used TRNSYS to simulate thermal and electric performance of hybrid system<br>• Optimisation of heliostat field, tower height, receiver geometry done using Solar-Pilot an algorithm from SAM software<br>• 3 operational strategies modelled using a controller in TRNSYS software | (Zurita et al, 2018) |
| "Simulation of hybrid solar power plants" | To evaluate the potential of software GREENIUS to carry out a techno – economic evaluation for hybrid solar power plants | • Simulated the hybrid system in two simulations using GREENIUS software to implement the operational strategy<br>• First simulated output for PV plant<br>• Modified the load profile (base load – PV output)<br>• Second simulation involved CSP following the modified load profile | (Dieckmann and Dersch, 2017) |
| "Combined CSP – PV plants for MENA Region" | To investigate the optimal configuration of solar power plants | • Simulated the performance of hybrid system using INSEL tool | (Benitez et al, 2018) |

| | | | |
|---|---|---|---|
| | for selected sites in Jordan, Tunisia, and Algeria | • Performed parametric study, optimisation, economic evaluation, and operational strategy implemented in INSEL | |

From the above table, TRNSYS and INSEL are the two software packages with the capability of simulating the PV – CSP hybrid system in its entirety. SAM and GREENIUS can independently simulate PV and CSP and will need modifications to model PV – CSP as whole system. The main features of the mentioned software packages are given in the table 2.8 below:

Table 2. 8: Key features of selected software packages for PV- CSP hybrid

| Name and Developer | Key features | Technology simulated | Reference |
|---|---|---|---|
| • SAM – System Advisor Model<br>• National Renewable Energy Laboratory | • Parametric analysis, stochastic analysis, probability of Exceedance analysis, LK script, economic evaluation<br>• Price – Free<br>• Comment – need modifications to simulate PV – CSP, no global weather data | PV (with option for battery storage), High concentrated PV, CSP, Wind, Geothermal, Biomass combustion, Convectional thermal fossil fuel, Water heating | (SAM, 2020) |
| • TRNSYS – Transient System Simulation Program<br>• University of Wisconsin, TRANSSOLAR, Thermal Energy System Specialist | • Parametric runs, can model hybrid PV – CSP<br>• Price – US$2530 for 10 users<br>• Comment – the software is a simulation program and can not perform economic evaluation and optimisation | All thermal and renewable generation except Nuclear, Wave, Tidal, and Hydro | (TRNSYS, 2020) |

| | | | |
|---|---|---|---|
| • GREENIUS – Green Energy System Analysis<br>• German Aerospace Center (DLR) | • Economic evaluation, Performance simulation<br>• Price – Free<br>• Comment – Cannot perform hybrid analysis, No global weather data | Solar thermal, PV, Wind, Fuel cells | (GREENIUS, 2020) |
| • INSEL – Integrated Simulation Environment Language<br>• University of Oldenburg | • Worldwide weather database, ability to simulate hybrid systems, economic evaluation, performance simulation<br>• Price – Free | PV, Solar thermal | (INSEL, 2020) |

## 2.7 Comparison of PV + Battery vs CSP + TES

The tables 2.9 and 2.10 below show the comparison of two systems in terms of the important parameters:

Table 2. 9: Comparison of Capacity factors of different configurations of PV + Battery and CSP + TES (NREL, 2016)

| **Parameter** | **CSP + TES** | | | **PV + Battery** | | |
|---|---|---|---|---|---|---|
| Typical capacity factor (CF) | **SM** | **storage hrs** | **CF / %** | **ILR** | **storage hrs** | **CF / %** |
| | 1.5 | 3 | 37 | 1.5 | 3 | 36.8 |
| | 2 | 6 | 50 | 2.1 | 6 | 50 |
| | 2.5 | 9 | 60 | 2.6 | 9 | 60 |

Table 2. 10: Comparison of PV + Battery vs CSP + TES (Florin and Dominish, 2017)

| **Parameter** | **CSP + TES** | **PV + Battery** | | |
|---|---|---|---|---|
| | | **Lithium ion (NMC)** | **Lead acid** | **Sodium - based** |
| Energy Efficiency | depend on steam temperature and capability of storage material withstanding higher working temperature | Mean roundtrip efficiency = 90% | Mean roundtrip efficiency = 82% | Mean roundtrip efficiency = 81% |

| | | | | |
|---|---|---|---|---|
| Lifecycle greenhouse efficiency | cradle to gate (manufacturing and production): low<br>5-25 kgCO2e/MWh<br>20% from storage system | cradle to gate: low<br>25 kgCO2e/MWh<br>mostly from nickel and cobalt | cradle to gate: high<br>75kgCO2e/MWh | cradle to gate: medium<br>50kgCO2e/MWh |
| Raw material availability | potential constraints in the supply of silver (used for reflectors) and silvering process which uses cerium which is a rare earth material<br>no issues with TES | presents of graphite, cobalt and fluorine not easily accessed<br>potential issues in the supply of lithium | lead is highly recyclable hence less critical | uses graphite hence potential issues |
| Material intensity | relatively highly intensive | high material demand | high material demand | low material demand than alternative battery types |
| Recyclability | relatively long lifespans (30yrs) and rate of degradation of molten salts is very slow minimal need to refresh material | high potential of recycling | high potential of recycling | high potential of recycling |
| Environmental Impact | Significant water usage<br>land footprint is relatively high | Air pollution from graphite dust<br>water pollution from cobalt | heavy metal contamination of water, soil, and plants | air pollution from graphite |
| Health and safety | relatively safe as it has established operating protocols | risk to consumers of fire due to thermal run away | potential emission of corrosive and potential explosive mix of hydrogen and oxygen in the last stages of charging | relatively safe |

| | | | | |
|---|---|---|---|---|
| | nitrate salts are non-toxic | | sulphuric acid as electrolyte can harm if exposed | |

# 3.0 Methodology

## 3.1 Model Description

The techno-economic models for PV, PV + Battery, CSP, and CSP + Thermal Energy Storage (TES) were developed for a typical mining load in Zimbabwe. Evaluation was based on technical and economic performance using System Advisor Model (SAM) software. The table 3.1 below describes the process taken:

Table 3. 1: Methodology

| Stage | System / Description | Aim | Steps |
|---|---|---|---|
| 1 | Demand profile | To develop typical hourly load profile from the given monthly data | Understand the given load data and the billing structure<br>Analyse the typical working pattern and use it to develop hourly profile |
| 2 | PV | To analyse the viability of integrating Solar PV at Mimosa mine | Design the capacity and optimise technical parameters (tilt angle, orientation and interrow distance)<br>Analyse technical and economic metrics of the modelled results (annual energy produced, LCOE, Savings, Net Present value) |
| 3 | PV + Battery | To analyse the viability of integrating Solar PV + Battery at Mimosa mine | Design and determine the optimal size for PV and Battery for a given dispatch<br>Analyse technical and economic metrics of the modelled results (annual energy produced, LCOE, savings, Net Present value) |
| 4 | CSP | To analyse the viability of integrating CSP at Mimosa mine | Design the capacity and optimise technical parameters (solar multiple, design point DNI)<br>Analyse technical and economic metrics of the modelled results (annual energy produced, LCOE, savings, Net Present value) |
| 5 | CSP + Thermal Energy Storage | To analyse the viability of integrating CSP + TES at Mimosa mine | Design and determine the optimal size for CSP and TES for a given dispatch<br>Analyse technical and economic metrics of the modelled results (annual energy produced, LCOE, savings, Net Present value |
| 6 | Repeat stage 2 to 5 but considering energy export | To analyse the techno-economic performance of the systems when exports are allowed | Design and determine the optimal size for PV, CSP and TES/Battery<br>Analyse technical and economic metrics of the modelled results (annual energy produced, LCOE, savings, Net Present value |

The mentioned systems will be evaluated based on Key Performance Indicators (KPI) listed in the table 3.2 below:

Table 3. 2: Key performance Indicators used for evaluation

| KPI | Calculation/Comment |
|---|---|
| **Base case** | |
| Renewable Energy Contribution | This is shown as a percentage energy offset by the renewable energy system.<br>Calculated as $\frac{Net\ annual\ energy\ produced\ by\ system}{annual\ energy\ demand}\ x\ 100\%$ |
| Localised Cost of Energy (LCOE) – applies to export case | This metric will allow comparison of energy systems being considered based on technical performance, capital cost and operations and maintenance costs.<br>The formula used is given in Appendix C |
| Net Present Value (NPV) – applies to export case | This will be used to analyse the profitability of the system<br>The formula used is given in Appendix C |
| **Export case** | |
| Energy exported | This shows the percentage of energy exported from the system calculated as:<br>$\frac{Annual\ energy\ from\ system\ to\ grid}{Annual\ generated\ energy}\ x\ 100\%$ |
| Energy used locally | This shows the percentage of energy used to meet local generation from the system calculated as:<br>$\frac{Annual\ energy\ from\ system\ to\ load}{Annual\ generated\ energy}\ x\ 100\%$ |
| Renewable Energy contribution | This shows the percentage energy offset by the renewable energy system calculated as:<br>$\frac{Annual\ energy\ from\ system\ to\ grid}{Annual\ mine\ energy\ demand}\ x\ 100\%$ |
| Grid contribution (applies to base case as well) | This shows the percentage of energy used to meet the mine demand from the grid calculated as:<br>$\frac{Annual\ energy\ from\ grid\ to\ load}{Annual\ mine\ energy\ demand}\ x\ 100\%$ |

**System Advisor Model (SAM) software**

The SAM software will be used to model the renewable energy systems under consideration. This is a financial and performance model developed by National Renewable Energy Laboratory (NREL) funded by US Department of Energy (SAM, 2020). The target users for the software include:

- Project engineers and managers
- Developers
- Researchers
- Policy analyst

The model makes performance predictions and estimates energy cost for grid connected systems referencing the installation and operations cost and the design parameters inputted to the model (SAM, 2020). The projects can either be connected to:

- Customer side – buying and selling electricity at retail rates
- Utility side – selling electricity at a negotiated price through a power purchase agreement

The models require input data to describe the performance characteristics of the system's physical equipment and project costs. One disadvantage of the software is that it does not have weather database for the whole world hence there is need to source it from external if the desired area is not covered (SAM, 2020).

## 3.2 Candidate mine

### 3.2.1 Mimosa Mining Company

Mimosa mine is a Platinum Group Metal (PGM) and base metal mining company located in the Wedza sub-chamber of the Great Dyke of Zimbabwe (24 km west of Zvishavane town). The two figures below (figure 3.1 and 3.2) show the geographical location of Mimosa mine on the Great Dyke and the satellite picture (geographical coordinates with latitude -20.33 and longitude 29.83). It involves underground mining and plant processing activities with an estimated life of mine of 30 years. The output commodities of the mine include Platinum, Palladium, Rhodium, Gold, Nickel and Copper.

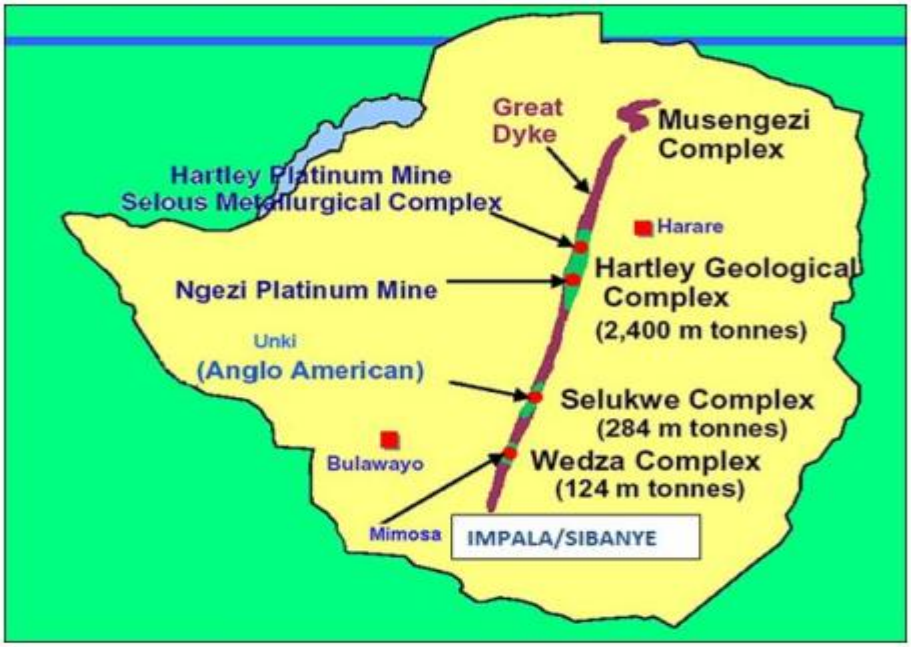


Figure 3. 1: The position of Mimosa mine on the Great dyke, Zimbabwe


Figure 3. 2: Satellite picture showing the position of mimosa mine (Google maps,2020)

### 3.2.2 Climate data

The climate data used in this project was sourced from Solcast. This is a data services company providing solar radiation data and solar forecasting globally using surface and satellite measurements (Solcast, 2020). Three set of data were acquired – Typical Meteorological Year (TMY) in csv format, data customised for SAM software and PVSyst. Solcast data sets have been validated showing 0% and 0.3% bias on Global Horizontal Irradiation (GHI) and Direct Normal Irradiation (DNI) data sets, respectively (Solcast, 2020).

Mimosa mine receives solar radiation of 2010 kWh/m$^2$/year of DNI and 2034 kWh/m$^2$/year of GHI according to Solcast data. The DNI value shows that the site is technically feasible to develop CSP as the minimum rule of thumb value required is between 1900 – 2000 kWh/m$^2$/year (Bousselamti and Cherkaoui, 2019). The figure 3.3 below shows the variation between monthly GHI and DNI for the candidate site - the site receives higher DNI values than GHI between April and September.

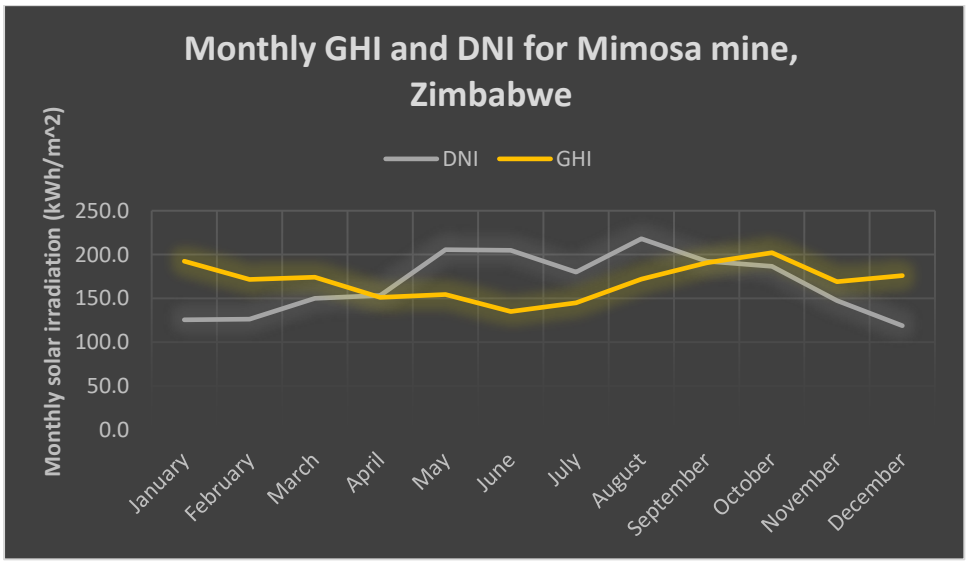


Figure 3. 3: Monthly GHI and DNI for Mimosa mine

The two figures below (figures 3.4 and 3.5) show the typical hourly variation of DNI, GHI and temperature of a day in summer and winter at the candidate site. For both figures, the GHI and DNI peak occurs around midday. The temperature in winter is below 25°C which could help PV system to perform better. However, the temperature in summer has a peak value of 35°C which could affect the performance of PV system.

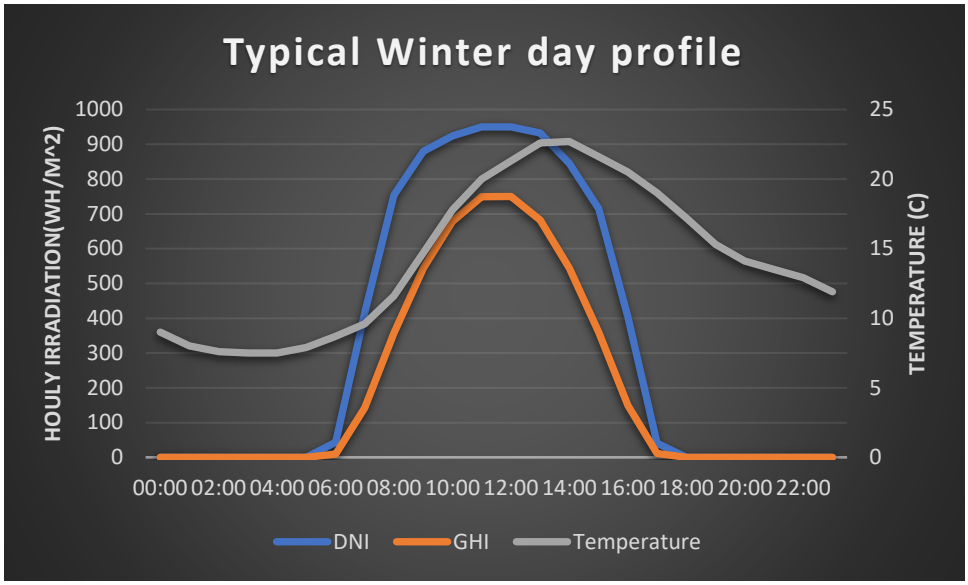


Figure 3. 4: Typical winter day (in June) profile at Mimosa mine

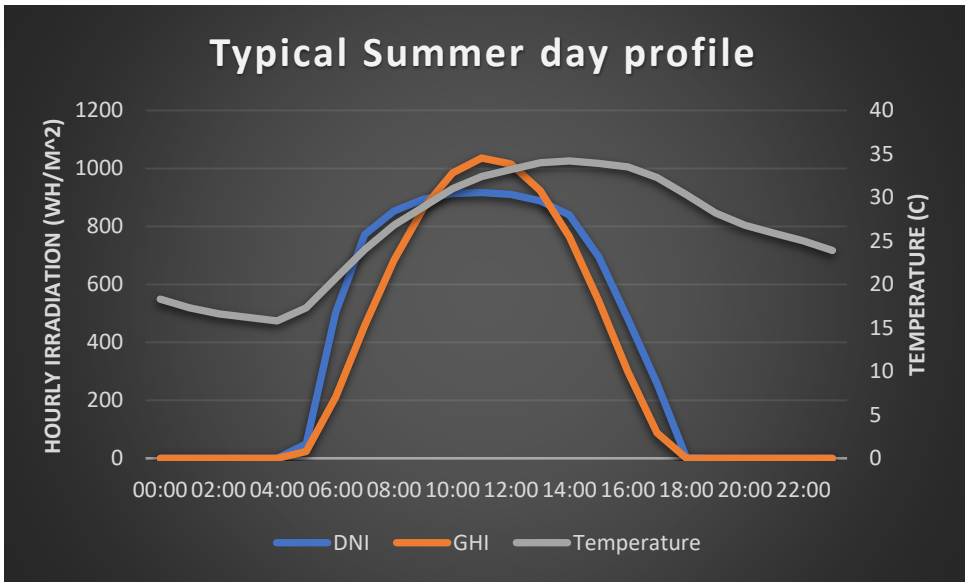


Figure 3. 5: Typical summer day (In October) profile at Mimosa mine

## 3.3 Mimosa Mine Demand Profile

### 3.3.1 Raw Data – Monthly profile 2015

Currently, the mine is grid connected with annual consumption of 165GWh according to 2015 figures. The peak demand in that year was recorded in December with a value of 28.4MW. The figure 3.6 below shows the monthly variation of the consumed energy and the corresponding peak power. The energy consumption graph has a minimum of 12.7GW (in October) and a maximum value of 14.9GW in June. There is a variation from month to month

of energy consumed due to maintenance activities. Taking for example, in October there was 5-day plant shut down (planned maintenance) which corresponded to the minimum monthly energy consumed that year.

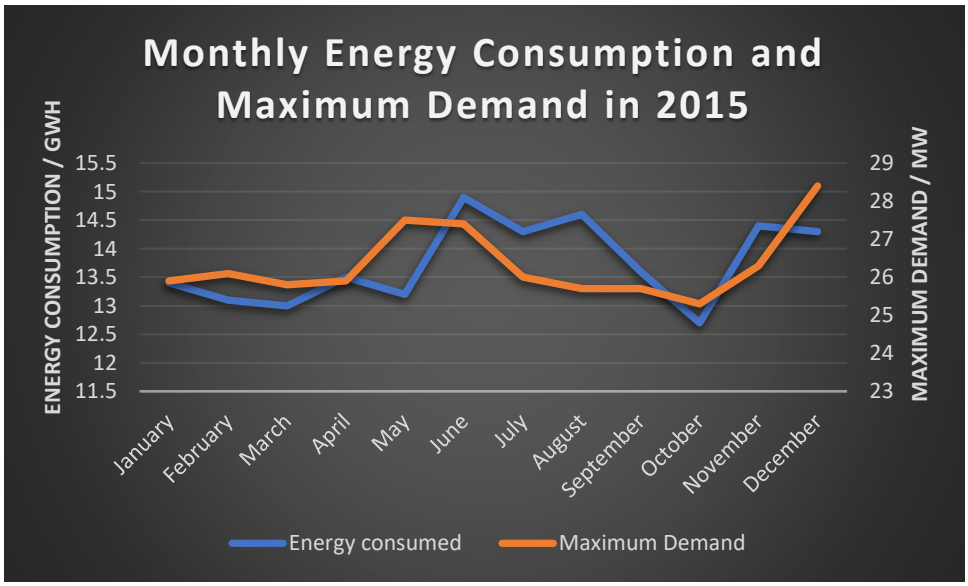


Figure 3. 6: 2015 monthly energy consumption and maximum demand for Mimosa mine

The data for the year 2015 shows that the mine consumes most of its energy during peak hours as shown in the figure 3.7 below. The table 3.3 below shows the time periods of on-peak, standard and off-peak with the corresponding time of use tariff. The off-peak tariffs show that the mine could benefit by load shifting to off-peak hours and by finding an alternative cheaper source of electricity during peak hours.

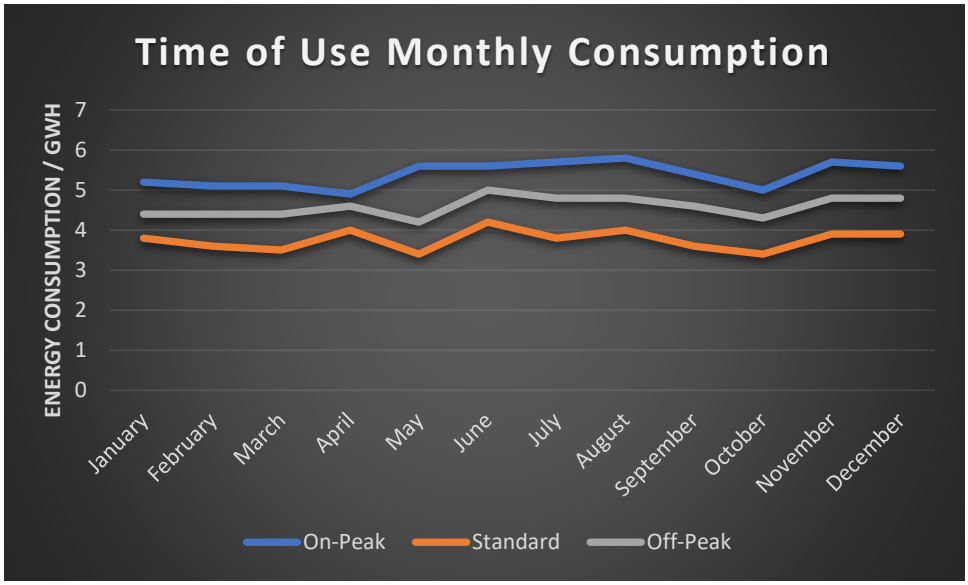


Figure 3. 7: Time of Use monthly consumption of Mimosa mine in 2015

Table 3. 3: Time of use periods and corresponding tariff

| | Hours | | | | | | | | | | | | | | | | | | | | | | Legend | | |
|---|---|---|---|---|---|---|---|---|---|---|---|---|---|---|---|---|---|---|---|---|---|---|---|---|---|
| Day of Week | 0 | 1 | 2 | 3 | 4 | 5 | 6 | 7 | 8 | 9 | 10 | 11 | 12 | 13 | 14 | 15 | 16 | 17 | 18 | 19 | 20 | 21 | 22 | 23 | Category | Color | Tariff/$USD per kWh |
| Sunday/Holiday | | | | | | | | | | | | | | | | | | | | | | | | | Peak | | 0.13 |
| Weekday | | | | | | | | | | | | | | | | | | | | | | | | | Standard | | 0.07 |
| Saturday | | | | | | | | | | | | | | | | | | | | | | | | | Off-peak | | 0.04 |

The 2015 mine consumption figures show that 40% of the load was consumed during peak times as illustrated by the pie chart (figure 3.8) below and this translates to high annual electric bill. In addition, the electric bill also includes the maximum monthly demand charge of USD2.6 per unit demand. The maximum demand charge is applied only during the peak and standard period to encourage customers to load shift wherever possible and not strain the system.

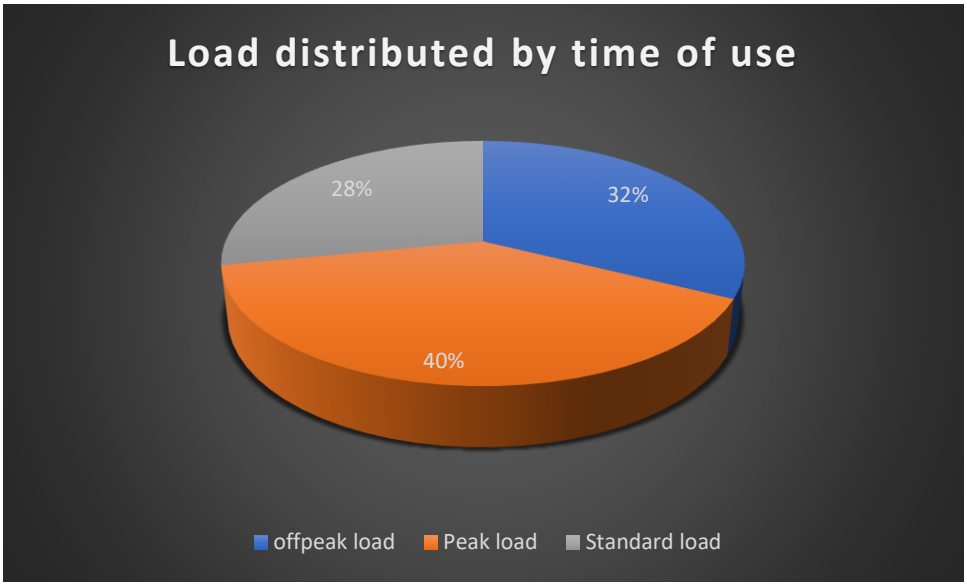


Figure 3. 8: A pie chart showing 2015 Mimosa mine load distribution by time of use

Lately, Zimbabwe has been facing power shortages which resulted in load-shedding with the most shed period being between 4pm and 9pm. Such scenario causes the mine to add another charge on the electric bill – uninterrupted demand charge of USD1.95 per unit demand on each hour supposed to be on load shedding. This shows that the mine can benefit by integrating reliable energy system that can offset or eliminate grid energy consumption during these risk hours. The peak period is also coincidentally the high-risk period in terms of load-shedding.

### 3.3.2 Synthesized hourly demand profile

Hourly demand profile for the mine was not provided (only monthly profile) hence there was need to produce one to use in the analyses. The following assumptions and consumption behaviours were used in estimating the hourly pattern from the given data:

- The hourly demand consumption is derived from time of use monthly consumption – peak, off-peak and standard energy consumptions
- The assumption is that each day of the month follow the same pattern and the cumulative total of energy consumption should be close to the given 2015 monthly and time of use figures

- The time of use hourly periods for the weekday will be used in estimating the pattern
- The mine has 2 shifts a day – day shift which starts at 7am to 4:30pm and night shift starting at 7pm up to 4am. The day shift consists of production and administrative teams while the night shifts only comprises of production teams.
- There will be two shift changeovers one in the morning from 4am to 7am and the other in the evening from 4:30pm to 7pm. During this time, key equipment that operate 24/7 (like Mills and Ventilation fans for underground) will be running.
- During the shift change over, the underground operations will stop to allow for blasting and no personal will be allowed underground for safety purposes. The technical team in the process plant (above ground) will continue to operate.
- Other machinery (process pumps, crushers, conveyer belts) will be switched on at 8am to 9am and 8pm to 9pm by the morning and night shift teams, respectively. This will correspond to peaks in the energy consumption pattern due to high starting currents of large motors involved. The value of the peak demand is estimated from the given maximum monthly demand from the 2015 data
- Each month will follow the same pattern but having different values as dictated by the given data. Figure 3.9 below show the typical hourly profile synthesized for the month of April:

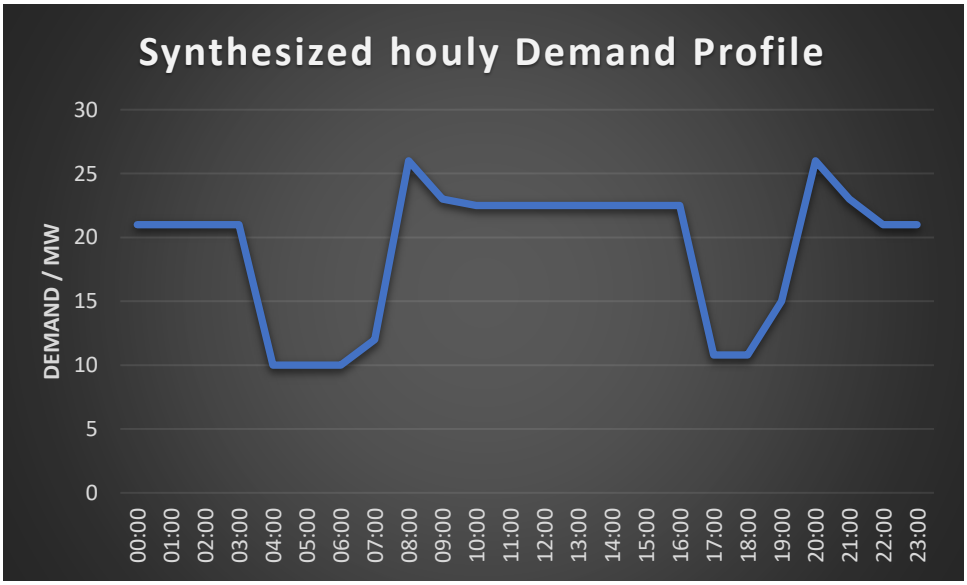


Figure 3. 9: Synthesized hourly profile for the month of April

- The synthesized hourly profile has an annual energy consumption of 165.7GWh with a peak demand of 28.4MW. The figure 3.10 below shows the monthly energy consumption comparison for raw data and synthesized data:

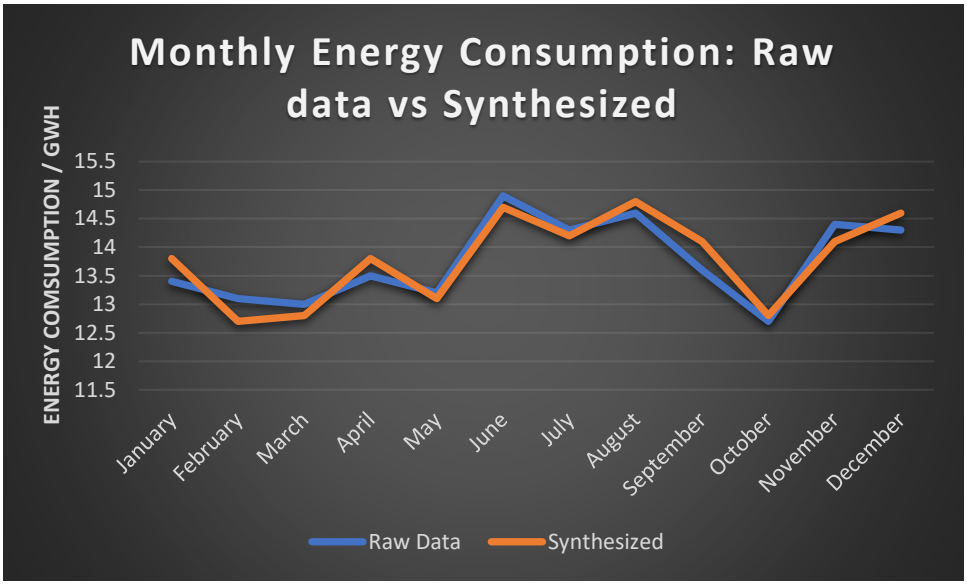


Figure 3. 10: Monthly energy consumption of raw data vs synthesized data

## 3.4 PV System

### 3.4.1 Plant Capacity

A PV plant differs from convectional electrical systems because their performance is naturally connected to unique details of the site and the specifics of the plant design. This makes it very difficult to calculate the required capacity of the plant. The equation used to calculate power in HOMER software is going to be utilised to estimate the rated capacity of this project (Homer, 2020). The rated capacity will assume that the modules are operating at Standard Test Conditions (STC).

$$Power = Rated\ Capacity\ x\ \frac{Net\ incident\ radiation}{incident\ radiation\ at\ STC}\ x\ Derating\ factor$$

Where:

Power = peak load/demand required (from load profile)

Rated capacity = unknown

Net incident radiation = incident radiation at STC = 1000 W/m$^2$ (Assumption)

Derating factor = 0.77 (NREL, 2013)

$$Rated\ Capacity\ (DC) = \frac{Peak\ load\ required}{Derating\ factor}$$

$$= \frac{28.4\ MW}{0.77} = 36.88\text{MW DC} \sim 37\text{MWDC}$$

The recommended DC to AC ratio (form factor) to avoid inverter clipping losses is between 1.0 – 1.1 (PVSyst, 2020). The proposed form factor for the project is 1.05. The tilt angle, azimuth angle and interrow space will be optimised through parametric analysis based on energy produced and LCOE. The key technical parameters used for the model are given in the table 3.4 below:

Table 3. 4: Technical parameters for PV plant (SAM, 2020)

| Parameter | Unit | Value (and comment) |
|---|---|---|
| Module type | - | Polycrystalline |
| Module DC capacity | W | 345 |
| Module Efficiency | % | 17.8 |
| Inverter | - | String inverter |
| Inverter Capacity | kW | 40 |
| Tilt angle | degrees | 0 – 60 (optimisation range) |
| Azimuth | degrees | 0 – 270 (optimisation range) |
| Module configuration | - | Landscape (based on literature review) |
| Far shading | - | Assumed no far shadings |
| DC / AC ratio | - | 1.05 |
| Ground cover ratio | - | 0.05 – 0.95 (optimisation range to determine interrow distance) |
| Soiling loss | % | 5 |
| DC losses | % | 4.4 (including module mismatch) |
| AC cabling losses | % | 2 |
| Degradation | %/year | 0.5 |

### 3.4.2 Financial inputs for PV System

The commercial model will be used to simulate the financial analysis of the PV system in SAM. This model assumes that the PV system will be developed, owned, and operated by the entity and in this case the Mimosa mining company. With this model, the entity will be able to buy and sell power at retail price. The metering and billing method to be used for this analysis is the net metering. This allows the PV system to supply the load with the shortfall being supplied from the grid. However, this type of system also mean excess generation of the system will be fed into the grid hence there is need to design it in such a way there is reduced excess generation. For the base case scenario, the excess generation will be curtailed based on the assumption that there is no agreement with the utility company to export power. The grid energy charges are based on the time of use for the weekday as defined in table 3.3 above in section 3.3.1.

The table 3.5 below shows the parameters to be used in the model to calculate LCOE, Net Present Value (NPV) and pay-back period. The formulas on how these are calculated in SAM are presented in Appendix C.

Table 3. 5: Commercial parameters for PV module (Zurita et al, 2020)

| **Parameter** | **Unit** | **Value** |
|---|---|---|
| **Direct Capital Cost** | | |
| Module cost | USD/Wdc | 0.30 |
| Inverter cost | USD/Wac | 0.05 |
| Balance of System | USD/Wdc | 0.17 |
| Installation cost | USD/Wdc | 0.10 |
| Installer margin and overhead | USD/Wdc | 0.05 |
| Contingency | % | 3 |
| **Indirect Capital Cost** | | |
| Sales tax | % | 5 |

| | | |
|---|---|---|
| Land purchase | USD/acre | 11000 |
| Operations and maintenance cost | USD/kW-year | 9 |
| **Analysis Parameters** | | |
| Project life | Years | 25 |
| Inflation | % | 2.5 |
| Discount rate | % | 6.4 |
| Interest rate | % | 5 |

## 3.5 PV + Battery System

### 3.5.1 Capacity design

The PV + Battery system in the model mainly aims to perform time of use arbitrage and to reduce the risk of losing grid power due to load-shedding (or paying uninterrupted charge). The AC connected behind the meter battery will utilise energy produced by PV system during the day and discharging it during peak periods. The two main design parameters for the PV + battery system are:

- Power to Energy ratio – this determines the battery storage hours
- PV size ratio – PV + battery plant capacity to PV (without storage) capacity. This determines capacity of the PV plant to service both the load and the battery

A parametric analysis will be carried out to optimise the design parameters based on return on investment (Net Present Value) and the ability of the system to supply the load during the most risk period from load shedding on a typical good day for PV production. From the load profile, the maximum energy required between 4am – 9pm is 138MWh (occurring in June) and this will be used to calculate the minimum required battery capacity (Bayod-Rujula et al, 2013):

$$E_{cap-min}(MWh) = \frac{110E_{req}(MWh/day)xD}{DOD\%}$$

Where:

- $E_{cap\text{-}min}$ = minimum battery capacity
- $E_{req}$ = peak energy consumption between 4pm and 9pm (inclusive) from load profile
- D = days of anatomy (1 will be used for estimation with parametric study to determine the final)
- DOD = depth of discharge (80% will be used) (Petrollese and Daniele, 2016)

$$= \frac{110\ x\ 138\ x\ 1}{80}$$
$$= 189.75 \sim 190MWh$$

Therefore, the minimum battery capacity for this model is 190MWh with rated power capacity of 30MW (based on peak demand of 28.4MW). The technical parameters used to model the battery are given in the table 3.6 below (the PV plant will use the same parameters as described in the above section 3.4.1):

Table 3. 6: Battery technical properties (SAM,2020)

| Description | Unit | Value |
|---|---|---|
| Battery type | - | Lithium ion: Nickel Manganese Cobalt Oxide (NMC/Graphite) |
| Maximum charge power | MWac | 30 |
| Maximum discharge power | MWac | 30 |
| Life cycle at 80% DOD | cycles | 2500 |
| Minimum State of Charge | % | 15 |
| Maximum State of Charge | % | 95 |
| Battery replacement threshold capacity | % | 50 |
| DC – AC efficiency | % | 96 |
| AC – DC efficiency | % | 96 |

### 3.5.2 Battery dispatch

A manual dispatch will be defined in SAM so as to input specific time frames, other than using the automatic peak shaving dispatch. The battery will only be allowed to charge from PV system (not from grid) and can only discharge during peak or standard period times (7am – 9pm). The power generated from PV system prioritise the load first and will only charge the battery when the generated PV is greater than the load. Just like with the PV system, the excess generated power will not be exported to the grid and will be reported as losses. In case the power from PV + Battery is not enough to supply the load: grid power will be used instead.

### 3.5.3 Economic inputs to PV + Battery System

The commercial model used for this system is the same as with PV system described in section 3.4.2 above. The table 3.7 below show the economic parameters for the battery system to calculate the LCOE, Net Present Value and payback period (for PV they are the same as described in the previous section 3.4.2):

Table 3. 7: Economic parameters for Battery storage (Zurita et al, 2020)

| Description | Unit | Value |
|---|---|---|
| **Battery Storage System** | | |
| Cost of storage | USD/kWh | 209 |
| Conversion system | USD/kW | 70 |
| Balance of System | USD/kW | 80 |
| **Operations and Maintenance (O/M)** | | |
| Fixed O/M | USD/kW-year | 6.9 |
| Variable O/M | USD/MWh | 2.1 |
| Battery Replacement Cost | USD/kWh | 2/3 of Cost of Storage |
| **Analysis Parameters** | | |
| Project life | Years | 25 |
| Inflation | % | 2.5 |
| Discount rate | % | 6.4 |
| Interest rate | % | 5 |

### 3.5.4 Practical considerations of PV + Battery system

The table 3.8 below shows typical practical challenges and corresponding best practises for a PV + Battery system:

Table 3. 8: Potential practical challenges of PV + Battery system (NREL, 2018)

| Subsection | Challenge | Best practice |
|---|---|---|
| Electrical and Balance of plant | • Degradation of cables and cable ties that are exposed to direct sunlight<br>• Cables exposed to animals (like rates, snakes) which can destroy/chew cable insulation resulting in faults | • Consider covering electrical cables that are in open air with conduits<br>• Employ animal repellent/deterrent system |
| PV module mounting | • Modules mounted too low causing difficulties in vegetation management | • Consider intended vegetation management during the design stage of the project |
| Environmental | • Hot spots from uneven soiling like bird droppings<br>• Flooding and soil erosion | • Regular checking and cleaning the PV modules – also consider installing birds spikes to prevent roosting<br>• Establish good drainage system at the site |
| Battery system | • Capacity degradation and shorter battery usable life due to operating outside optimum temperature range | • Effective and efficient (less power consumption) thermal management system of battery units recommended<br>• Usually air cooling and heating HVAC systems employed |

## 3.6 Concentrated Solar Power (CSP)

The system chosen for primary analysis in this project is the Parabolic trough CSP system. Based on the literature review, this is a more mature system (when compared to other CSP systems) with commercial operational plants around the world including in Africa.

### 3.6.1 System design

The recommended methodology to design and model parabolic trough CSP plant in SAM is given below (SAM, 2020):

- Define solar field design parameters
- Configure receiver and collector components
- Determine transport operational limits
- Configure the loop

- Specify power cycle design point
- Update cost and financials
- Optimise uncertain parameters – solar multiple, storage hours

The table 3.11 below shows the technical parameters used to develop the CSP parabolic trough system for this project. Details of the most important parameters are described below:

**Design point DNI**

This is used to calculate the aperture area required to drive the power cycle at its design capacity (SAM, 2020). Theoretically the value should be close to maximum DNI value of the site. A low DNI value results in excessive dumped energy while a high reference DNI value results in undersized solar field only operating at designed capacity for only few times (SAM, 2020). A parametric analysis will be used to determine the design point DNI.

**Solar Multiple (SM)**

This is defined as a multiple of aperture area required to operate the power cycle at its design capacity (SAM, 2020). An SM value of 1 defines an aperture area that will generate (when exposed to solar radiation equivalent to design point DNI) thermal energy required to drive power block at its rated capacity. A parametric analysis will be used to determine the optimal SM for this application.

**Design turbine gross output**

This is power cycle's design output (not including parasitic losses) used to determine solar field area (SAM, 2020). The value is determined from the maximum load required. The maximum load from demand profile is 28.4MW hence the net estimated output at design capacity is 29MW. The gross turbine output is determined using the following equation:

$$Estimated\ Net\ Output\ at\ Design = Design\ gross\ output\ x\ estimated\ gross\ to\ net\ conversion\ fractor$$

$$Design\ gross\ output = \frac{Estimated\ net\ output}{Estimated\ gross\ to\ net\ conversion\ factor}$$

$$= \frac{29MW}{0.9(SAM,2020)} = 32\text{MW}$$

**Heat rejection**

One of the criticisms of the CSP plant is based on its extensive use of water. This model is being proposed in area which is generally hot and dry with persistent droughts. In that regard, air cooled condenser is chosen for this model rather than the water cooled. Some of the advantages and disadvantages of air-cooled condenser over water condenser are given in the table 3.9 below:

Table 3. 9: Advantages and disadvantages of Air-cooled condenser over water condenser (Padillar, 2011)

| Advantages | Disadvantages |
|---|---|
| Reduced maintenance cost (no chemical additives or periodic cleaning) | Forced air heat transfer is less effective than evaporative heat transfer |

| | |
|---|---|
| Elimination of cooling tower plume | Large heat exchange areas required to achieve equivalent heat rejection |
| Reduced condensation on mirrors close to the cooling tower plume thus increased optical efficiency | Greater fan power required to achieve equivalent heat rejection |
| The waste products (warm, clean air) are environmentally friendly | Performance influenced by external conditions – dry bulb temperature |

Different types of dry cooling tower configurations are illustrated in Appendix D. In SAM software, the air flow generated by the fans can be modelled either at 50% or 100% of the designed air mass flow rate depending on the operating strategy (NREL, 2011). The strategy allows for either using two fixed fans, each supplying 50% of the load or only one fan to operate supplying 50% of the load. The air mass flow rate is calculated as (NREL, 2011):

$$m_{air} = \frac{Q_{rej}}{C_{p,air}\ x\ (T_{ITD} - \Delta T_{out})}$$

Where $Q_{rej} = Heat\ rejected\ at\ design$, $C_{p,air} = specific\ heat\ of\ air$, $T_{ITD} = initial\ temperature\ difference\ (steam\ to\ ambient)$, $\Delta T_{out} = temperature\ differnce\ at\ the\ hot\ side\ of\ the\ condenser$

The key performance indicators in dry cooled condensers are parasitic fan power and condenser pressure. The condenser pressure is determined from the condenser temperature which is illustrated in the figure 3.11 below:

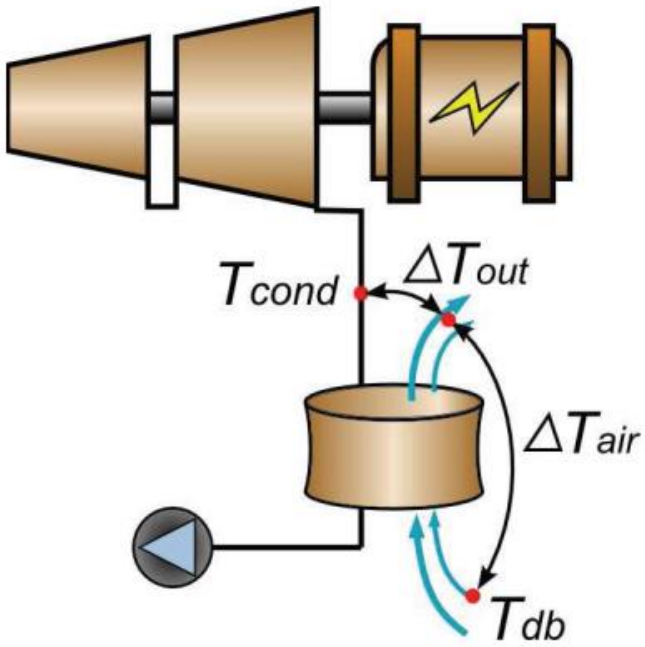


Figure 3. 11: Illustration of temperature variations influencing condenser pressure (NREL, 2011)

From the figure 3.11 above:

$$T_{cond} = T_{db} + T_{ITD}$$

Where $T_{ITD} = \Delta T_{out} + \Delta T_{air} = \Delta T_{out} + \frac{Q_{rej}}{m_{air}\, x\, C_{p,air}}$, $T_{db} = dry\ bulb\ temperature$ – with selected temperature being 3-5% of maximum summer conditions (Padillar, 2011).

The fan power is proportional to the enthalpy increase across the fan. Assuming that the ambient air behaves as ideal gas – no thermodynamic irreversibility – output isentropic temperature of the fan is given as (NREL, 2011):

$$T_{fan,out,s} = T_{fan,in}\, x\, r_p^{\frac{R}{C_{p,air}}}$$

Where $T_{fan,in} = T_{db}$, $R = gas\ constant\ for\ air$, $r_{p,cond} = condensor\ pressure\ ratio$

The isentropic enthalpy at fan outlet is determined as a function of the isentropic temperature and the actual outlet enthalpy is determined after considering the isentropic fan efficiency as shown below:

$$h_{fan,out} = h_{fan,in} + \frac{h_{fan,out,s} + h_{fan,in}}{\eta_{fan,s}}$$

Where $\eta_{fan,s} = isentropic\ enthalpy\ fan\ efficiency$ , $h_{fan,in} = fan\ inlet\ enthalpy$, $h_{fan,out,s} = isentropic\ fan\ outlet\ enthalp$

Therefore, the parasitic fan power is equal to:

$$W_{fan} = \frac{m_{air}\, x\, (h_{fan,out} - h_{fan,in})}{\eta_{fan}}$$

Where $\eta_{fan} = actual\ fan\ efficience$

**Heat transfer fluid (HTF)**

Majority of installed PTC solar power plants use an indirect system with the HTF (typically synthetic oil) exchanging thermal energy to a secondary circuit (Batuecas et al, 2017). Synthetic oil is limited on the operating temperature limits hence limiting the power cycle efficiency. Direct systems use molten salts, which have higher operating temperature limits, hence improved power cycle efficiency (Batuecas et al, 2017). In that regard, molten salts (Hitec Solar Salt) will be used as the HTF for this project. The properties of the salt together with that of a typically used synthetic oil (for comparison) are shown in the table 3.10 below:

Table 3. 10: Properties of Heat Transfer Fluids (SAM, 2020)

| **Name** | **Type** | **Minimum operating temperature / oC** | **Maximum operating temperature / oC** | **Freezing point / oC** |
|---|---|---|---|---|
| Hitec Solar Salt | Nitrate salt | 238 | 593 | 238 |
| Therminol VP-1 | Mixture of Biphenyl and Diphenyl Oxide | 12 | 400 | 12 |

However, one of the disadvantages of Hitec Solar Salt is the need for freezing point protection which leads to increased operations and maintenance cost (by employing a complicated HTF system which require power) and a drop in solar field efficiency.

**Optimum mass flow for HTF in the field**

The mass flow rate of the HTF determines the pressure exerted on the pipes/tubes with the pressure drop above the allowable limit from the HTF has the ability burst the pipes (SAM, 2020). Also, the number of collectors in the loop (hence loop configuration) will depend on the value of the mass flow rate. The procedure recommended in SAM help manual and videos is to iteratively solve pressure loss equations of a pipe. The procedure is described as follows (SAM, 2020):

1. **Establish a reference pressure loss for a smooth pipe**

   The reference pressure loss for smooth pipes (at maximum allowable HTF velocity) used in the SAM software to model CSP parabolic trough is 1610 Pa

2. **Calculate HTF mass flow rate using energy balance equations**

   Absorption energy balance - $Q_{loop} = A_{sca} x\, \eta_{sca} x\, N_{sca} x\, I_{bn}$

   Heat added to the loop - $Q_{loop} = m_s\, x\, C_{sp}\, x\, \triangle_T$

   Rearranging gives - $m_s = \frac{A_{sca}\, x\, \eta_{sca}\, x\, N_{sca}\, x\, I_{bn}}{C_{sp}\, x\, \Delta_T}$

   Where: $A_{sca} = Area\ of\ collector$ , $\eta_{sca} = collector\ efficiency$ , $N_{sca} = number\ of\ collectors$ , $I_{bn} = design\ point\ DNI$ , $m_s = mass\ flow\ rate$ , $C_{sp} = specific\ heat\ capacity$ , $\Delta_T = temperature\ difference$

   The number collectors are initially estimated, and latter refined by iterations.

3. **Calculate the reference length and iterate until convergence on reference pressure**

   Velocity of mass flow rate - $V_s = \frac{m_s}{\rho_s\, x\, \pi\, x\, (R^2)}$ , where R is the radius of tube/pipe and $\rho_s = density\ of\ HTF\ (salt\ in\ this\ case)$

   Calculate Reynolds number – $Re = \frac{\rho_s\, x\, V_s\, x\, 2R}{\mu_s}$ , where $\mu_s\ is\ the\ viscocity\ of\ HTF$

   Look up for friction factor on moody chart (given in Appendix E) for smooth pipe

   Solve the pressure loss equation in a pipe for length - $L = \frac{\Delta P_{ref}\, x\, 4R}{\rho_s\, x\, (V_s^2) x\, f}$ , where L is the reference length (used as a factor to scale the number of collectors), $\Delta P_{ref}$ is reference pressure and *f* is friction factor.

   The new reference length is used to update the number of collectors and process repeated until convergence on reference pressure.

The described above process was carried out in SAM official video tutorial for maximum HTF flow rate and minimum HTF flow rate at 950W/m$^2$ design point DNI using Hitec solar salt as HTF and produced the following results:

- Number of collectors = 14
- Maximum HTF flow rate = 12.8 kg/s
- Minimum HTF flow rate = 1.75 kg/s

The figure 3.12 below shows the collector configuration (a single loop of 14 assemblies) used for this model based on the parameters above:

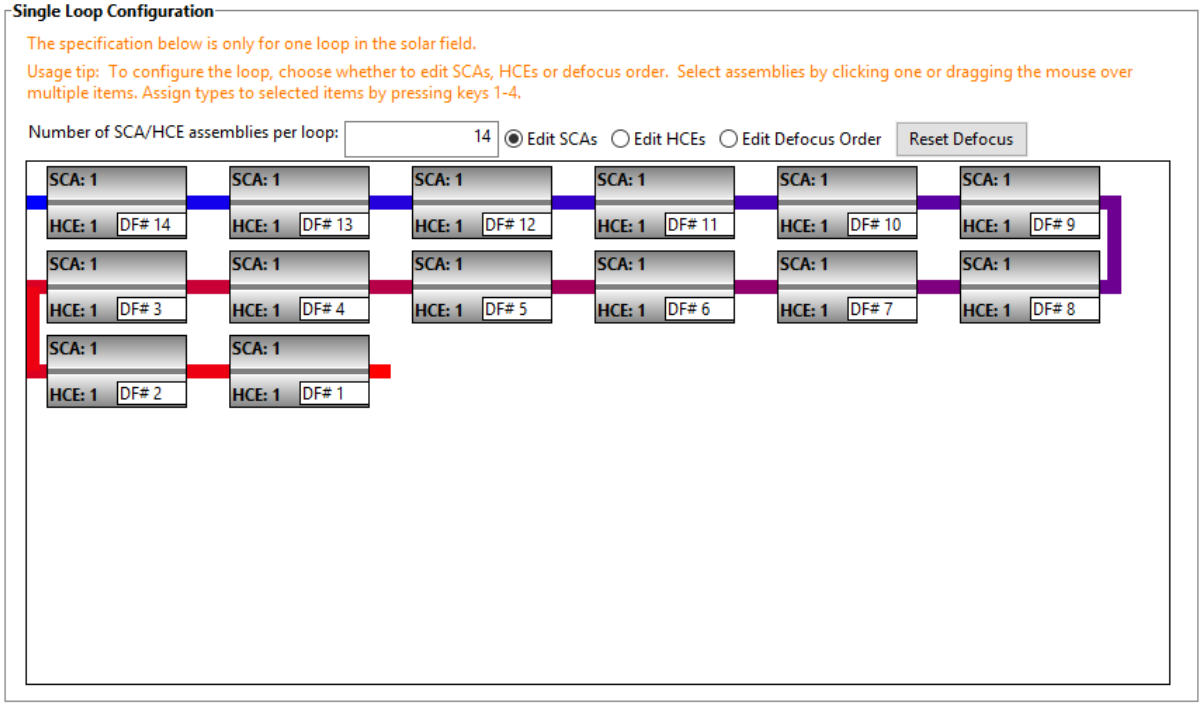


Figure 3. 12: A single loop of 14 collector assemblies

The table 3.11 below shows most of the specifications used to model the parabolic trough CSP system in SAM:

Table 3. 11: Technical parameters for CSP (SAM, 2020)

| Subsection | Parameter | Description |
|---|---|---|
| Solar field | Solar multiple (Option 1) | Parametric analysis to determine – 1 to 4 with 0.25 steps |
| | Number of field subsections | Parametric analysis to determine – 1 to 12 |
| | HTF pump efficiency | 0.85 |
| | Irradiation at design point | Parametric analysis to determine – 700 to 1000 W/m^2 with steps of 20 |
| | Design loop inlet temperature / C | 295 |

| | | |
|---|---|---|
| | Design loop outlet temperature /C | 550 |
| | Water usage per wash (L/m^2) | 0.7 |
| | Number of SCA per loop | 14 |
| Collectors (SCAs) | Configuration type | Solargenix SGX-1 |
| Receivers (HCEs) | Configuration type | Schott PTR80 |
| Power cycle | Design gross output | 32MW |
| | Estimated gross to net conversion | 0.9 |
| | Rated cycle conversion efficiency (Rankine) | 0.4 |
| | Condenser type | Air cooled |
| | Ambient temperature at design point / C | 32 |

### 3.6.2 Economic parameters for CSP

The commercial model used for this system is the same as with PV system described in section 3.4.2 above. The table 3.12 below show the economic parameters for the CSP system to calculate the LCOE, Net Present Value and payback period.

Table 3. 12: Economic parameters for CSP (Turchi et al, 2019)

| **Description** | **Unit** | **Value** |
|---|---|---|
| Solar field | USD/m$^2$ | 150 |
| Site improvements | USD/m$^2$ | 25 |
| Heat Transfer Fluid | USD/m$^2$ | 60 |
| Power plant | USD/kW | 910 |
| Balance of Plant | USD/kW | 32 |
| Contingency | % | 3 |
| Land cost | USD/acre | 11000 |
| Sales tax | % | 5 |
| **Operations and Maintenance** | | |
| Fixed cost | USD/kW-year | 66 |
| Variable cost by generation | USD/MWh | 4 |
| **Financial parameters** | | |
| Project life | Years | 25 |
| Inflation rate | % | 2.5 |
| Discount rate | % | 6.4 |
| Interest rate | % | 5 |

## 3.7 CSP + Thermal Energy Storage (TES)

### 3.7.1 Capacity design

Just like the PV + Battery system described in section 3.5, the main aim of adding thermal energy storage is to assess the potential of performing time of use arbitrage and reducing the risk of losing grid power due to load-shedding (or paying the uninterrupted charge). The storage hours of the system and solar multiple are the two main design parameters of the CSP + TES system. A parametric analysis will be carried out optimise the two design parameters based on LCOE and the ability of the system to supply the load during the risk period of load-shedding on a typical good day for CSP production.

Besides the solar multiple, the CSP + TES will utilise the CSP technical and commercial parameters as described in section 3.6. A direct system where molten salts are used both as a heat transfer fluid and storage will be utilised for this project because of improved efficiency advantage over indirect system. The table 3.13 below describes the TES technical (and economic) parameters to be utilised:

Table 3. 13: TES technical and Economic parameters (SAM, 2020)

| Parameter | Units | Value |
|---|---|---|
| Storage fluid | - | Hitec Solar Salt |
| Storage hours | hrs | Parametric analysis to determine – 1 to 14 with steps of 1 |
| Solar Multiple | - | Parametric analysis to determine – 1 to 4 with 0.25 steps |
| Tank orientation | - | Parallel |
| Tank height | m | 15 |
| Parallel tank pairs | - | 2 |
| Cold tank heater temperature set point | $^{o}$C | 238 |
| Hot tank heater temperature set point | $^{o}$C | 525 |
| **Economic parameter** | | |
| Storage cost | USD/kWht | 62 |

### 3.7.2 Dispatch Control

The CSP + TES system will dispatch energy from 7am to 9pm (peak and standard periods) with the off-peak period (11pm to 6am) - when the tariff is cheap - is left for the grid alone. The figure 3.13 below shows the dispatch control for the system implemented in SAM – period 1 shows when CSP + TES can dispatch power to the load with grid power able to fill in the shortfall while period 2 show that the system output will be zero hence the grid covering the load alone.

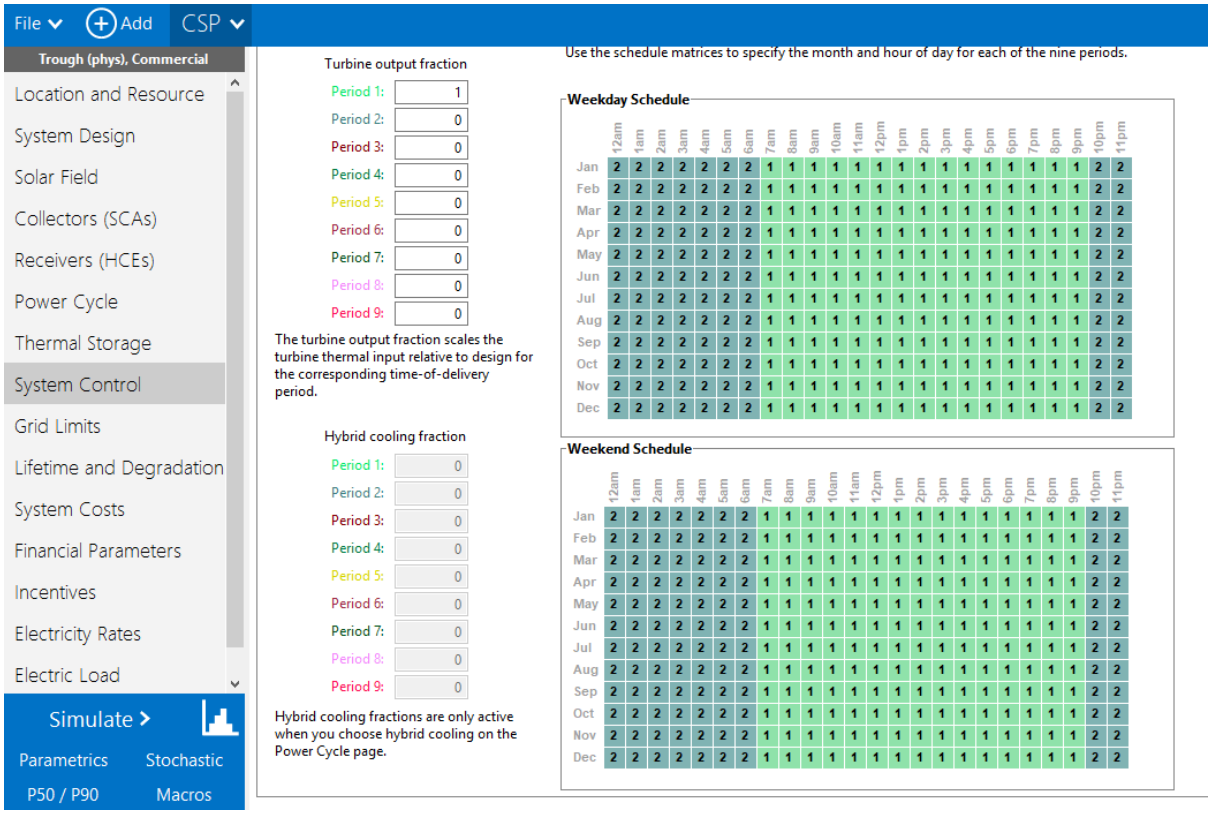


Figure 3. 13: Dispatch control for CSP + TES in SAM

### 3.7.3 Parasitic losses for CSP + TES in SAM

Several critical components require electrical energy to operate in a CSP plant which includes tracking devises, fans, pumps, and site lighting (NREL, 2011). This power is siphoned off from the plant generator output before it reaches the grid or load. If the plant is not actively producing power (like at night or overcast periods), then this power must be sourced from the grid or any other external source. The table 3.14 below shows losses accounted for in SAM in a CSP + TES model:

Table 3. 14: Parasitic losses for CSP + TES in SAM (NREL, 2011)

| Loss | Sub-system |
|---|---|
| Tracking device power consumption | Solar field |
| Solar field HTF pumps | Solar field |
| Piping freezing protection | Solar field |
| Storage HTF pumps | Storage |
| Balance of plant | Controller |
| Auxiliary heater operation | Controller |
| Heat rejection equipment | Power cycle |
| Storage heat trace heater | Storage |

### 3.7.4 Practical considerations for CSP + TES plant

#### 3.7.4.1 Solar collector

The desired features of parabolic trough collectors are given below (NREL, 2020):

- High reliability and availability

- Good optical and thermal efficiency
- Stiff structure to maintain optical performance
- Strong enough to withstand adverse weather conditions like strong wind, earthquakes
- Low initial cost and maintenance requirements

The chosen SGX-1 collector for this model has the following practical advantages (NREL, 2007):

- 50% fewer parts than DS-1 collector
- 30% lighter
- Less time required for field assembly
- Low cost extruded parts

#### 3.7.4.2 Receivers

The most important parameter of receivers are reliability and long lifespan. Receiver failure rates can be attributed to breakages and hydrogen build-up (which increase thermal losses) (NREL, 2011). Breakages are mainly caused by mirrors breaking and falling on the receiver, torque from ball joints, and operational problems like HTF flow rate causing build-up of HTF hence increasing the pressure on the receiver. Hydrogen from the breakdown of HTF tends to build-up in the receiver's vacuum annulus. Hydrogen is a good heat transfer medium hence any build up will increase the thermal losses to the glass envelope (NREL, 2020).

The chosen receiver for this model, Schott PTR 80 is equipped with sufficient getter material to capture hydrogen for at least 25 years (Schott Solar, 2020). The receiver has also improved the glass to metal seal design to reduce breakages (Schott Solar, 2020).

#### 3.7.4.3 HTF

The HTF system include the HTF pump, valves, piping, ullage system, instrumentation and control, and auxiliary heating system (NREL, 2020). The table 3.15 below summarises the common practical challenges of the HTF system and suggested best practices:

Table 3. 15: Potential challenges and best practices on HTF (NREL, 2020)

| Subsection | Potential challenge | Best practice |
|---|---|---|
| HTF pumps | • Pump failure affecting plant availability<br>• Lack of variable frequency drives (VFD) damaging HTF control valves | • Installation of (n+1) pumps to increase plant reliability<br>• VFD driven pumps reduce the duty and stress of solar field control valves |
| HTF valves | • External valve leakage | • Bellows sealed bonnet valves preferred<br>• Shroud-less bellows seal design valve |
| Ullage system | • Inability to remove by-products associated with degradation of HTF like hydrogen | • Installation of high and low boilers and hydrogen treatment design capable of treating HTF for the life of the project |

| | | |
|---|---|---|
| | | • The system should have the capability to remove water in the HTF |
| HTF instrumentation and control | • HTF flowmeter malfunction | • Installation of quality and reputable brands |
| Auxiliary HTF heaters | • Wrong sizing | • The heater should be designed larger than the minimum capacity required to start up and maintain load on turbine |

### 3.7.4.4 TES

The table 3.16 below summarises potential challenges and best practises when using molten salts as a TES:

Table 3. 16: Potential challenges and best practices on TES (NREL, 2020)

| Subsection | Potential Challenges | Best practice |
|---|---|---|
| Chemical composition | • Corrosion issues due to presents of chlorine<br>• Inorganic impurities clogging pipes, valves, pumps, and heat exchangers | • Use salt consisting of a total chloride concentration below 0.1%<br>• The salt should free of impurities |
| TES tank | • Corrosion issues | • Installation of corrosion monitoring systems – like ultrasound measurements of tank wall thickness |
| Process design | • Difficulty to control mass flow rate of HTF during start-up and during TES - Solar transition<br>• Complexity and availability challenges from using external heating system | • Installation of VFD salt pumps and split ranges controls to manage HTF flow rates during transition, start-up, and normal operation<br>• Bayonet heaters installed in tank walls preferred.<br>• Good salt circulation also needed to mix and distribute the heat |

### 3.7.4.5 Power cycle and balance of plant

The table 3.17 below shows typical challenges and corresponding best practices for CSP power block and balance of plant:

Table 3. 17: Typical challenges on CSP power cycle and balance of plant (NREL, 2020)

| Subsection | Potential Challenge | Best practice |
|---|---|---|
| Steam generation | • High stress on heat exchangers during start up | • Installation of bypasses on high pressure feedwater heaters recommended |
| Steam turbine | • Low start-up efficiency | • Consider thicker turbine castings (hence hold heat much better) to improve start-up time<br>• Heating blankets can also be considered but a cost benefit analysis needed to justify the investment |
| Generator | • Complexity of maintaining hydrogen system at remote areas – hence complicating operations and maintenance of hydrogen cooled generators | • Consider using air cooled generators |
| Electrical system | • Lack of emergency power system – equipment in the solar field could be damaged due to loss of power | • Consider installing Uninterruptable Power System (UPS) or hydraulic accumulators to power solar field drive units in case of loss of power |

## 3.8 System with Exports

### 3.8.1 Technical consideration

The current transmission line supplying the mine is rated at 132kV, 100MVA feeding into 2 x 20MVA, 132kV/11kV transformers connected in parallel. The maximum demand (according to 2015 figures) at the mine is 28.4MW. Taking these figures into consideration, the grid exports from the renewable system will be limited to 60MW for this analysis. The table 3.18 below shows the procedures taken to analyse the systems:

Table 3. 18: Methodology to simulate system with exports

| System | Description |
|---|---|
| PV | • The system will use the generic and optimised parameters for the base case scenario as described in section 3.4<br>• The desired PV plant capacity will be determined by parametric analysis. The analysed range is from 20MW to 120MW in steps of 5MW |
| PV + Battery | • The system will inherit the generic and optimised parameters for the base case scenario as described in section 3.5<br>• The battery being simulated is behind the meter hence exports from the hybrid system will be from excess PV |

| | |
|---|---|
| | generation. Behind the meter batteries in SAM are used to meet the load and cannot export energy to the grid<br>• The desired battery capacity (storage capacity) and the corresponding plant size will be determined by parametric analysis. Battery storage size ranges from 2hours to 14hours in steps of 1hr and PV plant size ranges from 55.5MWdc to 185MWdc in steps of 18.5MW |
| CSP | • The system will inherit the generic and optimised parameters for the base case scenario as described in section 3.6<br>• The desired gross power output and solar multiple will be determined by parametric analysis. Gross power output will range from 20MW to 60MW with 10MW steps and solar multiple will range from 1 to 4 with steps of 0.25 |
| CSP + TES | • The system will inherit the generic and optimised parameters for the base case scenario as described in section 3.7<br>• The desired gross power output, solar multiple and thermal storage hours will be determined by parametric analysis. Gross power output will range from 30MW to 75MW with steps of 5MW, solar multiple will range from 1 to 4 with steps of 0.25, and thermal storage hours will range from 1hr to 14hrs in steps of 1hour |

### 3.8.2 Economic consideration

Net billing will be used to compensate the energy generated by the renewable system. In SAM, the difference between generated energy and load in each simulation time step over a month is evaluated. For months with excess generation, the dollar value of the excess generation is credited to the month's bill with the value of credit determined by the sale rate. The usual procedure to determine the sale rate is through Power Purchase Agreement with the Utility provider. However, for this analysis an assumption will be made to equate the sale rate and time of use tariff as described in section 3.3.1.

# 4.0 Results and Discussion

## 4.1 PV System Results

### 4.1.1 Tilt angle optimisation

A parametric study was performed to determine the optimum tilt angle for the site. The figure 4.1 below shows the variation of annual energy produced and LCOE for 37MW DC PV plant with tilt angle. The annual energy increases with tilt angle increase (0 – 20º) from 53.1GWh to 55.1GWh. Once the tilt angle is greater than 20º, the annual energy starts to decrease. The curve for LCOE is a mirror image of the annual energy with its lowest value (US$0.048 / kWh) at tilt angle of 20º. This result is consistent with literature review which pointed out that the latitude of the site is usually the optimum angle hence the tilt angle of 20º will be used in the model.

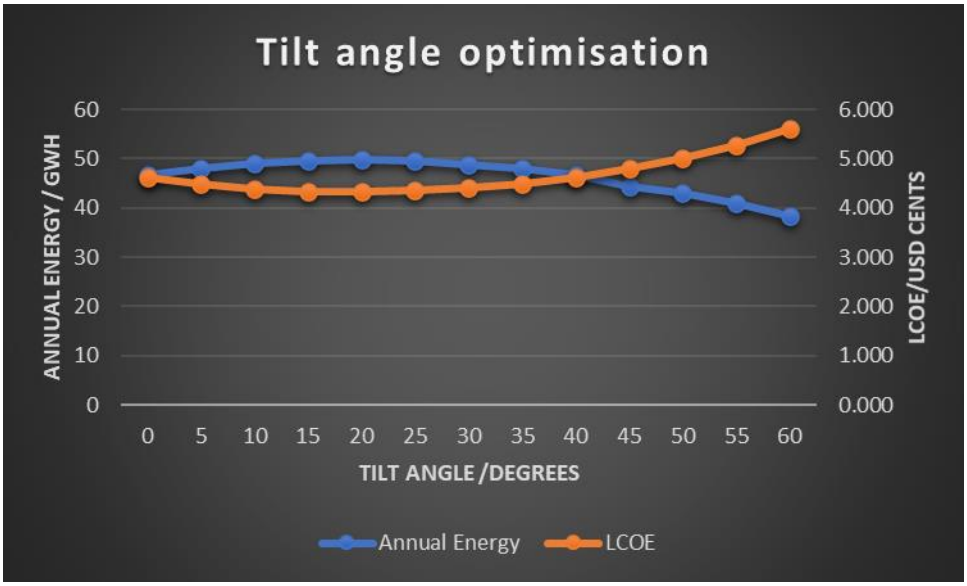


Figure 4. 1: Variation of annual energy and LCOE with tilt angle

### 4.1.2 Azimuth angle optimisation

The highest energy generated was found at azimuth angle of $0^0$ (North facing) and together with the lowest value of LCOE as shown in the figure 4.2 below. This is consistent with the literature review that the best orientation for PV plants in the southern hemisphere should be facing the North.

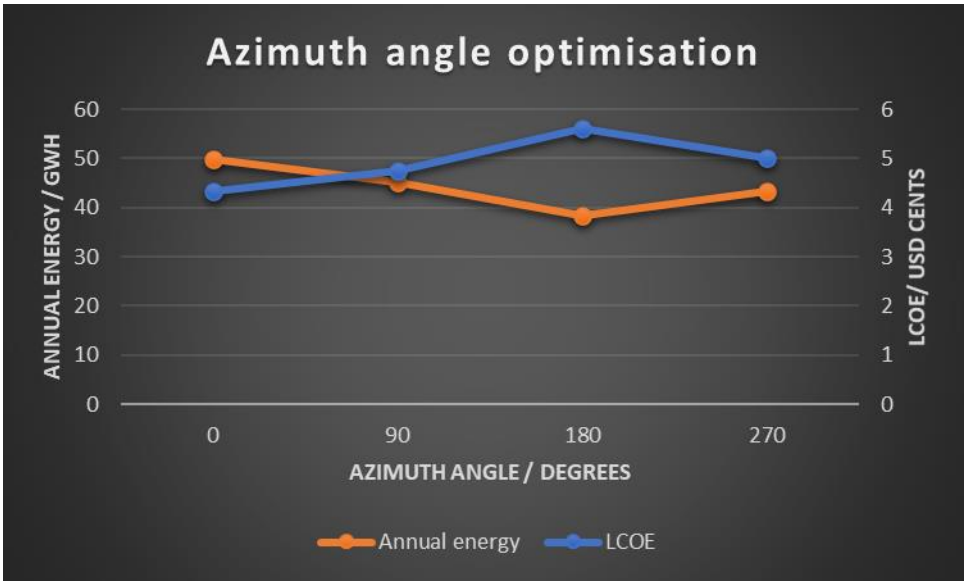


Figure 4. 2: Variation of annual energy and LCOE with azimuth angle

### 4.1.3 Interrow distance optimisation

The interrow distance is inversely proportional to the Ground Cover Ratio (GCR). This defined as the area between PV modules and total ground area. The figure 4.3 below shows the variation of annual energy generated and LCOE with GCR. The annual energy generated shows that as the GCR reduces (hence interrow distance increases) the annual energy increases steadily up to a GCR of 0.45 where it starts to flatten out. This means the lower the interrow distance the more chances of shading leading to reduced generated energy. As the interrow distance increases (GCR decreases), the generated energy will not vary much because the factor of self-shading would have been eliminated.

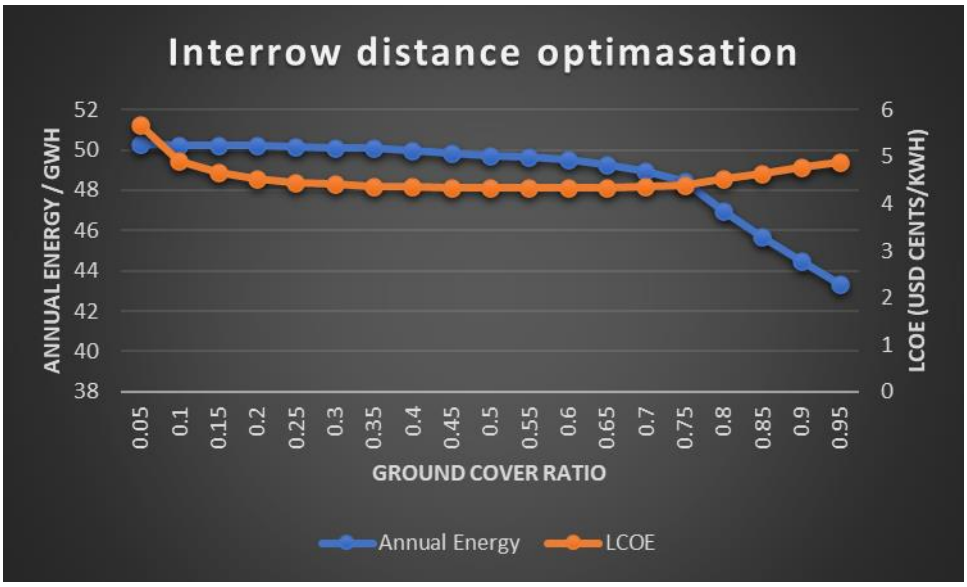


Figure 4. 3: Variation of annual energy and LCOE with Ground Cover Ratio

The LCOE in the above figure 4.3 resembles a bowl or parabolic shape. Very low values of GCR (high values of interrow distance) have a high LCOE even though the generated energy is high. This is because the greater the interrow distance the more land area required thereby

increasing installation cost. On the other hand, high GCR values (low interrow distance) mean more chances of self-shading leading to reduced generated energy which increases the LCOE. The optimum GCR value is the point where annual energy starts to flatten showing that the interrow distance is now just enough to eliminate interrow shading and on this case its 0.45 giving interrow distance of 2.4m.

### 4.1.4 Technical performance of optimised PV model

The simulation of the optimised 37MW DC PV plant predicts an output of 55.13GWh during the first year of operation (lifecycle output is shown in Appendix F). This is approximately 33.3% of the annual demand of the mine. The figure 4.4 below shows the monthly load vs the generated PV energy. The graph for the generated energy shows limited seasonal variation due to the optimisation of the tilt angle.

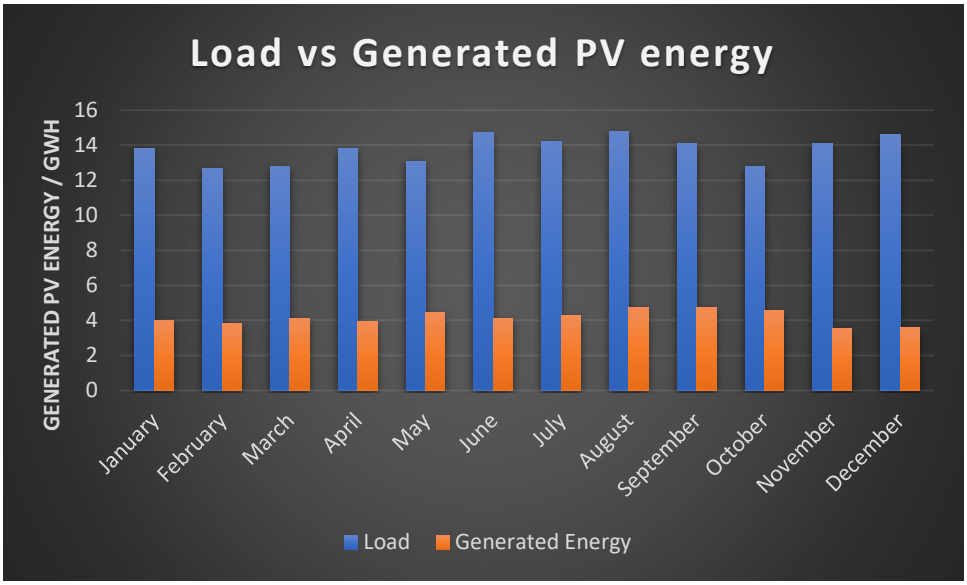


Figure 4. 4: Monthly variation of load vs generated PV energy

The expected capacity factor of the PV plant in the first year is 19% which compares with the 2019 weighted average capacity factor according to IRENA database (IRENA, 2020). The performance ratio of the plant is predicted at 77% with major losses including soiling, module mismatch and cable losses. The most significant loss however is that caused by grid limit (generation exceeding load and no exporting power) which accounted for 10.3%. The full loss diagram is given in Appendix F.

On a typical good PV production day, as shown in the figure 4.5 below, the PV plant is able supply the mine load alone (on this day 23MW) for 4 hours between 9am to 1pm. However, the morning spike is largely being covered by the grid because of the time it occurs (8am) there will be not enough irradiation. The graphs show that on a typical good day, the PV generated could be higher than the energy from the grid from 6am up to 3pm. As expected, the load during the night is supplied from the grid.

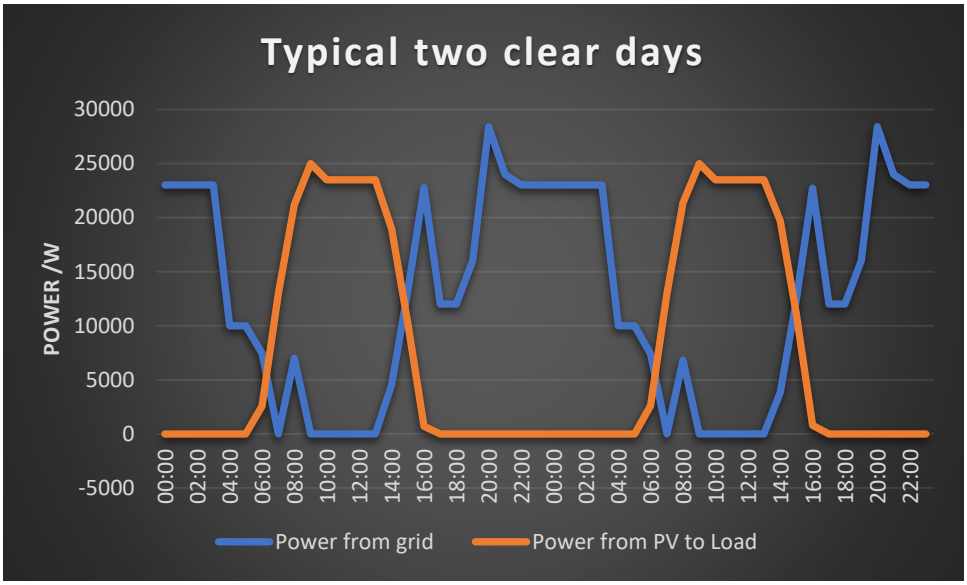


Figure 4. 5: Typical two consecutive days with good PV production

On a typical bad day for PV production, as shown in the figure 4.6 below, the generated PV peak could be as low as 5MW with no point in time where the PV generated is higher than the energy from the grid.

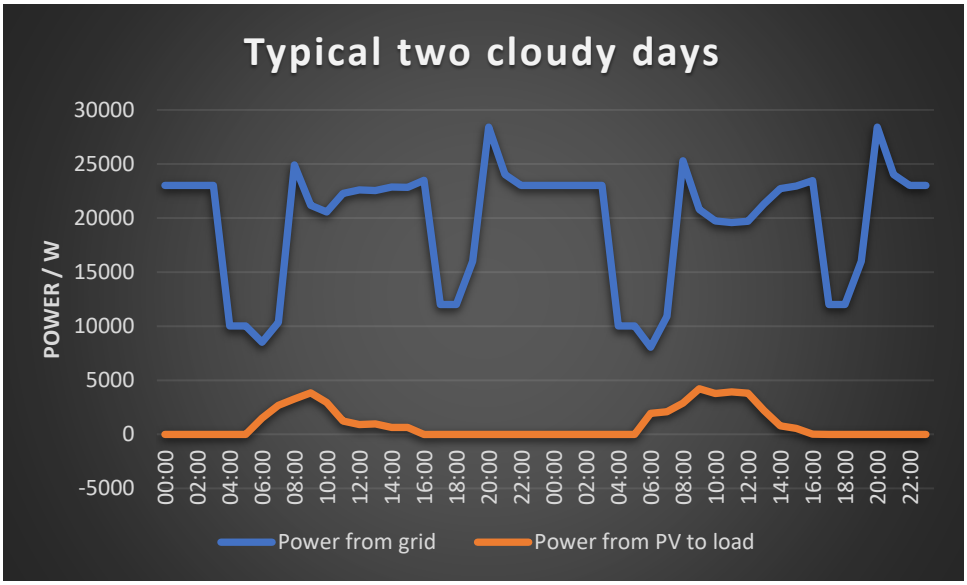


Figure 4. 6: Typical two consecutive days with bad PV production

### 4.1.5 Comparing PVSyst and SAM

For comparison purposes, the identical PV system (37MWdc, 1.05 DC/AC ratio, same PV, and inverter efficiencies) was modelled in PVSyst software version 6.43. The only adjustment that was made is on the grid limitation with the PVSyst allowed to export all the generated energy without limitation from the load profile (the same adjustment was made to the SAM model). The results show that the energy produced from the two software packages differ by only 1.65% with the largest difference being on performance ratio as shown in the table 4.1 below. The summary results from PVSyst simulation is given in Appendix G.

Table 4. 1: Comparison between PVSyst and SAM

| Parameter | SAM | PVSyst | % Difference with reference to PVSyst |
|---|---|---|---|
| Produced Energy (unlimited User) | 61.5 GWh | 60.5 GWh | +1.65% |
| Specific production | 1662 kWh/kW/year | 1632 kWh/kW/year | +1.84% |
| Performance ratio | 77% | 74.5% | +2.5% |

### 4.1.6 Economic performance of optimised PV model

The installation cost of the project is predicted at USD 0.76 per DC Watt which is comparable to the projects done in India in 2019 which had a weighted average installation cost of USD 0.62 per DC Watt (IRENA, 2020). Similarly, the predicted LCOE of this PV system is USD 0.048/kWh which is comparable to the weighted average LCOE of USD 0.045/kWh of projects done in India in 2019 (IRENA, 2020). The predicted Net Present Value of the project is about USD 41Million with a pay-back period of 5.1 years reinforcing the economic viability of this project. The table 4.2 below shows the main economic indicators for this project:

Table 4. 2: Economic performance indicators for the PV system

| Parameter | Unit | Value |
|---|---|---|
| Localised Cost of Energy | USD/kWh | 0.048 |
| Annual Electric Bill without PV system | USD | 13.69 Million |
| Annual Electric Bill with PV system | USD | 8.021 Million |
| Net annual savings | USD | 5.672 Million |
| Net Present Value | USD | 41.39 Million |
| Simple pay back | Years | 5.1 |

The first-year figures show that the annual energy electric bill is reduced from USD13.7 million to 8.02 million. This means by reducing the annual load by about 33.3%, the system will be able to save about 41.4% of the annual electric bill. The difference in two numbers is caused by the fact that the PV System is offsetting the load during the peak and standard tariff periods while the grid electricity is mainly used during off-peak hours. The figure 4.7 below shows the monthly bill of electricity with PV system and without.

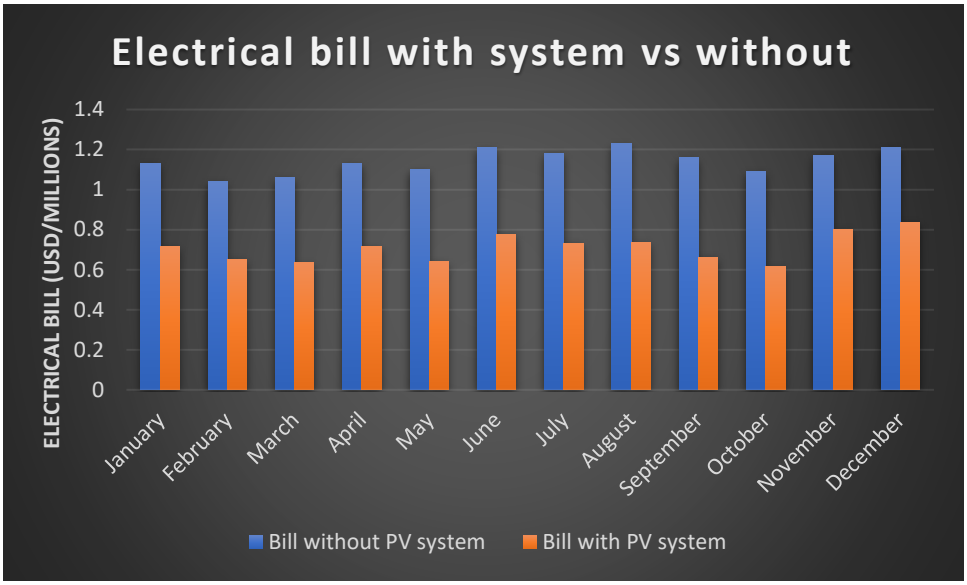


Figure 4. 7: Monthly electric bill with PV system vs without

## 4.2 PV + Battery Results

### 4.2.1 Battery and PV plant capacities optimisation

A parametric analysis was carried out to determine the optimum storage hours (hence battery capacity) and PV size based on the load profile, desired operation and return on investment. The trend from the two figures (figure 4.8 and 4.9) below shows that in general, the smaller the PV plant and the lower the storage hours the more viable the system. PV size ratios of 1.5 and 2 have a positive NPV value for the whole range of storage sizes simulated (2hrs to 12hrs) while the 2.5 PV size ratio is only viable up to 9hrs of battery storage. The PV size ratios from 3 up to 5 are not viable for this designed application for all simulated storage hours. For storage hours, the viability decreases with increase of storage size. The 2hour storage battery has 3 PV sizes viable while the 12hour battery storage is only viable for 2 PV sizes.

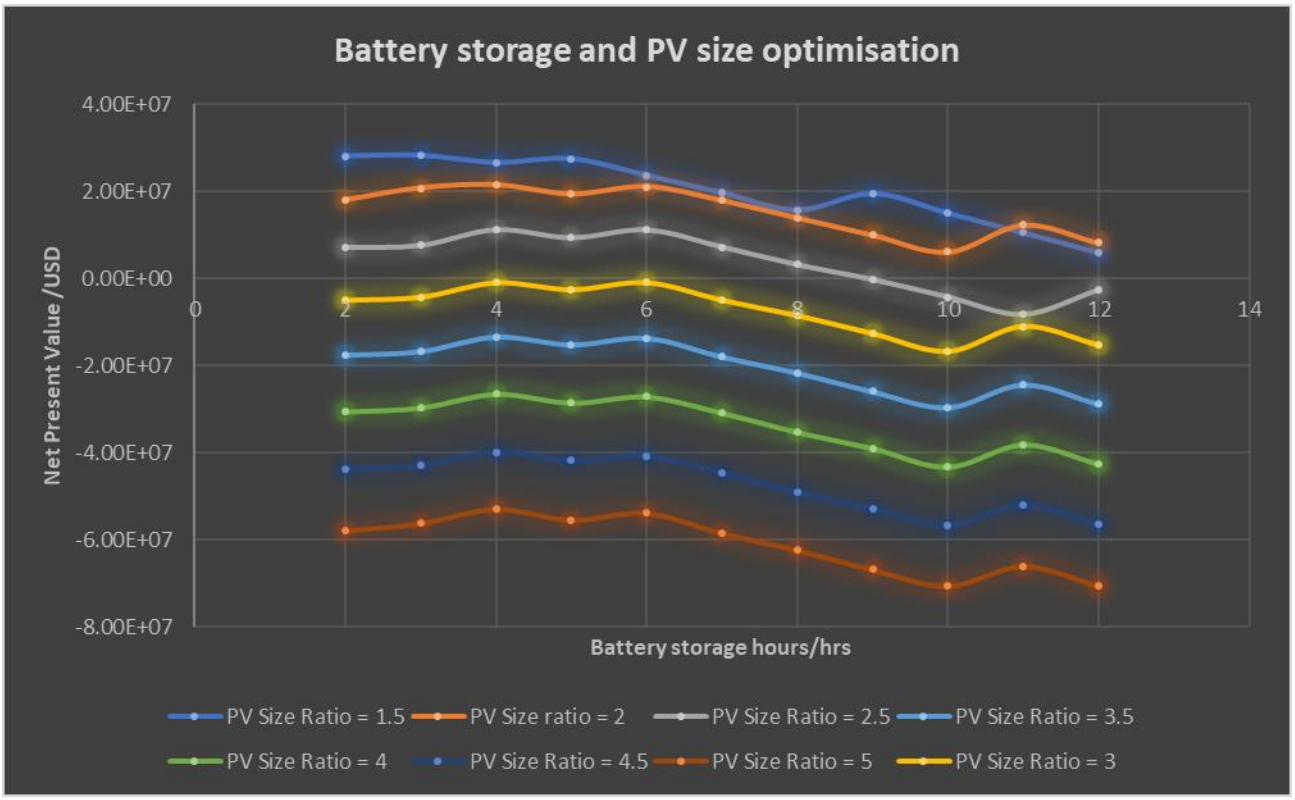


Figure 4. 8: Battery and PV plant capacities optimisation

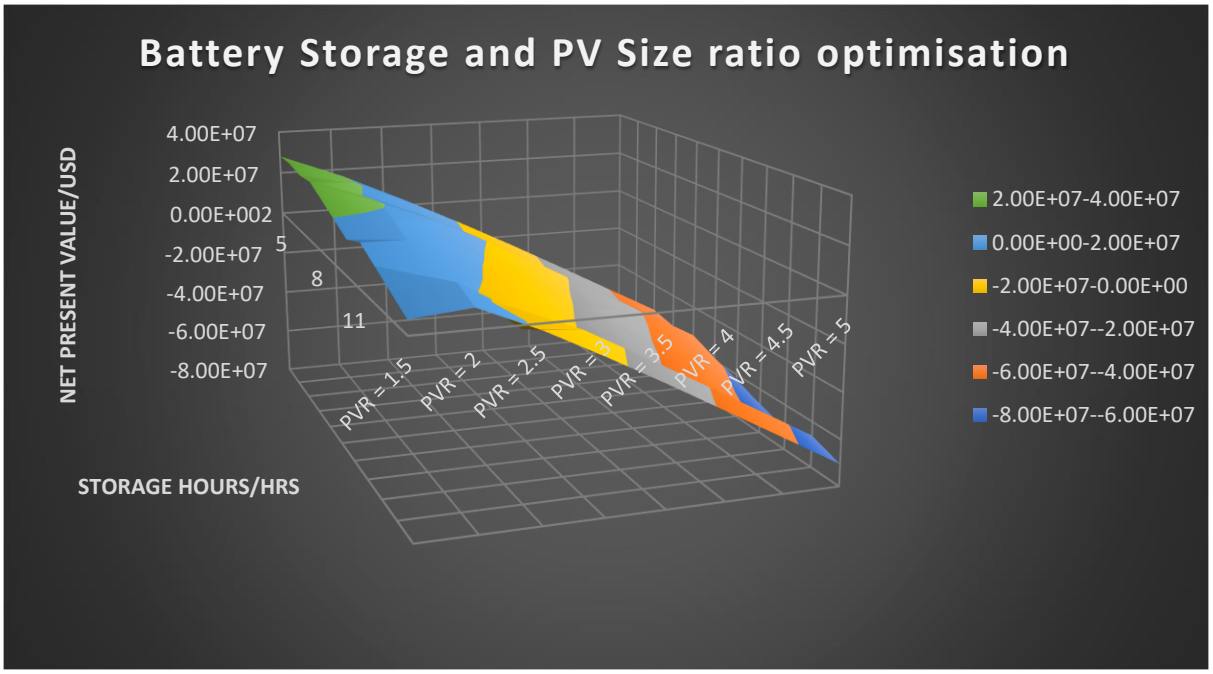


Figure 4. 9: 3D graph showing Battery and PV capacity optimisation

To determine the optimum system for the model, the minimum storage required for the battery to supply load during high risk load-shedding period must be considered. The calculated minimum battery capacity is 190MWh which translate to 6.3hrs of storage (190MWh/30MW). Using the graph above, the chosen battery storage capacity is 7hrs translating to 210MWh (30MW x 7hrs). For 7 hours of storage, the PV ratio sizes of 1.5, 2,

and 2.5 have a positive NPV value. The 2.5 PV size ratio was not chosen because the NPV value was way below for the other two sizes. Although the 1.5 PV size ratio has a slight better NPV value (by approximately USD2 million), the PV ratio of 2 performed better in terms of annual energy produced hence chosen for the model.

The optimum combination chosen is:

- PV size ratio of 2 which translate to 2 x Peak power for PV without storage = 2 x 37MW DC (The designed PV system in section 3.3) = 74MW DC
- Power to Energy ratio of 1:7 translating to 7hrs of battery storage meaning battery capacity of 210MWh

### 4.2.2 Technical performance of the optimised PV + Battery System

The simulation of the optimised 74MW DC PV plant + 210MWh of battery storage predicted an annual energy output of 103GWh in the first year (lifecycle output is shown in Appendix H). This is approximately 63% of the annual mine load – 41% from PV and 22% from battery – as shown in the pie chart below (figure 4.10). The design was meant to cater for the peak and standard periods which constitute about 68% of the load (from the load profile) hence the system was 5% less from the target with the grid covering the slack.

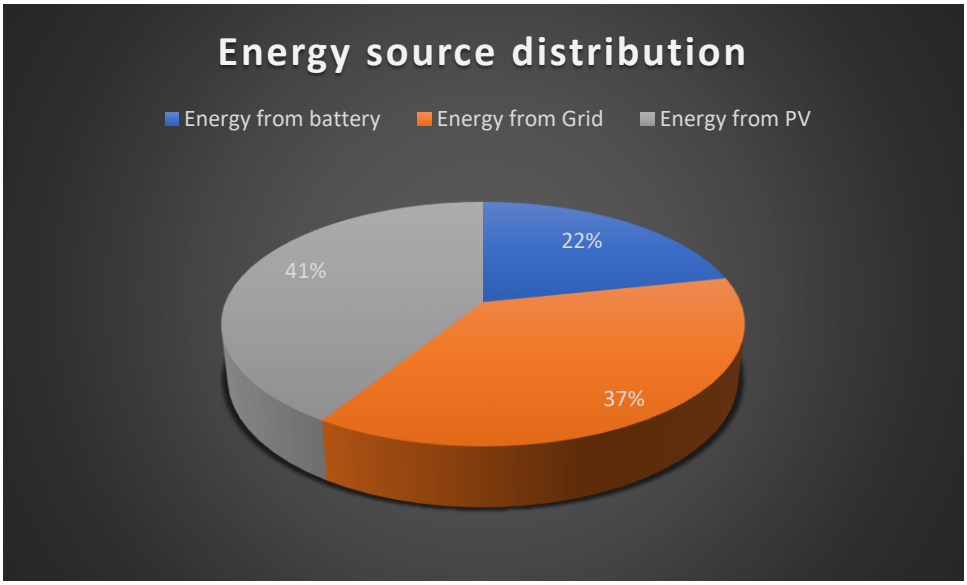


Figure 4. 10: Energy distribution of the PV + Battery System

The expected capacity factor of the system is 18.6% with a performance ratio of 75% and a battery roundtrip efficiency of 92.7%. The losses resembled that of the modelled PV with the addition of the battery losses. As with the PV system, the most significant loss is the grid connection limit with a value of around 13%. The full loss diagram is given in Appendix H.

On a typical good day of PV production, as shown in figure 4.11 below, the hybrid system is able to supply the load over the designed periods (peak and standard). The PV plant will supply the load alone from 7am to 2pm. The Battery and PV plant will supply the load from 2pm up to 5pm then the battery cover alone up to 9pm. The grid will then pick it up from 10pm to 6am which is off-peak period.

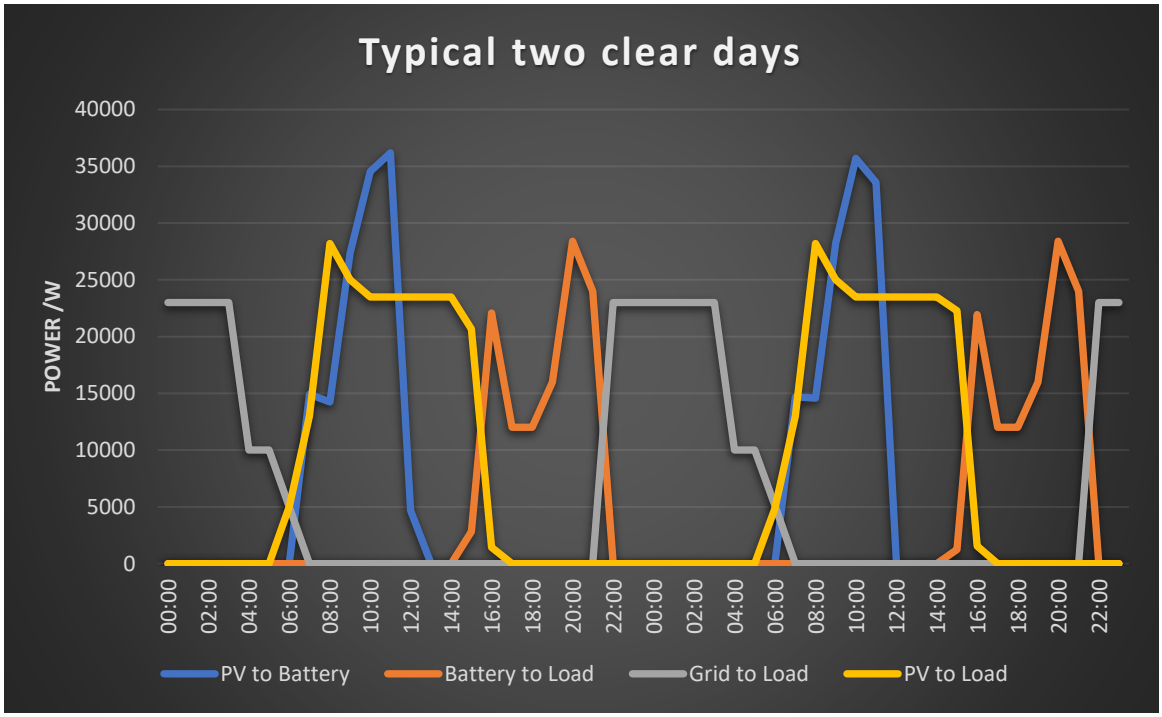


Figure 4. 11: Typical two consecutive days with good PV production

The state of charge of the battery of the same period is shown in the figure 4.12 below. The battery is charged by the PV plant between 7am to 12pm where it would have reached maximum designed state of charge (95%). It would then discharge from 3pm to 9pm reaching a state of charge of 40%.

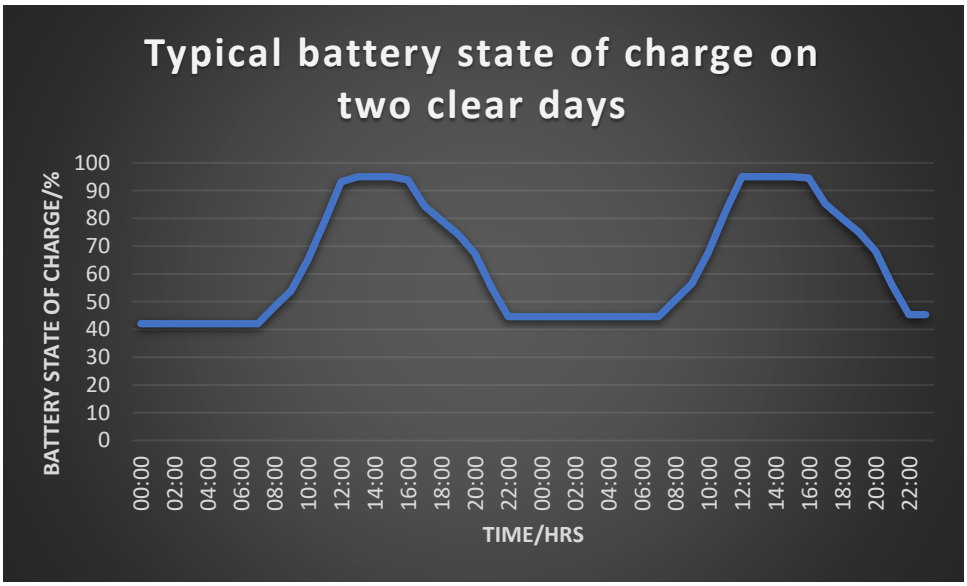


Figure 4. 12: Battery state of charge on two consecutive days with good PV production

On a typical bad day (like cloudy day) for PV production, as shown in the figure 4.13 below, the PV + Battery system only covers the load alone between 7am and 10am on the first day of the period. The grid power will then be used thereafter with a little help from the PV plant in the next day.

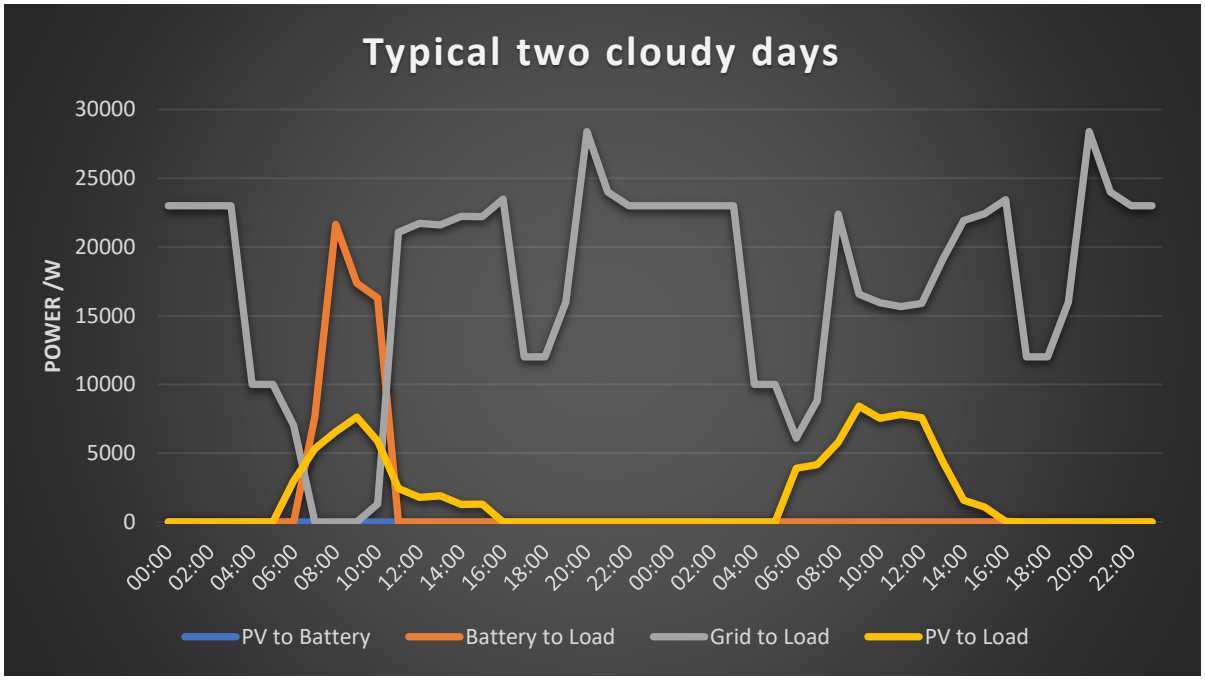


Figure 4. 13: Typical two consecutive days with bad PV production

The state of charge of battery on the same period is shown in the figure 4.14 below. The PV production is not enough to charge the battery and to cover the load. The battery will start discharging from 44% up to 15% which is the minimum designed state of charge between 6am and 11am. The battery will stay in that state up until the PV production is high enough to charge it again.

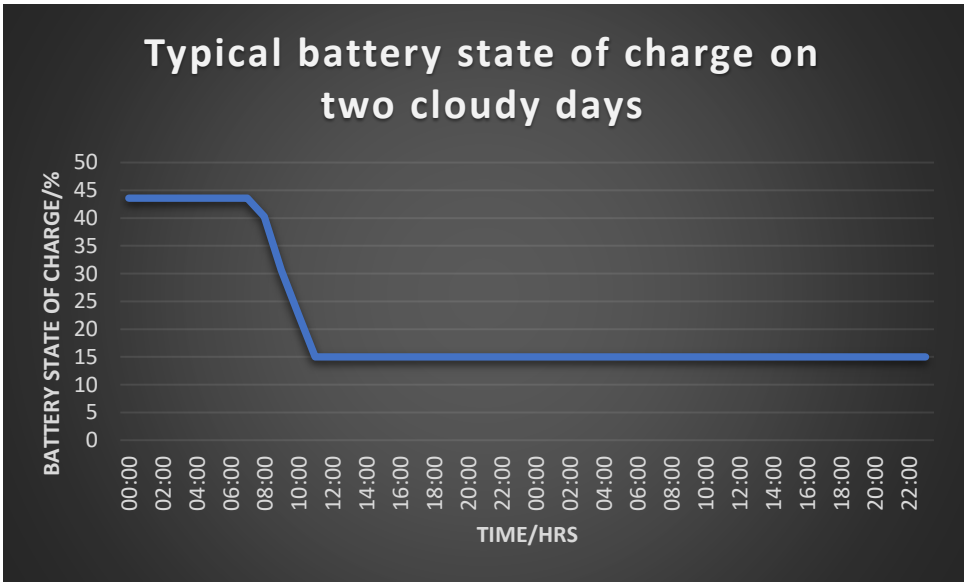


Figure 4. 14: Battery state of charge on two consecutive days with bad PV production

### 4.2.3 Economic performance of optimised PV + Battery System

The installed cost of PV + Battery system is USD 1.5/Wdc with the cost of storage contributing 43.3%. The LCOE of the system is USD 0.106/kWh – this is more than double than that of PV system alone. The predicted simple pay-back period is 10.8 years with an

NPV value of USD 19.26 Million. The table 4.3 below show the main economic indicators of the project:

Table 4. 3: Economic performance indicators for the PV + Battery System

| Parameter | Unit | Value |
|---|---|---|
| Localised Cost of Energy | USD/kWh | 0.106 |
| Annual Electric Bill without PV system | USD | 13.7 Million |
| Annual Electric Bill with PV system | USD | 3.0 Million |
| Net annual savings | USD | 10.7 Million |
| Net Present Value | USD | 19.3 Million |
| Simple pay back | Years | 10.8 |

The first-year simulation results show that the annual electric bill is reduced from USD13.7 million to USD 3 million. This represents about 78% in electric bill reduction after offsetting 63% of the load. As with PV system, the difference in the two figures is because the grid power is mainly used during off-peak period which is cheaper than the periods covered by the PV + Battery system. The graph below (figure 4.15) shows the monthly bill of electricity with PV + Battery and without.

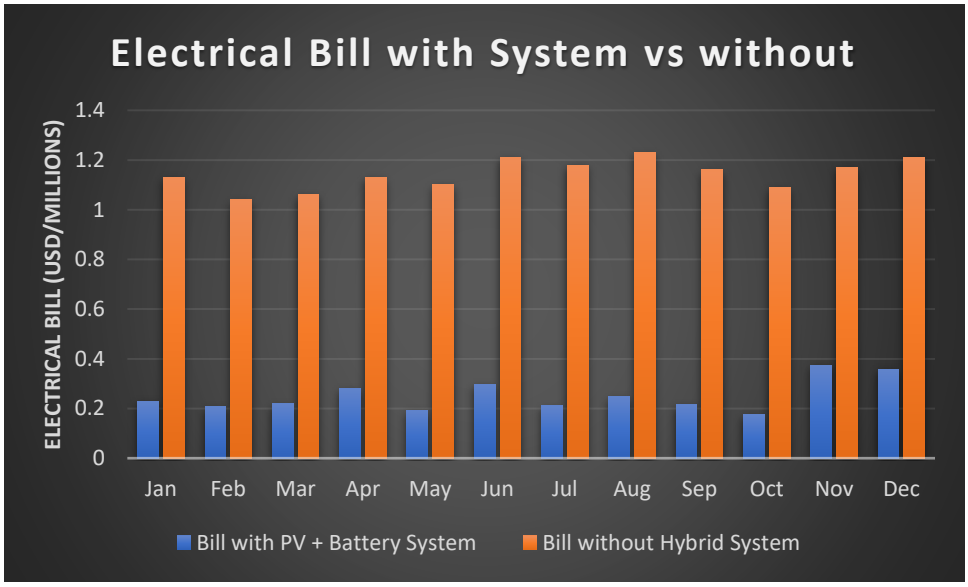


Figure 4. 15: Monthly electric bill with PV + Battery system vs without

## 4.3 CSP Results

### 4.3.1 Design point optimisation

The graph below (figure 4.16) shows the variation of LCOE with design point DNI with minimum LCOE occurring at 860W/m$^2$. Values higher than this DNI have high LCOE because the system is oversized and operates at design capacity for a limited time. Below 860W/m$^2$, the LCOE is higher (even though the is more generated energy) because the solar field area increase with low design point DNI hence increasing the installation cost.

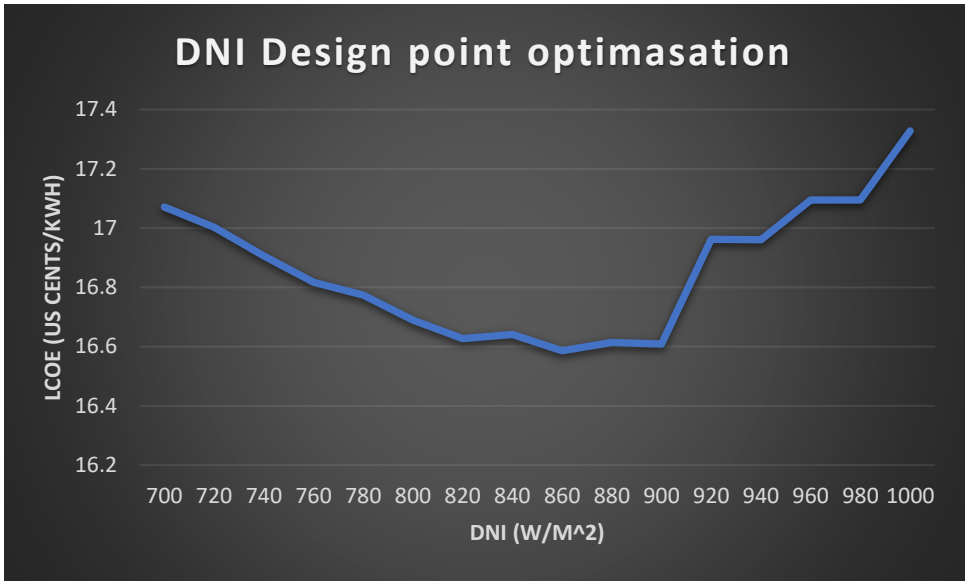


Figure 4. 16: Design point optimisation

### 4.3.2 Solar Multiple optimisation

The optimum solar multiple for the system from the graph (figure 4.17) below is 1.25. This value is consistent with literature review that revealed that a solar multiple of 1.3 is a typical optimum for no storage CSP system. Although the values higher than solar multiple 1.25 have higher energy produced, the increase in land size increases the LCOE.

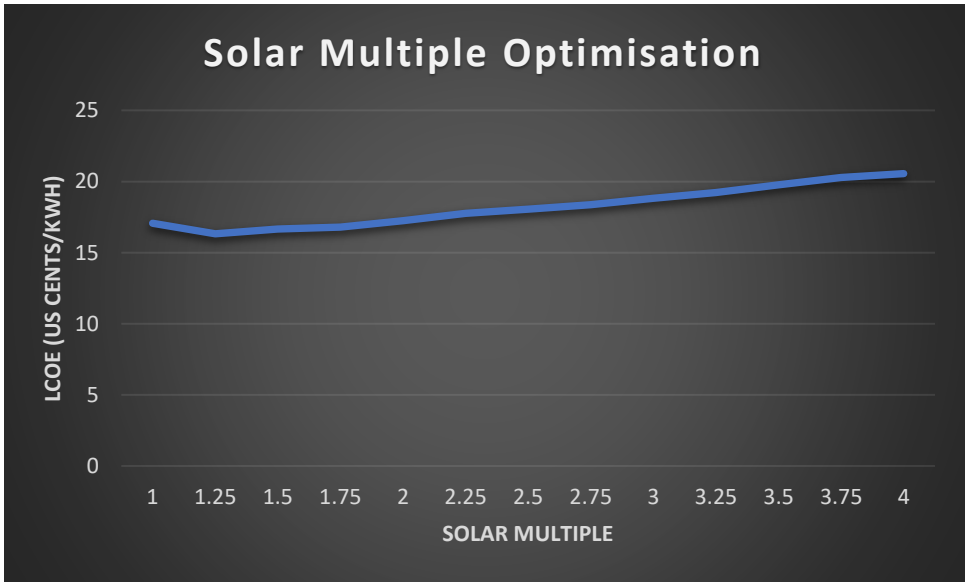


Figure 4. 17: Solar multiple optimisation

### 4.3.3 Field subsections optimisation

The shape and location of header piping delivering heat to the power cycle is determined by the number of field subsections. The orientation will directly affect the amount of heat loss in the pipes. The graph below (figure 4.18) shows that the optimal number of subsections is 2 based on the lowest LCOE and highest generated energy.

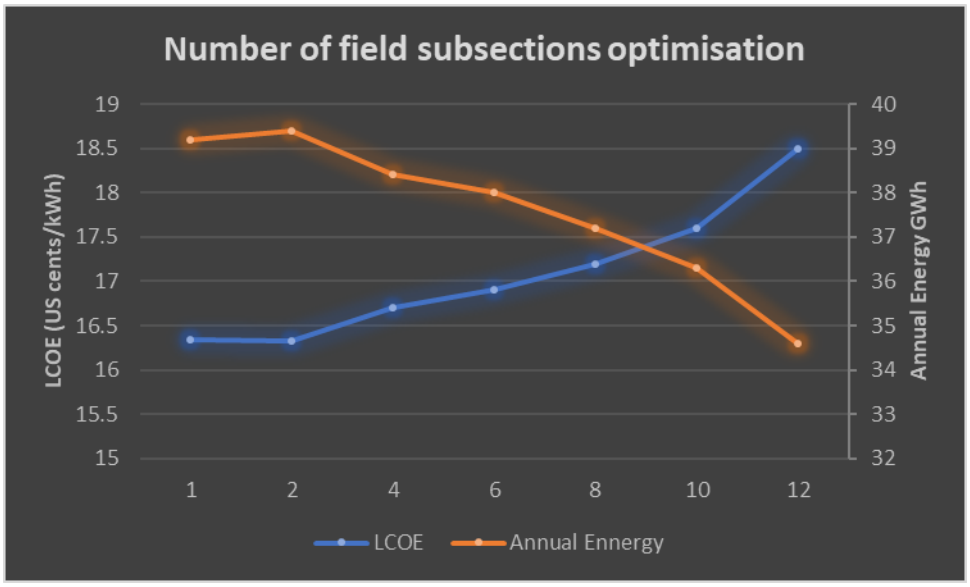


Figure 4. 18: Number of field subsections optimisation

### 4.3.4 Technical performance of the optimised CSP

The simulation of the optimised 32MW gross output, solar multiple of 1.25, and DNI design point of 860W/m$^2$ predicts a net annual electricity energy production of 39.3GWh during the first year of operation (Summary results from SAM are given in Appendix I). This is approximately 23.7% of annual demand of the mine with a capacity factor of 20.6%. The predicted capacity factor compares with figures given in IRENA (2019) for no storage CSP systems which has values ranging from 21% to 23%. The figure 4.19 below shows the monthly production of CSP energy vs the monthly demand of the mine.

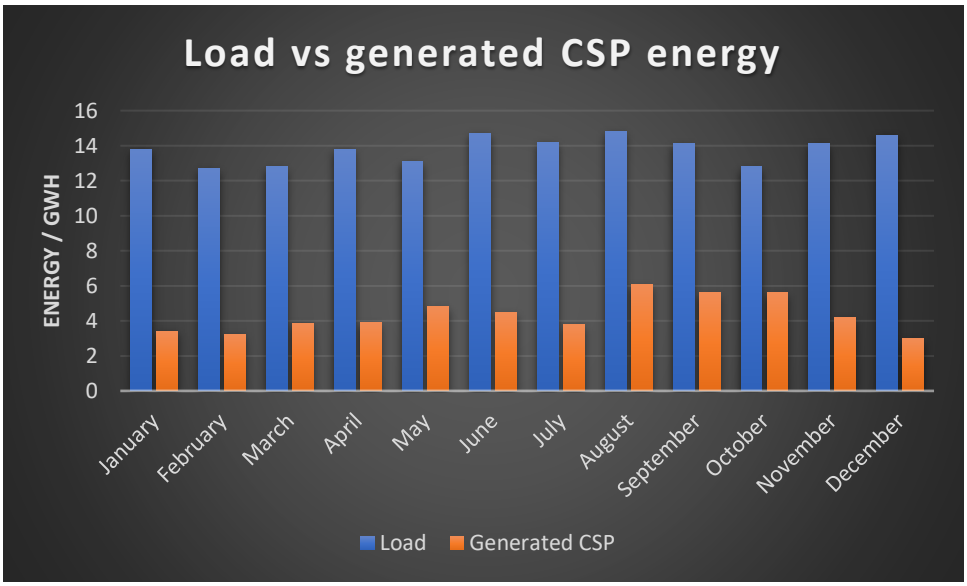


Figure 4. 19: Monthly generated CSP vs monthly demand

On a typical good day for CSP production, as shown in the figure 4.20 below, the system is able to supply the load from 8:00am to 2:00pm. The grid power will start to compliment the CSP after 2:00pm up until 4:00pm where CSP production will fall to zero. From then on, the grid will supply the load up until the next day.

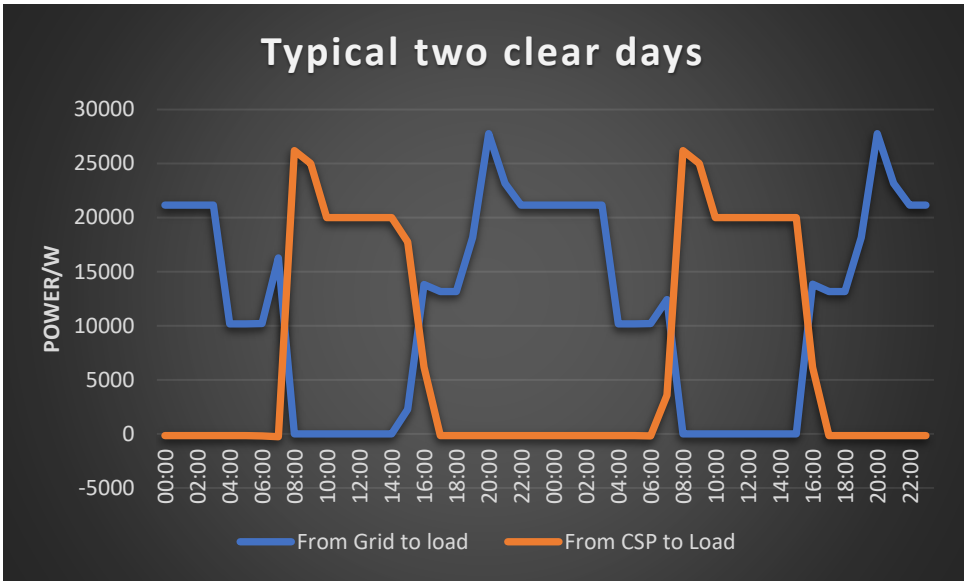


Figure 4. 20: Typical two consecutive days with good CSP production

On a typical overcast day, as shown in the figure 4.21 below, the CSP system will be absorbing power from the grid (for auxiliary circuits) instead of generating. The grid power will supply the load during the day and night.

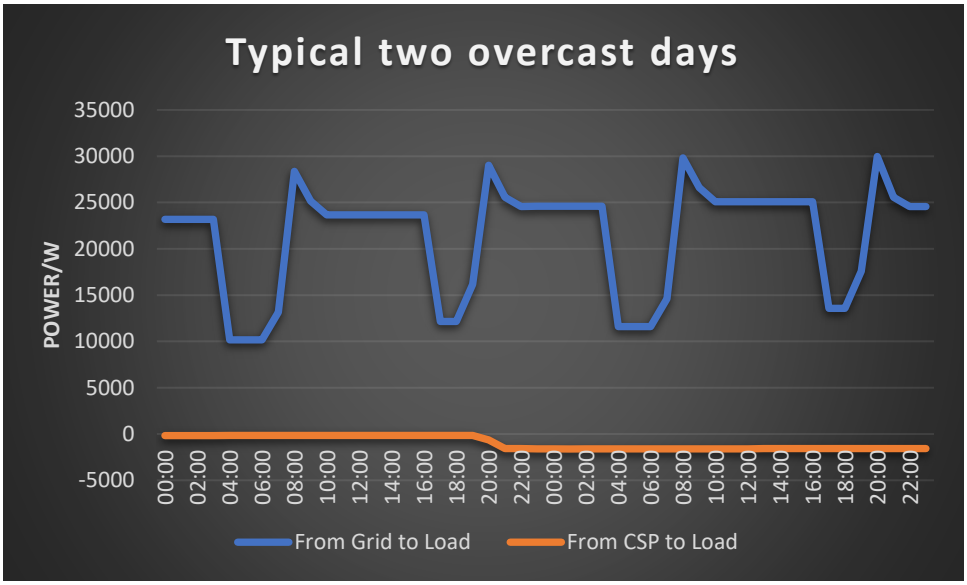


Figure 4. 21: Typical two consecutive days with bad CSP production

### 4.3.5 Economic performance of optimised CSP system

The installation costs of the system are predicted at USD 2479/kW. The IRENA renewable cost database for CSP commissioned in 2019 showed installation costs ranging between USD 3704/kW and USD 8645/kW – with the exception that these figures are for systems with storage hence higher. The predicted LCOE of the system is US cents 16.32/kWh which is slightly lower to the weighted average of LCOE (US cents 18.2/kWh) of CSP system in 2019 (IRENA, 2019). However, the predicted NPV for the system is below zero making it unattractive option to invest. The table 4.4 below show the main economic indicators of the system:

Table 4. 4: Economic performance indicators for the CSP System

| Parameter | Unit | Value |
|---|---|---|
| Localised Cost of Energy | USD/kWh | 0.16 |
| Annual Electric Bill without CSP system | USD | 13.69 Million |
| Annual Electric Bill with CSP system | USD | 9.63 Million |
| Net annual savings | USD | 4.06 Million |
| Net Present Value | USD | -13.6 Million |
| Simple pay back | Years | Not available |

The first-year simulation figures show that the annual electric bill is reduced from USD 13.69 million to 9.63 million. This represents a cost reduction of approximately 29.8% on the annual electric bill after offsetting approximately 23.7% of the annual load. The figure 4.22 below shows the monthly bill of electricity with PV system and without.

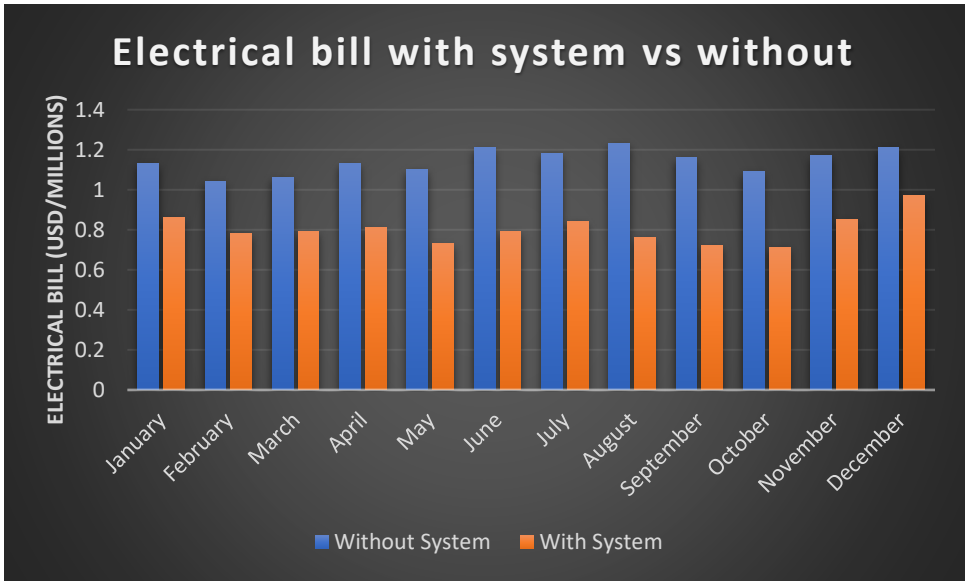


Figure 4. 22: Monthly electric bill with CSP system vs without

## 4.4 CSP + TES Results

### 4.4.1 Storage hours and Solar multiple optimisation

A parametric analysis was carried out to determine the optimum storage hours and solar multiple based on the load profile, location, desired dispatch and LCOE. The trends from the two figures below (figure 4.23 and figure 4.24) show that for low values of SM (1 – 1.5) the LCOE varies linearly, with a positive gradient, with TES storage hours. For solar multiple 2 – 4, low values of TES storage hours have high LCOE values which starts to decrease with increase in storage hours. The optimum values of LCOE occur between storage hours between 5 – 6 before the trend starts to increase gradually with increase in storage hours. This is because at low values of storage hours, the energy produced will be too low to justify the investment (the system will be undersized). At high values of storage hours, although the energy produced will be high, the system will be oversized for the application hence higher values of LCOE. From the analysis, optimum LCOE occurs at SM = 2.5 and storage hours of 5 hours.

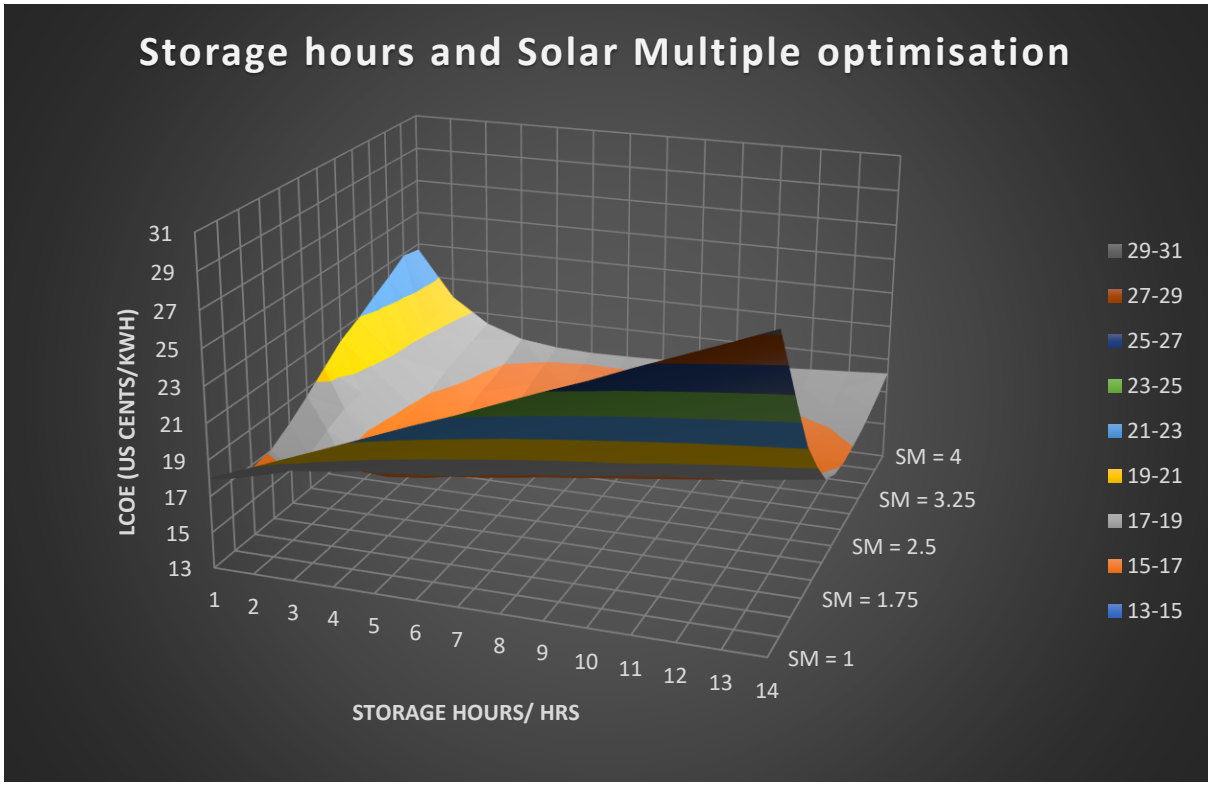


Figure 4. 23: 3D graph showing optimisation of storage hours and solar multiple

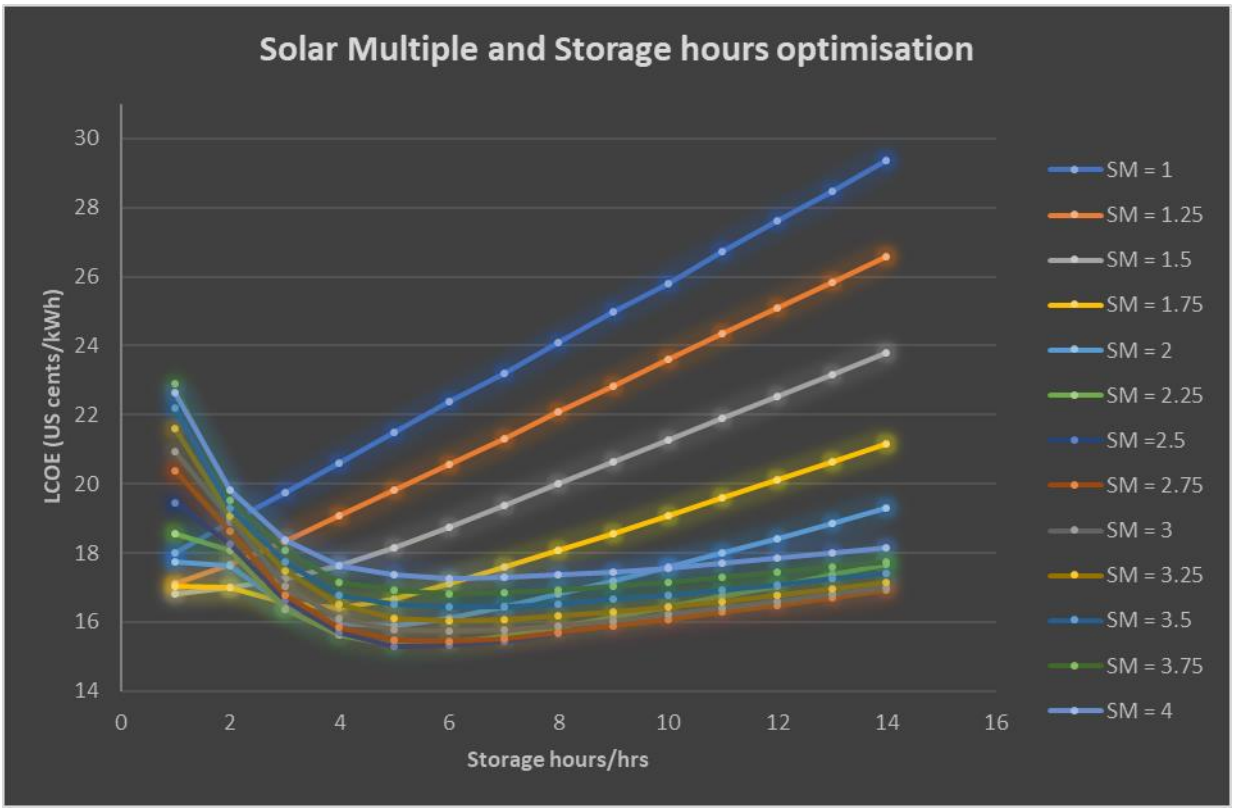


Figure 4. 24: Solar multiple and storage hours optimisation

For the system to cover the high-risk period from load shedding, the required storage hours are 6.3 hours (calculated in section 4.2.1). Therefore, the optimum SM and storage hours

chosen for this project is 2.5 and 7 hours respectively – this combination has the lowest LCOE at TES values greater than 6.3 hours.

### 4.4.2 Technical performance of the optimised CSP + TES system

The simulation of the optimised 32MW gross output, solar multiple of 2.5, storage hours of 7hrs at design point of 860W/m$^2$ predicts an net annual electricity production of 68.4GWh during the first year of operation (summary results from SAM are given in Appendix J). This is approximately 41.3% of annual demand of the mine at a capacity factor of 40.5%. The predicted capacity factor compares with figures given in IRENA (2012) for SM 2.5 and storage of 7 which has values ranging from 42 – 45%. The figure 4.25 below shows the monthly production of CSP + TES system vs the monthly demand of the mine:

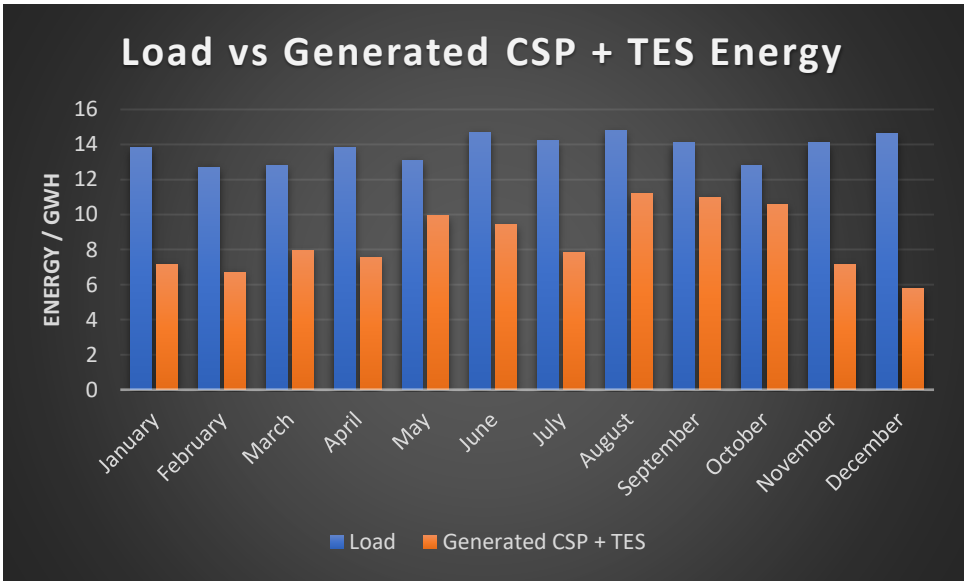


Figure 4. 25: Monthly generated energy from CSP + TES vs monthly load

On a typically good day for CSP production, as shown in the figure 4.26 below, the CSP + TES system is able to supply the load (without the grid) over the designed periods (7am to 9pm). The grid will supply the load during off-peak hours.

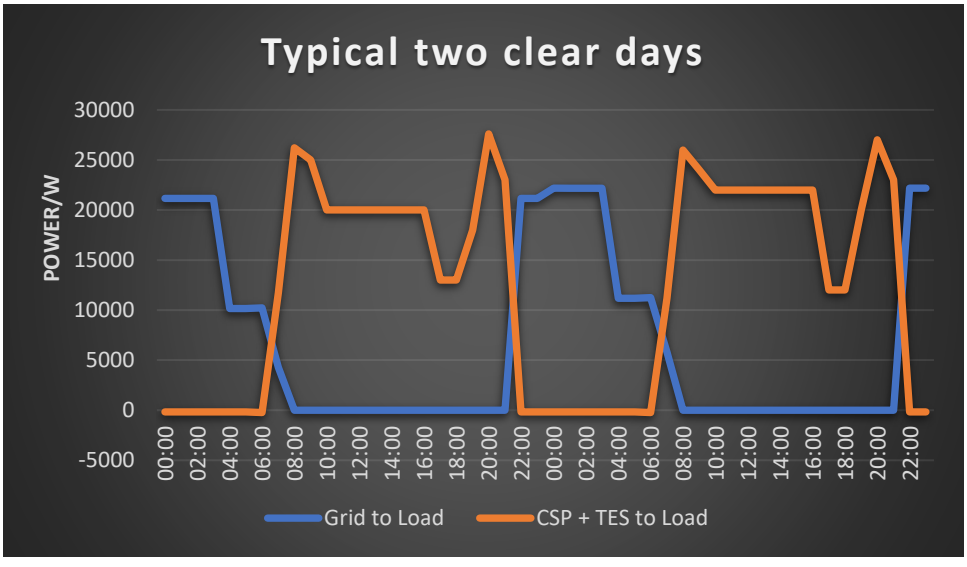


Figure 4. 26: Typical two consecutive days with good CSP production

The state of charge of TES on a typical good day is shown in figure 4.27 below. The graph shows that the TES briefly discharges in the morning from 7am – 8am before being charged from 8am to 12pm where it reaches a capacity just above 500 MWht. The TES will start to discharge from 3pm to 10pm reaching a capacity of approximately 200MWht.

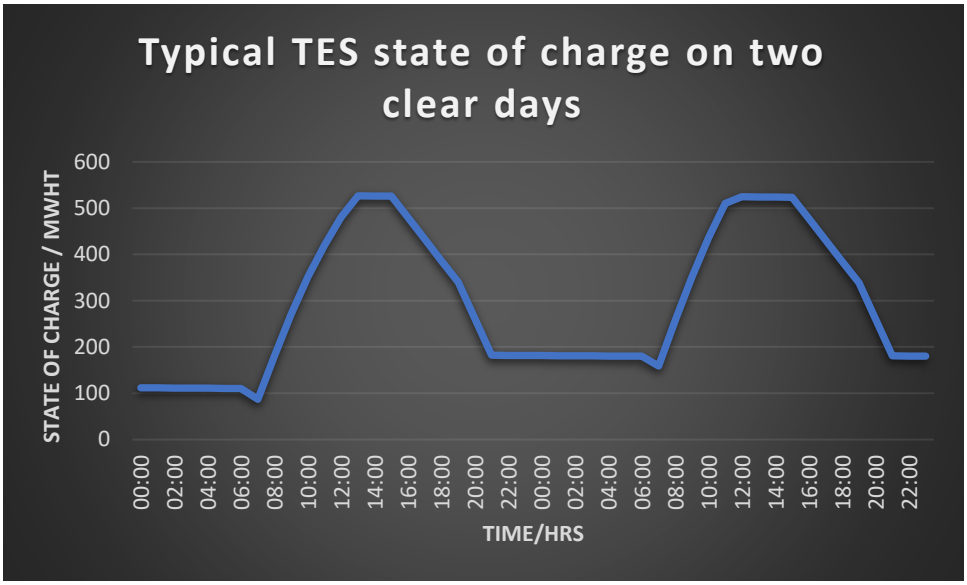


Figure 4. 27: TES state of charge on two consecutive days with good CSP production

On a typical overcast day, as shown in the figure 4.28 below, the CSP + TES system only supply the load from 6am to 8am from storage before the grid power covers the slack. The following day, the grid supplies the load without any contribution from CSP + TES system.

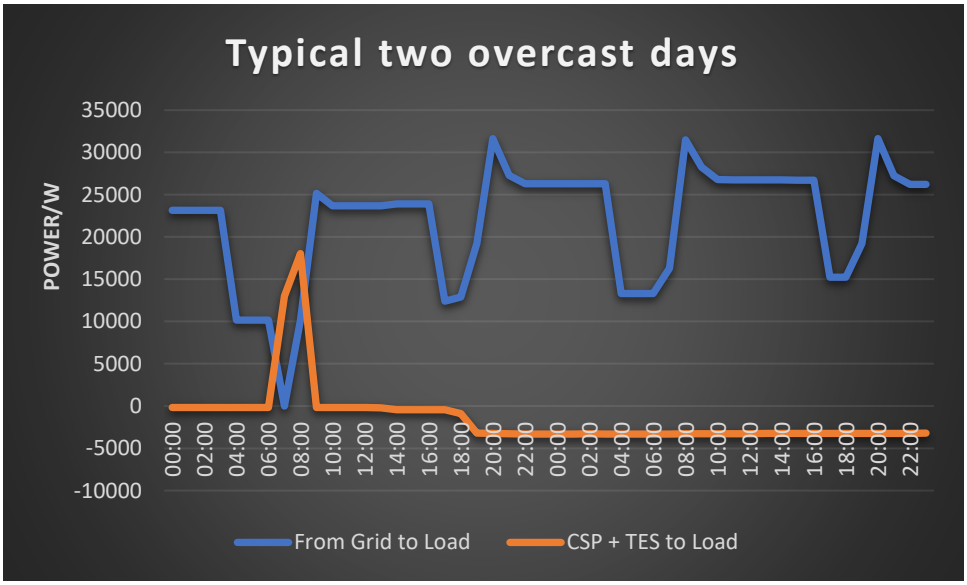


Figure 4. 28: Typical two consecutive days with bad CSP production

The state of charge of a typical overcast day is shown in the figure 4.29 below. The graph shows that the TES discharges from a capacity of 100 MWht to zero between 6am to 8am. The state of charge is maintained the following day up until the system receives direct irradiation

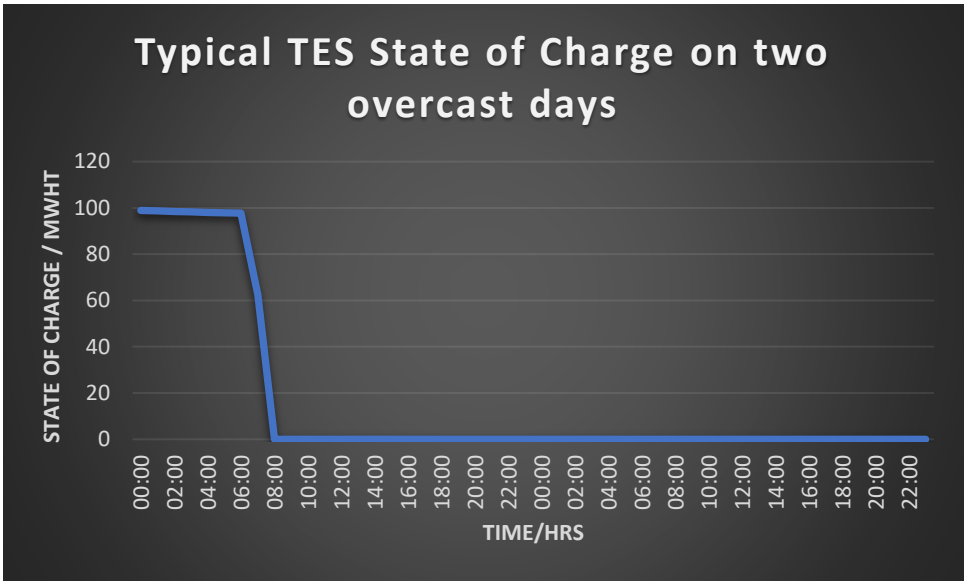


Figure 4. 29: TES state of charge on two consecutive days with bad CSP production

### 4.4.3 Economic performance of optimised CSP + TES system

The installation cost of the CSP + TES system is predicted at 5593.7/kW. This value is comparable with IRENA database for CSP systems commissioned in 2019 which showed installation cost ranging between USD 3704/kW and USD 8645/kW (IRENA, 2019). The predicted LCOE of the system is US cents 15.44/kWh which is lower to the weighted average LCOE (US cents 18.2/kWh) of CSP systems commissioned in 2019. However, the predicted simple payback period is 20.9 years with a negative NPV value making the system unattractive option to invest. The table 4.5 below shows the main economic indicators of the system:

Table 4. 5: Economic performance indicators for the CSP + TES System

| **Parameter** | **Unit** | **Value** |
|---|---|---|
| Localised Cost of Energy | USD/kWh | 0.15 |
| Annual Electric Bill without CSP system | USD | 13.69 Million |
| Annual Electric Bill with CSP system | USD | 6.54 Million |
| Net annual savings | USD | 7.15 Million |
| Net Present Value | USD | -17.3 Million |
| Simple pay back | Years | 20.9 |

The first-year simulation figures show that the annual electric bill is reduced from 13.69 million to 6.54 million. This represents a cost reduction of approximately 52.2% on the annual electric bill after offsetting approximately 41.3% of the annual load. The figure 4.30 below shows the monthly bill of electricity with CSP + TES system and without.

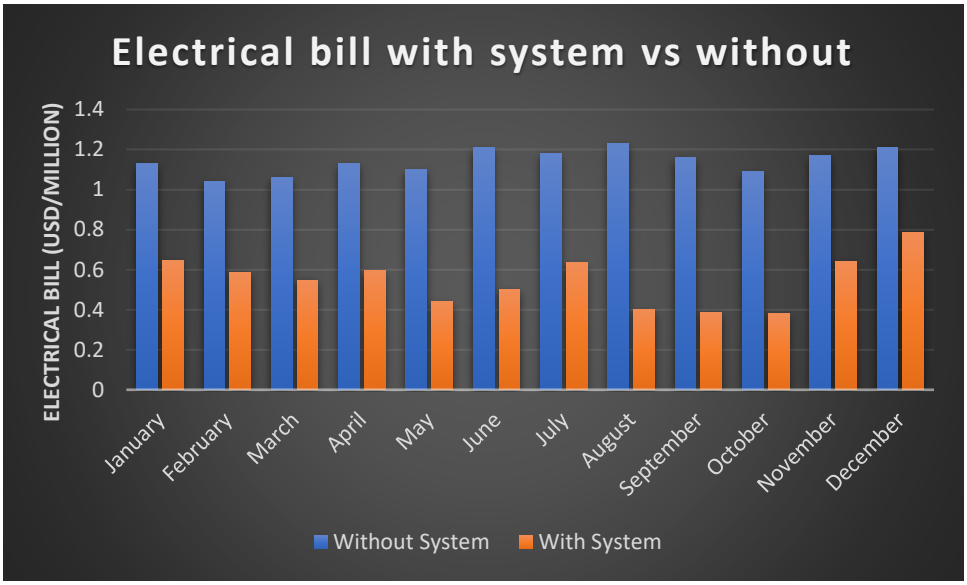


Figure 4. 30: Monthly electric bill with CSP + TES system vs without

## 4.5 Uncertainty and Sensitivity analysis for base case scenario

Assumptions were made to the cost of parameters used in the above models. Uncertainty and sensitivity analysis were carried out on each model to understand how uncertainty influence the optimal design and to identify the most influential uncertain parameter. The parameters were modelled over 100 samples using Monte Carlo technique in SAM software.

### 4.5.1 PV System

The table 4.6 below shows the cost parameters that were allowed to vary in the PV system:

Table 4. 6: Uncertain parameters for PV system

| Parameter | Base cost | Distribution | Standard deviation |
|---|---|---|---|
| Module cost | USD 0.30/Wdc | normal | 50% |
| Inverter cost | USD 0.05/Wac | normal | 20% |
| Balance of Plant cost | USD 0.17/Wdc | normal | 15% |
| Land cost | USD 11000/acre | normal | 50% |

The table 4.7 and graph (figure 4.31) below show the results of the uncertainty analysis. The 90% confidence interval from the analysis ranges from US cents/kWh 3.12 to 6.05 for LCOE. The NPV and simple pay back graphs are given in Appendix K.

Table 4. 7: Results of uncertainty analysis for PV system

| | Mean | Variance | P05 | P95 |
|---|---|---|---|---|
| LCOE (US cents/kWh) | 4.76 | 0.77 | 3.12 | 6.05 |
| NPV (USD) | 4.14E+07 | 2.14E+13 | 34612505 | 50047255 |
| Simple Pay Back (years) | 5.13 | 1.20 | 3.08 | 6.74 |

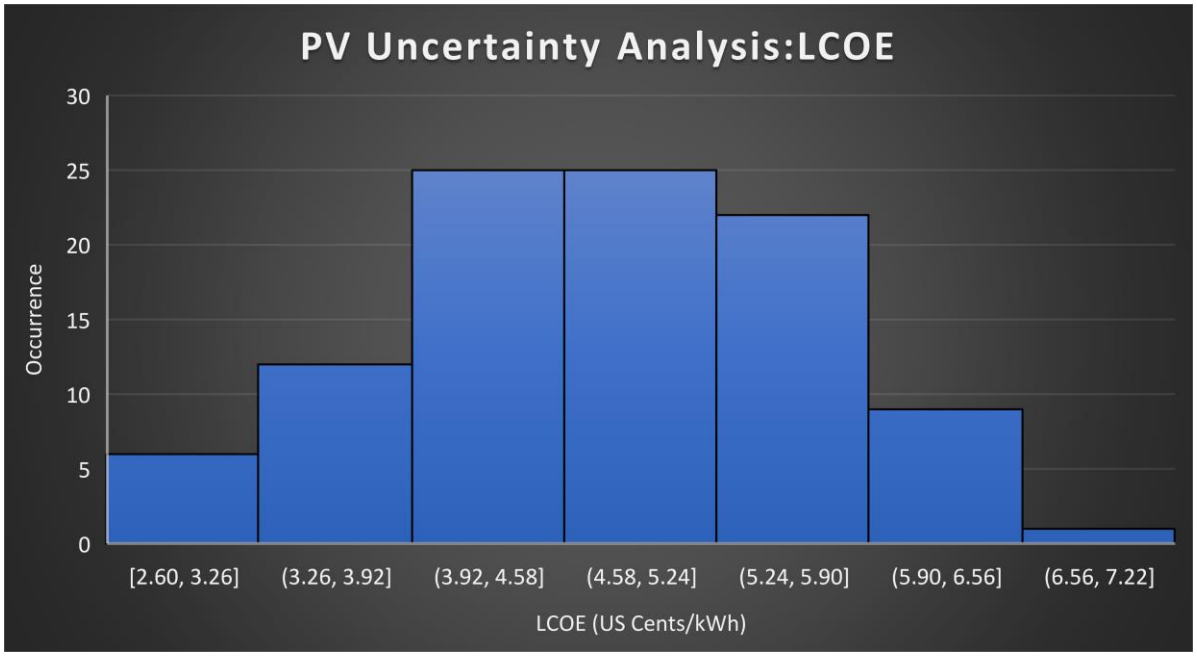


Figure 4. 31: Uncertainty analysis LCOE distribution for PV system

The tornado chart from the sensitivity analysis is shown below (figure 4.32). The results show that the PV module cost has the most influence on the LCOE followed by BOP cost with the inverter cost having the least.

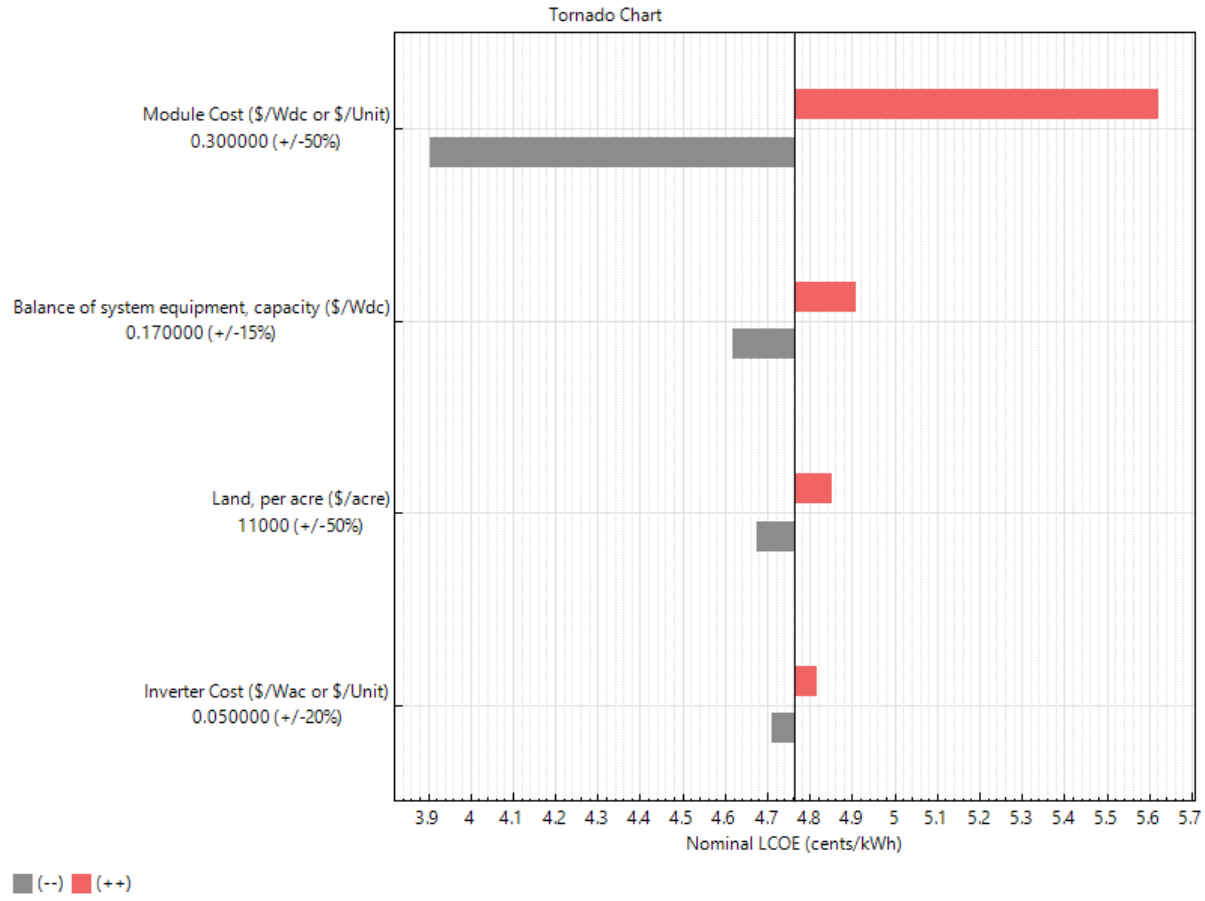


Figure 4. 32: Tornado chart showing the sensitivity analysis results for PV system

### 4.5.2 PV + Battery system

The table 4.8 below shows the cost parameters that were allowed to vary in the PV + Battery system:

Table 4. 8: Uncertain parameters for PV + Battery system

| Parameter | Base cost | Distribution | Standard deviation |
|---|---|---|---|
| Module cost | USD 0.30/Wdc | normal | 50% |
| Inverter cost | USD 0.05/Wac | normal | 20% |
| Battery cost | USD 209/kWh | normal | 30% |
| Replacement cost | USD 140/kWh | normal | 30% |
| Land cost | USD 11000/acre | normal | 50% |

The table 4.9 and graph (figure 4.33) below show the results of the uncertainty analysis. The 90% confidence interval from the analysis ranges from US cents/kWh 7.95 to 12.64 for LCOE. The NPV and simple pay back graphs are given in Appendix L.

Table 4. 9: Results of uncertainty analysis for PV + Battery system

| | Mean | Variance | P05 | P95 |
|---|---|---|---|---|
| LCOE (US cents/kWh) | 10.67 | 1.83 | 7.95 | 12.64 |
| NPV (USD) | 1.93E+07 | 1.81096E+14 | -301508 | 46345900 |
| Simple pay back (years) | 10.91 | 4.40 | 7.99 | 15.83 |

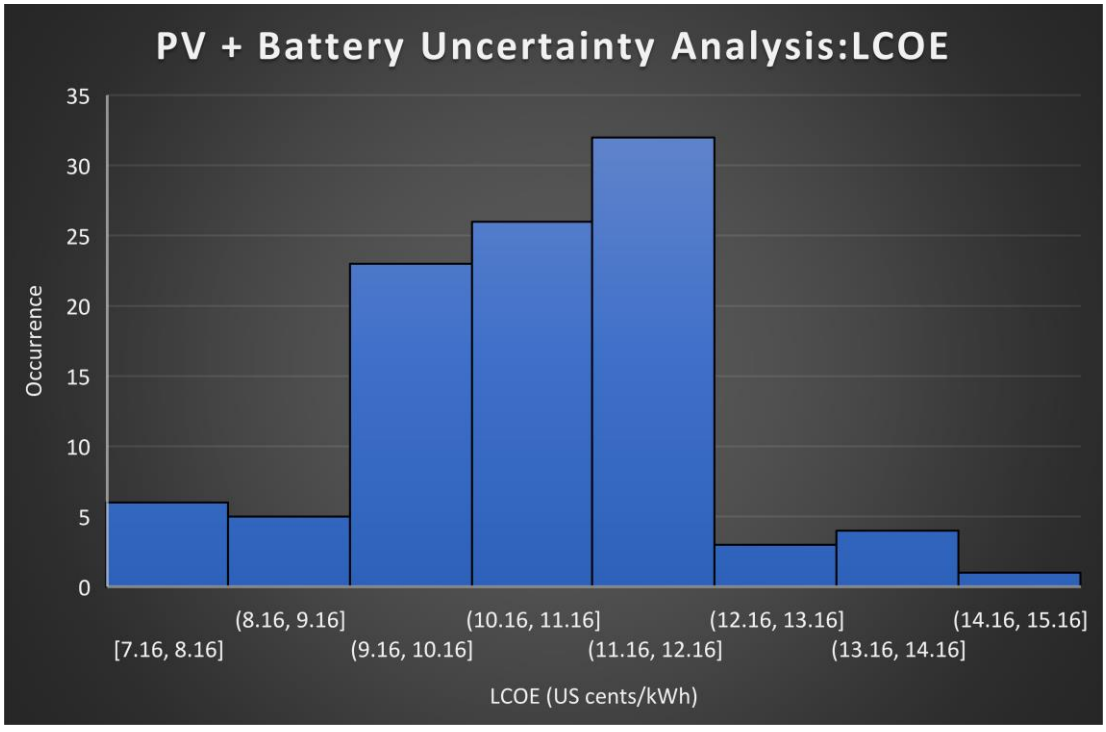


Figure 4. 33: Uncertainty analysis LCOE distribution for PV + Battery system

The tornado chart from the sensitivity analysis is shown in figure 4.34 below. The results show that the Battery cost has the most influence on the LCOE followed by the module cost with the inverter cost having the least.

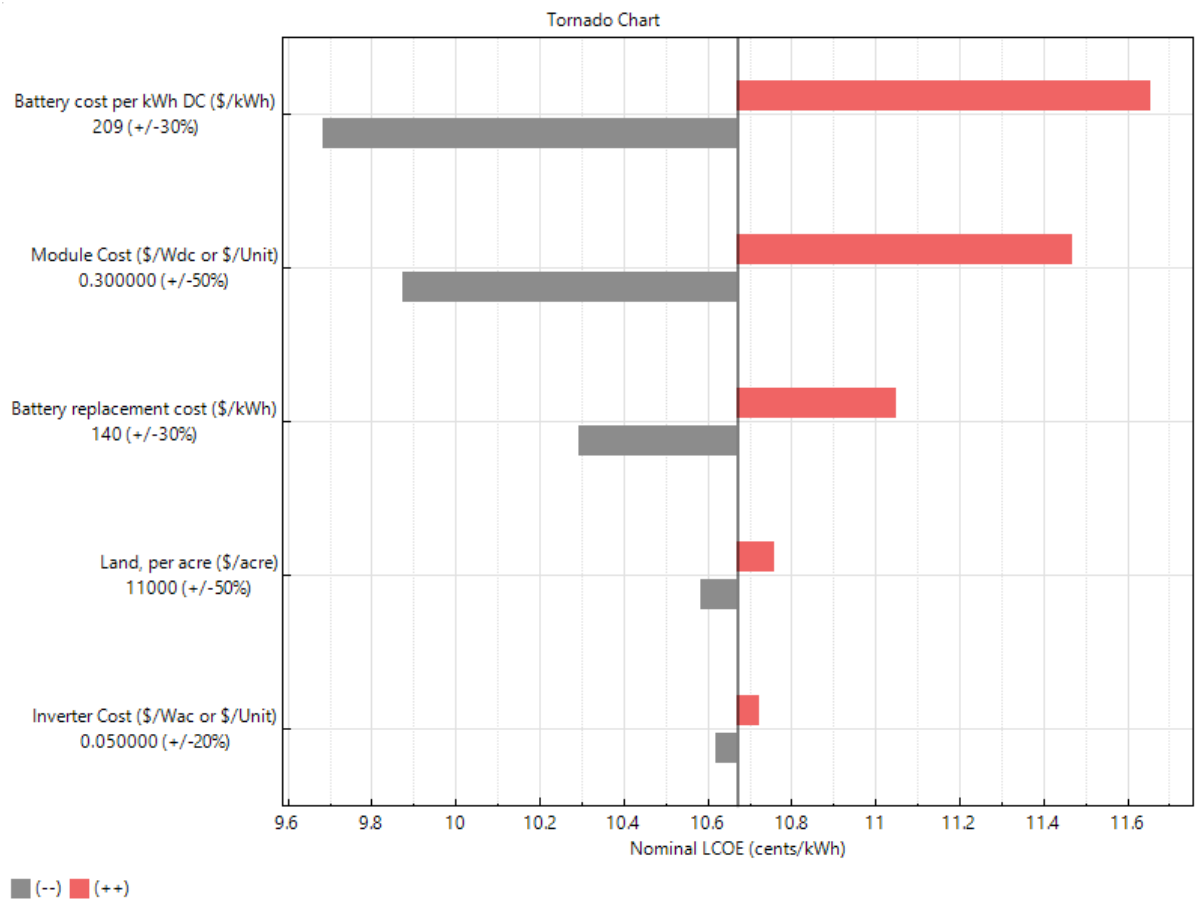


Figure 4. 34: Tornado chart showing the sensitivity analysis results for PV + Battery system

### 4.5.3 CSP System

The table 4.10 below shows the cost parameters that were allowed to vary in the CSP system:

Table 4. 10: Uncertain parameters for CSP system

| Parameter | Base cost | Distribution | Standard deviation |
|---|---|---|---|
| Solar Field cost | USD 150/$m^2$ | Normal | 30% |
| HTF cost | USD 60/$m^2$ | Normal | 20% |
| Power plant cost | USD 910/kWe | Normal | 20% |
| Land cost | USD 11000/acre | Normal | 50% |

The table 4.11 and graph (figure 4.35) below show the results of the uncertainty analysis. The 90% confidence interval from the analysis ranges from US cents/kWh 14.05 to 18.65 for LCOE. The NPV graph is given in Appendix M.

Table 4. 11: Results of uncertainty analysis for CSP system

| | Mean | Variance | P05 | P95 |
|---|---|---|---|---|
| LCOE (US cents/kWh) | 16.33 | 1.92 | 14.05 | 18.65 |
| NPV (USD) | -1.39E+07 | 2.82598E+13 | -22795305 | -5113653 |

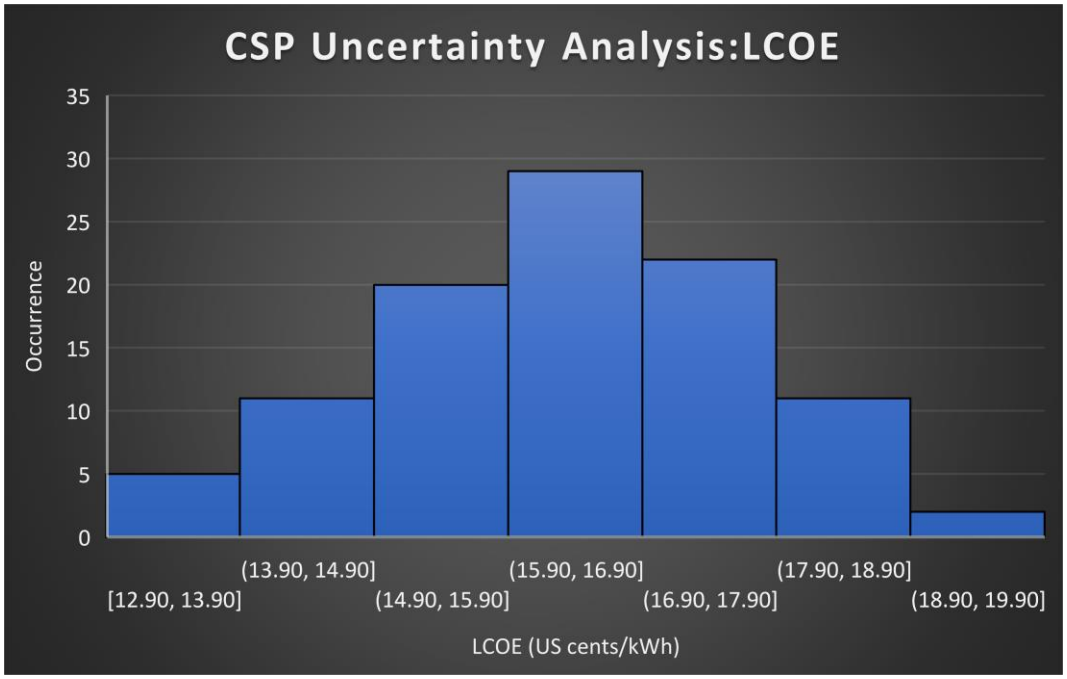


Figure 4. 35: Uncertainty analysis LCOE distribution for CSP system

The tornado chart from the sensitivity analysis is shown (figure 4.36) below. The results show that the Solar field cost has the most influence on the LCOE followed by the power plant cost with the land cost having the least.

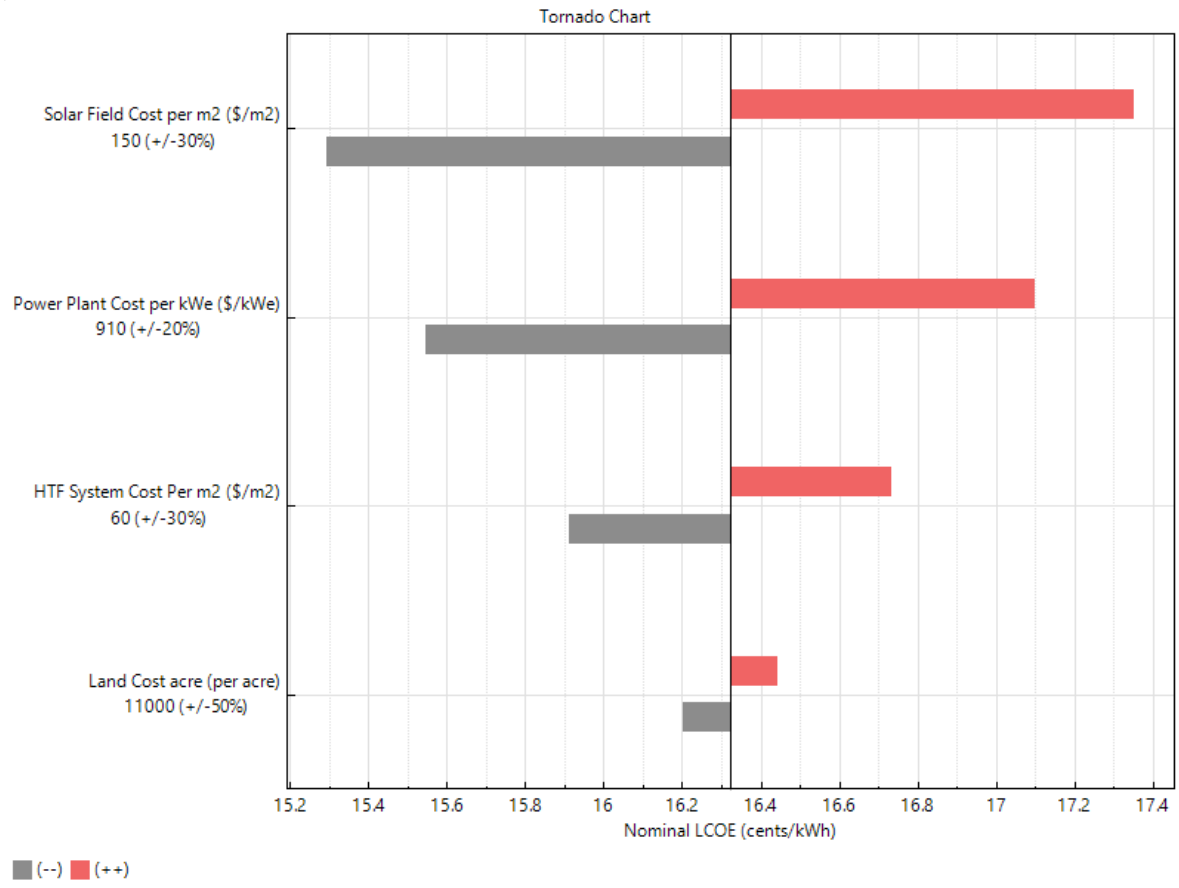


Figure 4. 36: Tornado chart showing the sensitivity analysis results for CSP system

### 4.5.4 CSP + TES

The table 4.12 below shows the cost parameters that were allowed to vary in the CSP + TES system:

Table 4. 12: Uncertain parameters for CSP + TES system

| Parameter | Base cost | Distribution | Standard deviation |
|---|---|---|---|
| Solar Field cost | USD 150/$m^2$ | Normal | 30% |
| HTF cost | USD 60/$m^2$ | Normal | 20% |
| Power plant cost | USD 910/kWe | Normal | 15% |
| Storage cost | USD 62/kWht | Normal | 30% |
| Land cost | USD 11000/acre | Normal | 50% |

The table 4.13 and graph (figure 4.37) below show the results of the uncertainty analysis. The 90% confidence interval from the analysis ranges from US cents/kWh 12.71 to 17.7 for LCOE. The NPV graph is given in Appendix M.

Table 4. 13: Results of uncertainty analysis for CSP + TES system

| | Mean | Variance | P05 | P95 |
|---|---|---|---|---|
| LCOE (US cents/kWh) | 15.45 | 2.42 | 12.71 | 17.7 |
| NPV | -1.73E+07 | 1.07918E+14 | -32378535 | 940789.3 |

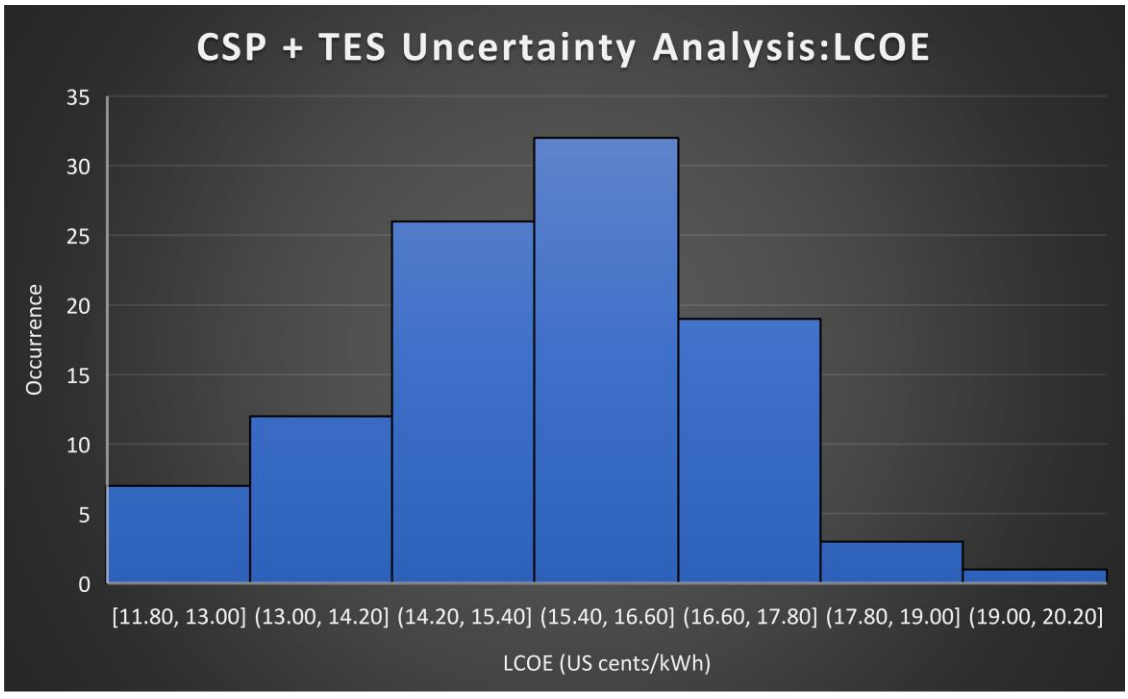


Figure 4. 37: Uncertainty analysis LCOE distribution for CSP + TES system

The tornado chart from the sensitivity analysis is shown in figure 4.38 below. The results show that the Solar field cost has the most influence on the LCOE followed by the storage cost with the land cost having the least.

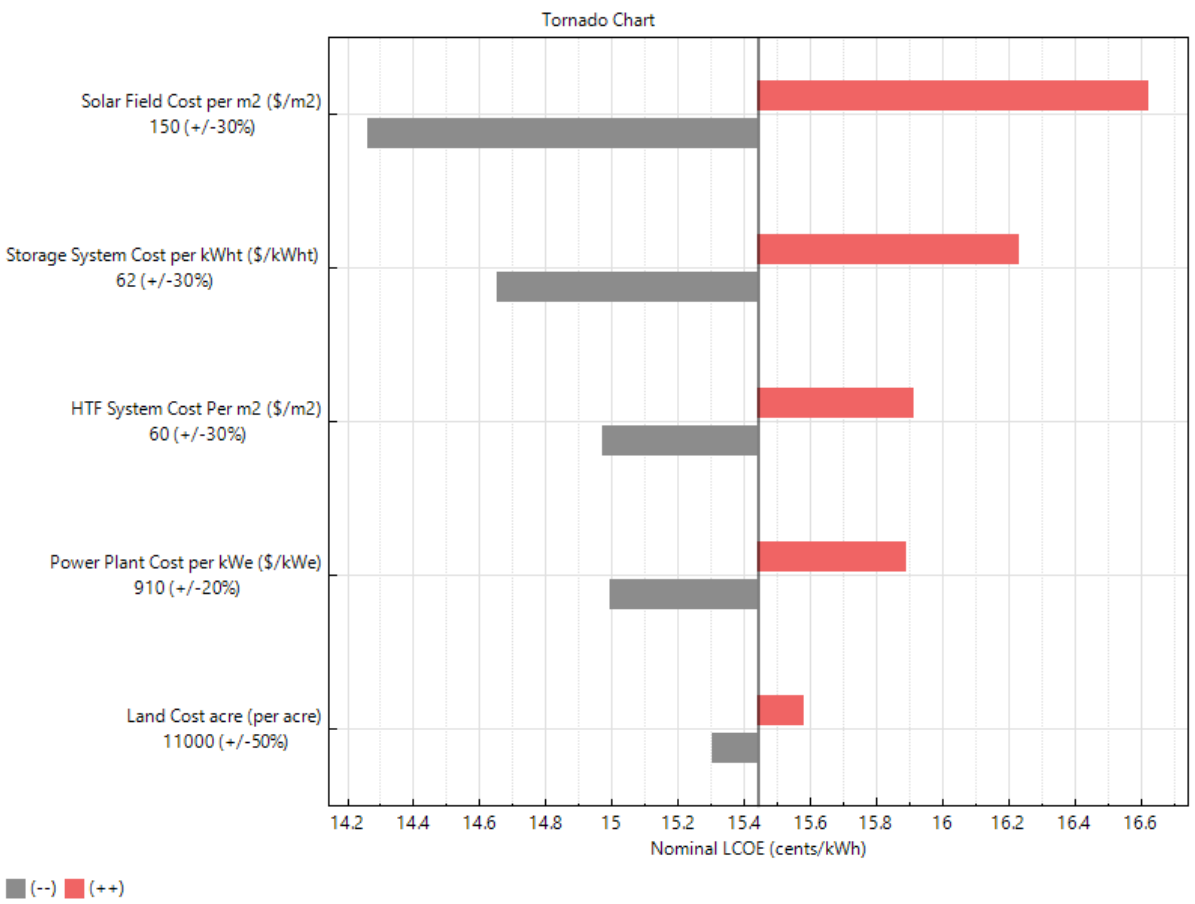


Figure 4. 38: Tornado chart showing the sensitivity analysis results for CSP + TES system

## 4.6 PV with Exports Results

### 4.6.1 Desired PV Plant Optimisation

A parametric study was carried out to determine the optimum size of the PV plant. The figure 4.39 below shows the variation of NPV with plant size. The NPV increases with increase of plant size from 20MW to 60MW, where it peaks, before starting to decrease. From 20MW to 60MW, the PV plant is operating efficiently with the generated energy either being used for local load or exported to the grid. After 60MW, although the energy produced is increasing, the plant is no longer operating efficiently as some energy is being curtailed due to the grid limit. From the analysis, the optimum PV plant size is 60MWdc hence chosen for the model.

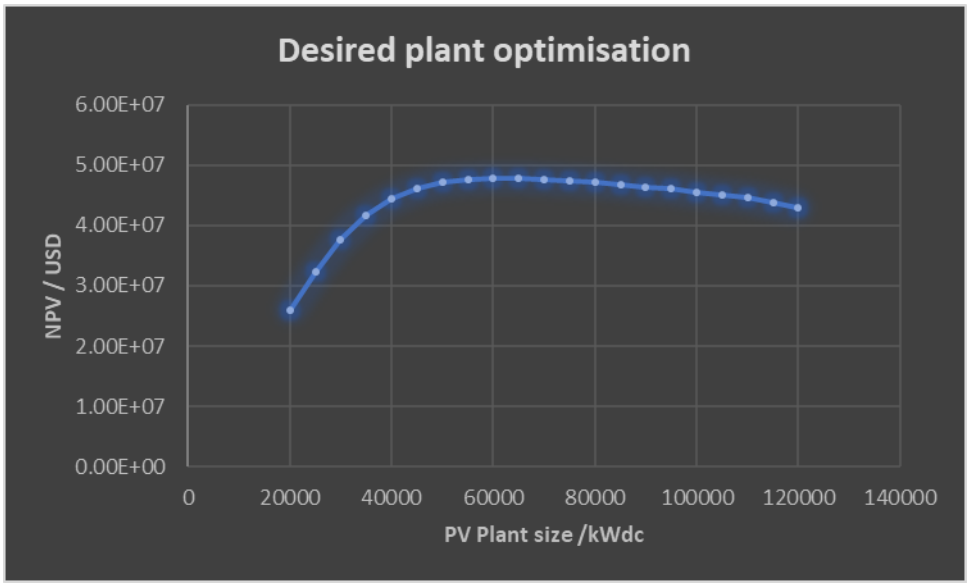


Figure 4. 39: Desired PV plant size optimisation

### 4.6.2 Technical performance of PV model

The simulation of the optimised 60MWdc PV plant predicts an output of 99.7GWh during the first-year operation (life cycle and loss diagram given in Appendix N). 65% of the generated PV energy is used by the local mine load with the remaining 35% exported to the grid as shown in the figure 4.40 below. However, most of the energy to supply the load is supplied from the grid (61%) with the PV system only contributing 39% of the load as shown in the figure 4.41 below.

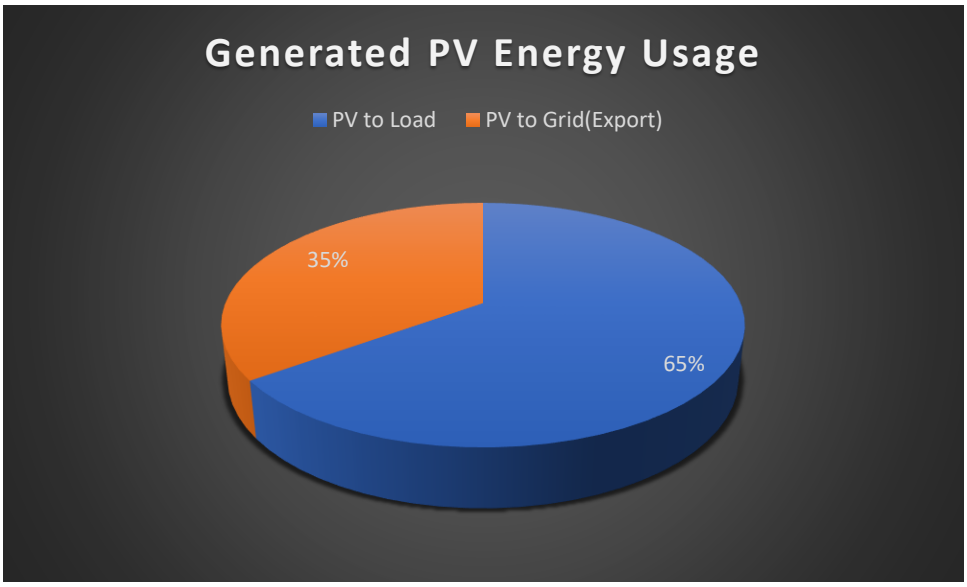


Figure 4. 40: Generated PV Energy usage

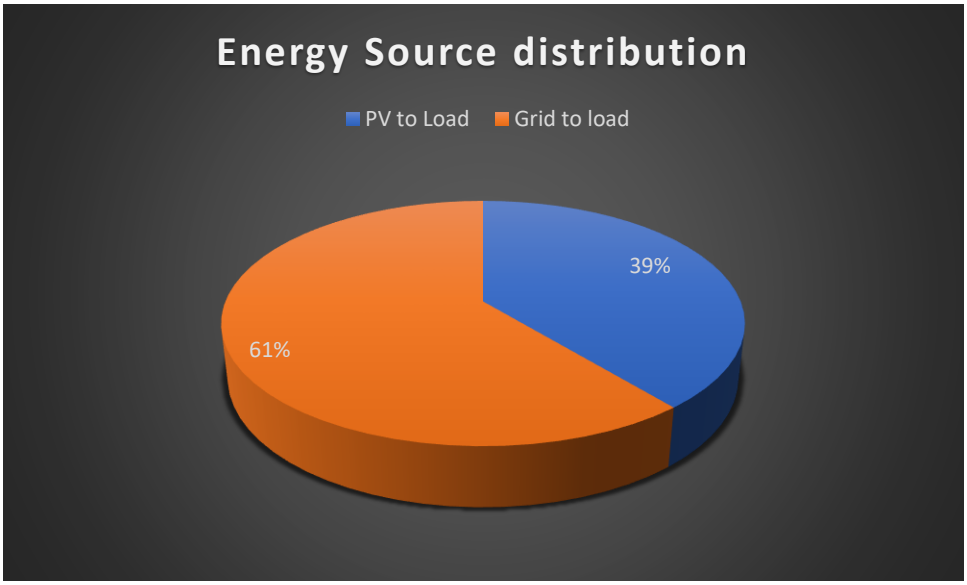


Figure 4. 41: Energy source distribution

On a typical good day for PV production, as shown in the figure below 4.42, the PV system is able to supply the mine load from 7:00am up to 2pm. During this period, the system will also be exporting to the grid with a typical peak power exported reaching 25.5MW at 11am. By around 3pm, there will no power being exported, and the grid power will start to compliment the PV system to supply the mine load. From 4pm, the grid will be supplying the load alone until the next day.

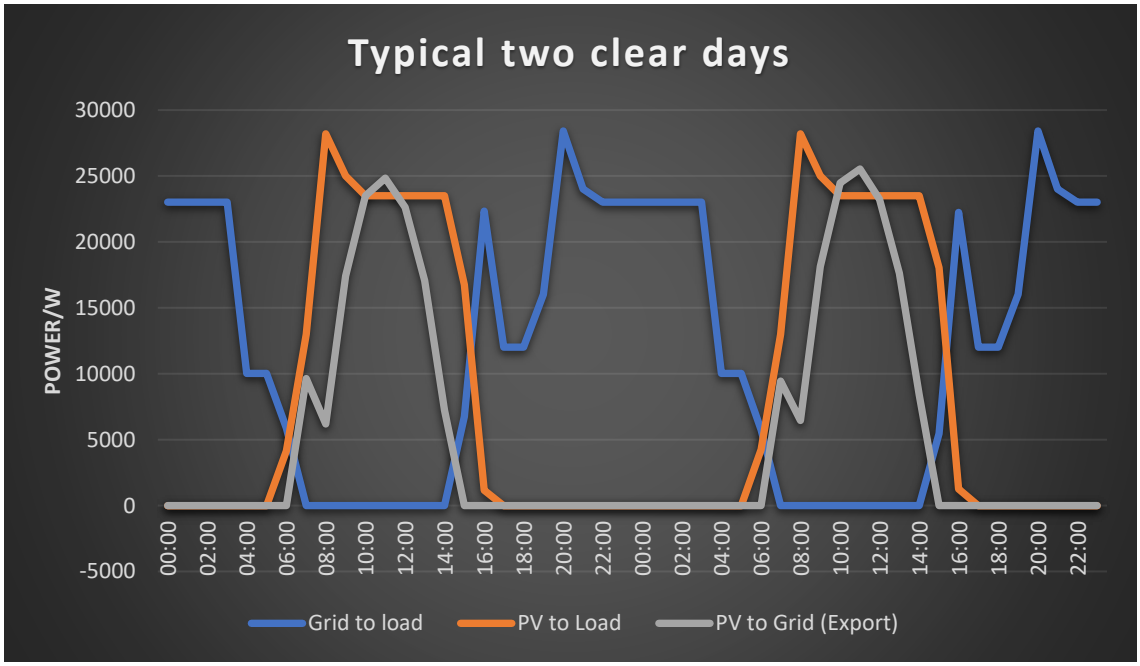


Figure 4. 42: Typical two good days for PV production

On a typical bad day for PV production, as shown in the figure 4.43 below, the generated PV energy peak output is just above 5MW with no exports at any given point in time.

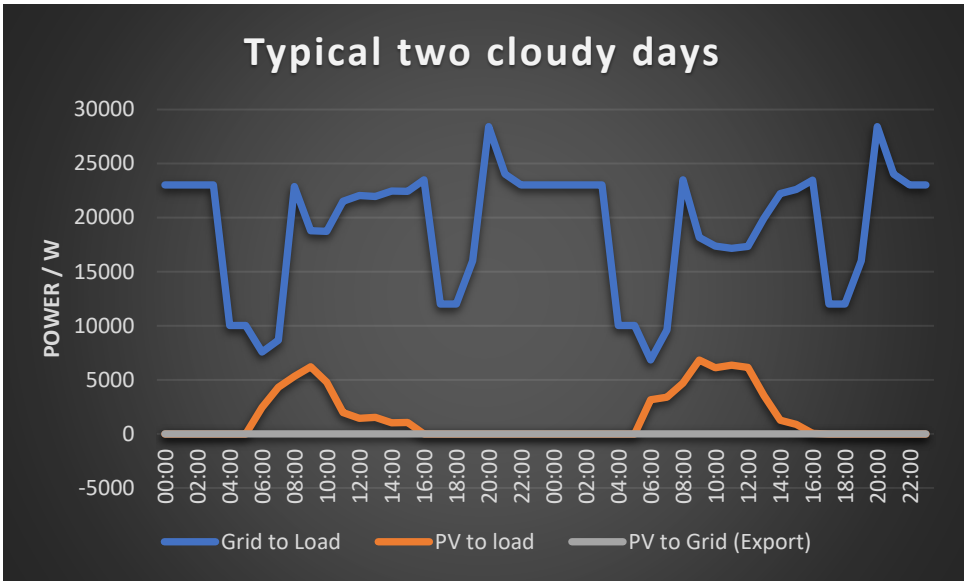


Figure 4. 43: Typical two bad days for PV production

### 4.6.3 Economic performance of PV model

The installation cost of the system is predicted at USD 0.76 per DC watt with the predicted LCOE at US cents 4.34 per kWh. The NPV of the system is estimated at 47.7 million with a simple pay-back period of 6.3 years. The table 4.14 below shows the main economic indicators of the system:

Table 4. 14: Economic indicators for PV system

| **Parameter** | **Unit** | **Value** |
|---|---|---|
| Localised Cost of Energy | USD/kWh | 0.0434 |
| Annual Electric Bill without CSP system | USD | 13.69 Million |
| Annual Electric Bill with CSP system | USD | 6.17 Million |
| Net annual savings | USD | 7.52 Million |
| Net Present Value | USD | 47.7 Million |
| Simple pay back | Years | 6.3 |

The simulation results show that the annual electric bill liable is reduced from USD 13.7 million to USD 6.17 million. This means by reducing the annual energy demand by 39% and exporting 35% of the generated energy, the system is able to save about 55% of the annual electric bill. The figure 4.44 below shows the monthly bill of electricity with PV system vs without.

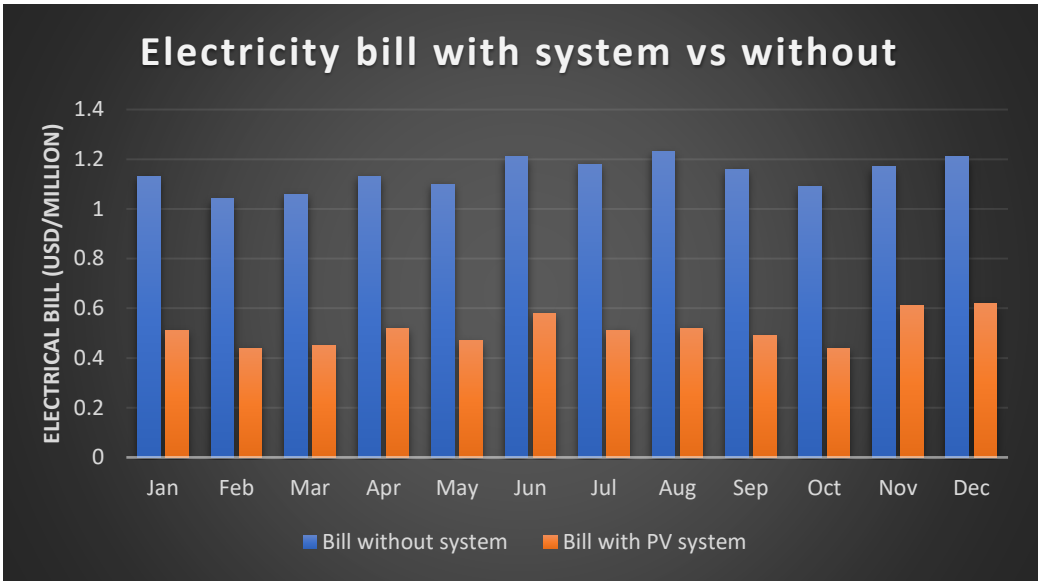


Figure 4. 44: Monthly electric bill with PV system vs without

## 4.7 PV + Battery with exports

### 4.7.1 Battery and PV plant capacity optimisation

A parametric study was carried out to determine the optimum storage hours of the behind the meter battery and corresponding PV size based on the load profile, desired operation, and return on investment. The two figures below (figure 45 and 46) show that in general, the smaller the PV plant size and the lower the storage hours the more viable the system. PV size ratio of 5 is not viable for the whole range of storage hours while PV size ratio 1.5 to 3.5 is viable for all analysed storage hours.

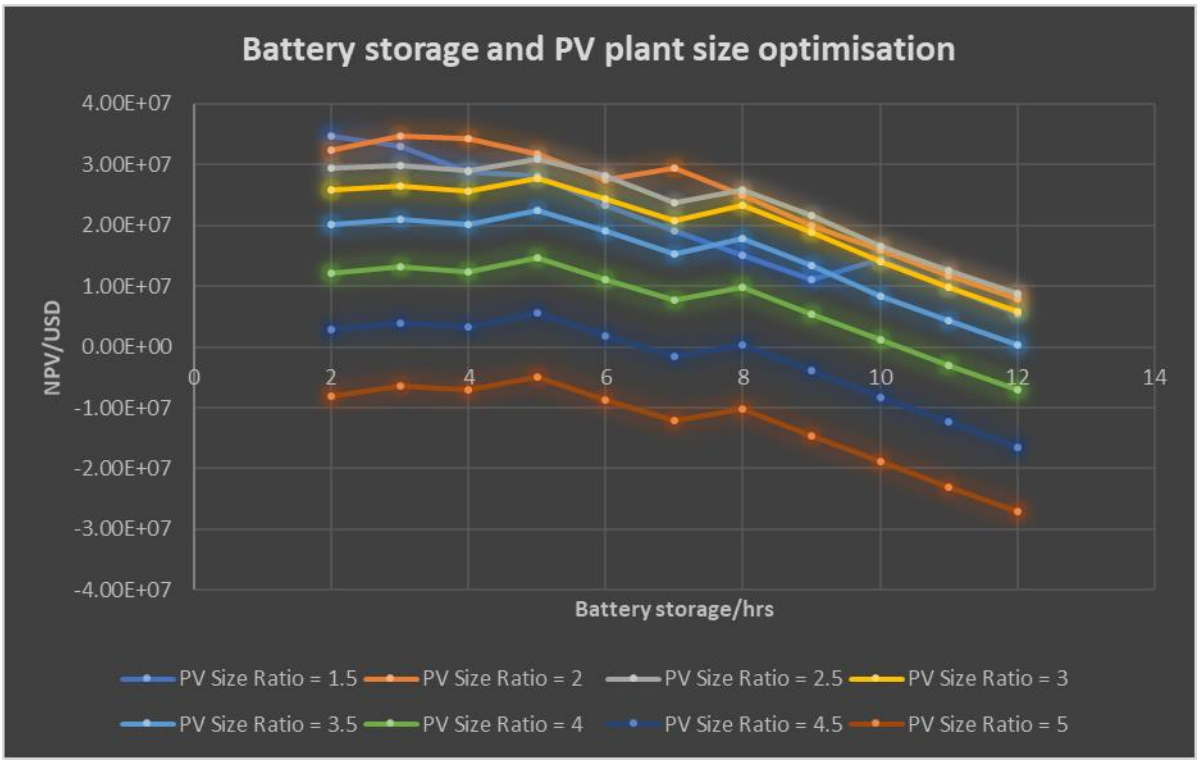


Figure 4. 45: Storage hours and PV plant optimisation for PV + Battery

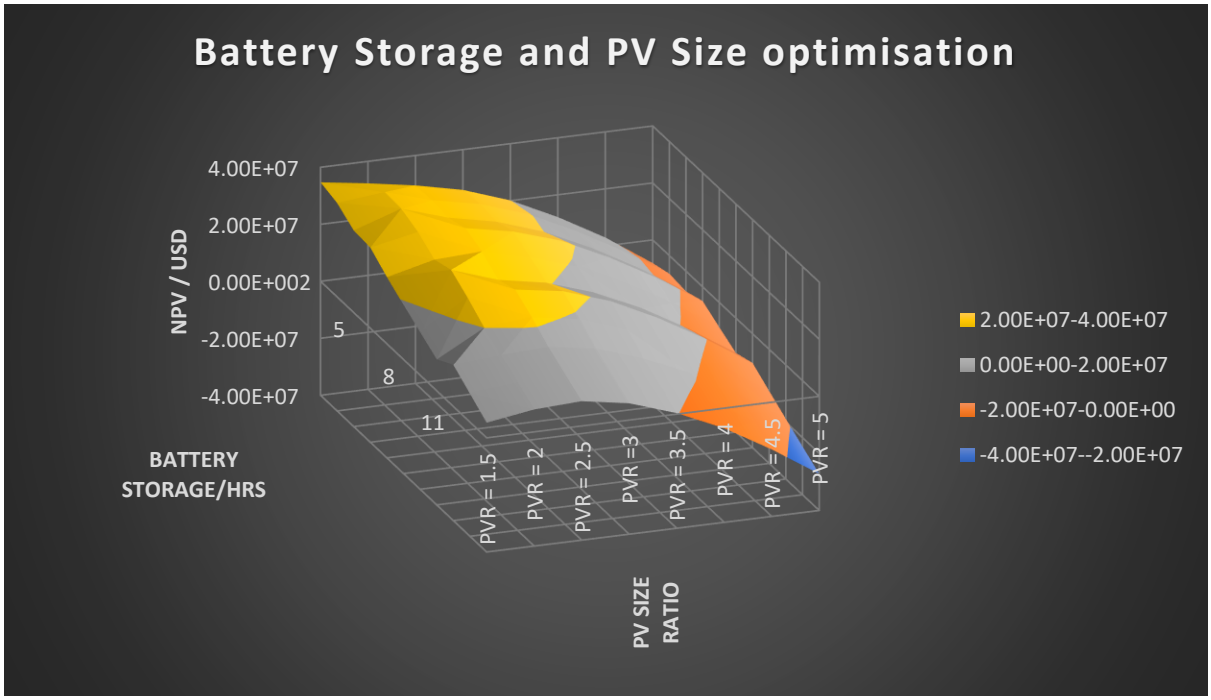


Figure 4. 46: 3D Battery storage and PV plant optimisation

To determine the optimum system, the minimum storage required for battery to supply load during the high-risk load-shedding period must be considered. From section 4.2.1, the minimum required storage hours are 7 hours. From the analysis, the PV size ratio with maximum NPV at battery storage of 7 hours or more is 2. Therefore, the optimum battery size is 210MWh with a PV plant size of 74MWdc.

### 4.7.2 Technical performance of PV + Battery

The simulation of the optimised 74MWdc PV plant + 210MWh of battery storage predicted an annual output of 120.5 GWh in the first year (lifecycle and loss diagram are shown in Appendix O). 55% of the generated energy by PV system is used to supply the load with 31% used to charge the battery (and eventually supply the load) with the remaining 14% exported to the grid as shown in figure 4.47 below. 63% of the load is supplied from local generation (41% from PV and 22% from battery) with 37% supplied from the grid as shown in the figure 4.48 below.

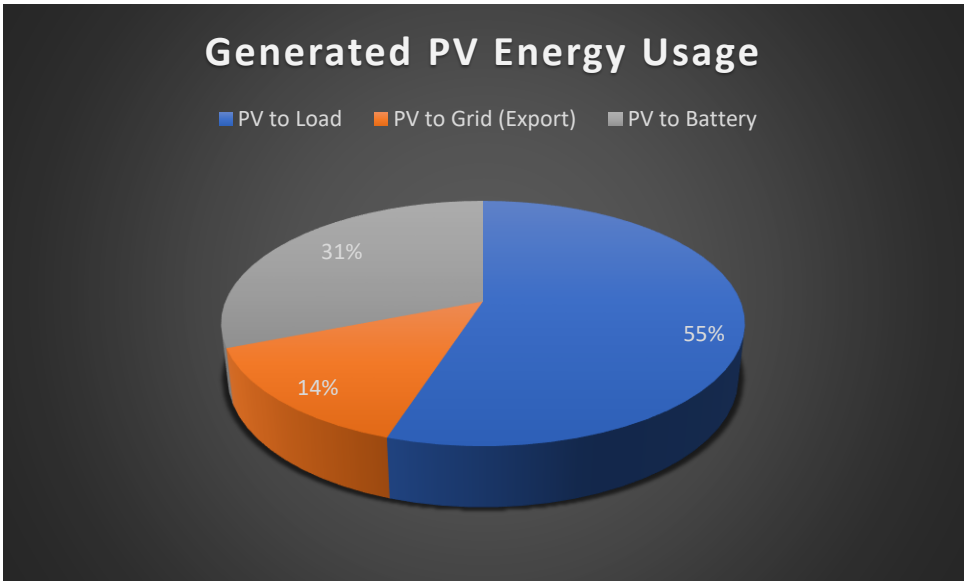


Figure 4. 47: Generated PV Energy usage

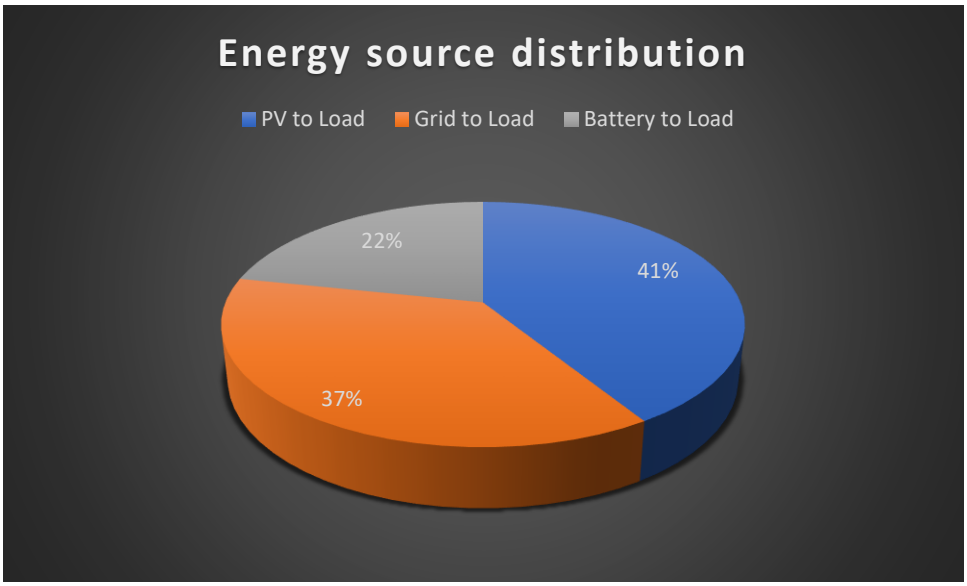


Figure 4. 48: Energy source distribution for PV + Battery

On a typical good day of PV production, as shown in the figure 4.49 below, the hybrid system is able to supply the load over the peak and standard periods. The PV plant will supply the load alone from 7am to 2pm while at the same time charging the battery. Energy exports starts -when the battery has reached full capacity – from 11 am up to 3pm. The battery and PV plant will complement each other from 2pm to 5pm with the battery latter suppling the load alone up to 9pm. The grid will supply the off-peak period from 10pm to 6am.

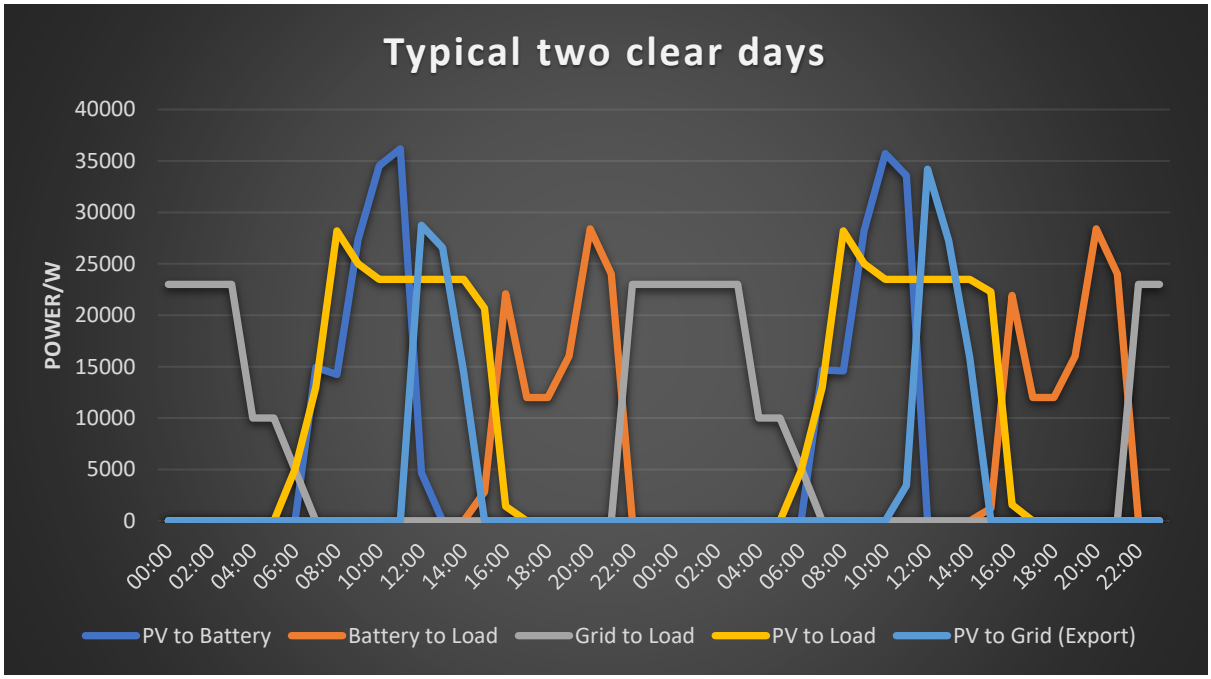


Figure 4. 49: Typical two good days for PV production

On a typical bad day for PV production, as shown in the figure 4.50 below, the hybrid system only covers the load alone between 7am and 10am. The grid power will then be used thereafter with a little help from PV plant in the next day. There will be no energy exports during the period.

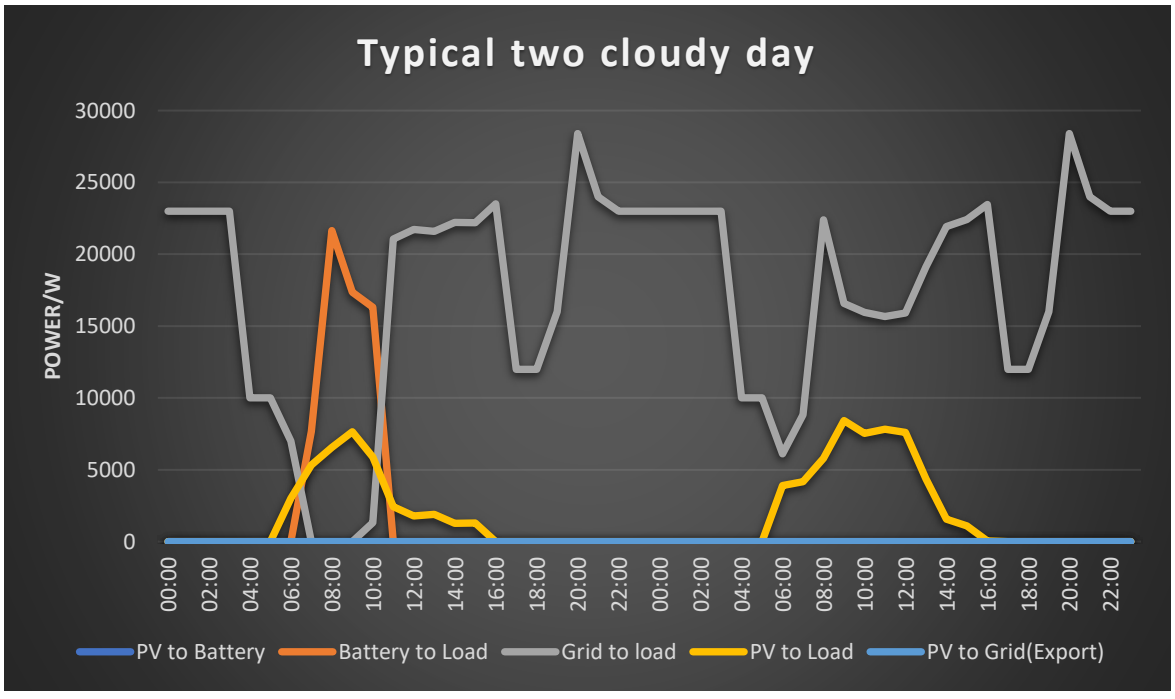


Figure 4. 50: Typical two bad days for PV production

### 4.7.3 Economic performance of the PV + Battery

The installation cost of the system is estimated at USD 1.5/Wdc with the predicted LCOE at US cents 9.40 per kWh. The predicted NPV of the system is about USD 31.4 million with a

simple pay back of 9.7 years. The table 4.15 below shows the main economic indicators of the system:

Table 4. 15: Economic indicators for PV + Battery

| Parameter | Unit | Value |
|---|---|---|
| Localised Cost of Energy | USD/kWh | 0.094 |
| Annual Electric Bill without CSP system | USD | 13.69 Million |
| Annual Electric Bill with CSP system | USD | 1.7 Million |
| Net annual savings | USD | 11.99 Million |
| Net Present Value | USD | 31.4 Million |
| Simple pay back | Years | 9.7 |

The first-year simulation results show that the annual electric bill liable is reduced from USD 13.7 million to USD 1.7 million. This means by reducing the annual load by 63% and exporting 14% of the generated energy, the system is able to save about 86.6% of the annual electric bill. The figure 4.51 below shows that in the month of October there will be a cash inflow rather than outflow as far as electric bill is concerned.

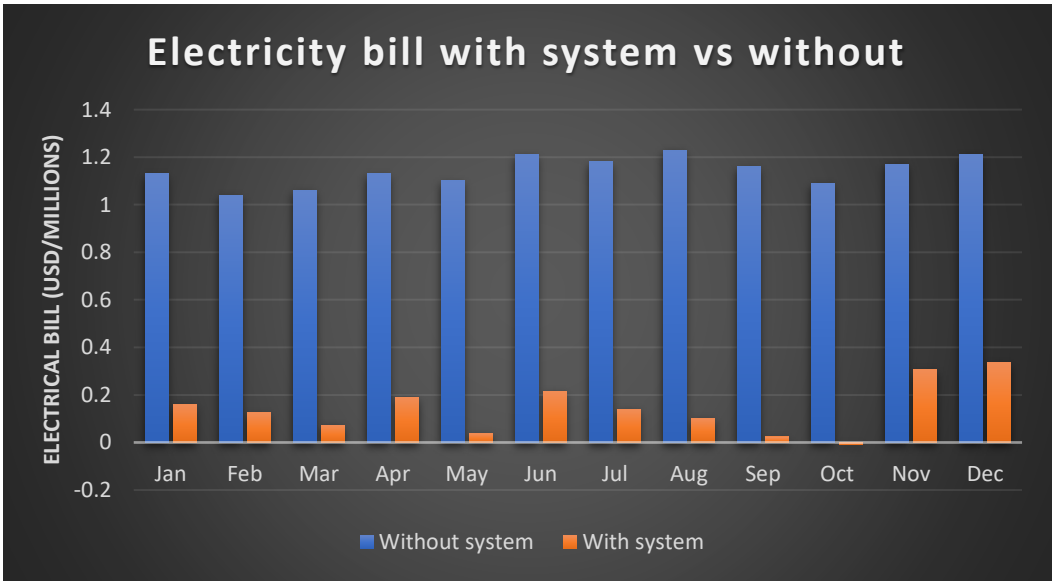


Figure 4. 51: Monthly electric bill with system vs without for PV + Battery

## 4.8 CSP with exports results

### 4.8.1 Solar multiple and Power output optimisation

A parametric study was carried out to determine the optimum solar multiple and gross power output. The figure 4.52 below shows that the LCOE reduces as SM varies from 1 to 1.75 before starting to increase. The variation of LCOE with gross output power is not significant but the general trend is it is higher on the extremes (20MW and 60MW) and lowest between 40 – 50 MW. From the analysis, the lowest LCOE occurs at SM = 1.75 and gross power output of 50MW.

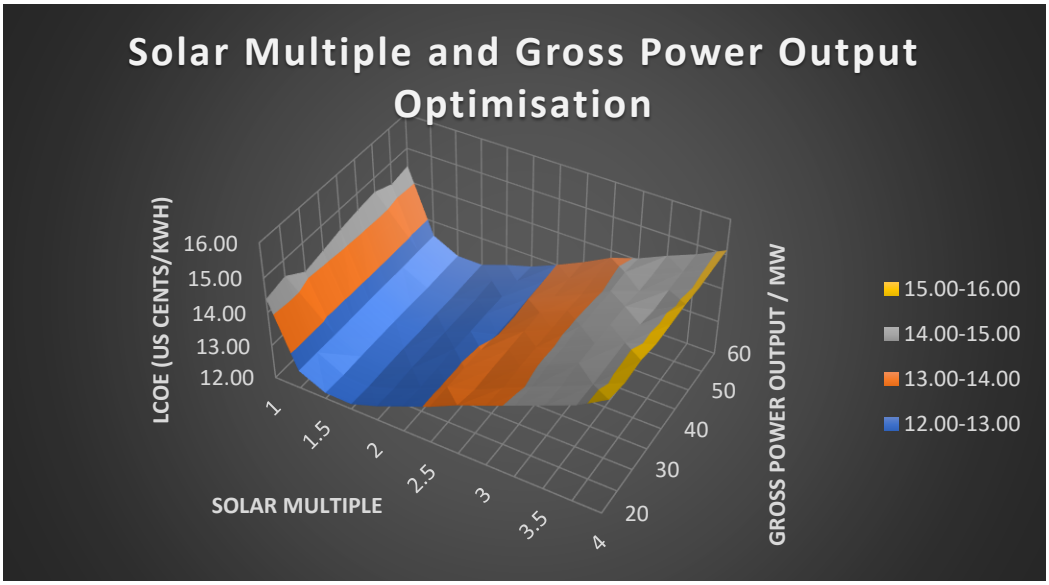


Figure 4. 52: Solar Multiple and Gross power output optimisation

### 4.8.2 Technical performance of optimised CSP

The simulation of the optimised 50MW gross output, solar multiple of 1.75 and DNI design point of 860W/m$^2$ predicts a net annual electrical energy production of 94.7GWh during the first-year operation (summary results from SAM are given in Appendix P). 49% of the generated CSP energy is used to supply the load while 51% is exported to the grid as shown in the figure 4.53 below. Energy supplied to the load covers 28% of the annual load with the remaining 72% coming from the grid as shown below in figure 4.54.

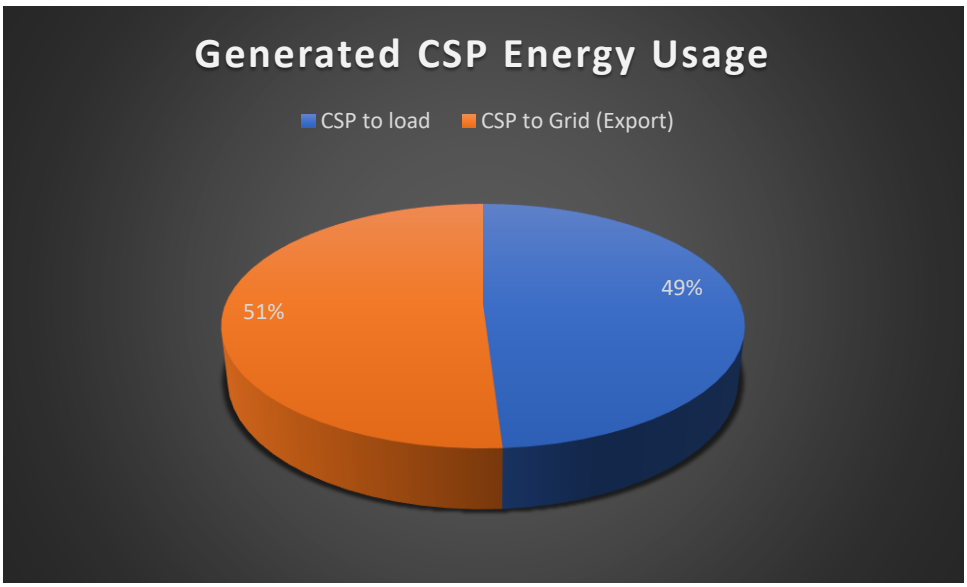


Figure 4. 53: Generated CSP Energy Usage

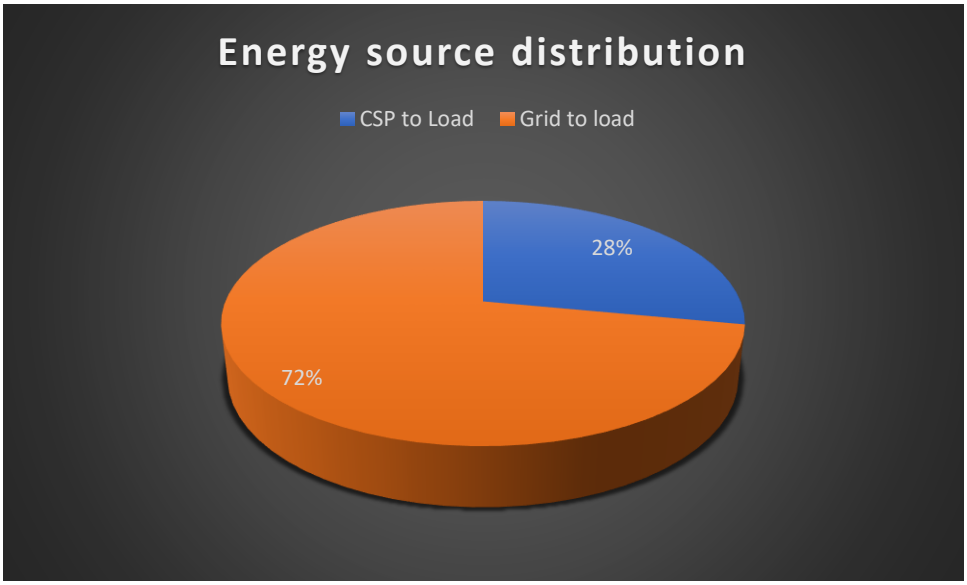


Figure 4. 54: Energy source distribution for CSP

On a typical good day for CSP production, as shown in the figure 4.55 below, the system is able to supply the local load from 7:00am to 2pm. During this time, the system will also be exporting power to the grid (with a typical peak power of 32MW). The energy exports stop at around 3pm, with the grid power starting to compliment the CSP to supply the local load. From 5pm, the grid power will be supplying the load alone up until the next day.

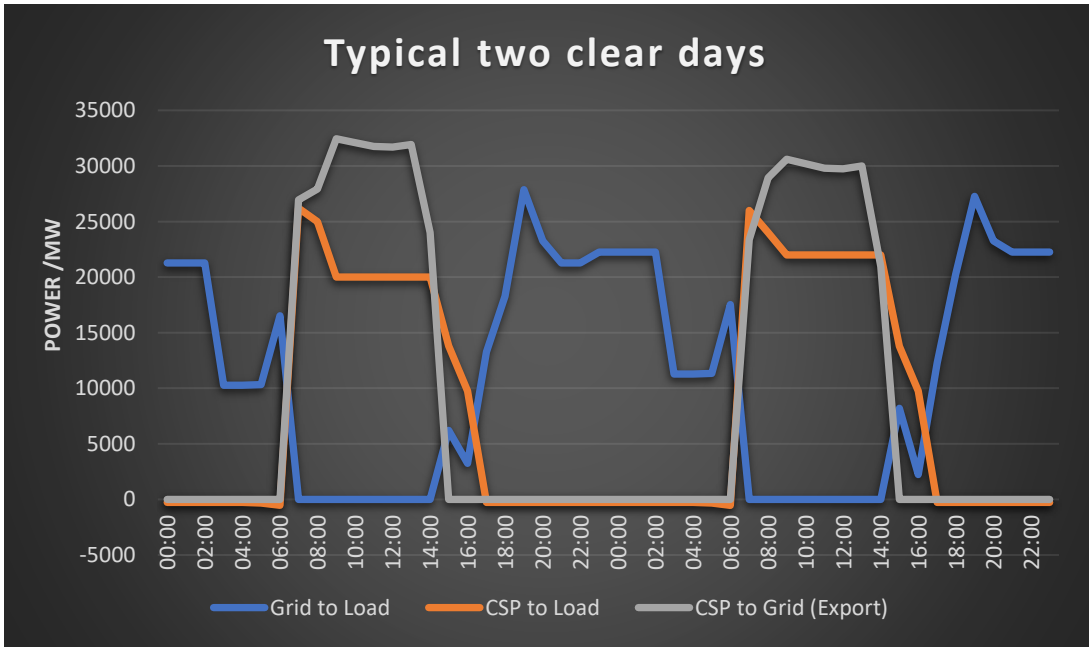


Figure 4. 55: Typical two good days for CSP production

On a typical bad day for CSP production, as shown in the figure 4.56 below, there will be neither energy to cover the load nor to export to the grid. The grid will supply the load (together with ancillary equipment like freeze protection heaters) during the day and night.

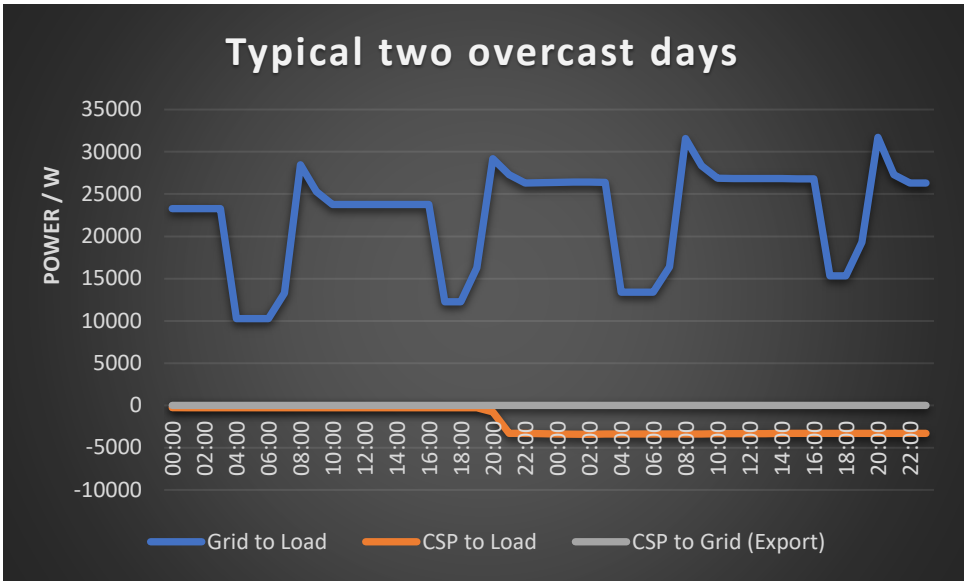


Figure 4. 56: Typical two bad days for CSP production

### 4.8.3 Economic performance of CSP

The installation cost of the system is predicted at 3347/kW with LCOE at US cents 12.13/kWh. The predicted NPV is USD 3.96 million with a simple pay-back period of 15.7 years. The main economic indicators of the system are given in the table 4.16 below:

Table 4. 16: Economic indicators for CSP

| **Parameter** | **Unit** | **Value** |
|---|---|---|
| Localised Cost of Energy | USD/kWh | 0.12 |
| Annual Electric Bill without CSP system | USD | 13.69 Million |
| Annual Electric Bill with CSP system | USD | 4.01 Million |
| Net annual savings | USD | 9.68 Million |
| Net Present Value | USD | 3.96 Million |
| Simple pay back | Years | 15.7 |

The first-year simulation results show that the amount of annual electric bill liable is reduced from USD 13.69 million to 4 million. This means by reducing the annual load by 28% and exporting 51% of the generated energy, the system is able to save about 70.6% of the annual electric bill. The figure 4.57 below shows the monthly electric bill of the mine with system vs without system:

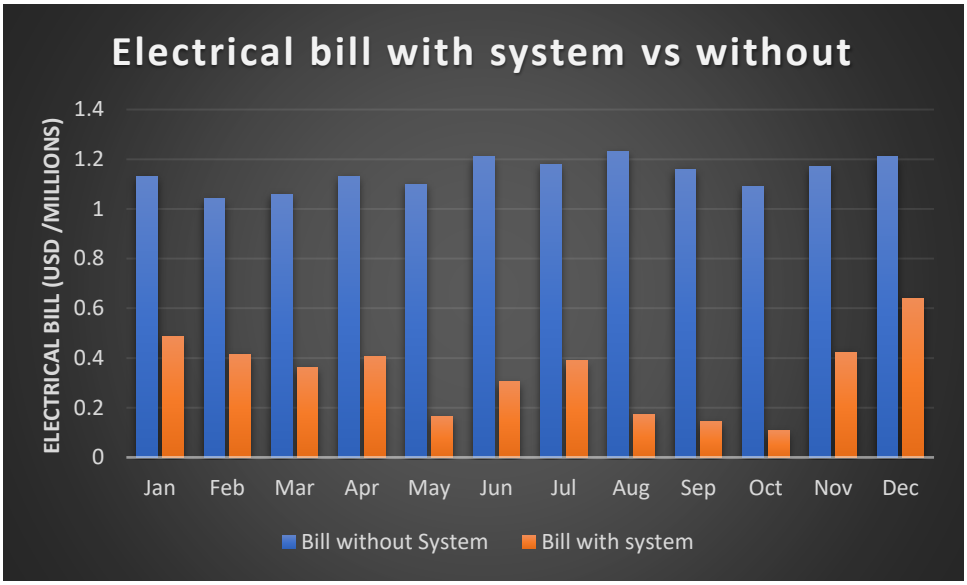


Figure 4. 57: Monthly electric bill with system vs without for CSP

## 4.9 CSP + TES with Exports Results

### 4.9.1 Desired Power Output Optimisation

A parametric study was carried out to determine the optimum output size for CSP + TES system. As shown in the figure 4.58 below, there is little variation on LCOE with gross power output. However, the analysis shows that the minimum LCOE occurs at power output of 40MW.

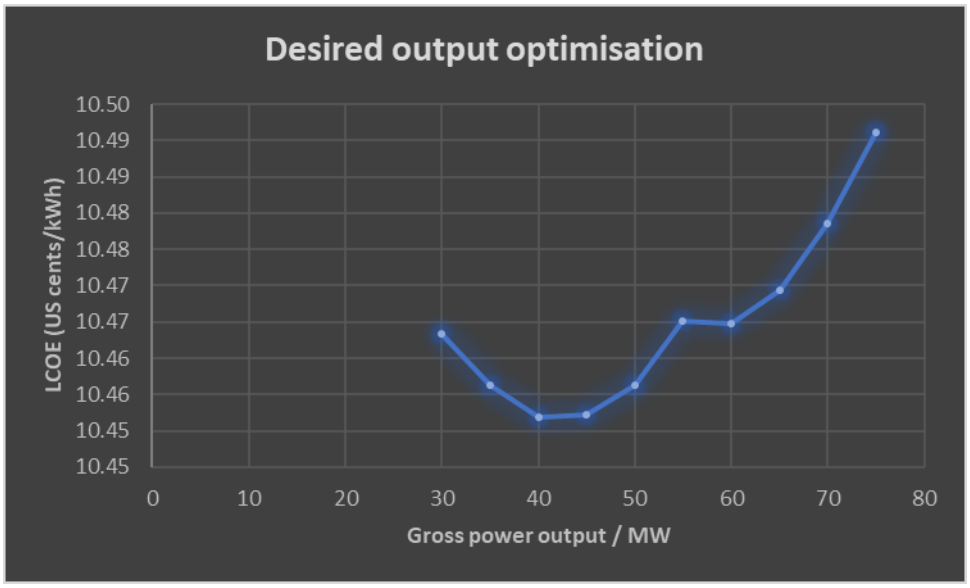


Figure 4. 58: Desired power output optimisation for CSP + TES

### 4.9.2 Storage hours and Solar Multiple Optimization

The figure 4.59 below shows the results of the parametric analysis carried out to determine the optimum solar multiple and storage hours. In general, the LCOE is higher for smaller solar multiple values and decreases with increase in solar multiple reaching the trough at SM = 2.25 to 2.75. For SM 1 to 1.5, the LCOE increases with increase in storage hours while for SM 1.75 to 4, the LCOE is higher at the extremes of storage hours (1 and 14) with minimum

occurring between storage hours 5 and 7. The analysis shows that the optimum SM value is 2.5 and the minimum required storage hours for the system to supply the high risk period is 7hrs.

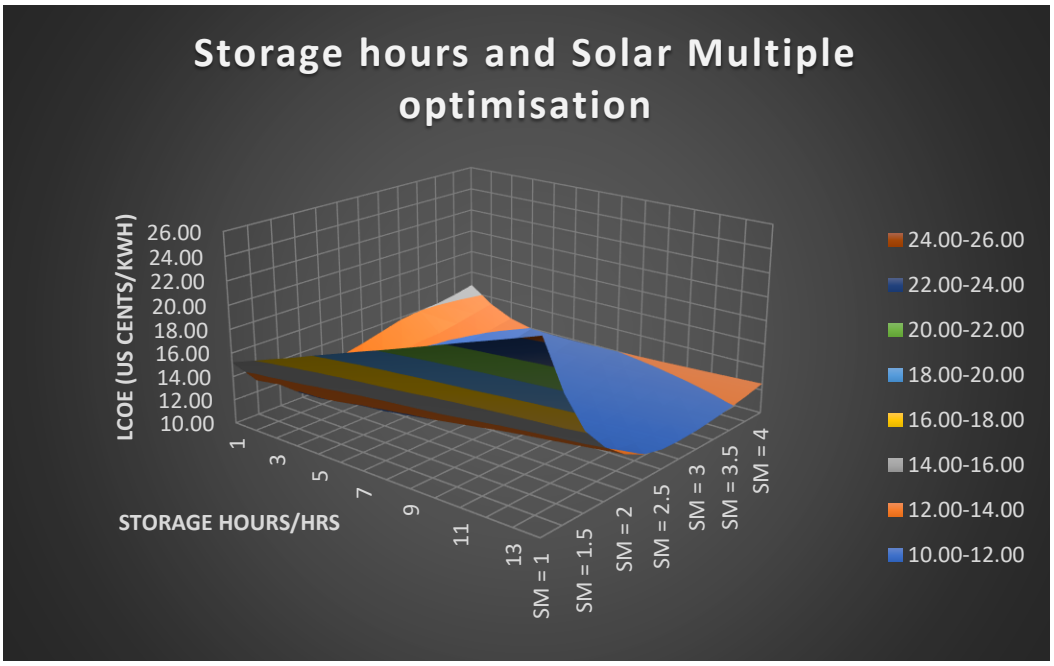


Figure 4. 59: Storage hours and Solar Multiple optimisations for CSP + TES

### 4.9.3 Technical performance of CSP + TES

The simulation of the optimised 40MW gross output, SM = 2.5, and storage hours of 7 predicts a net annual electrical energy of 127.4GWh during the first-year operation (summary results from SAM are given in Appendix Q). 54% of the generated CSP + TES energy is used to supply the local mine load with the remaining 46% exported to the grid as shown in the figure 4.60 below. Energy supplied to the load covers 41% of the annual mine load with the remaining 59% supplied from the grid as shown in the figure 4.61 below.

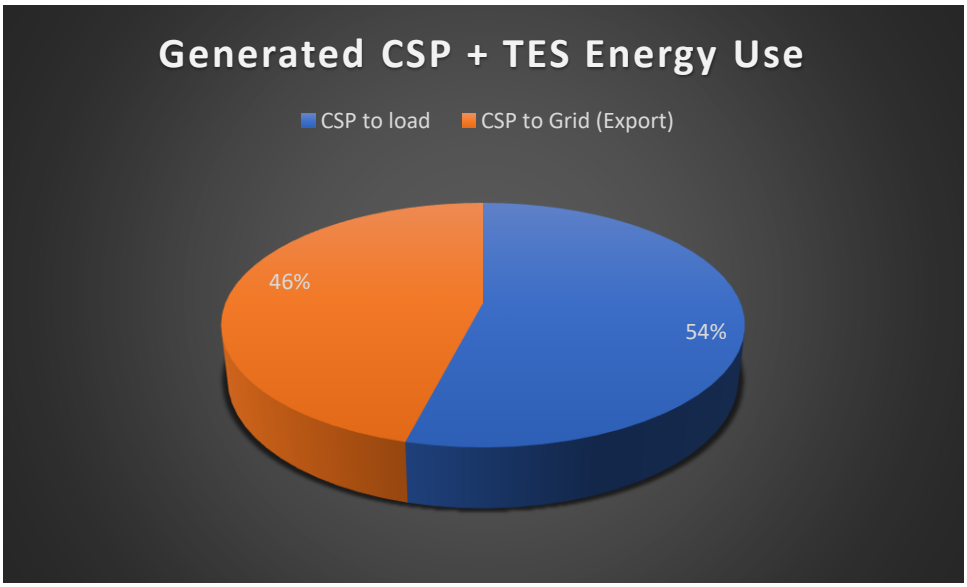


Figure 4. 60: Generated CSP + TES Energy use

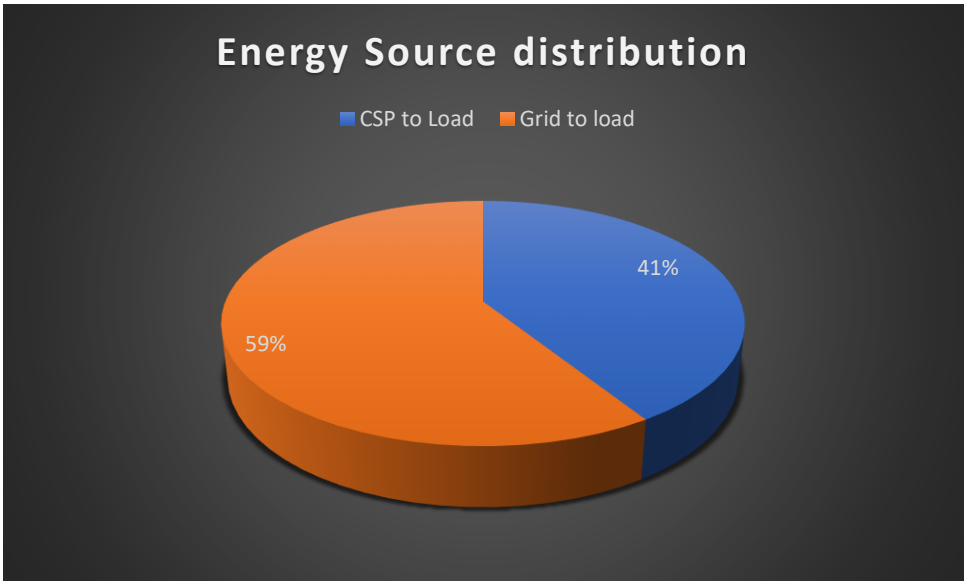


Figure 4. 61: Energy source distribution

On a typical good day for CSP production, as shown in the figure 4.62 below, the system is able to supply the local mine load from 7am to 9pm while at the same time exporting to the grid. The grid power is only used during off-peak period as per design.

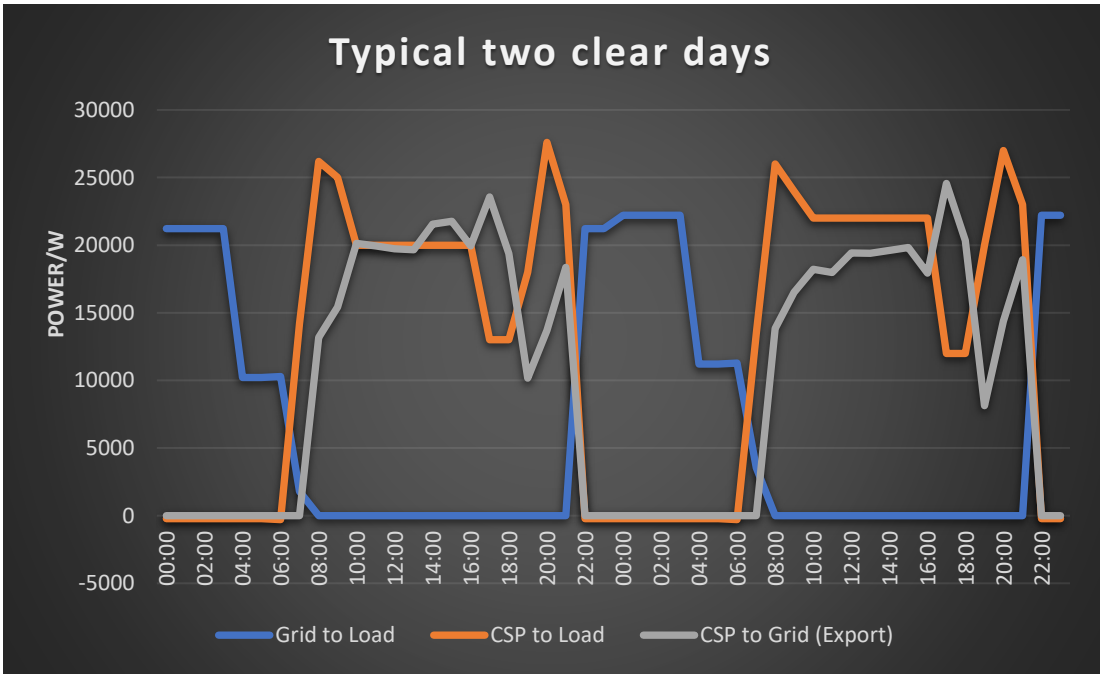


Figure 4. 62: Typical two good days for CSP + TES production

On a typical bad day for CSP production, as shown in the figure 4.63 below, there will be neither energy to cover the load nor to export to the grid. The grid will supply the load (together with ancillary equipment like freeze protection heaters) during the day and night.

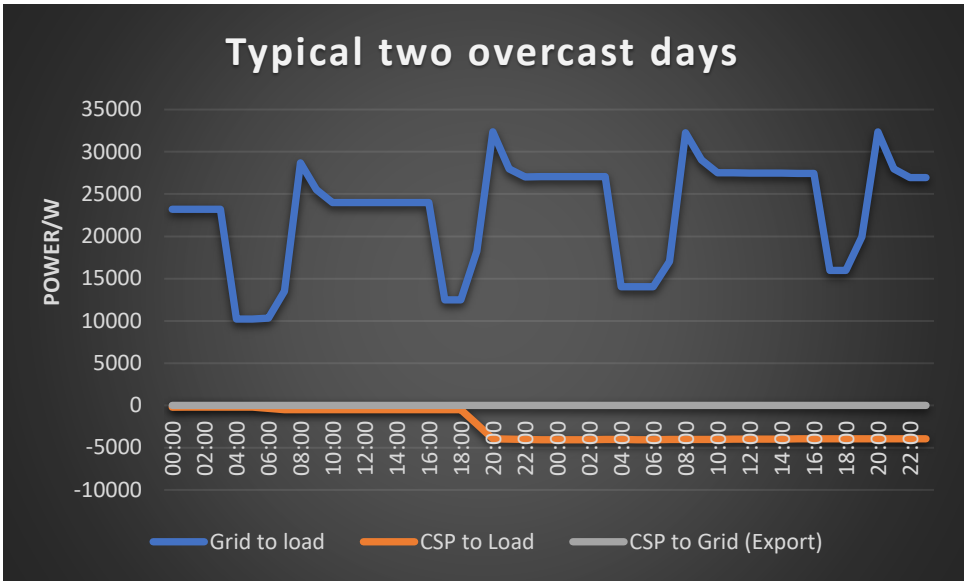


Figure 4. 63: Typical two bad days for CSP + TES production

### 4.9.4 Economic performance of CSP + TES

The installation cost of the system is predicted at USD 5546/kW with LCOE at US cents 10.45 per kWh. The predicted NPV is USD 28.6 million with simple pay back of 12.9 years. The main economic indicators of the system are given in the table 4.17 below:

Table 4. 17: Main economic indicators for CSP + TES

| **Parameter** | **Unit** | **Value** |
|---|---|---|
| Localised Cost of Energy | USD/kWh | 0.10 |
| Annual Electric Bill without CSP system | USD | 13.69 Million |
| Annual Electric Bill with CSP system | USD | 0.472 Million |
| Net annual savings | USD | 13.22 Million |
| Net Present Value | USD | 28.6 Million |
| Simple pay back | Years | 12.9 |

The first-year simulation results show that the amount of annual electric bill liable is reduced from USD 13.69 million to 0.472 million. This means by reducing the annual load by 41% and exporting 46% of the generated energy, the system is able to save about 96.6% of the annual electric bill. The CSP + TES system exports energy during the peak time where the tariff is highest hence a higher return on investment. The figure 4.64 below shows 4 months with cash inflows instead of outflows.

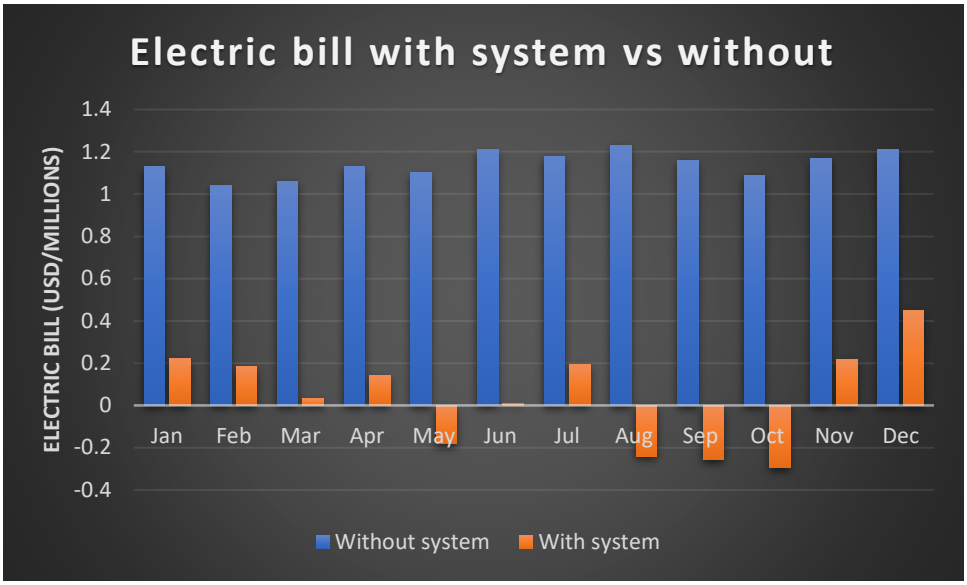


Figure 4. 64: Monthly electric bill with CEP +TES system vs without

## 4.10 Discussion of Results

The table 4.18 below shows the summary of key results from the analysis. The key points from the results are:

- The addition of battery storage system to PV (on base case scenario) improved the percentage of load offset by renewable system and the generated energy by the renewable system by almost double. However, the installation cost, required land, LCOE, and simple payback also increased by approximately a factor of 2 while the NPV reduced by nearly half.
- The addition of thermal storage system to CSP (on base case scenario) increased the generated energy, capacity factor, and renewable energy contribution by approximately a factor of 2. Also, the LCOE improved due to increase in generated energy. However, the land required for development and installation costs also nearly doubled.
- For base case scenario, the CSP and CSP + TES system have a negative NPV making them commercial unviable options. However, the two systems have positive NPV values for export case. This concludes that CSP systems become more economically viable as the size of the system (hence generated energy) increases.
- For both cases, PV system performed better than CSP system both on the technical performance – generated energy, renewable energy contribution – and economic performance – NPV, LCOE, and simple pay back
- In general, systems with exports performed better in terms of technical and economic performance than base case scenarios. This is because the excess energy which could have been clipped is exported gaining revenue in the process.

| **Parameter** | **No Export (base case)** | | | | **With Export** | | | |
|---|---|---|---|---|---|---|---|---|
| | **PV** | **PV + Battery** | **CSP** | **CSP + TES** | **PV** | **PV + Battery** | **CSP** | **CSP + TES** |
| Installed capacity | 37MWdc | 74MW + 210MWh(7hrs) | 32MW | 32MW + 7hrs | 60MWdc | 74MW + 210MWh(7hrs) | 50MW | 40MW + 7hrs |
| Annual Energy generated (first year)/ GWh | 55.1 | 104 | 39.3 | 68.4 | 99.7 | 121 | 94.7 | **127** |
| Renewable Energy contribution (to load)/ % | 33.3 | **63** | 23.7 | 41.3 | 39 | **63** | 28 | 41 |
| LCOE (US cents/ kWh) | 4.76 | 10.67 | 16.32 | 15.44 | **4.34** | 9.4 | 12.13 | 10.45 |
| NPV / USD Million | 41.4 | 19.3 | -13.9 | -17.3 | **47.7** | 31.4 | 3.96 | 28.6 |
| Energy Exported by System / % | - | - | - | - | 35 | 14 | **51** | 46 |
| Grid contribution (to load) / % | 72.7 | **37** | 76.3 | 58.7 | 61 | **37** | 72 | 59 |
| Installation Cost / USD | **0.76/Wdc** | 1.5/Wdc | 2.75/Wac | 5.6/Wac | **0.76/Wdc** | 1.5/Wdc | 3.35/Wac | 5.5/Wac |
| Land used / acres | **114** | 228.2 | 178 | 355 | 185 | 228.2 | 383 | 437 |
| Capacity Factor / % | 19 | 18.6 | 20.6 | **40.5** | 19 | 18.6 | 24 | 40.4 |
| Energy yield (kWh/kW) | 1662 | 1629 | 1802 | **3552** | 1662 | 1629 | 2105 | 3540 |
| Simple pay back / years | **5.1** | 10.8 | - | 20.9 | 6.3 | 9.7 | 15.7 | 12.9 |
| Annual Electric bill savings / USD Million | 5.67 | 10.7 | 4.1 | 7.15 | 7.52 | 12 | 9.68 | **13.2** |

Table 4. 18: Summary of key results

- For base case scenario PV + Battery system performed better than the CSP + TES both technical and economic performance. With exports scenario, CSP + TES generated more energy (which was largely exported) than the PV + Battery because the simulated battery system was behind the meter hence exports were only limited to excess energy generated by PV system. However, due to high installation costs of the CSP + TES system, the PV + Battery performed better on the economic performance regardless of producing less energy.
- In terms of renewable energy contribution and grid reliance, PV + Battery system out-performed all other systems with 63% and 37% (on both scenarios) respectively. The least performing system was CSP base case.
- In terms of NPV and LCOE, PV system with exports performed better than other systems due to low installation cost and the ability to export energy (hence reduced clipping and grid limit losses). CSP with no exports performed least on LCOE while CSP + TES with no exports performed least as far as NPV is concerned.
- In terms of land use, the CSP + TES (with exports) required the biggest land for development while PV base case required the least.
- As far as installation cost is concerned, CSP + TES has the highest cost while PV system has the least. The sensitivity analyses showed that a reduction of about 30% in installation costs will improve the economic performance of CSP + TES system.

From the analysis above, PV + Battery will be the recommended system for development. This is mainly because the system was able to reduce the mine annual grid reliance to only 37% (considering that the dispatch design was not meant to include off-peak period which constitute 32% of the annual mine load). CSP + TES has the potential to be competitive economically if exports are allowed (hence bigger capacity) and installation cost reduce by at least 30%.

# 5.0 Conclusion

This research was aimed at analysing the technical and economic performance of CSP (+ thermal storage) and PV (+ battery storage) as applied to a typical mine in Zimbabwe. The analysis showed that the PV + Battery models could offset about 63% of the annual mine load. This is approximately double the contribution of PV system alone as the addition of battery firmed up the generation of the renewable system. However, there is need to optimise the PV size relative to the battery storage size (and load profile) as the analysis shows that the larger the capacity of the two systems the lower the economic performance.

The CSP + TES system managed to offset about 41% of the annual mine load against 24% (base case) of CSP alone. Design parameters like solar multiple, storage hours, design point DNI, and solar field subsection need to be optimised based on the given demand profile. The analysis shows that CSP systems performed better economically with exports allowed which translates to bigger plant capacity.

Both the technical and economic performances of all the simulated models performed better with the option to exporting to grid. For models with storage systems, the ability to export energy during peak periods where the electricity tariff is highest certainly boosted the economic performance thereof. With exports, CSP + TES LCOE was comparable to that of PV + Battery (US cents 10.45/kWh vs 9.4/kWh respectively) something that was not the case with no exports (US cents 15.44/kWh vs 10.67/kWh respectively).

The installation costs of CSP systems are currently still high when compared to PV systems. For instance, CSP + TES installation cost was over double than that predicted for PV + Battery. Also, the land required to develop the CSP technology is close to twice the land required for PV systems.

The recommended system based on the analysis carried out will be the PV + Battery system. The CSP + TES system shows great potential if the exports to the grid are allowed, bigger load, and the installation cost thereof fall by at least 30%.

# 6.0 Future Work

The exports scenario for PV + Battery was limited to behind the meter battery (due to software limitation) hence did not fully utilise the potential of the battery system. When simulating in-front of the meter battery in SAM there is no option for the system to supply the local load. There is need to explore the PV + Battery (Infront of the meter hence battery system can export to grid) where exports are allowed while suppling the local load. The system promises to improve the economic performance and overall generated renewable energy.

The combination of PV + CSP (+ Battery + TES) also need to be explored. The anticipated benefits from theory include improved capacity factor and reduced LCOE. A dispatch strategy will need to be formulated to exploit the unique characteristics of the systems. SAM software can be used as it has a way to simulate combined cases and a platform to develop a dispatch algorithm to control the combined cases.

The possibility of implementing demand side management at the mine like load shifting while evaluating different renewable energy sources need to be analysed. For instance, the possibility of utilising PV during the day to cover most of the load while reducing the peak load but at the same time exporting energy from battery system (during peak period) promises to have great economic benefits.

# References

Alsadi, S., Khatib, T., (2018), "Photovoltaic Power Systems Optimisation Research Status: A Review of Criteria, Constrains, Models, Techniques, and Software tools", Applied Sciences, Vol. 8, page 1 – 30

Arrif, T., Benchabane, A., Germoui, M., Bezza, B., Belaid, A., (2018), ''Optimisation of heliostat field layout for solar power tower systems using iterative artificial bee colony algorithm: a review and case study'', International Journal of Ambient Energy

Australian Renewable Energy Agency, 2017, ''Renewable Energy in the Australian mining sector'', available at https://arena.gov.au/knowledge-bank/renewable-energy-australian-mining-sector/

Australian Renewable Energy Agency, (2018), ''Hybrid power generation for Australian off-grid mines handbook, available at https://arena.gov.au/assets/2018/06/hybrid-power-generation-australian-off-grid-mines.pdf

Batuecas, E., Mayo, C., Diaz, R., Perez, F.J., (2017), "Life cycle assessment of heat transfer fluids in parabolic trough concentrating solar power technology", Solar Energy Materials and Solar Cells, Vol. 171, page 91- 97

Benitez, D., Kazantzidis, A., Al-Salaymeh, A., Bouaichaoui, S., Guizani, A., (2018), "Combined CSP – PV plants for Mena Region", GCREEDER 2018, Amman - Jordan, April 3rd – 5th 2018

Bhattacharya, P., Dey, S., Mustaphi, B., (2014), "Some analytical studies on the performance of grid connected solar photovoltaic system with different parameters, Procedia Material Science, Vol.6, page 1942-1950

Bousselamti, L., and, Cherkaoui, M., (2019), "Modelling and assessing the performance of hybrid PV-CSP plants in Morocco: A Parametric study", International Journal of Photoenergy, Volume 2019, Article ID 5783927, 15 pages, https://doi.org/10.1155/2019/5783927

Bravo, R. and Friedrich, D., (2018), ''Integration of energy storage with hybrid solar power plant'', Energy Procedia

Cerro Dominador website, (2020), https://cerrodominador.com/en/quienes-somos-en/

Cirocco, L., Belusko, M., Bruno, F., Boland, J., Pudney, P., (2014), ''Optimization of storage for concentrated solar plants, Challenges, Vol. 5, page 473 – 503

Columbia Center on Sustainable Investment, (2018), ''The Renewable power of the mine – Accelerating renewable energy integration'', available at http://ccsi.columbia.edu/files/2018/12/3418-CCSI-RE-and-mining-report-09-lr-reduced-optmized-07-no-links.pdf

Dieckmann, S., Dersch, J., (2017), "Simulation of hybrid solar plants", AIP Conference Proceedings 1850, 16005 (2017), https://doi.org/10.1063/1.4984539

Dieckmann, S., Dersch, J., (2015), "Techno – Economic evaluation of Renewable Energy projects using software GREENIUS", International journal of Thermal and Environmental Engineering, Vol. 10 No. 1, page 17 – 24

Eddhibi, F., Amara B.M., Balghouthi, M., Guizani, A., (2015), ''Optimal study of solar tower power plants'', Journal of physics: Conference Series 596 (2015) 012018

Florin, N., Dominish, E., (2017), "Sustainability evaluation of energy storage technologies", Institute of Sustainable futures for the Australian Council of learned academics", available at https://acola.org/wp-content/uploads/2018/08/wp3-sustainability-evaluation-energy-storage-full-report.pdf

Fouad, M.M., Shihata, A.L., Morgan, I.E., (2017), "An integrated review of factors influencing the performance of photovoltaic panels", Renewable Energy and Sustainable Energy Reviews, Vol. 80, page 1499 – 1511

Gharbi, E.N, Derbal, H., Bouaichaoui, S., Said, H., (2011), ''A comparative study between parabolic trough collector and linear Fresnel reflector technologies, Energy Procedia, Vol. 6, page 565 – 572

Green, A., Diep, C., Dunn, R., Dent, J., (2015), ''High Capacity Factor CSP-PV Hybrid Systems'', Energy Procedia, Vol. 69, page 2049-2059

Green Energy System Analysis (GREENIUS), (2020), GREENIUS Manual Version 4.5.0.1052, DRL Solar Research, Available at https://www.dlr.de/sf/de/Portaldata/73/Resources/sonstiges/greenius/Greenius_Manual.pdf

Hesse, C., H., Schimpe, M., kucevic, D., Jossen, A., "Lithium-ion battery storage system design tailored for application in modern power grids, Energies, Vol 10, page 1-42

Homer help manual, (2020), https://www.homerenergy.com/products/pro/docs/index.html

IEA Energy Efficiency Indicators Database, (2019), ''Kew world energy statistics'', available at https://www.iea.org/reports/key-world-energy-statistics-2019

International Renewable Energy Agency (IRENA), (2012), ''Renewable Energy Technologies (CSP): Cost analysis series'', Volume 1:Power sector, Issue 215, available at https://www.irena.org/documentdownloads/publications/re_technologies_cost_analysis-csp.pdf

International Renewable Energy Agency (IRENA), (2020), Renewable Power Generation Costs in 2019'' available at https://www.irena.org/publications

International Finance Corporation, (2015), "A project developer's guide to utility-scale photovoltaic power plants", available at https://www.ifc.org/wps/wcm/connect/topics_ext_content/ifc_external_corporate_site/sustainability-at-ifc/publications/publications_utility-scale+solar+photovoltaic+power+plants

International Renewable Energy Agency (IRENA), (2019), "Innovation landscape brief: Behind-the-meter batteries", available at https://www.irena.org/-/media/Files/IRENA/Agency/Publication/2019/Sep/IRENA_BTM_Batteries_2019.pdf

International Renewable Energy Agency (IRENA), (2019), "Innovation landscape brief: Utility scale batteries", available at https://www.irena.org/-/media/Files/IRENA/Agency/Publication/2019/Sep/IRENA_Utility-scale-batteries_2019.pdf

International Renewable Energy Agency (IRENA), (2020), Renewable Power Generation Costs in 2019'' available at https://www.irena.org/publications

INSEL website (2020), https://insel4d.ca/en/what-is-insel.html

Isalm, M.T., Huda, N., Abdullah, A.B., Saidur, R., (2018), ''A comprehensive review of state of the art concentrating solar power technologies: Current status and research trends, Renewable and Sustainable Energy Reviews, Vol. 91, page 987 – 1018

Ju, X., Xu, C., Hu, Y., Han, Y., Wei, G., Du, X., (2017), "A review on the development of photovoltaic/Concentrated Solar (PV – CSP) hybrid system", Solar Energy Materials and Solar Cells, Vol. 161, page 305 – 327

Kuravi, S., Trahan, J., Goswam, Y.D., Rahman, M.M., Stefanokos, E.K., (2013), Thermal energy storage technologies and systems for concentrating solar plants, Progress in Energy and Combustion Science, page 1 – 35

Liu, H., Zhai, R., Fu, J., Wang, Y., Yang, Y., (2019), "Optimization study of thermal storage PV – CSP integrated system based on GA – PSO algorithm", Solar Energy, Vol. 184, page 391 – 409

Liu, M., Steven Tay, N.H., Bell, S., Belusko, M., Jacob, R., Will, W.S., Bruno, F., (2016), ''Review on concentrating solar plants and new developments in high temperature thermal energy storage technologies'', Renewable and Sustainable Energy Reviews, Vol. 53, pp 1411-1432

May, J., G., Davidson, A., Monahov, B., (2018), "Lead batteries for utility energy storage: A review", Journal of Energy Storage, Vol. 15, page 145 – 157

National Renewable Energy laboratory (NREL), (2013), Technical Report NREL/TP-6A20-60272, available at https://www.nrel.gov/docs/fy14osti/60272.pdf

National Renewable Energy Laboratory, (2014), "Modelling Parabolic Trough systems", available at https://sam.nrel.gov/images/webinar_files/sam-webinars-2014-parabolic-trough-systems.pdf

National Renewable Energy Laboratory, (2018), "Best practices for operation and maintenance of photovoltaic and Energy Storage: 3rd Edition", NREL/TP-7A40-73822, available at https://www.nrel.gov/docs/fy19osti/73822.pdf

National Renewable Energy Laboratory, (2011), "Technical manual for the SAM physical trough model", NREL/TP-5500-51825, available at https://www.nrel.gov/docs/fy11osti/51825.pdf

National Renewable Energy Laboratory, (2020), "Concentrating solar power best practice study", NREL/TP-5500-75763, available at https://www.nrel.gov/docs/fy20osti/75763.pdf

National Renewable Energy Laboratory, (2007), "Parabolic trough technology development" available at https://www.nrel.gov/docs/fy07osti/41424.pdf

National Renewable Energy Laboratory (NREL), (2016), "Exploring the potential competitiveness of utility-scale photovoltaics plus batteries with concentrating solar power, 2015-2030", Technical report NREL/TP – 6A20 – 66592, available at https://www.nrel.gov/docs/fy16osti/66592.pdf

National Renewable Energy Laboratory, (2017), "Evaluating the technical and Economic performance of PV plus storage power plants", Technical report NREL/TP-6A20-68737, available at https://www.nrel.gov/docs/fy17osti/68737.pdf

Padilla, V.R., (2011), "Simplified methodology for designing parabolic trough solar power plants", available at https://scholarcommons.usf.edu/cgi/viewcontent.cgi?referer=&httpsredir=1&article=4585&context=etd

Pan, C.A., Dinter, F., (2017), "Combination of PV and central receiver CSP plants for base load power generation in South Africa", Solar Energy, Vol. 146, page 379 – 388

Parrado, C., Girrard, A., Simon, F., Fuentealba, E., (2016), ''2050 LCOE projection for a hybrid PV-CSP plant in the Atacama Desert in Chile'', Energy, Vol 94, page 422-430

Petrollese, M., Cocco, D., (2016), "Optimal design of a hybrid CSP-PV plant for achieving the full dispatchability of Solar Energy power plants", Solar Energy, Vol. 137, page 447 – 489

PVSyst help manual, (2020), https://www.pvsyst.com/help/

Rocky Mountain Institute, (2019), ''Renewable resources at mine tracker'', available at https://rmi.org/our-work/industry-and-transportation/material-value-chains/renewable-resources-at-mines-tracker/

SAM help manual, (2020), https://sam.nrel.gov/download.html

Schott solar, (2020), "Schott PTR 70 Receiver brochure" available at https://www.schott.com/d/csp/370a8801-3271-4b2a-a3e6-c0b5c78b01ae/1.0/schott_ptr70_4th_generation_brochure.pdf

Shahin, A., Shirouyehzad, H., Pourjavad, E., (2012), ''Optimal maintenance strategy: A case study in mining industry'', International Journal of Service and Operations Management, Vol 12, No.12, page 368-386

Singh, G., and, Singh, B.R., (2019), "Recent developments in hybrid solar power generation: A review", International Journal of Engineering research and technology, Vol. 8, Issue 06, page 1019 – 1031

Solcast website, (2020), https://solcast.com/

Starke, A.R, Cardemil, D.M, Escobar, R., Lolle, S., (2018), "Multi-objective optimisation of hybrid PTC + PV system using generic algorithm", AIP Conference Proceedings 2033, 180011 (2018), https://doi.org/10.1063/1.5067183

TRNSYS website (2020), http://www.trnsys.com/index.html

Turchi, Craig, S., Boyd, M., Kesseli, D., Kurup, P., Mehos, M., Neises, T., Sharan, P., Wagner, M., Wendelin, T., (2019).” CSP Systems Analysis – Final Project Report”, Golden, CO: National Renewable Energy Laboratory. NREL/TP-5500-72856, available at https://www.nrel.gov/docs/fy19osti/72856.pdf

Vidyanandan, K.V., (2017), “An overview of factors affecting the performance of Solar PV Systems”, Journal of Corporate planning, Issue 27, page 2-8

Zhai, R., Liu, H., Chen, Y., Yang, Y., (2017), “The daily and annual technical – economic analysis of the thermal storage PV – CSP system into two strategies”, Energy conversion and management, Vol. 154, page 56 – 67

Zhai, R., Chan, Y, Liu, H., Wu, H., Yang, Y., (2018), “Optimal design method of a hybrid CSP-PV plant based on Generic Algorithm considering the operational strategy”, International Journal of Photoenergy, Volume 2018, Article ID 8380276, 15 pages https://doi.org/10.1155/2018/8380276

Ziuka, S., Seyetin, L., Mapurisa, B., Chikodzi, D., van Kuijk, K., (2014), ‘’Potential of concentrated solar power (CSP) in Zimbabwe’’, Energy for sustainable development, No. 23, pp 220-227

Zurita, A., Mata-Torres, C., Valenzuela, C., Felbol, C., Cardemil, J.M., Guzman, A.M, Escobar, R.A, (2018), ‘’Techno-economic evaluation of a hybrid CSP + PV plant integrated with thermal storage and a large scale battery energy storage system for base generation’’, Solar Energy, Vol 173, page 1262-1277

Zurita, A., Mata-Torres, C., Cardemil, J.M., Escobar, A.R., (2020), “Assessment of time resolution impact on the modelling of a hybrid CSP-PV plant: A case of study in Chile”, Solar Energy, Vol. 202, page 553 – 570

# Appendix A – Characteristics of CSP (Islam et al, 2018)

| | Parabolic-trough collector (PTC) | Linear Fresnel reflectors (LFR) | Solar power tower (PTC) | Solar parabolic dishes (SPD) |
|---|---|---|---|---|
| **Capacity (MWe)** | 10-200 | 10-200 | 10-150 | 0.01-0.4 |
| **Concentration ratio** | 25-100 | 70-80 | 300-1000 | 1000-3000 |
| **Solar efficiency max** | 20% (expected) | 21% (demonstrated) | 20% (demonstrated) 35% (expected) | 29%(demonstrated) |
| **Annual solar-to-electric efficiency** | 15% | 8-10% | 20-35% (concepts) | 20-35% |
| **Optical efficiency** | Medium | Low | Medium | High |
| **Collector concentration** | 70-80 suns | > 60 suns (depends on secondary reflector) | > 1000 suns | >1300 suns |
| **Receiver/absorber** | Absorber attached to collector, moves with collector, complex design | Fixed absorber, no evacuation, secondary reflector | External surface or cavity receiver, fixed | Absorber attached to the collector, moves with collector |
| **Area requirement ($m^2$/MWh)** | 4 to 6 | 6 to 8 | 8 to 12 | 30 to 40 |
| **Thermal efficiency (%)** | 30-40 | - | 30-40 | 30-40 |
| **Plant peak efficiency (%)** | 14-20 | 18 | 23-35 | ~30 |
| **Capital cost (US$/kW)** | 3972 | - | 4000+ | 12578 |
| **Capital cost (US$/m^2)** | 424 | 234 | 476 | - |
| **Operation and maintenance cost ($/kW h)** | 0.012 − 0.02 | low | 0.034 | 0.21 |
| **Basic plant cost (US$/W)** | 3.22 | - | 3.62 | 2.65 |
| **Land use (m^2/MW h/year)** | 6 to 8 | 4 to 6 | 8 to 12 | 8 to 12 |
| **Specific power ($W/m_2$)** | 300 | - | 300 | 200 |
| **Water requirement (m^3/MWh)** | 3 (wet cooling), 0.3 (dry cooling) and 0.4-1.7 (hybrid) | 3(wet cooling) and 0.2 (dry cooling) | 2-3 (wet cooling), 0.25 (dry cooling) | 0.05-0.1 (mirror washing) |
| **Annual CF (%)** | 25-28 (no TES), 29-43 (7 h TES) | 22-24 | 55 | (10 h TES) 25-28 |
| **Grid stability** | Medium to high (TES or hybridization) | Medium (back-up firing possible) | High (large TES) | low |
| **Operating temperature of solar field (°C)** | 290-550 | 250-390, possible up to 560° C | 250-650 | 800 |

# Appendix B – Type and Characteristics of PV Cells (International Finance Corporation, 2015)

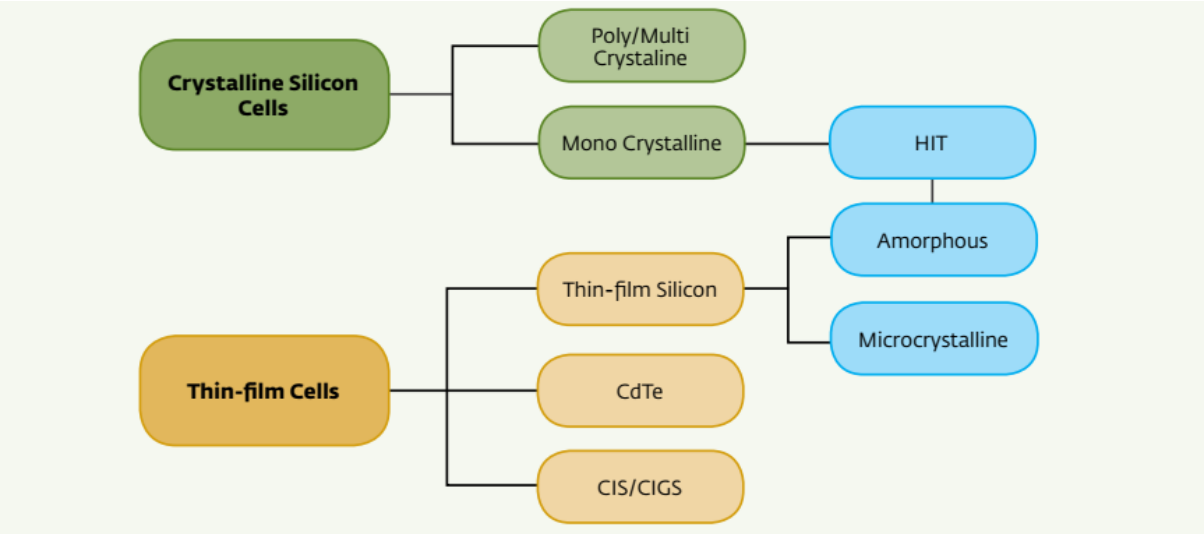


| Technology | Crystalline Silicon | Heterojunction with intrinsic Thin-film Layer | Amorphous Silicon | Cadmium Telluride | Copper Indium Gallium Di Selenide |
|---|---|---|---|---|---|
| Category | c-Si | HIT | a-Si | CdTe | CIGS or CIS |
| Current commercial efficiency (Approx.) | 13%-21% | 18%-20% | 6%-9% | 8%-16% | 8%-14% |
| Temperature co-efficient for power a (Typical) | -0.45%/ºC | 0.29%/ºC | -0.21%/ºC | -0.25%/ºC | -0.35%/ºC |

# Appendix C – SAM Calculations for LCOE and NPV

$$\text{Levelized cost (nominal)} = \frac{-C_0 - \frac{\sum_{n=1}^{N} C_n}{(1+d_{nominal})^n}}{\frac{\sum_{n=1}^{N} Q_n}{(1+d_{nominal})^n}}$$

Where:

- **$Q_n$** (kWh) is the electricity generated by the system in year n
- **N** is the analysis period in years
- **$C_0$** is project equity investment amount
- **$C_n$** is project annual costs in year n
- **$d_{nominal}$** is the discount rate

$$\text{NPV} = \sum_{n=0}^{N} \frac{C_n}{(1+d_{nominal})^n}$$

Where:

- **$C_n$** is the after-tax cash flow in year n
- **N** is the analysis period in years
- **$d_{nominal}$** is the discount rate

**Capacity factor in SAM**

$$Capacity\ factor = \frac{Net\ annual\ Energy\ (kWhac/year}{System\ capacity\ (kWdc\ or\ kWac) x\ 8760hrs}$$

# Appendix D – Configurations of Air Cooled Condensers (Padilla, 2011)

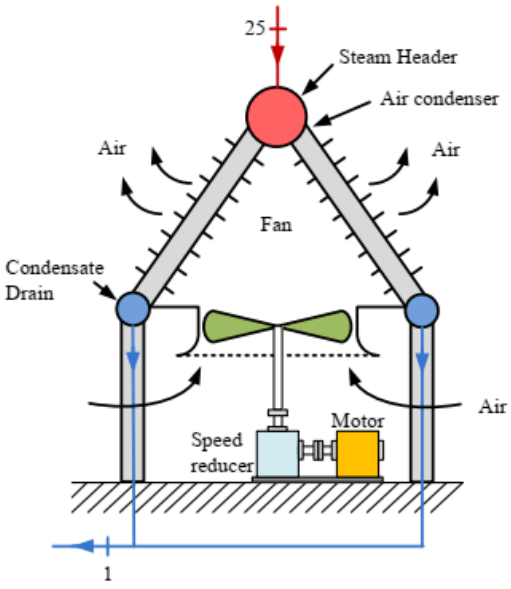


A frame air cooled condensor

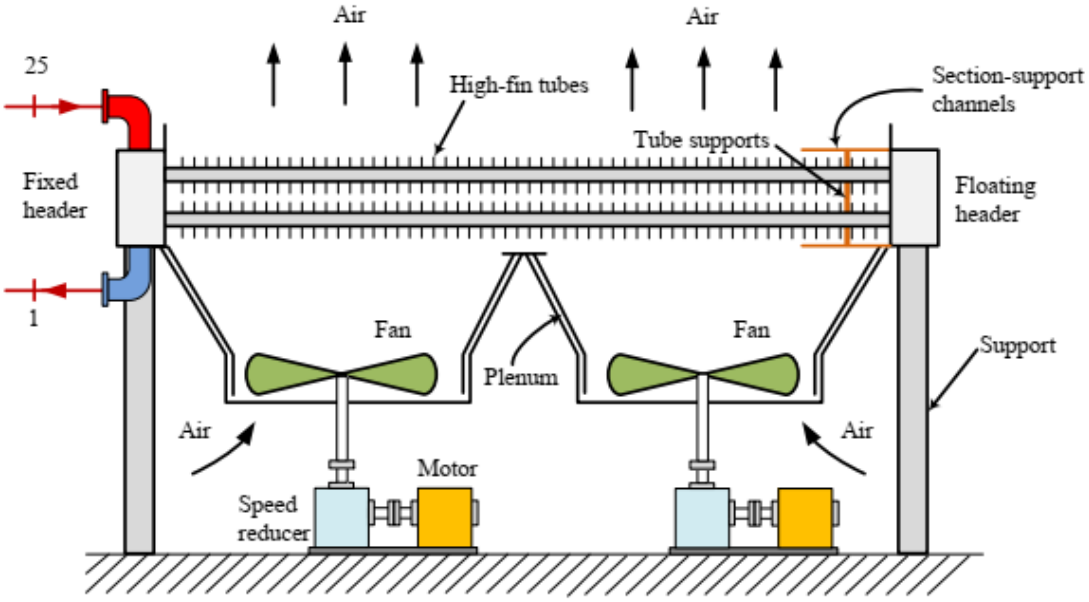


Air cooled heat exchanger using horizontal tubes: forced draft

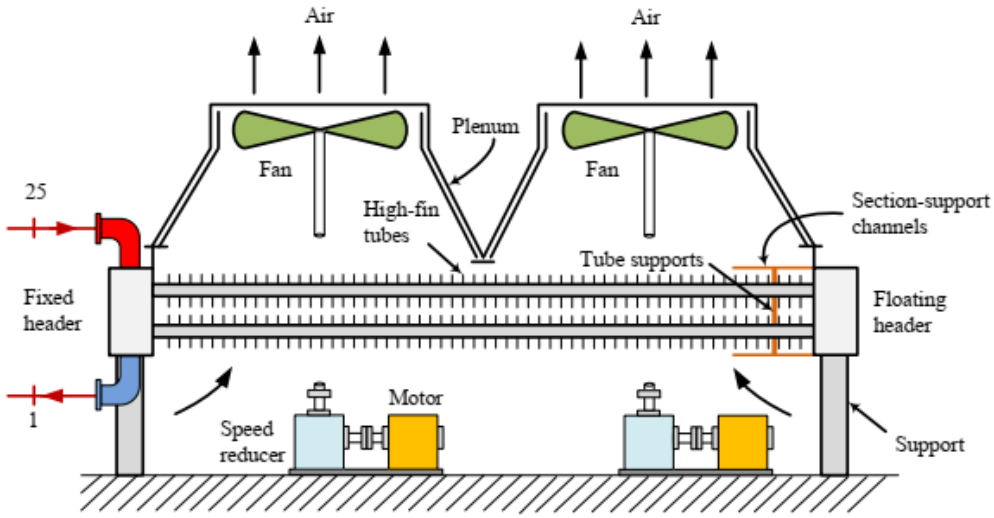


Air cooled heat exchanger using horizontal tubes: induced draft

# Appendix E – Moody Chart (NREL, 2014)

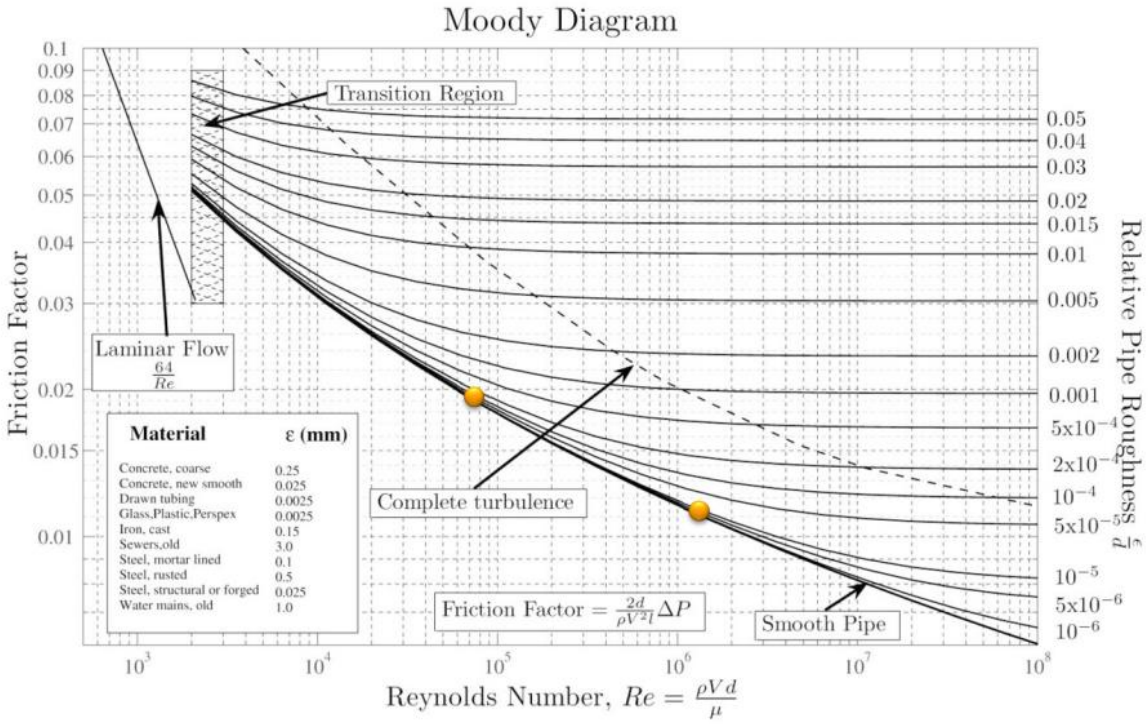

# Appendix F – PV System Loss Diagram and Lifetime production

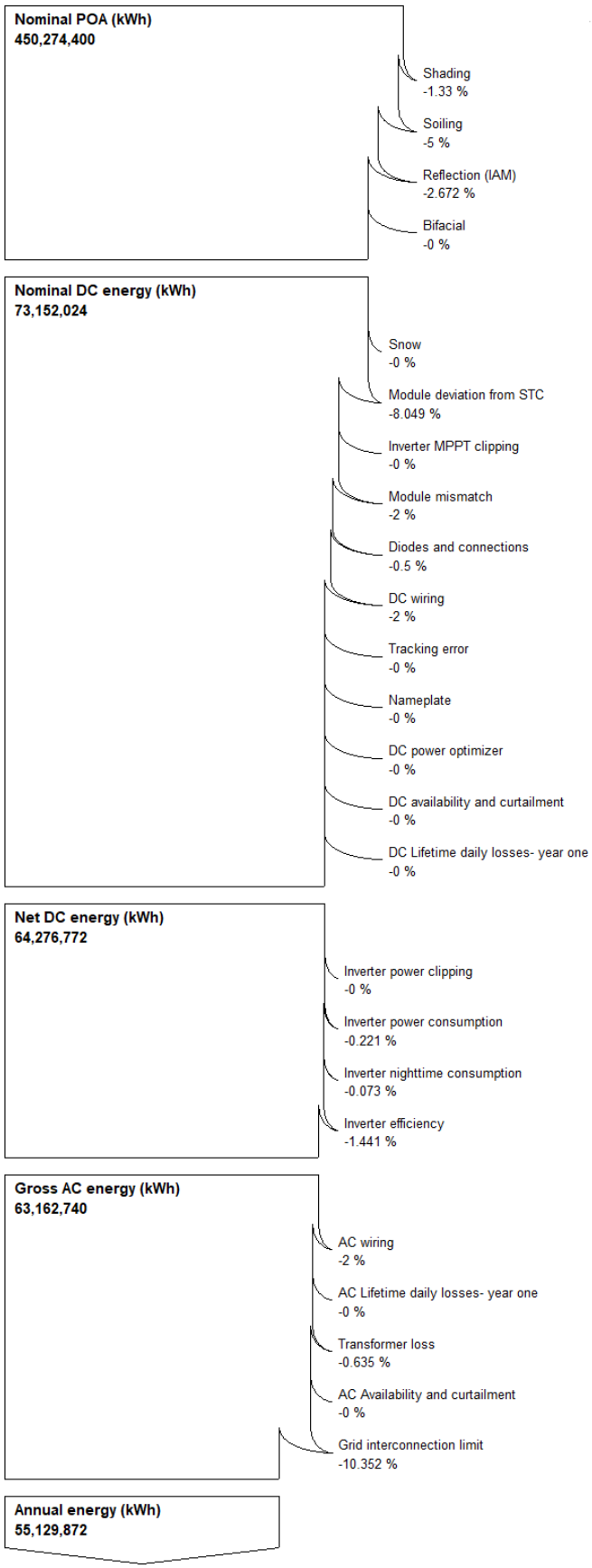


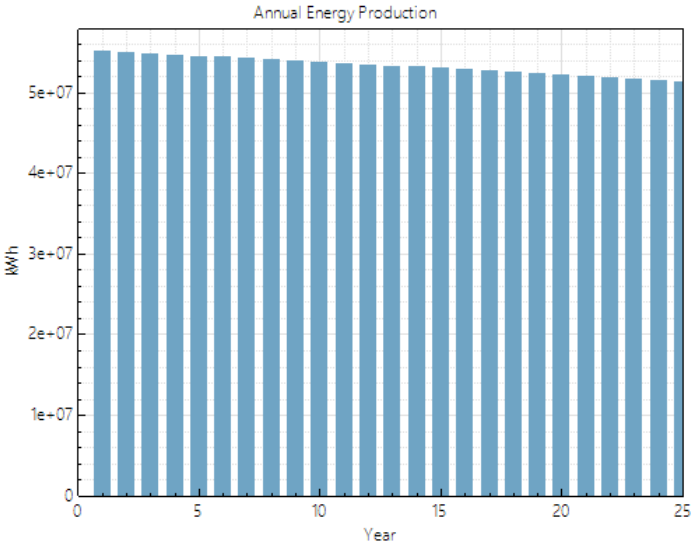

# Appendix G – PVSyst Summary results

| PVSYST V6.43 | | 12/07/20 | Page 3/5 |
|---|---|---|---|

## Grid-Connected System: Main results

**Project :** **Mimosa**

**Simulation variant :** **New simulation variant**

| | | | | |
|---|---|---|---|---|
| **Main system parameters** | System type | **Grid-Connected** | | |
| **Near Shadings** | Linear shadings | | | |
| PV Field Orientation | tilt | 20° | azimuth | 0° |
| PV modules | Model | Poly 285 Wp 72 cells | Pnom | 285 Wp |
| PV Array | Nb. of modules | 129975 | Pnom total | **37043 kWp** |
| Inverter | Model | 30 kWac inverter | Pnom | 30.0 kW ac |
| Inverter pack | Nb. of units | 1174.0 | Pnom total | **35220 kW ac** |
| User's needs | Unlimited load (grid) | | | |

| | | | | |
|---|---|---|---|---|
| **Main simulation results** | | | | |
| System Production | **Produced Energy** | **60457 MWh/year** | Specific prod. | 1632 kWh/kWp/year |
| | Performance Ratio PR | 74.5 % | | |
| Investment | Global incl. taxes | 29209745 US$ | Specific | 0.79 US$/Wp |
| Yearly cost | Annuities (Loan 5.0%, 25 years) | 2072503 US$/yr | Running Costs | 9 US$/yr |
| Energy cost | | **0.03 US$/kWh** | | |

**Normalized productions (per installed kWp): Nominal power 37043 kWp**

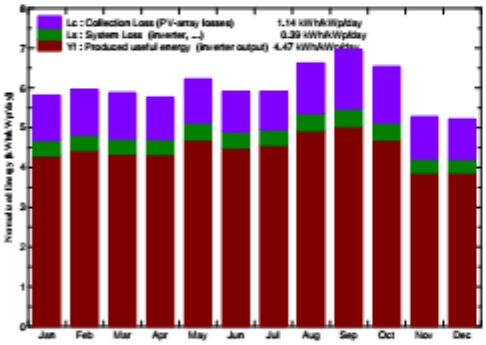


**Performance Ratio PR**

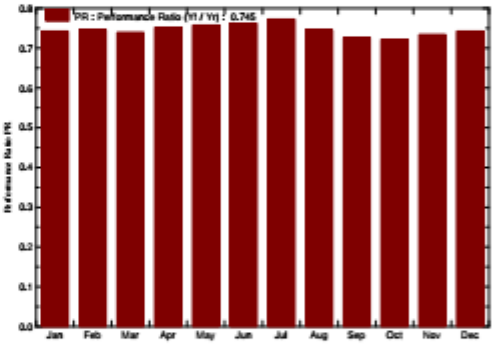


**New simulation variant**

**Balances and main results**

| | GlobHor kWh/m² | T Amb °C | GlobInc kWh/m² | GlobEff kWh/m² | EArray MWh | E_Grid MWh | EffArrR % | EffSysR % |
|---|---|---|---|---|---|---|---|---|
| January | 192.3 | 22.37 | 180.1 | 167.0 | 5389 | 4952 | 11.86 | 10.90 |
| February | 171.5 | 20.88 | 166.6 | 154.3 | 5003 | 4603 | 11.91 | 10.96 |
| March | 174.1 | 21.29 | 182.3 | 169.7 | 5430 | 4993 | 11.81 | 10.86 |
| April | 151.3 | 19.08 | 172.9 | 161.3 | 5240 | 4817 | 12.02 | 11.05 |
| May | 154.4 | 16.06 | 193.0 | 180.7 | 5892 | 5414 | 12.10 | 11.12 |
| June | 135.0 | 14.58 | 177.2 | 166.0 | 5446 | 5002 | 12.19 | 11.19 |
| July | 145.0 | 14.52 | 183.2 | 171.0 | 5693 | 5242 | 12.32 | 11.34 |
| August | 172.1 | 16.65 | 205.3 | 192.5 | 6162 | 5662 | 11.90 | 10.94 |
| September | 190.6 | 20.16 | 208.4 | 195.5 | 6092 | 5598 | 11.59 | 10.65 |
| October | 202.1 | 23.98 | 202.7 | 189.3 | 5894 | 5422 | 11.53 | 10.61 |
| November | 169.0 | 22.78 | 158.4 | 147.1 | 4694 | 4305 | 11.75 | 10.78 |
| December | 176.0 | 22.13 | 161.7 | 149.2 | 4842 | 4445 | 11.87 | 10.90 |
| Year | 2033.6 | 19.53 | 2191.7 | 2043.5 | 65778 | 60457 | 11.90 | 10.94 |

Legends: GlobHor Horizontal global irradiation; T Amb Ambient Temperature; GlobInc Global incident in coll. plane; GlobEff Effective Global, corr. for IAM and shadings; EArray Effective energy at the output of the array; E_Grid Energy injected into grid; EffArrR Effic. Eout array / rough area; EffSysR Effic. Eout system / rough area

# Appendix H– PV + Battery Loss diagram and Lifetime energy production

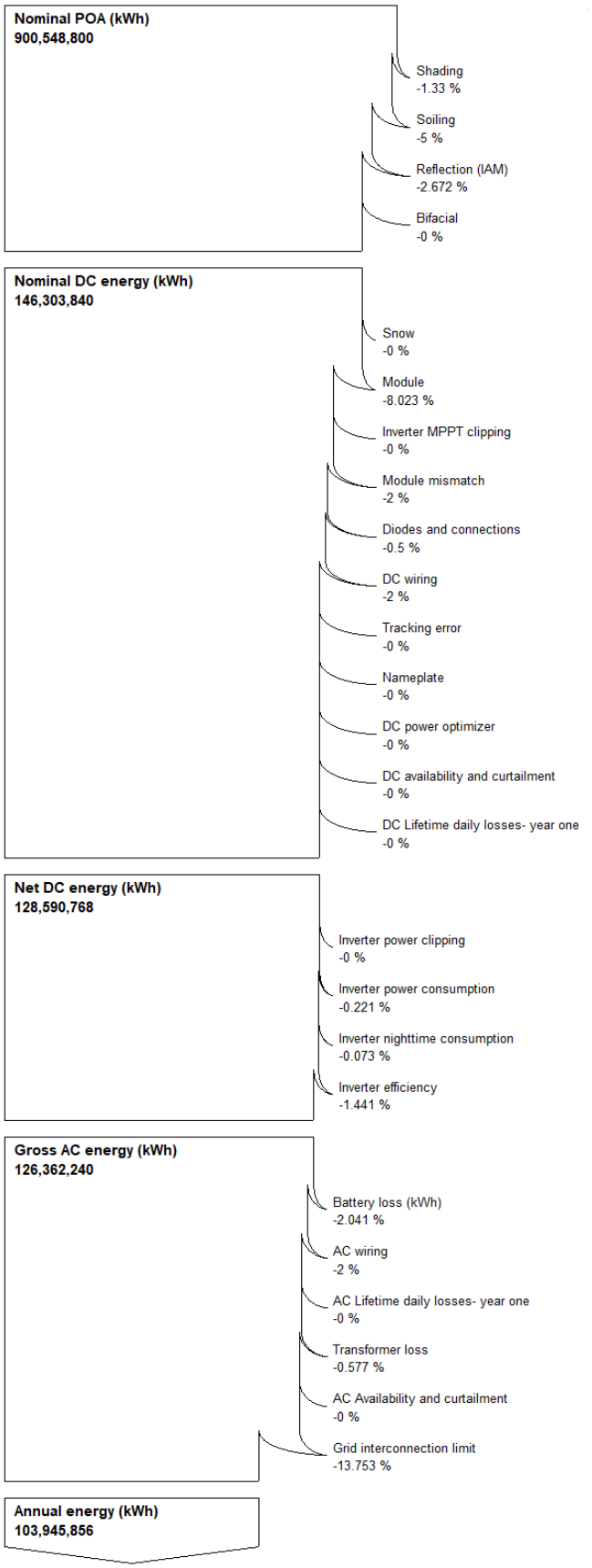


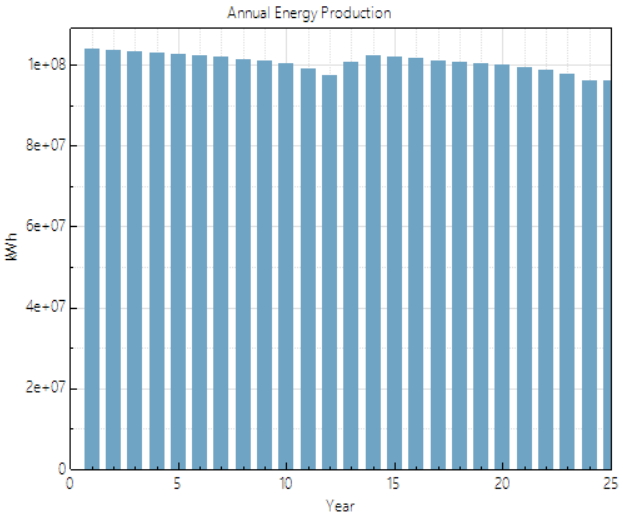

# Appendix I – Summary results of CSP system

| Metric | Value |
|---|---|
| Annual Net Electrical Energy Production | 39,284,100 kWh-e |
| Annual Freeze Protection | 656,100 kWh-e |
| Annual TES Freeze Protection | 0 kWh-e |
| Annual Field Freeze Protection | 656,100 kWh-e |
| Capacity factor | 20.6% |
| Power cycle gross electrical output | 57,764,008 kWh-e |
| First year kWh/kW | 1,802 - |
| Gross-to-net conversion | 89.9 % |
| Annual Water Usage | 11,397 m^3 |
| Levelized COE (nominal) | 16.32 ¢/kWh |
| Levelized COE (real) | 12.96 ¢/kWh |
| Electricity bill without system (year 1) | $13,693,863 |
| Electricity bill with system (year 1) | $9,629,363 |
| Net savings with system (year 1) | $4,064,500 |
| Net present value | $-13,859,520 |
| Simple payback period | NaN |
| Discounted payback period | NaN |
| Net capital cost | $79,326,496 |
| Equity | $0 |
| Debt | $79,326,496 |

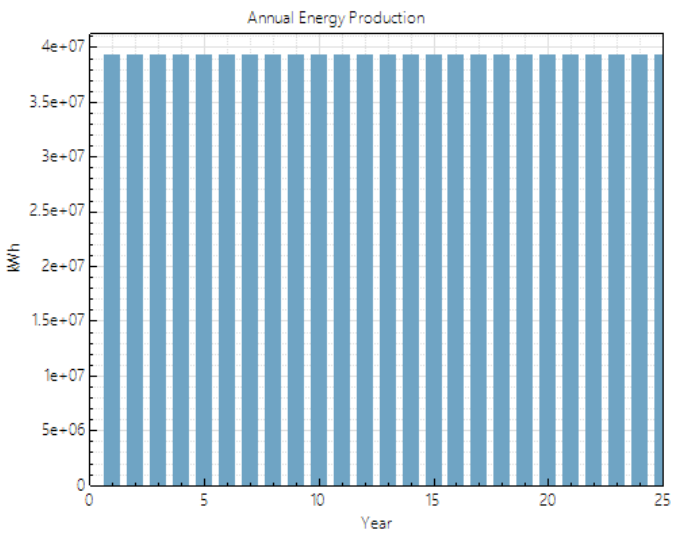

# Appendix J – Summary results for CSP + TES System

| Metric | Value |
|---|---|
| Annual Net Electrical Energy Production | 68,370,184 kWh-e |
| Annual Freeze Protection | 4,132,157 kWh-e |
| Annual TES Freeze Protection | 2,727,843 kWh-e |
| Annual Field Freeze Protection | 1,404,314 kWh-e |
| Capacity factor | 40.5% |
| Power cycle gross electrical output | 114,923,112 kWh-e |
| First year kWh/kW | 3,552 - |
| Gross-to-net conversion | 89.0 % |
| Annual Water Usage | 22,706 m^3 |
| Levelized COE (nominal) | 15.44 ¢/kWh |
| Levelized COE (real) | 12.26 ¢/kWh |
| Electricity bill without system (year 1) | $13,693,863 |
| Electricity bill with system (year 1) | $6,541,949 |
| Net savings with system (year 1) | $7,151,915 |
| Net present value | $-17,304,314 |
| Simple payback period | 20.9 years |
| Discounted payback period | Inf |
| Net capital cost | $161,098,432 |
| Equity | $0 |
| Debt | $161,098,432 |

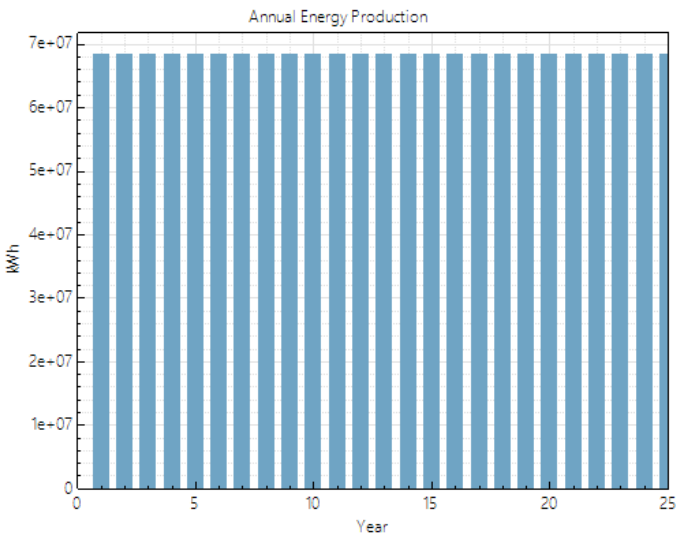

# Appendix K – Uncertainty Analysis for PV System

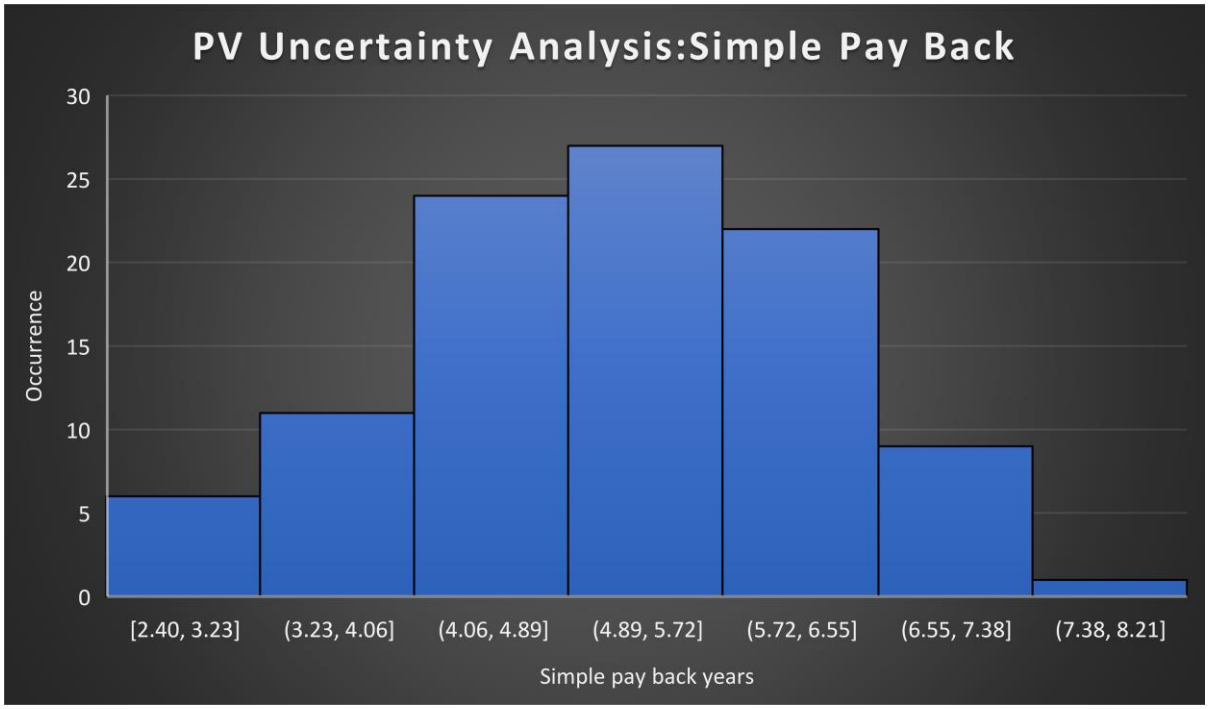


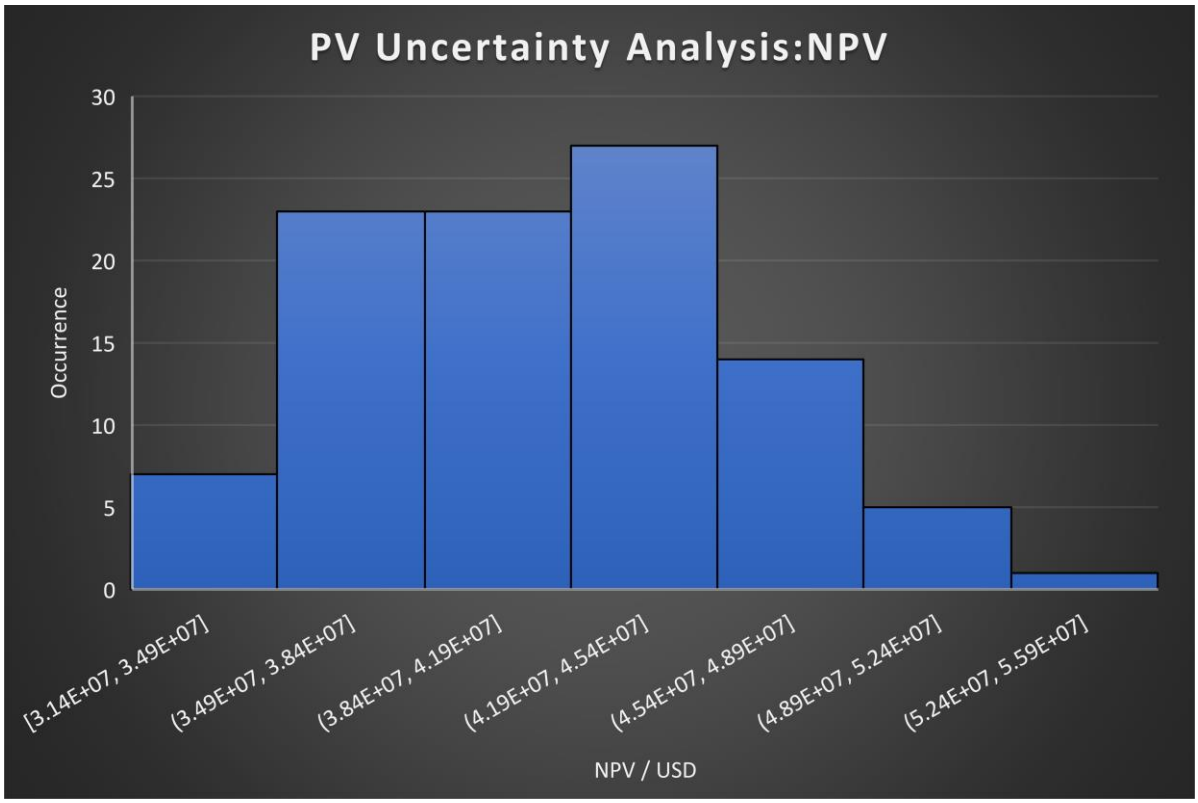

# Appendix L – Uncertainty analysis for PV + Battery

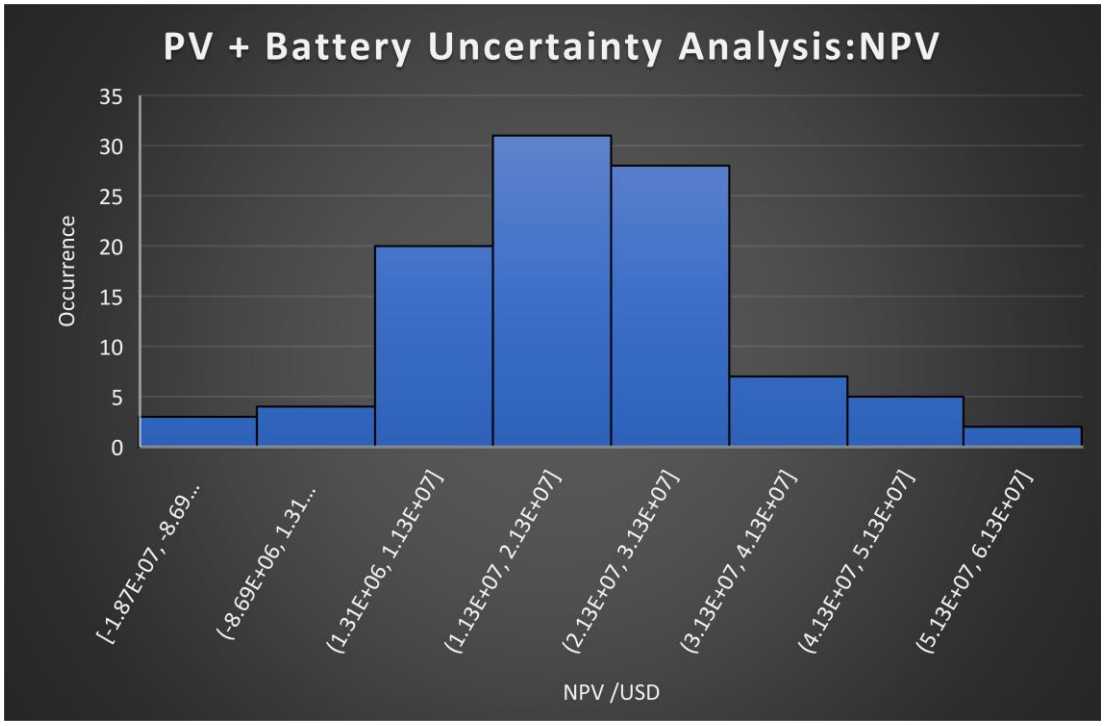


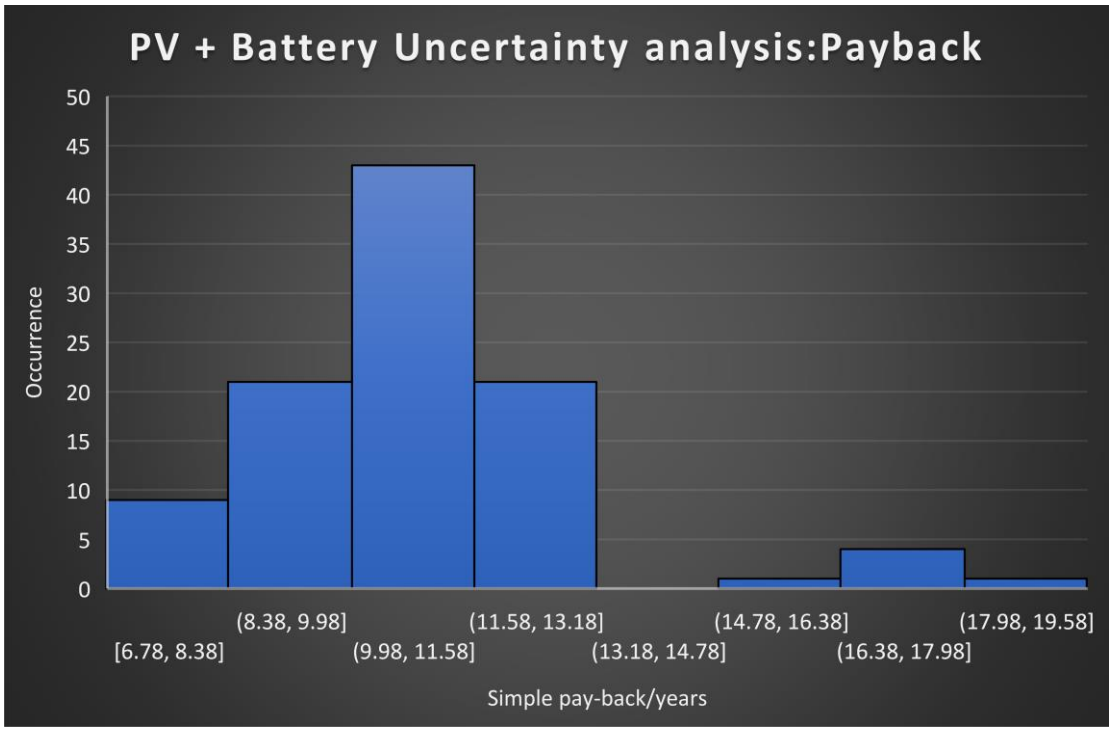

# Appendix M – Uncertainty analysis CSP and CSP + TES

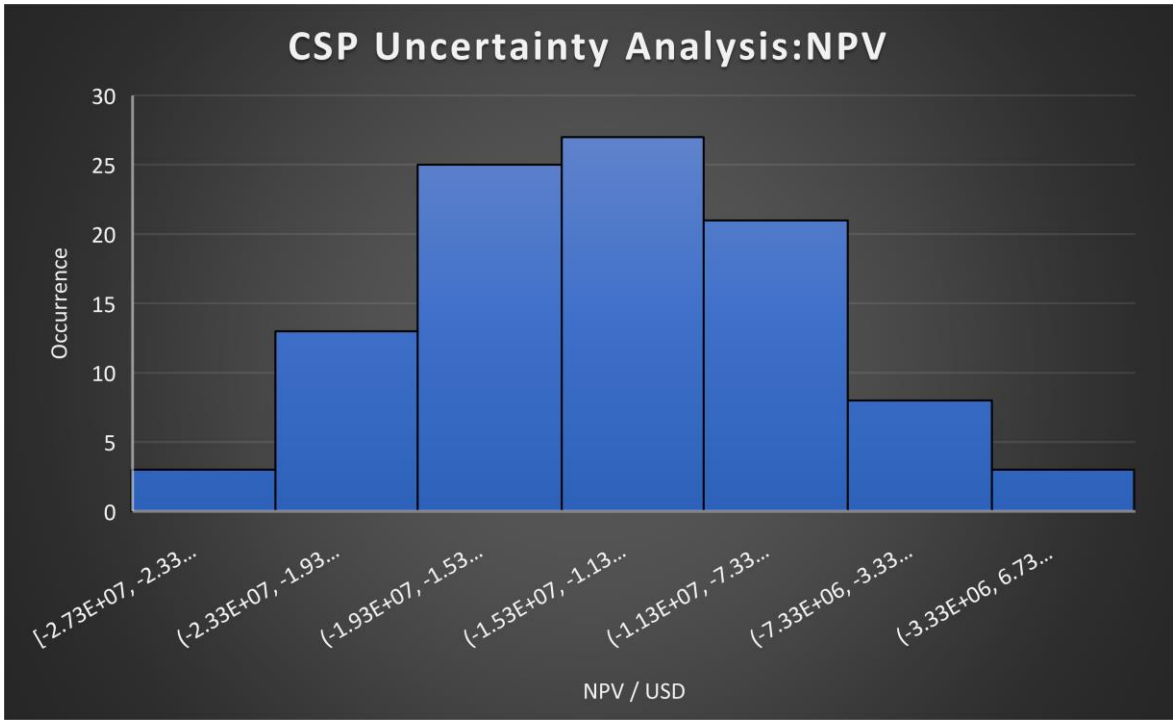


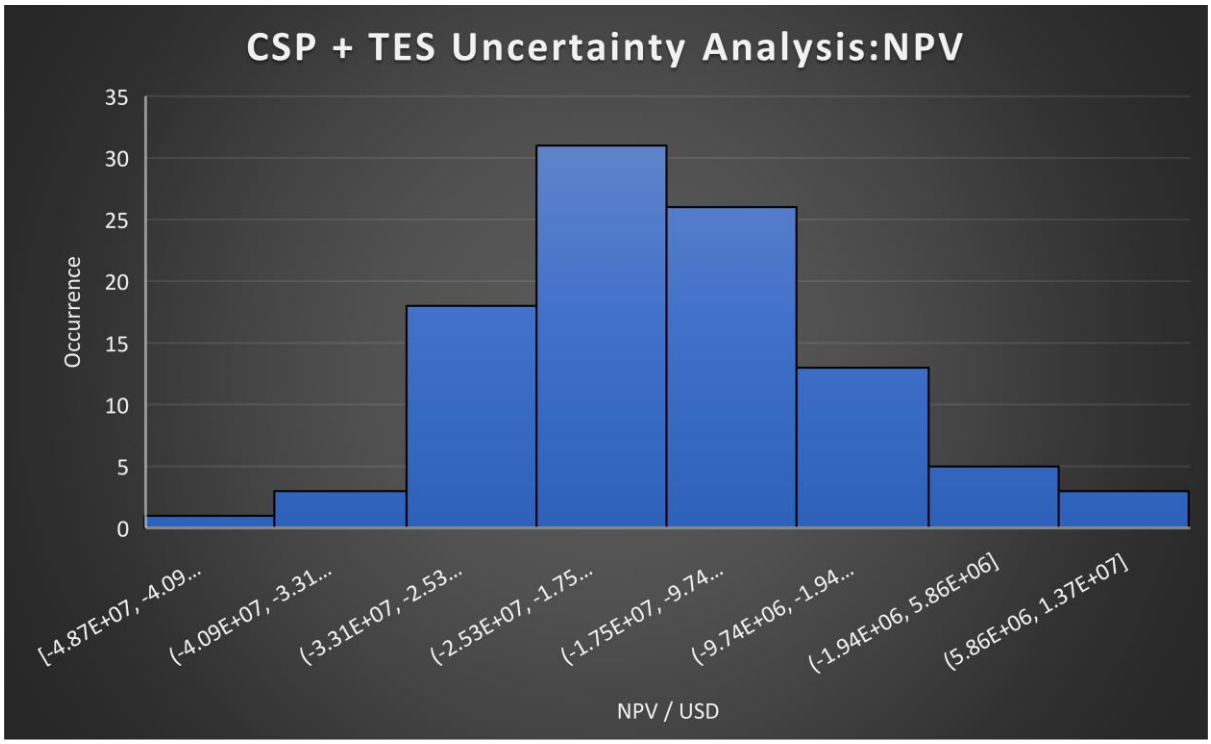

# Appendix N – PV with Exports loss diagram and lifetime production

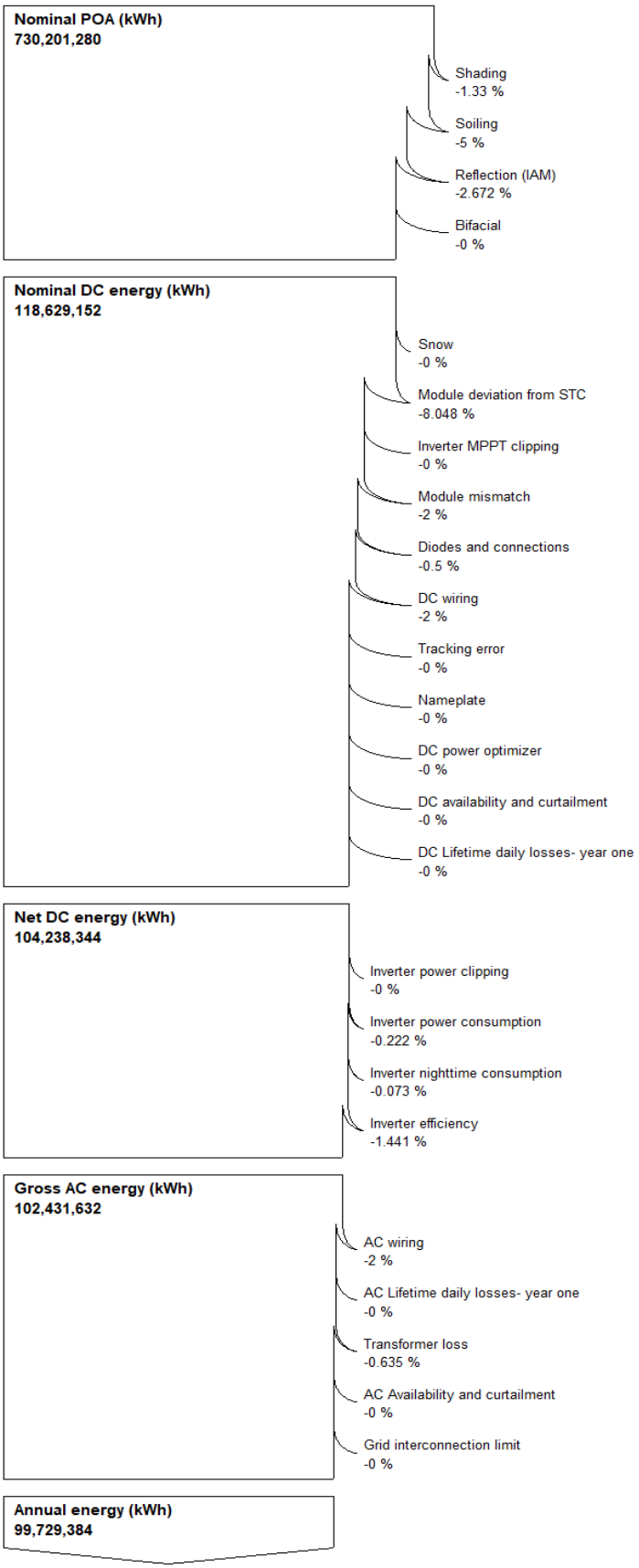


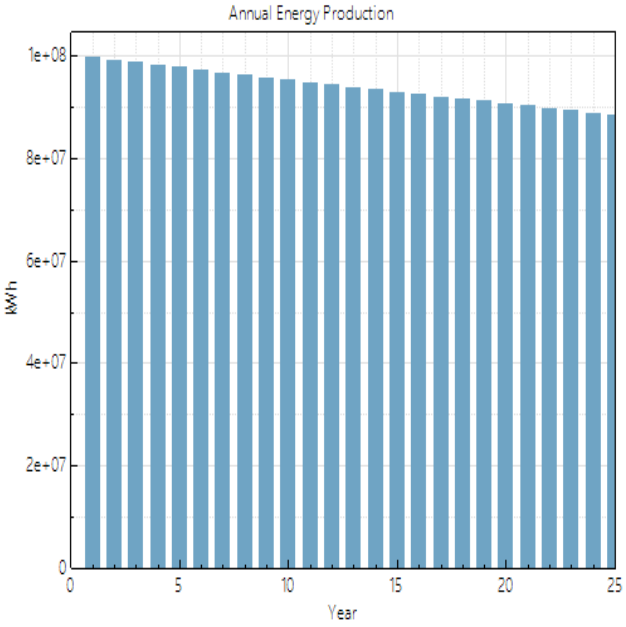

# Appendix O – PV + Battery with Exports loss diagram and lifetime production

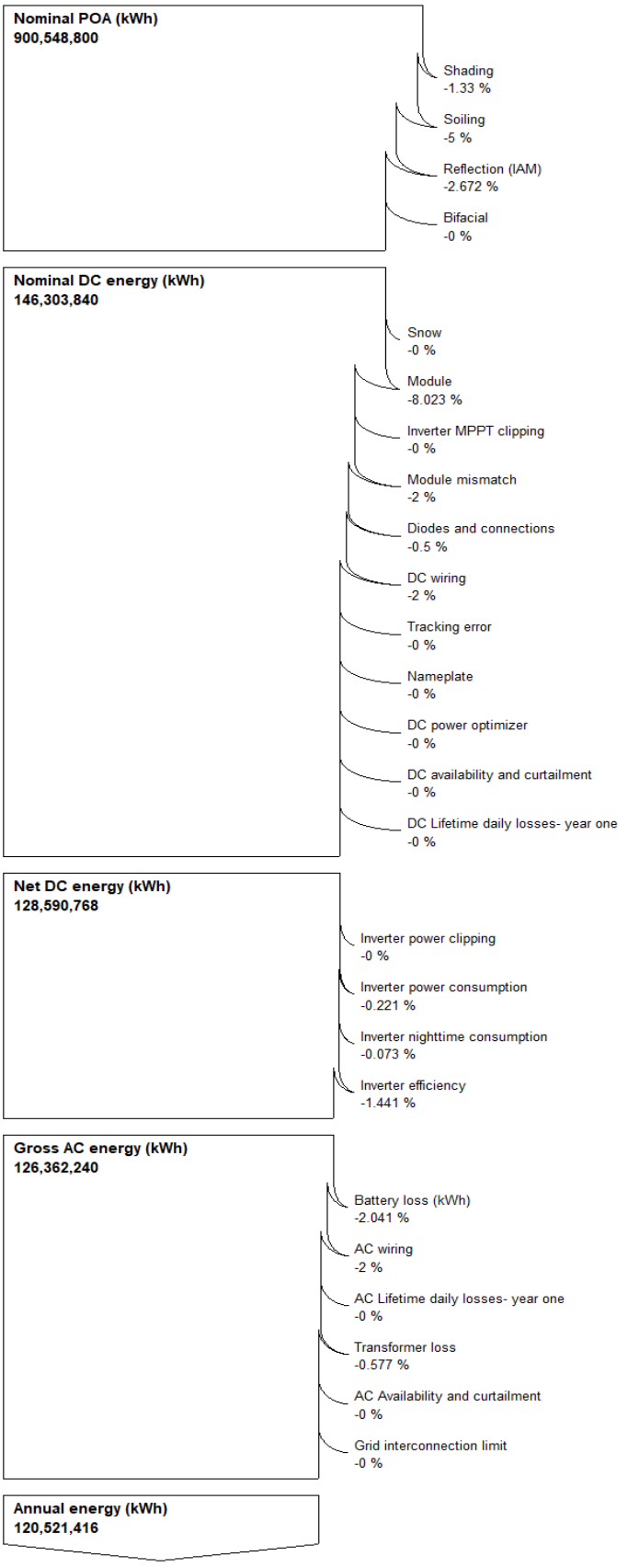


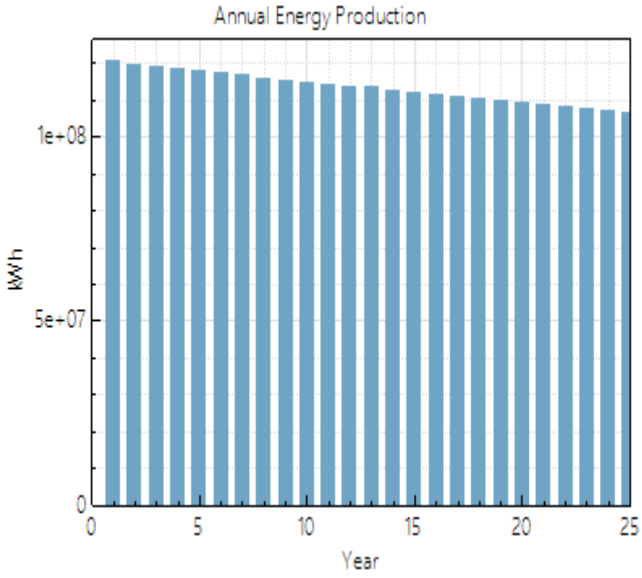

# Appendix P – Summary results for CSP with Exports

| Metric | Value |
|---|---|
| Annual Net Electrical Energy Production | 94,714,760 kWh-e |
| Annual Freeze Protection | 1,405,602 kWh-e |
| Annual TES Freeze Protection | 0 kWh-e |
| Annual Field Freeze Protection | 1,405,602 kWh-e |
| Capacity factor | 24.0% |
| Power cycle gross electrical output | 105,163,888 kWh-e |
| First year kWh/kW | 2,105 - |
| Gross-to-net conversion | 90.1 % |
| Annual Water Usage | 23,297 m^3 |
| Levelized COE (nominal) | 12.13 ¢/kWh |
| Levelized COE (real) | 9.63 ¢/kWh |
| Electricity bill without system (year 1) | $13,693,863 |
| Electricity bill with system (year 1) | $4,016,119 |
| Net savings with system (year 1) | $9,677,744 |
| Net present value | $3,956,226 |
| Simple payback period | 15.7 years |
| Discounted payback period | NaN |
| Net capital cost | $150,586,688 |
| Equity | $0 |
| Debt | $150,586,688 |

# Appendix Q – Summary results for CSP + TES with exports

| Metric | Value |
|---|---|
| Annual Net Electrical Energy Production | 127,436,792 kWh-e |
| Annual Freeze Protection | 5,106,000 kWh-e |
| Annual TES Freeze Protection | 3,417,043 kWh-e |
| Annual Field Freeze Protection | 1,688,957 kWh-e |
| Capacity factor | 40.4% |
| Power cycle gross electrical output | 143,142,176 kWh-e |
| First year kWh/kW | 3,540 - |
| Gross-to-net conversion | 89.0 % |
| Annual Water Usage | 28,059 m^3 |
| Levelized COE (nominal) | 10.45 ¢/kWh |
| Levelized COE (real) | 8.30 ¢/kWh |
| Electricity bill without system (year 1) | $13,693,863 |
| Electricity bill with system (year 1) | $472,424 |
| Net savings with system (year 1) | $13,221,439 |
| Net present value | $28,608,922 |
| Simple payback period | 12.9 years |
| Discounted payback period | NaN |
| Net capital cost | $199,640,416 |
| Equity | $0 |
| Debt | $199,640,416 |